THE UNIVERSITY OF MANITOBA

DOWNSLOPE MOVEMENTS AT SHALLOW DEPTHS RELATED TO DRAINED CYCLIC PORE PRESSURE CHANGES

by

Jean Paul Burak

A THESIS

SUBMITTED TO THE FACULTY OF GRADUATE STUDIES

IN PARTIAL FULFILLMENT OF THE REQUIREMENTS FOR THE DEGREE OF

MASTER OF SCIENCE

DEPARTMENT OF CIVIL ENGINEERING

WINNIPEG, MANITOBA

ISBN 0-315-33996-9

DOWNSLOPE MOVEMENTS AT SHALLOW DEPTHS RELATED TO DRAINED CYCLIC PORE PRESSURE CHANGES

BY

JEAN PAUL BURAK

A thesis submitted to the Faculty of Graduate Studies of the University of Manitoba in partial fulfillment of the requirements of the degree of

MASTER OF SCIENCE

ABSTRACT

This thesis investigates the effect of cyclic pore pressures on soil with regards to its deformation behavior. The observed behaviour is then correlated to actual field conditions in which shallow, slow ground movements have been measured.

The effect of fluctuating porewater conditions on slow ground movements has been studied by subjecting triaxial speciments to cyclic pore pressure changes. These changes were applied through a back pressure burette with full drainage being permitted throughout the duration of the tests. The tests were performed at constant total loads, and a total of 11 tests was completed.

Results from the laboratory tests showed permanent changes in volume and shape during the cyclic pore pressure changes. The deformation rates reached approximately constant values in the range of 30 cycles and were dependent on the magnitude of the pore pressure changes. The strain rates also increased linearly with an increase in the ratio $\Delta u/\Delta u_f$.

Correlations between the laboratory test results and the field soil behavior show that the displacements pattern

can be predicted from the cyclic pore pressure changes. The new analysis, however, seriously underpredicts the downslope movements, as the magnitude of the field displacements is much larger than those predicted.

ACKNOWLEDGEMENTS

The author greatly appreciates the help of all those who contributed to the completion of this thesis and wishes to express his sincere gratitude.

Special mention goes to Dr. K.D. Eigenbrod for suggesting this topic of research and for this invaluable advice and guidance during all stages of this study.

The author is grateful to Dr. J. Graham for his guidance and suggestions.

The author thanks his collegues for being available to discuss problems and assist during the preliminary testing.

Cominco Mines generously permitted access to the test site, and special thanks go to on-site personnel, Frank Mintert and Scotty Trotter for their logistic support and for obtaining instrument readings during the year.

The author thanks Rhonda Kelly for her time and effort in typing out the manuscript.

Thanks go to Lakehead University for their support during the research.

Finally, thanks go to the National Science and Energy Research Council of Canada, the Northern Training Program, Summer Canada 84 and Summer Canada 85, Government of Canada for providing financial assistance.

TABLE OF CONTENTS

LIST OF SYMBOLS

A_f	Porewater pressure coefficient at failure ($A_f = \Delta u/\Delta\sigma$ for $B = 1.0$)
B	Skempton porepressure parameter
C_v	Coefficient of consolidation
E'	Young's modulus in terms of effective stresses
F_s	Factor of safety against catastrophic slope failure
K_A	Coefficient of active earth pressure
K_o	Coefficient of earth pressure at rest (σ_3'/σ_1')
R	Thaw consolidation ratio = $(\alpha/2\sqrt{C_v})$
V	Specific volume
c'	Cohesion with respect to effective stresses
d	Depth of thaw
e	Void ratio (V_v/V_t)
p'	Effective octahedral stress = $(\sigma_1'+2\sigma_3')/3$
q	Deviator stress = $(\sigma_1'-\sigma_3')$
q_f	Deviator stress at failure
r_u	Porewater pressure ratio = $(u/\gamma z)$
t	Time
u	Porewater pressure
Δu	Change in porewater pressure
Δu_f	Change in porewater pressure required to bring sample to failure
$v, \dot{v}$	Volumetric strain, strain rate
z	Depth below ground surface
CIU	Consolidated, isotropically, undrained triaxial test

LIST OF SYMBOLS (cont'd)

γ, γ'	Specific weight of soil, effective
θ	Inclination of natural slope
γ_w	Specific weight of water $= 9.81$ kN/m^3
α	Constant
σ_1, σ_3	Major, minor principal stresses
σ_1', σ_3'	Major, minor effective principal stresses
$\sigma_{1_c}', \sigma_{3_c}'$	Major, minor principal effective consolidation stress
σ_v'	Vertical effective stress
σ_{vc}'	Vertical effective preconsolidation pressure
$\varepsilon_{13}, \dot{\varepsilon}_{13}$	Major, minor principal strains, strain rates
$\varepsilon_s, \dot{\varepsilon}_s$	Shear strain, strain rate
λ	Slope of normal consolidation line (negative)
κ	Slope of overconsolidation line (negative)
ϕ'	Angle of shearing resistance w.r.t. effective stresses
ν	Poisson's ratio

LIST OF TABLES

LIST OF FIGURES

LIST OF FIGURES (continued)

Figure | Page

LIST OF FIGURES (continued)

LIST OF FIGURES (continued)

I INTRODUCTION

Shallow, slow, irregular ground movements have been frequently observed in natural slopes of less than 10^{o} (Skempton and Delory, 1957, Williams, 1966)as well as in steeper slopes. It has been suggested that slow movements of this kind may at times result in slope failures (Yen, 1969), or may continue for long periods without leading to failure (Kojan, 1967). These movements may be of significant concern to engineers when they interfere with construction works or engineered structures (Eigenbrod, 1984, Chandler and Pochakis, 1973). In periglacial areas, continuous ground movements are referred to as solifluction (Bloom, 1978). The moving soil layer is saturated with water and many of the observed movements occur on slopes with angles as low as $2\text{-}5^{o}$ (Carson and Kirkby, 1972). Movements may also be due to the effects of frost: observed as heave of the soil during freezing followed by subsequent consolidation on thawing (Williams, 1966, Washburn, 1973). This phenomenon causes a step like behavior of the soil particles downslope.

Tavenas and Leroueil (1981) and McRoberts and Morgenstern (1974) suggest that these slow movements could also be related to fluctuating porewater pressure conditions. Tavenas and Leroueil (1981) stated that the "cyclic creep deformation behavior of natural slopes has not been investigated in detail."

In order to study the effect of fluctuating porewater conditions on slow ground movements a laboratory testing program was undertaken in which soil specimens were subjected to cyclic pore pressures, and an instrumentation program of a slope at Bluefish Lake N.W.T. initiated where slow shallow soil movements had been reported (Eigenbrod, 1984).

This thesis presents the results of the laboratory program and additional field observations obtained for the instrumented slope. The data is then related to results reported by other authors (eg. Williams, 1966, Tavenas and Leroueil, 1981, Washburn, 1973, McRoberts and Morgenstern, 1974).

Chapter II describes the site investigation which was carried out at the Bluefish Slope as well as the observations obtained from the instrumentation which was installed. A subsequent stability analysis is also presented. Chapter III presents brief summaries of other reports on continuous, slow soil movements as well as their respective field observations and discussions on the possible mechanisms causing the movements.

The laboratory programs undertaken, their results and respective discussions are given in Chapters IV and V, while Chapter VI attempts to correlate the laboratory test results with the actual field observations. Conclusions and recommendations for further study are given in Chapter VII.

II SLOPE AT BLUEFISH LAKE HYDRO

2.1. General Description

Bluefish Lake Hydro Electric Plant is located on the Yellowknife River System approximately 50 km north of Yellowknife, N.W.T. The wooden penstock of the hydro plant runs in a north-south direction along a south east facing slope (see Fig. 2.1). It is partly located on rock and partly on a slope underlain by clay and silt.

Slow, continuous slope movements have occurred over the years on the clay - silt slope, necessitating on two occasions within a period of 50 years, the removal and replacement of a section of the penstock. The piles on which the penstock was supported had tilted downhill. The only indication of downhill slope movements was soil having been pushed up against a series of piles on their uphill sides, while a gap had formed on their downhill sides. Tilting of the piles caused excessive distortion of the penstock leading to numerous leaks. Excessive movements of the piles became a concern approximately twelve years after their reconstruction in 1968. Eventually a portion of the pipe and its supports had to be replaced in 1983.

2.2 Geology

The topography in the vicinity of the site consists of smoothly rounded bedrock hills separated by valleys with maximum differences in elevation of up to 70 meters. According to Aspler (1984), the bedrock was exposed during advances of the Laurentide ice sheet. The local sequences of tills resting on glaciofluvial material are interpreted as the result of basal meltout coincident with deposition by streams flowing through the icesheet. Following deglaciation the area was subaerially exposed and sands and gravels were deposited in some of the deeper valleys.

The area was then inundated by glacial Lake McConnell which deposited silts and clays on topographic lows, but sands on topographic highs. Ice rafting resulted in various size clasts being incorporated into the sediments. Permafrost in the area is believed to have started to form as recently as 4000 BP.

2.3 Field Investigations

Conditions on the site seem to indicate that groundwater may be an important factor in the slope movements. Since its construction, the penstock has consistently leaked, contributing water to the groundwater regime. There is also an indication that groundwater from higher up in the slope flows down an access road then down a trough-like path on the slope under the section of penstock recently replaced. This is evident by an area of the access road which is constantly wet, even during the driest part of the summer, and by a spring which exits downslope of the penstock and just below the former alignment. The locations of these observations are indicated on Fig. 2-2 which shows the site layout as well as the locations of test holes, instruments installed and test pits.

Downslope of the penstock, the lower section of the slope consists of a permafrost feature in which massive ground ice was found between the depths of 2.0 and 8.5 m (Eigenbrod, 1984). It is believed that the degradation of this ice feature due to the water leaking from the penstock is initiating the slope movements. A marshy area is located at the toe of the slope where further degrading permafrost is evidenced by surface slumping and surface slope movements. A complete profile of the slope is given in Fig. 2-3. Fig. 2-3a shows the overall extent of the slope while Fig. 2-3b shows a more detailed profile of the instrumented area. The average slope angle is approximately 7^{o}.

The site was investigated by a total of 18 boreholes: five drilled in the fall of 1982 (Eigenbrod, 1984) and thirteen drilled in the summer of 1984. Two test pits were also excavated in the summer of 1984 and their locations are shown on Fig. 2-2. A total of six open standpipes was installed at the locations indicated in Fig. 2-2, as well as three electro-piezometers, with their tips located in the sand-gravel layer overlying the bedrock. Four slope indicator casings were also installed on the site in the summer of 1984. These installations provided information regarding the magnitude of slope movements and the fluctuations in the groundwater pressures in the sand and gravel layer underlying the clay deposit. A summary of the 1984 Field Drilling Program is given in Appendix B.

Two pressure cells were installed in Test Pit No. 1 against the foundation pier in order to measure the soil pressure exerted on them due to the movements. The data obtained from these pressure cells to date are not sufficient to permit their evaluation and therefore will not be discussed in the context of this study.

Three thermistor strings were installed; one in 1982 and two in 1984, and have provided pertinent information with regards to the ground temperature profile and the uphill extent of the permafrost feature. A description of the instruments installed as well as their installation procedures are given in Appendix B.

2.4 Field Observations

The site stratigraphy as shown in Figs. 2-3 and 2-4, is interpreted from the borehole logs and the laboratory classification test results presented in Appendix B; and from the site investigation performed previously (Eigenbrod, 1984).

A silty clay is found overlying sand and gravel deposited directly on the bedrock. The overburden ranges in thickness from 2.0m uphill of the penstock to 12.5 m downhill of the penstock. The clay is often varved, and contains ice-rafted pebbles and stones randomly deposited throughout. The top 0.5m of soil commonly contains boulders to a maximum size of 0.5m. At the location of Test Pit No. 2, the silty clay was only approximately 0.5m thick and below changed to a silt to a depth of 2m. The clay observed through-out most of the site was a light brownish-grey silty clay, nuggety, moist to wet at some locations, soft, and contained some organics. Pocket penetrometer readings taken at 1.35m depth in Test Pit No. 1 gave an average undrained shear strength of 200 kPa while torvane readings taken at the same depth gave an average result of 70 kPa.

The water tables observed in the standpipes varied throughout the year. Seasonal variations of the water pressure in the sand and gravel zone below the clay are indicated in Figs. 2-5, 2-6and 2-7. Figure 2-5 presents the height of the water in the standpipes, with respect to their tips, as observed at various times through the year. Figure 2-6 shows the piezometric levels for these readings as plotted on the slope profile, while Fig. 2-7 shows the change in r_u and the change in u, versus depth, for different locations, for the maximum level of water recorded (see List of Symbols page vi). The magnitude of the groundwater fluctuations in the slope is different for each location as shown in Fig. 2-7. With reference to a depth of 2.0m, the fluctuation is zero in the upper part of the slope, while further down in the area of STP-1 , the fluctuation is approximately 2.5m. The highest water levels were recorded in August, 1984 and September 1985.

The slope movements recorded from the slope indicator casings installed are shown in Figs. 2-8 to 2-11. The total deflections are plotted versus depth using the original set of readings obtained on August 16, 1984, soon after they were installed, as the reference line. Total deflections shown are deviations from this original profile. Each casing is oriented with the A+ axis pointing upslope (west), with the exception of installation SI-3 in which the A+ axis is pointing in the N.W. direction. The B+ axis corresponds to the groove which is 90° clockwise from the A+ groove.

The slope indicator readings as indicated in these figures show movements of the soil concentrated in the top 2m of the overburden. The rates of surface movements vary from 5mm/yr. for SI-4 at the upper margin of the slope, to 32 mm/yr for SI-2 in the upper centre of the slope area. For installation SI-1 downslope of the penstock in the centre portion a rate of 20 mm/yr was recorded and for SI-3 a rate of 14 mm/yr was recorded. These rates of movements are in the same range as those reported by Williams (1966) for a shallow slope located at a sub-artic location. He observed movements up to 18.7 mm/yr with flexible tubes inserted into the ground.

The temperature profiles obtained from the thermistor installations are shown in Appendix B, while, Figs. 2-12 to 2-14 show the yearly extremes of the temperatures variations. All thermistors show relatively stable ground temperatures below 5m depth. Thermistors TH-1 and TH-3 show an active zone of approximately 1.5m whereas thermistor TH-2, which was installed at a location which was believed to be at the boundary of the permafrost feature, showed an active zone of almost 5m thickness.

The average temperatures of the permafrost below 5.0m depth were -1.3°C for the thermistor TH-3, -1.0°C for thermistor TH-1, and -0.2°C for thermistor TH-2.

2.5 Stability Analysis

2.5.1 Infinite Slope Analysis - Seepage Slope

The slope at Bluefish Lake is a fairly uniform slope of relatively large extent in which the movements are shallow and may be assumed to be parallel to the ground surface. The appropriate way to analyse this slope with respect to its stability is by using "infinite slope" analysis with the assumption that the soil properties and pore water pressures at any given distance below the ground surface are constant. The factor of safety F_s for the condition of limit equilibrium using an effective-stress analysis ($c'\ \phi'$) becomes

$$F_s = \frac{c' + (\gamma - m\gamma_w) z \cos^2\theta \tan\phi'}{\gamma z \sin\theta \cos\theta} \qquad (2\text{-}1)$$

where the groundwater flow is parallel to the slope and the groundwater table is at a vertical height mz above the slip surface (ref. Fig. 2-15a). For no cohesion and the groundwater table at the surface, Eq. 2-1 reduces to

$$F_s = \frac{\gamma' \tan\phi'}{\gamma \tan\Theta} \qquad (2\text{-}2)$$

where γ'/γ is the ratio of effective total unit weight of the soil and is usually taken as approximately 0.5, ϕ' is the angle of shearing resistance in terms of effective stress and θ is the slope angle. Using $\gamma'/\gamma = 0.5$, the slope angle $\theta = 7^{o}$ and $\phi' = 31^{o}$ determined from CIU tests described in section 3.2.1, in Eq. 2-2, the factor of safety F_s is calculated to be 2.4.

From this simple calculation, it can be seen that the slope apparently has a very high factor of safety against catastropic failure, yet it is definitely experiencing movements.

Eq. 2-1, written in terms of r_u, where $r_u = u/\gamma z$ and $c' = 0$, yields

$$F_s = \frac{(\cos^2\theta - r_u)\ \tan\phi'}{\sin\theta\cos\theta} \qquad (2\text{-}3)$$

Using a safety factor of unity indicating failure conditions, and the parameters relevant to this slope, we find that the r_u required for failure is approximately equal to 078. This value is greater than the approximate value of 0.5 which correlates to the condition of the ground water table being at the ground surface.

2.5.2 Infinite Slope Analysis - Thaw Slope

McRoberts and Morgenstern (1974) have applied the thaw-consolidation theory to the prediction of slope stability on thawing slopes (Fig. 2-15b), contending that excess pore water pressures can be set up in thawing soils and that they are consequent upon thaw-consolidation. Solving the one-dimensional thaw-consolidation problem using the Newmann solution

$$d = \alpha\sqrt{t} \qquad (2\text{-}4)$$

where: d = depth of thaw

t = time

α = a constant

the solution is formulated in terms of a thaw consolidation ratio R, where:

$$R = \frac{\alpha}{2\sqrt{C_v}} \qquad (2\text{-}5)$$

where α is defined by Eq. 2-4 and c_v is the coefficient of consolidation. This ratio expresses the relative influence of the rate at which water is produced by thaw and the rate at which it may be squeezed out of the thawed soil overlying the moving thaw interface.

For an infinite soil mass thaw-consolidating under self weight conditions the excess pore presssure has been found to be

$$u = \frac{\gamma' d}{\left(1 + \frac{1}{2R^2}\right)} \qquad (2\text{-}6)$$

where $\gamma' d$ is the effective stress after complete dissipation of excess pore pressures.

Considering a slope, Fig. 2-15b, where the thaw front is at depth d, the effective stress on plane A-A would be $\gamma' d \cos\theta$, and the pore pressure would be

$$u = \gamma_w d\cos\theta + \gamma' d\cos\theta \left(\frac{1}{1 + \frac{1}{2R^2}} \right) \qquad (2\text{-}7)$$

and applying a statical balance of forces, the factor of safety becomes

$$F_s = \frac{\gamma'}{\gamma} \left(1 - \frac{1}{1 + \frac{1}{2R^2}} \right) \frac{\tan\phi'}{\tan\theta} \qquad (2\text{-}8)$$

for a thaw slope.

Applying the relevant slope parameters and a value of R of 0.65, the factor of safety against failure for this thawing slope becomes 1.12. It should be noted that the value of R was selected using $\phi' = 25^{\circ}$, $G_s = 2.70$ and a water content of 31%, because the solution for R was presented for these parameters only in the original publication. This value used for ϕ' is less than that actually measured for this soil, and the value $\phi' = 31^{\circ}$ would give an even more conservative factor of safety.

Again using $r_u = u/\gamma z$ and the expression given for u in Eq. 2.7, we find that

$$r_u = \frac{\gamma_w \cos^2\theta + \gamma' \cos^2\theta}{\gamma} \left(\frac{1}{1 + \frac{1}{2R^2}} \right) \qquad (2\text{-}9)$$

Using values of $\gamma_w = 9.81\ kN/m^3$, $\gamma' = 10\ kN/m^3$, $\gamma = 19.8\ kN/m^3$ and $R = 0.65$, an r_u value of 0.72 can be obtained, which is in the same order of magnitude as the value of 0.78 necessary for failure of this slope. The factor of safety obtained from the thaw slope analysis seems to indicate that excess pore pressures due to thaw consolidation may be an important factor to consider in the causes of slope movements.

III OTHER REPORTS ON CONTINUOUS, SLOW SOIL MOVEMENTS

3.1 Introduction

Several articles are summarized in this chapter which deal with shallow, slow movements in soil as well as the possible mechanisms which cause them. These summaries present the various mechanisms causing slope movements as well as presents quantitative data regarding shallow slope movements. Actual slope movements are recorded as well as pore pressures observed in thawing slopes. Subsequently, the movements and pore pressures recorded for these slopes, as well as the possible mechanisms causing the movements are summarized. These are later used in determining the correct analysis to use and in comparing results.

3.2 Slopes at Schefferville, P.Q. (P.J. Williams, 1966)

3.2.1 General

Downslope movements of a soil in a subarctic location were observed and reported by Williams (1966). Three sites near the town of Schefferville, P.Q. were selected in which 2.22 cm diameter polyethylene tubes up to 2 m long were inserted vertically in holes prepared with an auger in order to record the slope movements. The deformation of the tubes was measured using a probe which was lowered into each tube. The tubes were placed in 1958 and investigated in 1959, 1960 and 1961. The sites selected showed no indication of catastrophic instability.

3.2.2 General Description of Area and Slopes

The three sites investigated are in areas in which permafrost occurs discontinuously with their respective active layers generally 1.5 to 3.0 m deep.

Site 1, located 20 km northwest of Schefferville, is a terraced slope feature in which the terrace surface is sloped at an angle of varying from 4° to 9°, with a much steeper bluff of up to 30°. Six tubes were placed on this site (Fig. 3-1).

Site 2 is located 5 km northeast of the townsite. Overburden here varies between 1m to 2m depth and surface vegetation consists of older scrub and isolated spruce. The slope angle varies between 5° and 23°, and water reaches the surface at the foot of the slope. Six tubes varying in length from 0.4m to 1.2m were installed at the site (Fig. 3-1).

Site 3 is a vegetation-free slope with an angle of about 20° covered with small stones and located 300m southeast of Site 1. One tube was installed at this site.

Profiles showing the location of each installation relative to the slope are given in Fig. 3-1.

A composite curve presenting the grain size analysis of the three sites shows that the soil contains from 10-25% sand, 44-60% silt and 15-35% clay. A breakdown for each site shows that the site 1 is 25% sand, 60% silt and 15% clay; site 2 has 20% sand, 55% silt 25% clay; and site 3 has 12% sand, 44% silt and 34% clay.

3.2.3 Field Observations

Surface movements of up to 10cm were recorded for the slopes at site 1 and site 3. The movements decreased in depth, varying in intensity from year to year. Profiles showing the shape of the tubes in two sites is shown in Figs.3-2 and 3-3. Tubes B and C show a "concave" tube profile and movements downhill, while tubes A and D show a slight "concave" shape uphill (Williams, 1966). This was attributed to the tube's tendency to take on this form because of their transport to the site in a coil.

Fig. 3-4 shows a profile of average slope movements, per year for tube C at site 1. Site 2 showed very little movements, although deformations of the woody vegetation on the site seemed to indicate some.

3.2.4 Conclusions

Williams stated that "the concave downslope form assumed by the tubes shows that not only is the absolute displacement of the upper layers greater than that of the lower layers, but the differential movement within each layer increases towards the surface". A stability analysis utilizing Eq. 4-2 with $\gamma'/\gamma = 0.5$ shows that for failure the angle of internal friction (ϕ') on site 1 would have to be less than 18° (for $\theta = 9^{\circ}$), and less than 8° (for $\theta = 4^{\circ}$). For site 3, ϕ' would have to be less than 36°, which seems to indicate that the slope is at or close to failure. Because of the silty nature of the soil, it is evident that the angle of internal friction will be fairly high, and thus it was concluded that the movements (in site 1 anyway) are not susceptible to conventional stability analysis and require further explanations.

Considerations were then given to the possibility of movements due to freeze-thaw activity, the frost heave due to freezing being normal to the slope and the soil settling vertically due to gravity upon thawing (see Fig. 3-5). Using the equation $L = E \tan \theta$ (where L = downslope component of movement, θ = slope angle and E = frost heave), Williams found that the magnitude of frost heave required to cause the observed downhill movements was improbable for this case. He concluded that consolidation following frost heave is unlikely to be by itself responsible for the movements.

3.3 Frost Creep and Gelifluction (Washburn, 1973)

Washburn (1973) considers two processes by which a soil slope may move downhill; frost creep and gelifluction. He describes frost creep as "the ratchet like downslope movement of particles as the result of frost heaving of the ground and subsequent settling upon thawing, the heave being predominantly normal to the slope and the settling more nearly vertical." Gelifluction is presented as solifluction (movement of ground mass saturated with water) associated with frozen ground. Since the predominant characteristic of gelifluction is its dependency on moisture, it is contended that the reasons for the prominence of gelifluction in cold climates are two-fold: (1) the role of the frost table (permafrost table) in preventing the downward movement of moisture and creating saturated soil conditions and (2) the role in thawing ice and snow in providing moisture to the ground.

Rates of frost creep and gelifluction were reported for various locations including Greenland, Lapland, and Spitsbergen. The slopes varied from 5^{o} to 17^{o} and the rates recorded ranged between 9.0 mm/yr and 120.0 mm/yr. Washburn observed that the ratio of gelifluction to frost creep differed in successive years and thereby contended that both processes occur simultaneously, Either process can predominate in any given year. This combined process is illustrated in Fig. 3-6.

3.4 Seasonal Creep Due to Fluctuating Groundwater Table (Tavenas and Leroueil, 1981)

Tavenas and Leroueil (1981), in approaching the topic of seasonal soil creep of slopes, related the soil movements to the groundwater regime in the slopes. It was suggested that groundwater fluctuations can occur in the clay crust, or in surficial aquifers, or due to variations of artesian pressure in interval or underlying granular layers.

As a result of yearly and seasonal variations of the pore pressures in the slope, the effective stress conditions fluctuate. During periods of high pore pressures, the effective stresses are reduced towards failure (and higher creep rates). During periods of low-pore pressures, the effective stresses are higher and thus the slope is more stable. Although they referred to the creep rates reported by Mitchell and Eden (1972), they state that this 'cyclic creep deformation behavior of a natural slope has not been investigated in detail'.

3.5 Shallow Slope Movements Caused by Excess Pore Pressures due to Thaw-Consolidation (McRoberts and Morgenstern, 1974)

McRoberts and Morgenstern investigated several case studies which dealt with observations on slopes with inclinations ranging from 3° to 9°. Using infinite slope analysis, and pertinent soil data such as residual shear strength parameters, it was found that these slopes should all be stable for slope angles below 12.5°. They concluded that excess pore pressures are required to account for these low angle movements. By solving for the pore pressures required to cause failure, the pore pressures were expressed in terms of r_u and were recorded to vary from 0.6 to 0.86, as compared to an r_u of about 0.50 for hydrostatic conditions.

They associate these excess pore pressures to two possible mechanisms; thaw consolidation, and ice-blocked drainage. Thaw-consolidation refers to the release of water as frozen ground thaws and the subsequent settlement of the ground. If the rate of water generation exceeds the discharge capacity of the soil, excess pore pressures will develop (Andersland and Anderson, 1978).

Ice-blocked drainage results when a freezing front advances into a slope forming on impermeable frozen soil blanket. This blanket can then block or back-up the water flow and may produce excess pore pressures. McRoberts and Morgenstern contended that ice-blocked drainage, even though observed in the laboratory seems unlikely in the field since water will always be attracted to an advancing freezing front and 'pore water sub-pressures would be more reasonably expected'.

Two case records are presented in which excess pore water pressures were recorded during studies on thawing slopes. The first was in the Mackenzie River Valley near Fort Norman, N.W.T. The piezometers were installed in areas of silt-runs where free water was ponded at the surface. The measured pore pressures, expressed in terms of the r_u ratio, ranged from 0.88 to 1.09 as compared to an r_u of 0.52 for hydrostatic conditions. Thus the excess pore pressure ratios ranged betwen 0.36 to 0.57. The values of u and r_u

versus depth are plotted in Fig. 3-7.

The second case is referring to a study done by Chandler (1972) in which thawing slopes in Vestspitsbergen were investigated. Measurements were made at the base of the active layer as well as at intermediate depths. The pore pressures measured ranged from r_u values of 0.65 to 0.84, as compared to 0.50 for hydrostatic conditions. This gives excess r_u values ranging from 0.15 to 0.34. (See Figs. 3.9 and 3.10)

For both of these cases, it is suggested that the excess pressures are due to thaw-consolidation processes.

3.6 Deep Seated Movements in Clay Slopes (Mitchell and Eden, 1972)

Mitchell and Eden present measurements from inclinometer installations in three slopes in the Ottawa area. The slope angles ranged from 20^{o} to 28^{o}, with one installation on a 35^{o} slope. All the slopes are along rivers or creeks and are subject to toe erosion. Three inclinometers were installed in slopes that were similar to adjacent ones where recent landslides had occurred, and three were chosen because particular environmental factors were prevalent (eg. graded slope, outcropping marine clay and a natural slope subjected to unusually rapid erosion).

Three years of slope movement observations showed significant deep-seated movements in which the time of maximum movement for four of the installations was during the Spring. It is also believed that most of the movement occured during this time. The maximum rates of movements varied from 2 to 6 mm/month (during the Spring thaw) while the average movements over the three year period was 0.11 to 27 mm/yr.

In order to investigate the influence of changes in groundwater level on the deformation in the slopes, a sample of clay from one of the slopes (Rockcliffe Clay), was subjected to a normal drained compression test until the sample was at equilibrium under approximately 90% of its' failure load. The pore pressure was then cycled to simulate a 0.5 m variation in the goundwater level. The time intervals between the various cycles ranged between 1 min. and 4 min. After several cycles (number not mentioned), the sample had undergone about 3.5% axial strain without failure. No volume changes were mentioned. From this, Mitchell and Eden conclude that this test definitely supports the concept that slope movements are associated with seasonal high groundwater levels.

3.7 Artesian Pore Pressures in Shallow Slopes (Chandler, 1972)

Chandler (1972) investigated two slopes in Vestspitsbergen with inclinations in the range of $8\frac{1}{2}^{\circ}$ to 12° on which mudflows frequently occur in silty materials. Pore pressure measurements were obtained at the base of the thawing soil as well as at mid-depth of the thawing layer. Slope 1 was at the base of an abandoned cliff and consisted of a series of broad raised beach terraces of tertiary sediments. The overall slope from the crest of the rear scarp to the foot of the toe, was 10°. Slope 2 was at a site in which a number of small scale shallow mudslides had developed on the slope. Silt seeps were evident where emerging groundwater had brought the silt to the surface, indicating locally high water pressures.

The soil found at slope 1 was a relatively uniform silty sand with approximately 8% clay, 32% silt, 40% sand and 20% gravel. No grain size analysis was performed on soil from slope 2. Only slope 2 was investigated for slope movements, pore water pressures and ground temperatures. Three lines of pegs were set out across the slope to determine any surface movements. Over the two week observation period, none of the pegs showed any measurable movements.

Most of the piezometers installed (1 to 12, 20, 21) were simply open ended ½" diameter PVC tubes, while the remaining were electrical piezometers. The stand pipe piezometers were installed by pushing to refusal, presumably to the thawing depth. At four locations, pairs of piezometers (1,2; 3,4; 5,6 and 21,21) were installed, one tube to refusal, the other to a shallower depth. Figure 3-8 shows the locations of all piezometer installations as well as the general site layout.

Water pressures were recorded only by piezometers 1,2; 3,4; 20 and 21, while the remaining tubes were dry. Those piezometers which recorded water pressures were all sited in an area of the slope where there was a thin film of water flowing down the slope. The readings given by the electrical piezometers plotted against time are shown in Fig. 3-9. Fig. 3-10 gives a summmary plot in which the maximum observed heads of water above the piezometer tip are plotted versus the depths of piezometers. The data show a consistent record of artesian pressures.

Soil temperatures were measured at two points by driving to refusal a ½ inch bore metal tube into which a soil thermometer was lowered. The soil temperature profiles thus obtained indicate primarily the effect of air temperatures and thus are of little value.

After performing a stability analysis, Chandler showed that for the occurence of mudslides for the range of the slope angles at which they were observed, the pore pressures must have been considerally in excess of the hydrostatic condition. He concluded that the artesian pressures "are believed to be generated by layers of soil of contrasting permeability dipping downslope parallel to the ground surface. The presence of permafrost at a shallow depth prevents the movement of meltwater in any direction other than parallel with, or upwards towards the ground surface, and consequently the blanketing effect of the layers of lower permeability material results in the generation of artesian presures".

Another possible cause mentioned for the observed artesian pressures was overnight freezing of the surface. Chandler contends that surface freezing will be most likely to generate artesian pressures in the spring when the shallow depth of thaw ensures that melt water remains at or close to the ground surface.

3.8 Summary

The possible mechanisms mentioned which may be responsible for the observed shallow slow movements in natural slopes are: consolidation following frost heave

(Williams, 1966), frost creep and/or gelifluction (Washburn, 1973), seasonal variations of the pore pressures in the slope (Tavenanas and Lerouiel, 1981, and Mitchell and Eden, 1972), excess pore pressures due to thaw-consolidation and/or ice-blocked drainage (McRoberts and Morgenstern, 1974) and artesian pressures resulting from thawing (Chandler, 1972).

The observed slope movements ranged from 9.0 to 27.0 mm/yr for slopes in the range of 4^{o} to 23^{o} while one slope had movements as large as 120 mm/yr.

The measured pore pressure ratio in the thawing slopes investigated ranged from $r_u = 0.5$ to $r_u = 1.08$.

The types of mechanisms listed will be taken into consideration in the analysis chapter (Chapter VI) as well as the range of r_u observed. Chapter IV however, deals with the laboratory testing program performed using soil samples from the Bluefish Slope.

IV LABORATORY TESTING PROGRAM

4.1 Concept of Laboratory Program

The clay affected by the shallow slope movements at Bluefish Lake was tested using standard identification tests as well as specially designed Drained Triaxial Tests with Cyclic Pore Pressure Changes at Constant Total Load (DTTCP).

The DTTCP tests were undertaken in order to investigate the effects of cyclic pore water pressure changes on the behavior of soil, particularly with respect to related deformations.

4.2 Standard Soil Tests

4.2.1 Results

Water contents, Atterberg limits, grain size distributions and X-ray diffraction tests were determined for soil identification. In addition, consolidation tests (one-dimensional and isotropic) and consolidated isotropically undrained triaxial tests (CIU) with pore pressure measurements, were used to measure geomechanical properties. A summary of these tests and their results is presented in Table 4-1. Shelby-tube sample locations as indicated by borehole numbers and depth intervals are also shown.

The moisture contents obtained for the shelby tube samples ranged from 19% to 27% while those for a block sample that was taken from Test Pit No. 1 averaged 31%.

Two grain size analyses were performed by hydrometer method according to ASTM Standard D421-58. Their results are plotted in Fig. 4-1 and show average fractions of 73% clay, 26% silt and 1% sand.

Liquid and plastic limits tests were performed according to ASTM Standard 423-66 and D424-59. For the tube samples, liquid limits ranged from 29% to 35% and the plasticity indices from 11% to 14%; for the block sample, the average liquid limit was 43% and the plasticity index was 18%. The Atterberg Limits for the soil are plotted on Casagrande's plasticity chart presented in Fig. 4-2, and indicate a low plastic clay (CL).

X-ray diffraction tests were conducted on material from the block sample in order to identify the clay mineralogy of the soil. The diffractograms from these tests are included in Appendix B, along with the procedure used for the identification. The clay mineralogy, expressed as a percentage of the clay fraction was found to be:

Illite	48%
Chlorite	25%
Kaolinite	27%
Smectite	1%

Expressed as a percentage of the total soil sample in which 73% is clay we find that 35% is Illite, 18% is Chlorite, 20% is kaolinite and there is a trace of smectite.

Two types of compression tests were undertaken on one of the shelby tube samples (BH P-2, 1.8-2.0m depth). The first type of test was a one-dimensional test using a conventional oedometer ring, while the second type was an isotropic test utilizing a triaxial cell. Consolidation tests were also performed in the context of the CIU tests as well as the DTTCP tests. All of the consolidation tests, except the first three CIU tests, and the simple (one-dimensional) oedometer test, were performed against a back pressure. The back pressure ensured that the samples were saturated and any excess air was dissolved into solution, thus ensuring accurate volume readings. Sample preparation for the isotropic compression test was the same as for the CIU tests and the DTTCP tests and is described in detail in Appendix A. The results of both types of compression tests were plotted on a V-ln σ'_v diagram, and a

$V-\sigma_v'$ diagram as shown in Fig. 4-3. The consolidation stages from these tests, including those from the CIU and DTTCP tests, are compiled in Appendix C. It is common that the isotropic consolidation values should be above the oedometer values in Fig. 4-3. The mean pressures are higher. Typical time-consolidation results from the isotropic consolidation tests and one-dimensional consolidation tests are shown on Figs. 4-4 and 4-5 respectively.

Four CIU tests with porewater pressure measurement were performed at confining pressures of 15kPa, 27kPa, 40 kPa, and 300kPa, respectively. The results of these CIU tests are summarized on Figs. 4-6, 4-7 and 4-8 as well as in Appendix C (Fig. 4-8 shows the low-stress region of Fig. 4-7 to an enlarged scale). For the series of CIU tests undertaken in this study, failure was interpreted as the points at which the stress path, when plotted in q-p'space, intersected the Hvorslev surface. Further discussion regarding the definition of failure is presented in Appendix A.

4.2.2 Discussion of Standard Soil Test Data

For the majority of the tested samples as listed in Table 3-1, the water contents were close to their respective liquid limits resulting in Liquidity Index values around unity. This indicates a soft to very soft deposit. In this state the soil may be deformed or remolded without the formation of cracks and without any change in volume.

The clay mineralogy characterized by the high count of illite, chlorite and kaolinite, indicates a soil which has been affected by little chemical weathering. This is typical for clay deposits sedimented in a cold climate. The clay is relatively inactive and not susceptible to swelling.

The compression curves for both the isotropic and the one-dimensional consolidation tests are both shown in V- σ'_v and V-ln σ'_v diagrams in Fig. 4-3. Very gentle curves with little change in curvature in the range of the expected preconsolidation pressure, can be recognized. This shape may indicate sample disturbance (Holtz and Kovacs, 1981), and can be contributed to the soft nature of the soil in the tube samples (This will be presented later in section 3.3.1). The preconsolidation pressure was estimated to be between 200 and 250 kPa. A description of the method used of determining the preconsolidation pressure can be found in Appendix A. The slopes of the normal consolidation line (λ) and of the swelling line (κ), which are also shown on Fig. 4-3, were obtained from the one-dimensional compression curve and were found to be $\lambda = 0.388$ and $\kappa = 0.044$.

The pressure range which was utilized during the isotropic compression test was not quite adequate to obtain the virgin curve portion. It appeared appropriate however, to estimate the location of the isotropic virgin curve by drawing a line through the last point of the isotropic consolidation curve parallel to the virgin curve portion obtained from the one-dimensional test (see Fig. 4-3).

The two compression tests were performed from the same shelby tube sample. Therefore, it can be assumed that the samples were almost identical and that the two tests can be well compared. In fact, for most samples, during the consolidation stages, a similar behavior was observed in the volume readings of the isotropic compression test (see Fig. 4-4). During the initial stages of consolidation, pore water was expelled, indicating a reduction in volume. At a certain stage, however, when the test was in the secondary compression stage, the sample started to take water back in, apparently indicating an increase in volume. The net changes in volume neverthless showed a volume reduction.

The most likely reason for this behavior appears to be the presence of organic gases in the samples tested. Methane gas was indicated by its typical odour and by organic inclusions (rootlets) found in several samples. Methane gas was further observed during the preliminary

DTTCP test performed without back pressure in which the sample had to be continuously deaired on a daily basis. A volume of air (or gas) up to $4cm^3$ was removed each time. It can be visualized that as consolidation proceeds, the pore water pressure decreases and gas originally dissolved in the pore water will be released at lower pressures. The resulting gas voids will be filled by water which is drawn into the sample, indicating an apparent volume increase. The net volume increase was determined as the difference between the actual final volume reading and the volume reading at time zero extrapolated from the consolidation curve. Full equilibrium was accomplished in 24 hrs. for this fissured clay.

The load-deformation curves for the CIU tests, together with the related pore pressures are presented in Fig. 4-6. A strain hardening behavior is shown for the samples tested at low stress levels (p' varying between 15 and 40kPa) while slight strain softening is evident towards the end of the the CIU test at the higher stress level (p ' = 300 kPa). This strain-hardening behavior at the low stress levels may be due to the interaction of individual peds in the clay fabric resulting in a 'granular' behavior similar to a loose sand. The strain-softening observed for the high stress level however, is typical for over-consolidated clays. The u vs ε_1 , plots for all four tests in Fig. 4.6 show that positive pore pressures were initially generated, but later became negative as the test progressed. For the test at the high stress level, positive pore pressures were generated initially which were considerably higher than for the tests at the low stress levels.

In Fig. 4-7 and 4-8, the stress paths of the test samples are plotted in a q-p' diagram. The overconsolidated strength envelope in the Hvorslev surface can be established as the tangent to the various stress paths. It was found to have a slope M = 1.25. The resulting effective strength parameters were calculated to be $\phi' = 31^{o}$ and $c' = 12$ kPa.

4.3 Drained Triaxial Tests with Cyclic Pore Pressures Changes at Constant Total Load (DTTCP test)

4.3.1 Introduction

The drained triaxial tests with cyclic pore pressure changes at constant total load (DTTCP tests) were undertaken in order to examine soil behavior due to cycling pore pressures. The concept of the test is shown schematically in Fig. 4-9. The sample was placed into a triaxial cell and consolidated anisotropically, using a dead weight system for the axial load and an air pressure system for the confining pressure. It was then subjected to a cycling pore pressure,

Δu. The term $\Delta u/\Delta u_f$ used throughout the remaining thesis, represents the change in pore pressure, $\Delta u=(-\Delta p')$ as a fraction of the total pore pressure change measured which produced failure (see Fig. 4-9). The axial strains and volumetric changes were recorded and plotted during the test, from which the radial strains were also determined and plotted.

The following sections present the procedures followed for each test and contain discussions on the sample preparation and the test procedures (which includes a brief description of the apparatus, the consolidation stage, the cyclic pore pressure changes and the application of the failure loads). Because of the quantity of results and observations made, the following chapter is devoted to presenting and discussing the test results.

4.3.2 Sample Preparation

All the soil specimens were carved from the same block sample which was collected from a depth of approximately 2.0m below the ground surface in Test Pit No. 1. Because the clay was soft, nuggetty, and contained occasional pebbles and rootlets, it was very difficult to handle, and great care had to be taken during the trimming process. Handling procedure for the trimming and sample set-up stages of testing are described in Appendix A. These procedures were followed for all the clay samples prepared for the Drained Triaxial Tests with Cyclic Pore Pressure Changes (DTTCP).

4.3.3 Test Procedure for the DTTCP Tests

4.3.3.1 Equipment Set Up

The equipment setup for the DTTCP tests is shown schematically on Fig. 4-10. The sample specimen was enclosed in two rubber membranes which were lubricated with silicone oil, and placed inside the triaxial cell which was subsequently filled with water. Constant axial loading was applied by deadweights on a hanger, sitting on the piston which passed through the top of the cell. The cell was equipped with a rotating bushing to minimize the friction between the cell top and the piston.

Compressed air was used to provide the pressure required for cell and pore pressures. The air supply lines were rerouted through a pressure container to minimize fluctuations in the air pressure supply.

Volumetric changes in the sample were measured by means of a backpressure burette. This consisted of a cylinder which was enclosed within a clear plastic chamber which could be pressurized to the level of the required sample pore pressure.

Vertical displacements of the sample top were measured by means of a dial gauge, as well as a Linear Variable Differential Transformer (LVDT). Pore pressures were measured by pressure transducers and were recorded at fifteen minute intervals by an automatic data-logger along with the vertical displacements. The volumetric readings as well as the dial gauges for displacement readings were recorded manually at 2 hour intervals during daily working hours.

The sample specimens were consolidated anisotropically at total stress conditions similar to those estimated for the field conditions. Cell and pore pressures were applied simultaneously by opening the valves connected to the cell base, while the hanger load was applied slowly to the top of the specimen by gently releasing a mechanism holding the hanger in place. Pore pressures were cycled by using two bleeding air pressure valves set to the upper and lower stress levels of the load cycles and a solenoid switch connected to a timer set to change the pressure at specified intervals.

4.3.3.2 Consolidation Stage

The samples were consolidated at stresses equivalent to the site stress levels found at depths of 1.5m, 2.0m, and 3.0m using coefficients of lateral earth pressures between 0.3 and 0.6. This range was selected because the estimated K_A is 0.3 for this soil and the estimated K_o value was 0.6. All tests were consolidated against a backpressure of 240 kPa. Durations of the consolidation stages of the tests ranged between 3840 min and 4320 min. This included some secondary consolidation. At the end of each consolidation stage, change in length and the total volume change were recorded.

4.3.3.3 Cyclic Pore Pressure Changes

After completion of the consolidation stage, the samples were subjected to cyclic pore pressure changes. These changes were selected such that they were in the same order of magnitude as the seasonal pore pressure changes which were estimated for the field conditions, and varied between 0 and 30kPa. A second criterion which was applied for choosing the magnitude of the pore pressure changes was related to the proximity of the stress points to the no-tension line on the q -p' plot shown in Fig. 4-8. This was done in order to determine if there was different soil behavior for those samples consolidated to different K_o values. Each pore pressure change was held for two hours to ensure pore water pressure equalization, even though it appeared that pore pressure equalization was practically completed within half an hour after the pore pressure change. Thus, the time required for a full cycle was four hours.

Values for cell pressure, pore pressure and vertical displacement were recorded automatically every fifteen minutes by means of a data logger, and every two hours manually during the day hours. For each test, between 60 and 100 cycles were applied, resulting in a total test duration of approximately three weeks for each test. A total of 11 DTTCP tests was completed during the testing program, plus one additional preliminary test.

4.3.3.4 Application of Failure Loads

At the end of each test series, the samples were brought to failure by increasing the pore pressure in increments of 1.0 to 2.0 kPa, allowing adequate time (2 hrs.) for pore water pressure stabilization for each increment (see Fig. 4-8). This provided additional data for failure values in the low stress no tension region. After failure, the final values of pressure, height and volume of the samples were recorded and the apparatus disassembled. The samples were visually inspected, photographed (samples B-9, B-10, B-11 and B-12) and final moisture contents were taken.

V RESULTS OF THE DTTCP TESTS

5.1 Introduction

A total of 11 DTTCP tests was completed during the testing program, in which the specimens were subjected to cycling pore pressures. For each test, between 60 and 100 cycles were applied, resulting in a duration of approximately three weeks for each test. The results obtained from these tests are presented, discussed and then summarized.

5.2 Presentation and Discussion of Test Results

Figures 5-1 to 5-7 present typical data from the DTTCP tests. The complete set of test data can be found in Appendix C. Figure 5-1 shows plots of the volume changes and the axial deformation changes versus log-time for a typical consolidation stage on sample number B-4. The same anomaly described before for the routine consolidation tests (water being apparently absorbed into the sample during the later stages of the test) was also evident during each of these tests. Consolidation was complete after one day, but was continued both for convenience and to ensure sample saturation for three days (over a weekend period). Similar plots are presented for each DTTCP test in Appendix C.

Figure 5-2 presents the change in height which was measured during cycling for a typical test (test sample B-4). Upon pore pressure increase, the sample would increase in height (dial gauge reading reducing) and when this pore pressure was released, the sample would consolidate to a height less than prior to the increase. As cycling continued, the sample reduced in height. The permanent axial deformation is shown on this figure. A large portion of the total change in height occured within the first twenty minutes of the pressure change. The permanent axial and volumetric deformations were recorded and were plotted versus the number of cycles as shown on Fig. 5-3. The complete set of plotted results can be found in Appendix C.

On Fig.5-3a and 5-3b, the permanent axial strain (ε_1) and permanent relative volumetric strains (ε_v) after each full cycle are respectively plotted versus the number of cycles for a typical test. The rate of axial strain $\dot{\varepsilon}_1$, is the fastest at the beginning of the cycling, decreases with increasing cycling, and reaches a constant rate of deformation after approximately 30 cycles. The permanent relative volumetric strain as plotted in Fig. 5-3b versus number of cycles, although very small, show a similar behaviour as the axial strains. Logarithmic plotting of ε_1 and ε_v versus log (No. cycles) do not yield a straight line.

The volumetric strains recorded during cycling (see complete set of data in Appendix C) were very small, generally less than 0.8%, but never more than 1.2%.

The curves suggest that changes in strain occur in a step-like fashion. The plots of permanent volumetric strain (ε_v) versus cycle (Fig. 5-3b) typically shows that the ε_v remains constant at a certain value for a few cycles then suddenly increases for a few cycles until again a constant value is reached for several more cycles. This sequence continues in this way throughout the test. The same step-like behavior is also evident for the axial strains (ε_1). An observation made during the testing was that as the test progressed, a step-like increase in the sample volume would result in a step-like increase behavior in the sample length. As the volume then remained constant, the sample would continue to decrease in length.

A composite plot of all tests, cycled at different $\Delta u/\Delta u_f$ values ranging between 0 and 1.0 is presented in Fig. 5-4. The smaller the ratio of pore pressure change, the smaller are the axial strains and the lower the strain rate.

For the sample which failed during cycling (test B-8), failure was very quick, thus having a very high strain rate. For those tests with intermediate ratios of $\Delta u/\Delta u_f$, the steady state strain rate falls between the two extremes shown. It can be seen that these curves resemble those from typical constant stress creep tests in which the stresses are kept constant and the axial strain is measured. These constant stress creep curves typically show a primary creep zone in which the creep rate decreases, a steady state creep zone where the creep rate remains constant and a tertiary creep zone where the creep rate increases to failure (Nelson and Thompson, 1977). The curves from this investigation include the first two zones, primary and constant rate, while no observations were made to suggest that the tertiary zone had been reached. However, it should be noted that these are not typical creep curves since displacements were not taking place at constant effective stresses.

In Fig. 5-5, radial strains, ε_3, are plotted versus the number of cycles for test sample B-9. The values of ε_3 for each cycle were determined from the permanent axial deformation and the volume changes at the end of that cycle. These were related to obtain the change in diameter using the relationship:

$$\Delta D = D - 2\sqrt{\frac{V - \Delta V}{\pi(H - \Delta H)}}$$

where: D = original sample diameter

V = original sample volume

H = original sample height

ΔD = change in sample diameter

ΔV = change in sample volume

ΔH = change in sample height.

A detailed derivation of this relationship is given in Appendix A. The radial strain ε_3 was determined by dividing the original sample diameter by this change in diameter after consolidation. The same behavior can be observed in this plot as for the measured deformations: the rate of radial strain $\dot{\varepsilon}_3$, decreases with the number of cycles and reaches a constant value at approximately 30 cycles. A complete set of plotted results can be found in Appendix C.

Two samples (B-5 and B-8) which were cycled too close to the failure line failed during the cycling. Figures 5-6 and 5-7 show the axial deformations plotted versus number of cycles for these tests. It can be observed that once failure was initiated, both samples failed in step like fashion. For sample B-8, part of this behavior, however, may be attributed to the cycling of the pore pressure because the decrease in pore pressure stabilizes the soil. A similar step-like deformation behavior had also been observed during cycling of the other tests, as mentioned, however, it was not as pronounced as in these cases. Test B-8 on Fig. 5-7 was interrupted when the load ram began to rest on a support, although once the support was lowered, it continued to fail.

The stress conditions for each test, the magnitude of the pore pressures cycles, and the rate of strains obtained from the above plots ($\dot{\varepsilon}_1$, $\dot{\varepsilon}_v$, $\dot{\varepsilon}_3$ and $\dot{\varepsilon}_s$) are summarized in Table 5-1, where $\dot{\varepsilon}_s$ is the shear strain rate and was determined from the values of $\dot{\varepsilon}_1$ and $\dot{\varepsilon}_3$ in the same test using the relationship $\dot{\varepsilon}_s = 2/3\ (\dot{\varepsilon}_1 - \dot{\varepsilon}_3)$, (see List of Symbols).

Figure 5-8 shows for sample B-4 the vertical displacements observed during the incremental pore pressure increases which were applied, subsequent to the cycling tests, until the samples failed, in a settlement versus time plot. With each pore pressure increment, the sample increased in length. As the stress conditions approached failure, the rate of increase in length decreased. Eventually the sample length decreased slowly (pt. A), until with a further pore pressure increment sudden total failure occurred. Table 5-2 summarizes the failure stresses for each DTTCP test together with the volume changes observed immediately before failure.

The results of these test series are further summarized by using the invariant effective stress q, p', V space commonly associated with critical state soil mechanics, where $q = \sigma_1' - \sigma_3'$, $p' = (\sigma_1' + 2\sigma_3')/3$, and $V = 1 + e$ (Schofield and Wroth, 1968). This method presents clearly the stress paths followed in each test and gives a proper understanding of the soil behavior. The test results are presented in this manner in Figs. 5-9, 5-10 and 5-11 and are also listed in Tables 5-1 and 5-2. Figure 5-9 presents a composite plot of the stress paths at initial cycles for each DTTCP test in a q-p' diagram. The theoretical no-tension line and the Hvorslev failure line are also shown on this plot. The proximity of each test cycle to the theoretical failure line can be recognized. The failure points line up close to the theoretical 'no tension' line, although a majority of them fall slightly to the left of the line, indicating negative σ_3' values at failure and implying a positive value of c' in this region. This indicates, according to Atkinson and Bransby (1978), that the soil can sustain tensile effective stresses. Failure point B-9 shows a high cohesion intercept, which may be related to the reinforcing effect of rootlets which were found in the sample, different from the other samples. As well Fig. 5-9 shows a plot of the failure points in V-p' space along with the estimated failure line parallel to the isotropic consolidation line obtained from the isotropic compression tests.

The stress paths during pore pressure cycling can be presented in more detail in q-p' plots and V-p' plots as shown for a typical test (B-6) in Fig. 5-10. The sample was consolidated to point A, then cycled to point B by increasing the pore pressure, Δu, then subsequently decreasing the pore pressure by Δu back to the area of pt. A. Because the total stresses were kept almost constant, the effective stresses changed only as the pore pressures changed. During each cycle, changes in volume and shape occurred due to the changes in effective stress which were not reversible. Subsequently, the sample never returned to its original shape and volume. Thus, as cycling continued, the sample decreased in height, increased in volume and accordingly increased in diameter. Therefore, because the sample diameter increased, while the axial load remained constant, the major principle stress decreased. This slight decrease in σ_1 is shown in the q-p' plot and the V-p' plot in Fig. 5-10 by the migration of points A and B at the beginning of the test to points C and D for the final cycles. The incremental pore pressure increase applied to fail the sample subsequent to cycling is indicated by pt. E. Similar stress paths are plotted for each of the DTTCP test and are presented in Appendix A.

The failure points were further plotted in a V-log p' stress space as shown in Fig. 5-11. The slope of the resulting failure lines is theoretically about the same as the slope of the isotropic plastic compression line plotted in the same stress space. Because of the scatter of the failure points in the low stress region, the failure point from the CIU test performed at a confining pressure of 300 kPa was utilized in order to establish more clearly the location of the failure line in q-log p' space.

All the samples bulged at failure and for some samples failure zones rising at approximately 55^{o} from the horizontal were indicated (For example B-3, B-5, B-6, B-7, B-8, B-9, B-10, B-11 and B-12). Total failure for all of the samples happened suddenly, mainly indicated by rapid compression after the failure stresses were exceeded. Failure for all of the tests was defined as the point at which a change in soil behavior occurred, and not by a predetermined strain. Sudden axial compression was also accompanied by an increase in volume. For the tests in which the stresses were increased to negative σ'_3 values, however, the sudden change in volumetric reading is not indicative of a corresponding increase in sample volume, as much of the measured water inflow was due to water accumulating between the membrane and the sample. In order to obtain the correct stress state of the sample at failure, the cell pressure was momentarily increased so that $\sigma'_3 = 0$, and the correct volume reading was taken.

The results from the DTTCP tests show that a constant strain rate ($\dot{\varepsilon}_1$, $\dot{\varepsilon}_3$ and $\dot{\varepsilon}_v$ and $\dot{\varepsilon}$s) is attained after a linear behavior of the sample is reached, usually around 30 cycles. The rate of deformations after 30 cycles was estimated from the slopes of the ε_1, ε_3 and ε_v plots after this point of cycling. These rates of deformations, $\dot{\varepsilon}_1$, $\dot{\varepsilon}_v$ and $\dot{\varepsilon}_3$ and $\dot{\varepsilon}_s$ are summarized in Table 5-1 and are also plotted in Figs. 5-12, 5-13, 5-14 and 5-15 versus the change of pore pressure ratio $\Delta u/\Delta u_f$, in which Δu_f is the total pore pressure required to produce failure at the theoretical failure line. These strain rates are also plotted versus $\Delta u/\Delta u_f$ in Appendix A. For all the strain-rate versus $\Delta u/\Delta u_f$ plots, an almost linear rate increase with $\Delta u/\Delta u_f$ ratio can be seen.

The relative scatter of data points in the plots of the strain rates vs $\Delta u/\Delta u_f$ may be related to the method of obtaining the slope from the strain curves in the steady state region. The strain rates were determined from the slopes of an average line drawn through the stepped portions of the curves, believed to represent the general, overall behavior of the sample. Thus the rates obtained depend very much on the selection of the slope of the average curve:

whether to take the slope along individual 'steps' or the slope of the line averaging a larger portion of the curve (see Fig. 5-3b and diagrams in Appendix C.). There is also the possibility that the steps did not reflect soil behavior, but were due to disturbances during the duration of the tests, such as power failures and careless movement around the apparatus, or to insensitivity in the instrumentation.

A value of $\Delta u/\Delta u_f$ equal to unity represents pore pressure changes up to the theoretical no-tension line and thus theoretically constitutes the limit to which the porewater pressure can be cycled without causing failure. The strain rates for the tests cycled to this limit could not be clearly defined because the samples which failed when cycled to this level, did so at different rates. This may be an indication of uncontrolled rates in this area. It was evident however that the strain rates developing during cycling increased rapidly when the stresses were cycled close to, or at the failure line. For the lower $\Delta u/\Delta u_f$ values, however, strain rates increased almost linearly with number of cycles. The best correlation was obtained for the volumetric strain rate $\dot{\varepsilon}_v$ (Fig. 5-14). Failure occurred only when the pore pressure changes reached the failure line.

It is possible that the ratio $\Delta u/\Delta u_f$ may not be the most convenient way of presenting the test results. The reason being that at different stress levels q, the same $\Delta u/\Delta u_f$ ratio is possible and different behavior may be evident. A third parameter that may take this into account is K, which more precisely indicates the stress state.

5.3 Summary of Experimental Results

The most important results from the DTTCP tests appear to be the following points:

1) During cycling of pore pressures, permanent change of volume and shape can be achieved.

2) The smaller the ratio of pore pressure change, the smaller the axial strains.

3) Deformation rates expressed in terms of strain rates increased with the number of cycles but reached a constant value after approximately 30 cycles .

4) The strain rate is dependent on the magnitude of the pore pressure changes.

5) The strain rates ($\dot{\varepsilon}_1$, $\dot{\varepsilon}_3$, $\dot{\varepsilon}_v$, $\dot{\varepsilon}_s$) increase linearly with

an increase in the ratio $\Delta u/\Delta u_f$ almost up to $\Delta u/\Delta u_f$ = 1.0

6) An abrupt change of conditions from constant rate of strain to failure is indicated at the point $\Delta u/\Delta u_f$ = 1.0.

7) Failure at low stress levels is defined by a curve slightly left of the theoretical no-tension line.

VI CORRELATION BETWEEN DTTCP TEST OBSERVATIONS AND OBSERVED MOVEMENTS IN THE FIELD

6.1 Introduction

This chapter deals with correlating the results obtained from the DTTCP test and the actual measured movements in the Bluefish Slope.

Firstly, the relationship between triaxial test conditions and plane strain field conditions is discussed to determine the corrections required for the DTTCP test results so they can be compared with the field plane strain condition.

Secondly, because the deformation characteristics obtained from the DTTCP tests were related to the pore pressures at failure, the failure conditions in the slope must also be expressed in terms of pore pressures. The pore pressures at failure are expressed as a function of depth D for the Bluefish Slope using relevant slope parameters such as slope inclination θ, angle of friction ϕ' of soil and the unit weight γ of the soil. The difference between the pore pressures at failure u_f and the lowest existing pore pressures u in the slope defines the pore pressure change Δu_f required to cause failure. The ratio $\Delta u/\Delta u_f$ is plotted versus depth and related to the strain rates observed from the DTTCP tests, where Δu is the change in pore pressure observed for a particular depth.

Thirdly, the pore pressure changes in the surficial portions of the Bluefish Slope affected by movements must be estimated. The pore pressure readings obtained in the Bluefish Slope were not measured directly in the surface zones affected by movements but in the silty sand zone at the very base of the clay deposit. Pore pressure changes in the surface zones must therefore be estimated from these readings as well as from other data reported for surficial soil layers. The estimated pore water fluctuations Δu are then used to calculate $\Delta u/\Delta u_f$ values at various depth levels below the ground surface. By relating the ratio of $\Delta u/\Delta u_f$ to the shear strain rate $\dot{\varepsilon}_s$ from the lab testing program, data are obtained which show the shear strain distribution versus the depth. Thus, soil movements can be calculated for these cyclic pore pressure values. The calculated movements are then compared to those obtained from the slope indicators installed in the slope.

6.2 Correlation Between Triaxial Test Conditions and Plane Strain Field Conditions

6.2.1 General

In this section the correlation betwen the triaxial test conditions in the DTTCP tests and the plane strain conditions assumed for the field will be discussed. Generalized stress strain relationships are presented, and then using the conditions for each case, a relationship is obtained between the strains ε_1, ε_v and ε_3 and ε_s and the pore pressure ratio $\Delta u/\Delta u_f$. The two relationships will be compared in order to determine the correction factor required to transfer the results obtained in the triaxial DTTCP tests to field conditions. Because the actual behavior of soil is non-elastic, it should be noted that the relationship derived for purely elastic behavior is not in full agreement with the results of the testing program.

The stress-strain behavior of an ideal elastic material is given by the generalized form of Hooke's Law:

$$\begin{aligned}
\delta\varepsilon_x &= [\delta\sigma_x' - \nu'\delta\sigma_y' - \nu'\delta\sigma_z']/E' \\
\delta\varepsilon_y &= [\delta\sigma_y' - \nu'\delta\sigma_x' - \nu'\delta\sigma_z']/E' \qquad (6\text{-}1) \\
\delta\varepsilon_z &= [\delta\sigma_z' - \nu'\delta\sigma_x' - \nu'\delta\sigma_y']/E'
\end{aligned}$$

where E' and ν' are the Young's Modulus and Poisson's ratio, appropriate for the stress strain correlation in terms of effective stresses. The values of E' and ν' for soils can be assumed to remain constant over small increments of stress and strain only. That is, when the stress and strain changes considered are small, and the stresses are generally clearly below failure, almost linear elastic conditions can be assumed. In this case, the above equations (6-1) can be written:

$$\begin{aligned}
\Delta\varepsilon_x &= [\Delta\sigma'_x - \nu'\Delta\sigma'_y - \nu'\Delta\sigma'_z]/E' \\
\Delta\varepsilon_y &= [\Delta\sigma'_y - \nu'\Delta\sigma'_x - \nu'\Delta\sigma'_z]/E' \qquad (6\text{-}2) \\
\Delta\varepsilon_z &= [\Delta\sigma'_z - \nu'\Delta\sigma'_x - \nu'\Delta\sigma'_y]/E'
\end{aligned}$$

In terms of effective principal stresses and strains, the equations become:

$$\begin{aligned}
\Delta\varepsilon_1 &= [\Delta\sigma_1 - \nu'\Delta\sigma'_2 - \nu'\Delta\sigma'_3]/E' \\
\Delta\varepsilon_2 &= [\Delta\sigma'_2 - \nu'\Delta\sigma'_1 - \nu'\Delta\sigma'_3]/E' \qquad (6\text{-}3) \\
\Delta\varepsilon_3 &= [\Delta\sigma'_3 - \nu'\Delta\sigma'_1 - \nu'\Delta\sigma'_2]/E'
\end{aligned}$$

6.2.2 Axial Symmetry (Triaxial Test)

For the case of axial symmetry as it applies for the triaxial test, the following conditions are valid: $\sigma'_2 = \sigma'_3$ and $\varepsilon_2 = \varepsilon_3$. Substituting these conditions into Eq. 6-3,

$$\Delta\varepsilon_1 = [\Delta\sigma'_1 - 2\nu'\Delta\sigma'_3]/E'$$

and

$$\Delta\varepsilon_2 = \Delta\varepsilon_3 = [\Delta\sigma'_3(1-\nu') - \nu'\Delta\sigma'_1]/E' \qquad (6\text{-}4)$$

For the DTTCP tests, $\Delta\sigma'_1 = \Delta\sigma'_3 = \Delta u$. Therefore, we can express the axial and radial strain changes in terms of pore pressure changes Δu:

$$\Delta\varepsilon_1 = \Delta\varepsilon_2 = \Delta\varepsilon_3 = [(1-2\nu')\Delta u]/E' \qquad (6\text{-}5)$$

and for the shear strain changes:

$$\Delta\varepsilon_3 = 0$$

6.2.3 Plane Strain

For plane strain conditions as they apply approximately for the slope in question, the lateral strain parallel to the slope ε_2 is zero; hence from Eq.6-3,

$$\Delta\varepsilon_2 = 0 = [\Delta\sigma'_2 - \nu'\Delta\sigma'_3 - \nu'\Delta\sigma'_1]/E'$$

or

$$\Delta\sigma'_2 = \nu'[\Delta\sigma'_1 + \Delta\sigma'_3] \qquad (6\text{-}6)$$

and substituting this into Eq. 6-3,

$$\Delta\varepsilon_1 = \Delta\varepsilon_3 = [\Delta\sigma_1'(1-\nu^2) - \Delta\sigma_3'(\nu' + \nu'^2)]/E' \qquad (6\text{-}7)$$

Substituting $\Delta\sigma_1' = \Delta\sigma_3' = \Delta u$ into Eq. 6-7, we get for lateral and vertical strain changes due to pore pressure changes Δu:

$$\Delta\varepsilon_1 = \varepsilon_3 = [\Delta u'(1-\nu'-2\nu'^2)]/E' \qquad (6\text{-}8)$$

and for the shear strain changes:

$$\Delta\varepsilon_3 = 0$$

6.2.4 Discussion

By comparing the stress strain conditions for plane strain and axial symmetry (Eqs. 6-5 and 6-8, respectively) it is evident that the ratio $\Delta\varepsilon_3$ (plain strain)/ $\Delta\varepsilon_3$ (triaxial) increases as ν increases for values between 0 and 0.5 (Fig. 6-1). For example, for a value of $\nu = 0$, the ratio is equal to one and for a value of $\nu = 0.25$, the principal strain at plane strain conditions will be approximately 25% larger than for the axial symmetric conditions.

For dense soils and solid granular materials such as concrete or sandstone, Poisson's ratio increases from small values of the order of 0.2 at low stress to more than 0.5 at very high stresses (Terzaghi, 1942). A value of $\nu = 0.5$ applies also for materials in which no volume changes occur, for example, for clay soils at undrained conditions. For the case of the DTTCP tests, the stress range used is very low, therefore it can be assumed that Poisson's ratio might be $\nu = 0.2$ to 0.3. Thus, for relating the plane strain field situation to the triaxial test results which were obtained from the DTTCP tests, the data will be corrected accordingly by a factor of 1.25 using the assumption that $\nu = 0.25$. This factor applies for all the strains (ε_1, ε_3 and ε_s).

6.3 Formulation of Failure Criteria for Slope at Bluefish Lake

The pore pressure at failure is obtained from a stability analysis of the slope at Bluefish Lake by using the infinite slope method with ground water flow parallel to the slope. The factor of safety Fs for the condition of limit equilibrium of a shallow slope in terms of effective stresses is:

$$F_s = \frac{c' + z\cos^2\theta(\gamma - m\gamma_w)\tan\phi'}{\gamma z \sin\theta\cos\theta} \tag{6-9}$$

where the groundwater table is at a vertical height mz above the slip surface. The total unit weight of soil is γ, and

γ_w is the unit weight of water. The slope angle is θ, and ϕ is the effective angle of internal friction of the soil and c' is the effective cohesion value for the soil. Because the cohesion in weathered soils can reasonably be assumed close to zero (Rivard and Lu, 1974), Eq. 6-9 can be written in terms of the pore pressure ratio r_u as follows;

$$F_s = \frac{(\cos^2\theta - r_u)\tan\phi'}{\sin\theta\cos\theta} \qquad (6\text{-}10)$$

where $r_u = \dfrac{u}{\sigma_v} = \dfrac{u}{\gamma z}$

For a slope inclination of 7^o and an angle of friction of 31^o in the clay, the pore pressure ratio required for failure r_{uf} for the Bluefish Slope becomes:

$$r_{uf} = \frac{u_f}{\gamma z} = 0.78 \qquad (6\text{-}11)$$

Now substitute H for Z, and $\gamma_w H_{wf}$ for u_f, where H is the depth of soil element and H_{wf} is the height of the water level at failure above the soil element. If we then assume γ_w/γ approximately equal to 0.5,

$$r_{uf} = \frac{0.5H_{wf}}{H} = 0.78 \qquad (6\text{-}12)$$

or

$$H_{wf} = 1.57H \qquad (6\text{-}12)$$

That is, the height of water above the soil element at depth H required to give an r_u value of 0.78 is a function of the depth H. Using the relationship $u_f = H_{wf} \cdot \gamma_w$, the pore pressure required for slope failure can also be expressed as a function of depth below the ground surface. Using γ_w = 9.81 kN/m^3;

$$u_f = 15.38H \qquad (6\text{-}13)$$

Thus, the change in pore pressure required to produce failure in the slope is

$$\Delta u_f = 15.38H - \gamma_w H_w \quad \text{(kPa)} \qquad (6\text{-}14)$$

where $\gamma_w H_w$ is the lowest pore pressure in the slope at the depth H.

It should be noted that this relationship was formulated for the Infinite Slope in which the seepage flow is parallel to the slope. This is in fact contrary to the thaw slope analysis criteria stated by McRoberts and Morgenstern in which the flow direction is horizontal, out of the slope. Nevertheless, in order to keep the analysis simple, the same relationship (Eq.6-14) will be used for both conditions of pore pressure changes; due to groundwater level changes and due to thawing.

For the field situation, the ratio $\Delta u/\Delta u_f$ will be expressed in terms of the range of pore pressures Δu observed in the field, and the change of pore pressure required for failure, Δu_f, calculated using Eq. 6-14. For values of $\Delta u/\Delta u_f = 1.0$, failure conditions already exist in the slope, and the soil behavior described by the DTTCP tests is not valid.

6.4 Estimate of Cyclic Pore Pressure Changes in the Field

The measurements of pore pressure fluctuations in the Bluefish Lake Slope were obtained in the sand layer at the very base of the clay deposit as presented in Chapter II, Fig. 2-6.

In the following two different sources of pore water pressure changes will be discussed; a) those due to groundwater level changes, and b) those due to thawing processes.

In some areas of the Bluefish Slope there is an indication that the deposit is either silt or a silty clay which is extensively fissured. These soil conditions would allow seepage of the groundwater from the lower sand layer to the upper zones of the clay deposit. It would seem then, that the pore pressure changes observed at the bottom of the clay deposit are approximately the same throughout the clay deposit up to the very top. This assumption is subsequently used when analyzing the fluctuations in pore pressures in the Bluefish Slope with regards to the estimated strain profile.

The groundwater variations measured near location SI-1 in the Bluefish Slope will be considered and compared to the slope indicator profile obtained at that location.

As indicated on Fig. 2-6, the piezometric elevation ground water levels at the location of SI-1 varied from a depth of 2.2m below the ground surface in June to 0.2m below the ground surface in September. It can be seen that this variation in H_w is well lower the piezometric elevation that would be required to cause failure. The pore pressure variation over the depth of the clay zone at this location is shown on Fig. 6-2, where line AB shows the pore pressure distribution for the lowest groundwater level and line CD shows the pore pressure distribution for the highest groundwater level. The pore pressure change Δu is the difference between the two lines.

For thaw-effects; pore pressures at very shallow depth have been previously observed in thawing silt and clay slopes by McRoberts and Morgenstern (1974a) and by Chandler (1972). The reported data are plotted in Fig. 6-3 in terms of head of water above the piezometer tip versus depth of piezometer tip. In terms of pore pressure ratio r_u, the r_u values vary from 0.5 to 1.08 in which $r_u = 0.5$ represents a water level at ground surface. Relating these data to the thawing surface zones of the Bluefish Slope, it can be stated that r_u is definitely less than the pore pressure ratio $r_{u_f} = 0.78$ which is required to cause failure, since no slope failure has occurred.

It is doubtful that the high thaw pore pressures observed in the upper 1.0m by McRoberts and Morgenstern and Chandler, are also valid for greater depths; mainly because thaw at greater depths occurs more slowly, permitting the dissipation of pore pressures as they develop.

For the thaw analysis, a thaw pore pressure distribution to a depth of 2m will be used as shown on Fig. 6-4(a). The pore pressure change Δu is obtained by relating these pore pressures to zero as the minimum value. Zero pore pressures can be accepted as a lower bound as zero pore pressures are likely to occur at freezing conditions for fine-grained soils at low stress levels (McRoberts and Morgenstern, 1974b).

Maximum pore pressure changes due to thaw and due to water pressure at the base of the clay zone do not occur simultaneously, the first probably in early June and the second in late August. Thus, both cases will be considered separately. For each case the cycle length is assumed equal to one year.

6.5 Correlating Pore Pressure Changes to Strain Rate

The possible deformation profiles for the slope will be determined from the above pore pressure changes due to the variation in ground water level and subsequently will be compared to the deformation profile obtained from the slope indicator at the location of SI-1. In order to make the correlation, it is assumed that the slope is at a plane strain condition in which downhill lateral stress release is occurring - enabling downhill movements to take place. It is also assumed that cycling of the porewater pressures has been an on-going process and thus the lateral strain rates determined from the DTTCP tests can be utilized in this correlation, which implies that the lateral strains are continuing at a constant rate with continued pore pressure cycling.

The effect of the pore pressure fluctuation at the location of SI-1 (shown in Fig. 6-2a) on the shear strain with depth, is shown in the same figure, by plotting ε_s and $\Delta u/\Delta u_f$ versus depth using Eq. 6-14 for the determination of Δu_f ,and recalling the relationship obtained between $\dot{\varepsilon}_s$ and $\Delta u/\Delta u_f$ from Fig. 5-15 in Chapter V. The shear strain rate ε_s, can be converted to shear strain, ε_s, by multiplying $\dot{\varepsilon}_s$ by one cycle.

Fig. 6-5 shows the relationship between pure shear strain ε_{zx} (equivalent to ε_s) and engineers shear strain γ_{zx}. From Fig. 6-5(a) we can see that γ_{zx} is the change in angle between two fibres in the x:z plane which were originally at right angles to one another and is equal to

$$\gamma_{zx} = \lim_{\delta z \to 0} \frac{\delta x}{\delta z} \tag{6-15}$$

By rotating the strained element in Fig. 6-5(b) counterclockwise about O', the element in Fig. 6-5(c) is obtained similar to Fig. 6-5(a). Comparing Figures (a) and (b), it is evident that $\gamma_{zx} = 2\varepsilon_{zx}$, or in other words, engineers' shear strain is simply twice the pure shear strain. From Fig. 6-5(a), it can be seen that for any element of height Δz, the displacement

$$\Delta x = \gamma_{zx} \cdot \Delta z \tag{6-16}$$

but

$$\gamma_{zx} = 2\varepsilon_{zx} \tag{6-17}$$

therefore,

$$\Delta x = 2\varepsilon_{zx} \cdot \Delta z$$

or with

$$\varepsilon_{zx} = \varepsilon_s \quad : \quad \Delta x = 2\varepsilon_s \cdot \Delta z \qquad (6\text{-}18)$$

Therefore, in order to obtain the horizontal displacements for layer of thickness Δz, Eq. 6-18 is utilized. For a layer of soil of greater thickness, such as in Fig. 6-2 for location SI-1, an infinite number of layers must be taken, and the displacement of each summed up. For example, the shear strain profile in Fig. 6-2(b) must be integrated from the bottom up in order to obtain the displacement profile shown in Fig. 6-2(c).

A similar shear strain profile and displacement profile can be constructed for the deformations due to pore pressure changes due to thaw, using the pore pressure distribution shown in Fig. 6-4(a). These ε_s and Δx profiles are shown in Figs. 6-4(b) and (c) to a depth of 2.0m.

The individual displacement profiles as shown in a composite plot in Fig. 6-6(a) were added together in Fig. 6-6(b) to give the combined displacement profile for the two conditions.

6.6 Discussion

The displacement profile due to the cycling pore pressures related to the water pressure in the sand layer shown in Fig. 6-2(c) indicates a similar shape as the slope indicator profiles measured in the bluefish Slope (Chapter II) and those reported by Williams (1966) as presented in Chapter III. From Fig. 6-2(c) it can also be seen that the maximum surface movements are approximately 0.45 mm as estimated for one cycle, assumed to be over a one-year period.

The displacement profile shown in Fig. 6-4(c) due to pore pressure cycles related to thaw also shows a similar shaped curve as described above, with maximum surface displacements in the order of 0.2 mm for one cycle assumed to be over a one-year period.

The displacement profile shown in Fig. 6-6(b) again represents the sum of the two sets of data indicating a similar shape as before with maximum total surface displacements for approximately 0.6 mm over a one year period.

When comparing to the slope indicator profile for installation SI-1 shown in Fig. 2-8, it can be seen that the maximum displacement measured is 22 mm for a one year period and is thus considerably greater than the predicted maximum displacement of 0.6 mm. The discrepancies between the calculated and the measured displacements over the one-year period may be the result of deficiencies in the assumptions used for the analysis.

Firstly, only one cycle was assumed to occur within a one year time period for each of the conditions the cycling pore pressure related to the water pressure in the sand layer and the pore pressure changes due to thaw. It may be possible that more than one cycle for each condition can occur in one year.

Secondly, for the determination of pore pressures to failure an infinite slope analysis was used with flow parallel to the slope even though the actual flow direction of the porewater may be horizontal out of the slope as suggested by McRoberts and Morgenstern (1974) for thaw slope.

Thirdly, it is possible that the range of pore pressures utilized at location SI-1, related to the water pressure in the sand layer may not truly represent actual field conditions. It may be that the maximum height of water is greater than those recorded, as well, the water pressure may fall lower than the minimum value measured or assumed. This would have a significant affect on the shear strain profile, especially at the shallower depths, and subsequently on the displacement profile.

Fourthly, other mechanisms are at work which cause further displacements, such as frost-creep described by Washburn (1973). From the slope indicator profiles measured at the Bluefish Slope, it is evident that a majority of the displacements occurred between the October 1984 to June 1985 time period. It is possible that some of the displacements are a result of the slope indicator casing 'setting', however, this can only be verified by further monitoring to establish a more consistent data base for the slope movements. It was also observed during the June 1985 readings of the slope indicators at the Bluefish Slope that the casings had experienced heaving of up to 3 cm during the time interval mentioned above, which would result in a horizontal deformation of 4 mm.

Despite the discrepancies, it can be seen that the methods used to estimate the displacment profiles does produce profiles similar in shape at least to the actual field displacments.

VII CONCLUSIONS AND SUGGESTIONS FOR FURTHER RESEARCH

7.1 Conclusions

The following conclusions can be drawn from this study:

1) Permanent changes in volume and shape are experienced in clay samples during cyclic pore pressure changes.

2) Deformation rates expressed in terms of strain rates/cycles decrease initally with the number of cycles but reach approximately constant values in the range 30-80 cycles.

3) The constant strain rate reached in each DTTCP test is dependent on the magnitude of the cyclic pore pressure changes.

4) The strain rates ($\dot{\varepsilon}_1$, $\dot{\varepsilon}_3$, $\dot{\varepsilon}_v$, and $\dot{\varepsilon}_s$) increase linearly with an increase in $\Delta u/\Delta u_f$ almost up to $\Delta u/\Delta u_f = 1.0$, where Δu is the magnitude of the cyclic pore pressure changes; Δu_f is the magnitude of the pore pressures required to obtain failure.

5) An abrupt change of conditions from a constant rate of strain to failure is indicated at the point $\Delta u/\Delta u_f = 1.0$

6) Failure at low stress levels is represented by a failure line close to the theoretical no-tension line but it does indicate some cohesion (c' = 12 kPa)

7) Observations of a slope exhibiting shallow soil movements shows movement to a depth of approximately 2m, with no clearly defined failure zone. The absolute displacement of the upper layers is greater than that of the lower layers and the movements increase from the lower layers to the upper layers at an increasing rate.

8) Correlations between the laboratory test results and the field soil behavior show that the displacements pattern can be predicted from the cyclic pore pressure changes. The magnitude of displacements depends on the number of cycles, the surface zone is exposed to.

9) The new analysis underpredicts the downslope movements. The magnitude of the field displacements is much larger than those predicted using this analysis.

7.2 Suggestions for Further Research

The DTTCP test results show that a constant rate of strain is reached after approximately 30 cycles, and remain unchanged until about 80 cycles. Further research is suggested for a larger range of cycles in order to find out if the strain rates remain constant. Further research is also recommended using a similar laboratory testing program in order to enlarge the data base for this type of soil testing.

The failure points in the low stress range indicated a small cohesion intercept (c' =12 kpa). It is recommended to expand the testing program for low stress ranges in order to define more clearly the low-stress failure envelope.

Different soil types which may be subject to cyclic pore pressures should be investigated in a similar testing program in order to determine if the behavior in other soils is similar to the behavior found for the Bluefish clay.

The field program should be expanded in order to obtain a broader data base for shallow slope movements, over a longer time period, along with continuous measurements of the field pore pressures at these shallow depths. This is important to determine the number and magnitude of pore pressure cycles occurring throughout the year.

LIST OF REFERENCES

Andersland, O.B. and Anderson, D.M., 1978. Geotechnical Engineering for Cold Regions. McGraw-Hill Inc., U.S.A.

Aspler, L.G., 1984. Surficial Geology, Permafrost and Related Engineering Problems, Yellowknife, N.W.T. Internal Report, D.I.A.N.D., Geology Office, Yellowknife, N.W.T., pp. 119-135.

Atkinson, J.H. and Bransby, P.L., 1978. The Mechanics of Soils - An Introduction to Critical State Soil Mechanics. McGraw-Hill, London.

Berre, T., 1983. Triaxial Testing at the Norwegian Geotechnical Institute. Norwegian Geotechnical Institute Publication, Vol. 81, No. 95936, pp. 1-17.

Bishop, A.W. and Henkel, D.J., 1962. The Measurement of Soil Properties in the Triaxial Test. Edward Arnold, London, 2nd edition.

Bloom, A.L., 1978. Geomorphology - A Systematic Analysis of Late Cenozoic Landforms. Prentice-Hall, Inc., New Jersey.

Budynas, R.G., 1977. Advanced Strength and Applied Stress Analysis. McGraw-Hill, New York.

Carson, M.A. and Kirkby, M.J., 1972. Hillslope Form and Process. Cambridge University Press, London, England.

Chandler, R.J., 1972. Periglacial Mudslides in Vestspitsbergen and Their Bearing on the Origins of Fossil 'Solifluction' Shears in Low Angled Clay Slopes. Q.J Engineering Geol., Vol. 5, pp. 223-241.

Chandler, R.J. and Pachakis, M., 1973. Long-Term Failure of a Bank on a Solifluction Sheet. Eighth International Conference on S.M.F.E., Moscow, Vol. 2.2, pp. 45-41.

Eigenbrod, K.D., 1984. Personal Communication.

Graham, J., Pinkney, R.B., Lew, K.V. and Trainor, P.G.S., 1982. Curve-Fitting and Laboratory Data. Canadian Geotechnical Journal, Vol. 19, pp. 201-205.

Holtz, R.D. and Kovacs, W.D., 1981. An Introduction to Geotechnical Engineering. Prentice-Hall, New Jersey.

Hutchinson, J.N., 1974. Periglacial Solifluxion: An Approximate Mechanism for Clayey Soils. Geotechnique 24, pp. 438-443.

Kojan, E., 1967. Mechanics and Rates of Natural Soil Creep. 5th Annual Eng. Geol. and Soils Eng. Symposium, Pocatello, Idaho, pp. 233-253.

McRoberts, E.C. and Morgenstern, N.R., 1974. The Stability of Thawing Slopes. Canadian Geotechnical Journal, Vol. 11, No. 4, pp. 447-469.

McRoberts, E.C. and Morgenstern, N.R. 1974. Pore Water Expulsion During Freezing. Canadian Geotechnical Journal, Vol. 12, pp. 130-138.

Mitchell, R.J. and Eden, W.J., 1972. Measured Movements of Clay Slopes in the Ottawa Area. Canadian Journal of Earth Sciences, Vol. 9, pp. 1001-1013.

Schofield, A.N. and Wroth, C.P., 1968. Critical State Soil Mechanics, McGraw-Hill, London.

Skempton, A.W., and DeLory, F.A., 1957. Stability of Natural Slopes in London Clay. Forth International Conference on S.M. & F.E., London, England, Vol. 2, pp. 378-381.

Tavenas, F. and Leroueil, S., 1981. Creep and Failure of Slopes in Clays. Canadian Geotechnical Journal, Vol. 18, pp. 106-120.

Terzaghi, K. and Peck, R.B., 1968. Soil Mechanics in Engineering Practice. John Wiley and Sons, Inc., New York, 2nd edition.

Terzaghi, K., 1942. Theoretical Soil Mechanics. John Wiley and Sons, New York.

Washburn,A.L., 1973. Periglacial Processes and Environments, St. Martin's Press, New York, pp. 170-191.

Williams, P.J., 1966. Downslope Soil Movement at a Sub-Arctic Location with Regard to Variations with Depth. Canadian Geotechnical Journal, Vol. 8, No. 4, pp. 191-203.

Yen, B.C.Y., 1969. Stability of Slopes Undergoing Creep Deformation. Journal of the Soil Mech. and Foundations Div., Proc. of ASCE, pp. 1075-1096.

BOREHOLE NUMBER	DEPTH INTERVAL	MOIST. CONT.	BULK DENS.	ATTERBERG LIMITS			GRAIN SIZE DISTRIBUTION				SOIL DESCRIPTION
				W_L	WP	IP	CLAY	SILT	SAND	GRAV	
	metres	%	Mg/m	%	%	%	%	%	%	%	
STP-2	1.3 - 1.6		2.02	33	22	11					CIU-2
	1.3 - 1.6	19		35	21	14					CL - CLAY
	1.3 - 1.6	24	2.03	34	20	14					CIU-1 CL - CLAY
	1.85	27		29	18	11					CL - CLAY
	1.85	27									
	2.0										
SI-2	1.5 - 1.8	27		27	20	7					ML - SILT
	1.5 - 1.8	20									
	1.8 - 2.0	26		22	N/P						
	1.85	27		32	18	14					CIU-4 CL - CLAY
	1.85			35	21	14					CIU-4 limits on clay fraction only
P-2	1.8 - 2.0										
	2.4										
PIT 1	1.8	32		43	25	18	75	23	2	tr.	35% Illite,18% Chlorite,
		32					70	29	1		20% Kaolinite,tr.Smectite
		31									
		31									
		30									
		32									
		32									
		31									
		31									
		32									

TABLE 4-1 SUMMARY OF STANDARD SOIL TESTS

TABLE 5-1 SUMMARY OF DTTCP TESTS

TEST	σ_{1c} (kPa)	σ_{3c} (kPa)	k_{cons}	q (kPa)	p' (kPa)	Δu (kPa)	Δu_f (kPa)	$\Delta u/\Delta u_f$	$\dot{\varepsilon}_1$ (cycle^{-1})	$\dot{\varepsilon}_3$ (cycle^{-1})	$\dot{\varepsilon}_v$ (cycle^{-1})	$\dot{\varepsilon}_s$ (cycle^{-1})
B-2*	48.0	28.6	0.60	19.4	35.1	15.0	28.6	0.52	0.5×10^{-5}	-8.04×10^{-5}	-15.83×10^{-5}	5.69×10^{-5}
B-3	48.0	28.6	0.60	19.4	35.1	18.7	30.6	0.61	1.09×10^{-5}	-3.57×10^{-5}	-6.70×10^{-5}	3.11×10^{-5}
B-4	48.0	28.6	0.60	19.4	35.1	22.9	31.7	0.72	1.48×10^{-5}	-0.86×10^{-5}	-0.0	1.56×10^{-5}
B-5	38.2	10.1	0.26	28.1	19.5	10.1	10.8	0.94	1.77×10^{-5}	-7.27×10^{-5}	-9.84×10^{-5}	6.03×10^{-5}
B-6	62.0	20.7	0.33	41.3	34.5	10.5	20.3	0.52	0.70×10^{-5}	-3.80×10^{-5}	-5.10×10^{-5}	3.00×10^{-5}
B-7	52.2	26.0	0.50	26.2	34.7	16.7	28.0	0.60	1.00×10^{-5}	-4.44×10^{-5}	-7.40×10^{-5}	3.63×10^{-5}
B-8	59.2	16.8	0.28	42.4	30.9	16.7	17.0	0.98	-	-.150000	-	-
B-9	30.4	18.3	0.60	12.1	22.3	16.7	22.7	0.74	0.49×10^{-5}	-3.33×10^{-5}	-4.90×10^{-5}	2.55×10^{-5}
B-10	44.9	18.0	0.40	26.9	27.0	5.8	19.6	0.31	0.80×10^{-5}	-1.40×10^{-5}	-2.50×10^{-5}	1.45×10^{-5}
B-11	34.5	14.5	0.42	20.0	21.2	5.8	16.7	0.35	1.30×10^{-5}	-2.69×10^{-5}	-4.50×10^{-5}	2.66×10^{-5}
B-12	59.6	35.0	0.58	24.6	43.2	33.0	36.8	0.90	3.30×10^{-5}	-6.20×10^{-5}	-10.0×10^{-5}	6.33×10^{-5}

* note: Test B-2 was a preliminary test and these results are subsequently not used

TABLE 5-2 CONDITIONS AT FAILURE FOR DTTCP TESTS

TEST NO.	σ_{1f} (kPa)	σ_{3f} (kPa)	u_f (kPa)	p'_f (kPa)	q'_f (kPa)	Δv_f (cm^3)	V_f
B-2	-	-	-	-	-	-	-
B-3	288.1	269.1	270.9	4.5	19.0	2.7	1.842
B-4	287.1	269.1	271.7	3.4	18.0	4.0	1.928
B-5	277.6	251.4	251.4	8.7	26.2	1.9	1.878
B-6	301.6	261.7	260.8	14.2	39.9	2.0	1.883
B-7	299.2	276.0	277.0	6.7	23.2	3.0	1.887
B-8	297.2	255.8	255.7	13.9	41.4	1.1	1.840
B-9	269.1	257.3	261.6	-0.4	11.8	1.9	1.850
B-10	284.2	257.5	258.0	8.4	26.7	1.1	1.850
B-11	273.6	254.0	256.0	4.5	19.6	1.45	1.877
B-12	298.1	275.0	276.3	6.4	23.1	3.10	1.899

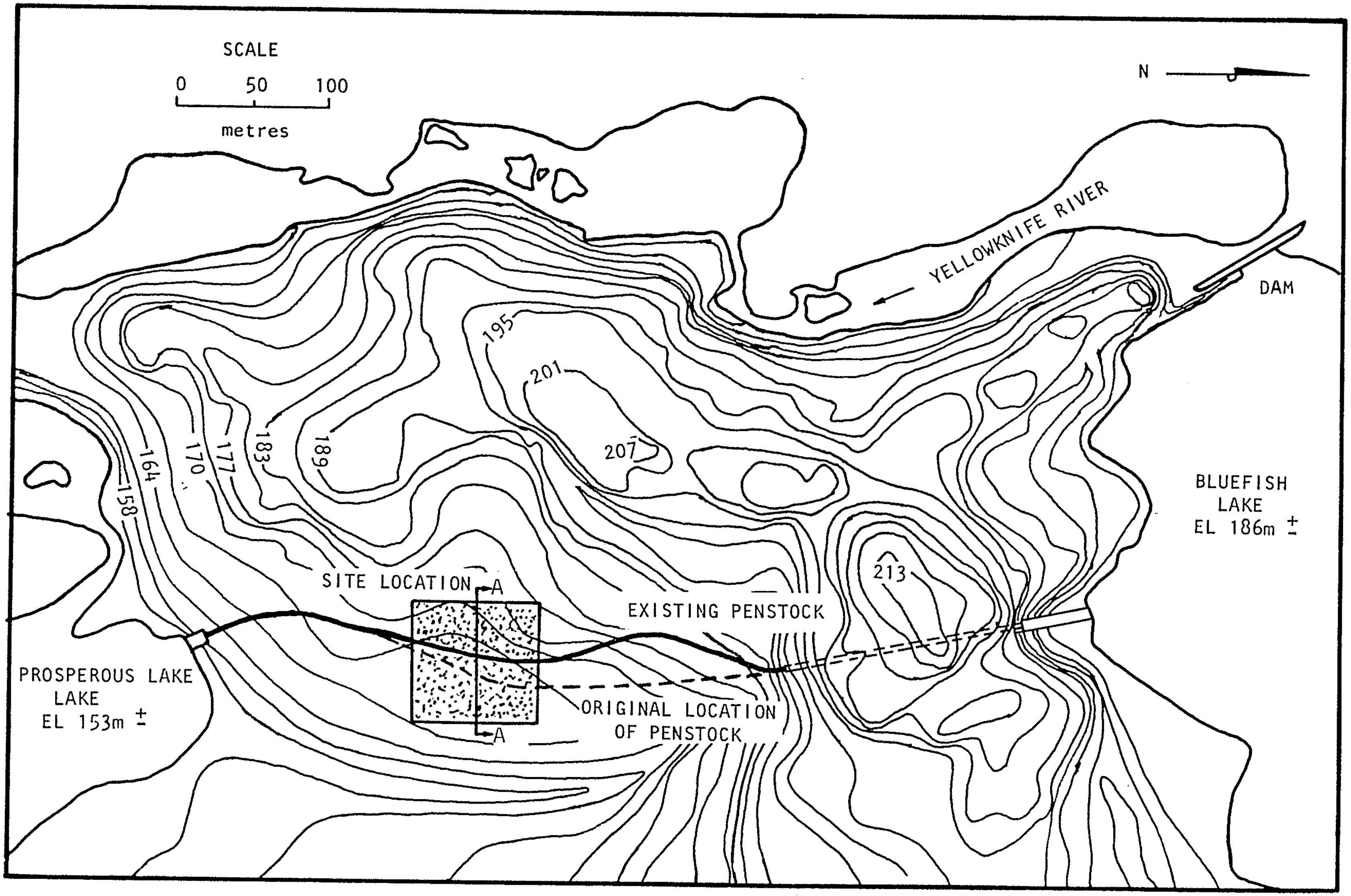

FIG.2-1 SITE LOCATION

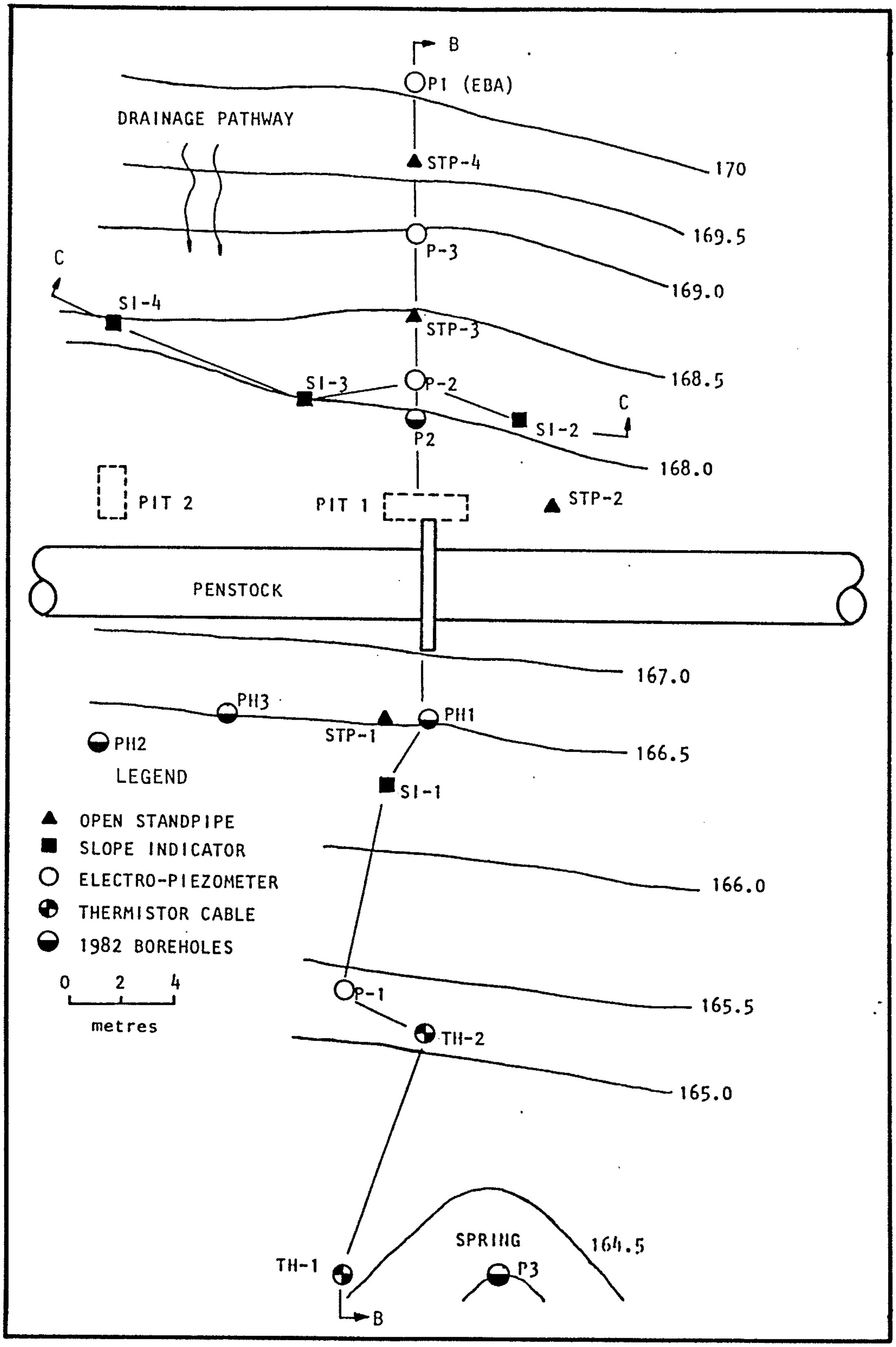

FIG. 2-2 SITE LAYOUT

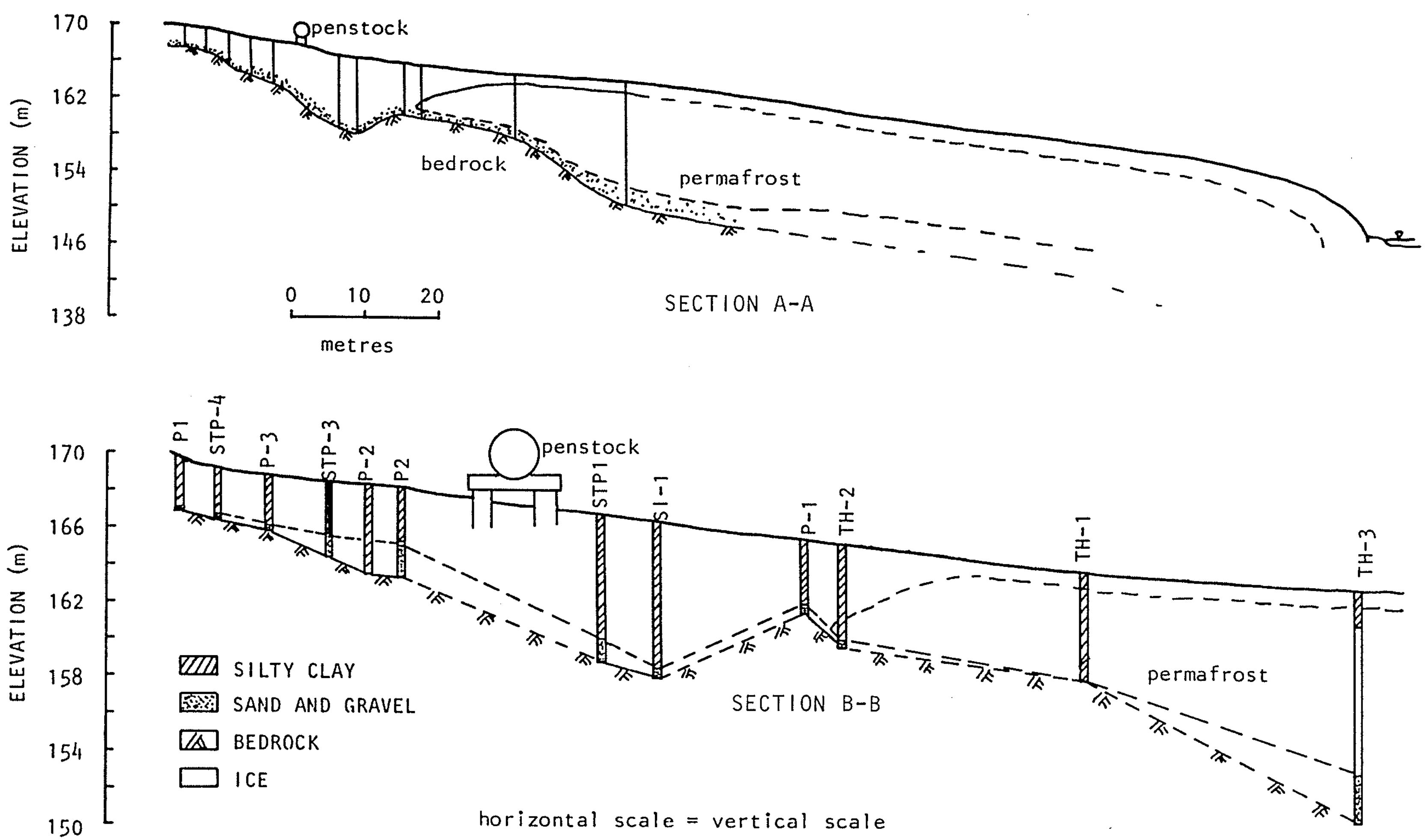

FIG. 2-3 SLOPE PROFILES FOR BLUEFISH SITE

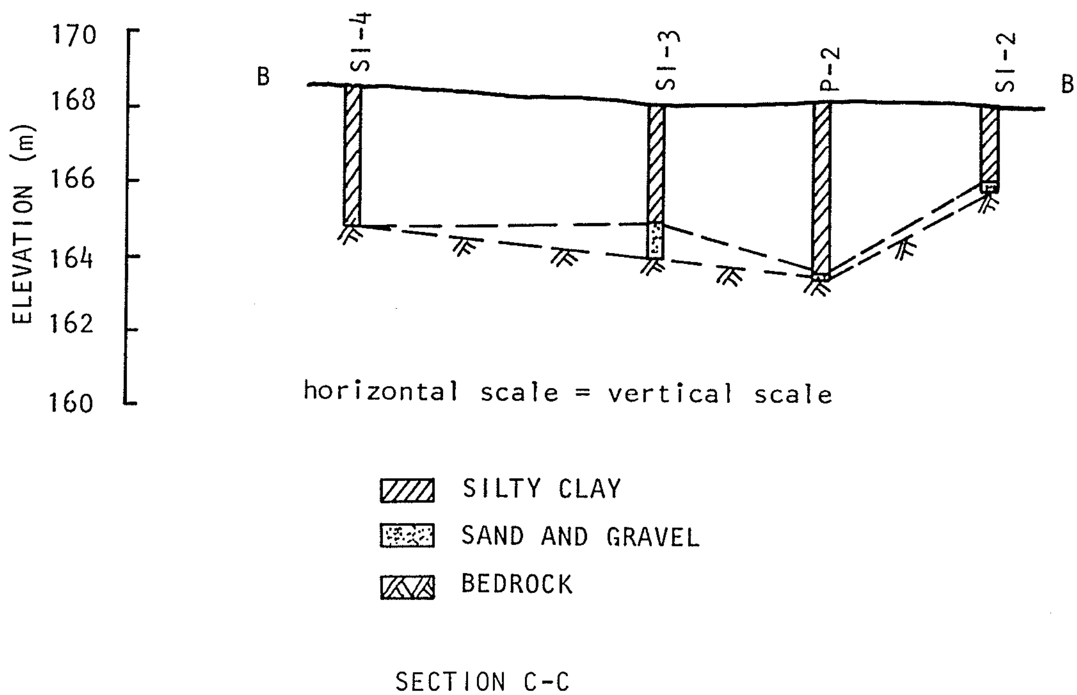

FIG. 2-4 SECTION C-C FOR BLUEFISH SLOPE

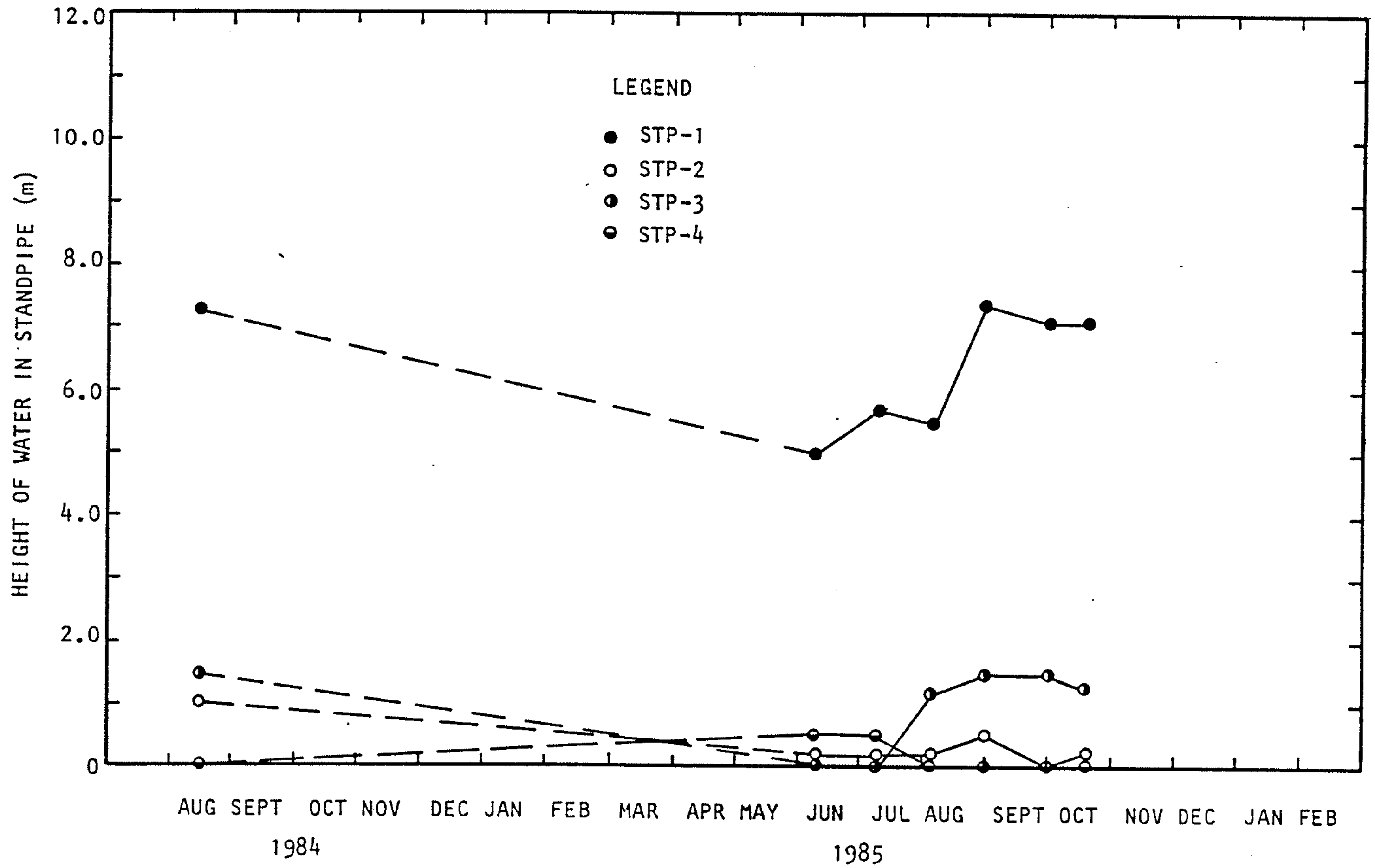

FIG. 2-5 HEIGHT OF WATER ABOVE STANDPIPE TIPS
VERSUS TIME OF YEAR

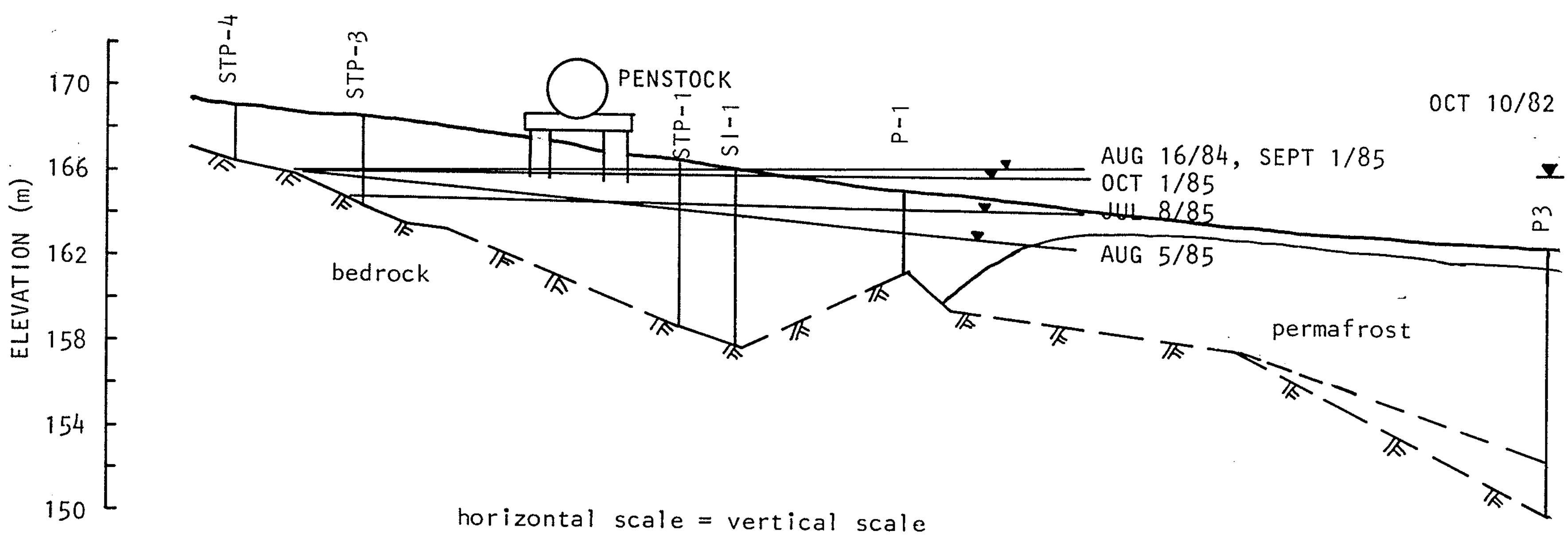

FIG. 2-6 PIEZOMETRIC VARIATION OF SAND AQUIFER

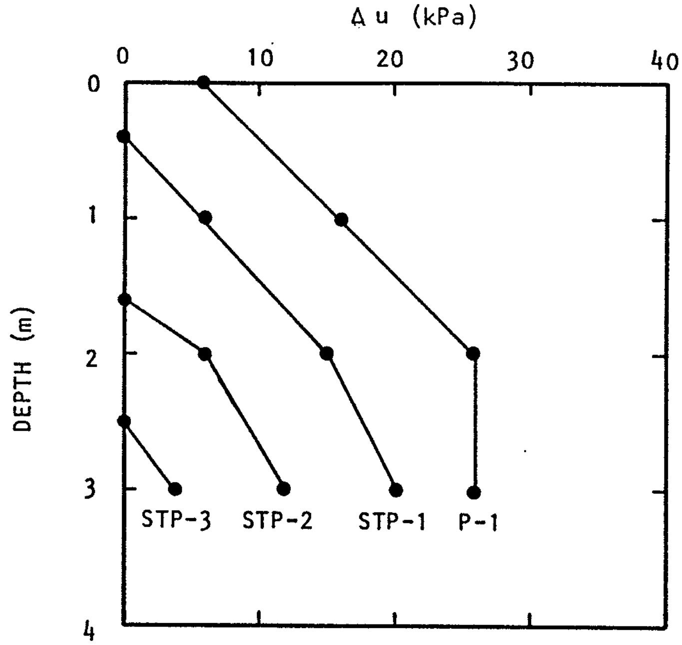

(a)

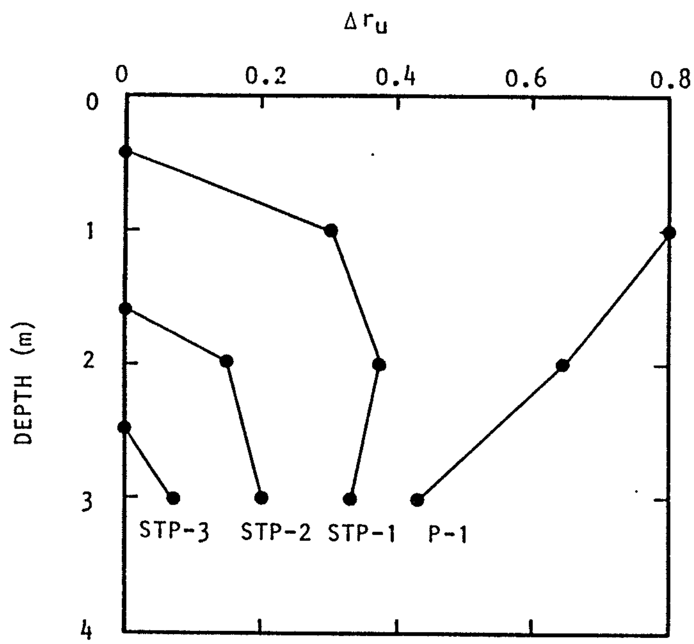

(b)

FIG. 2-7 PORE PRESSURE VARIATION VERSUS DEPTH FOR BLUEFISH SLOPE

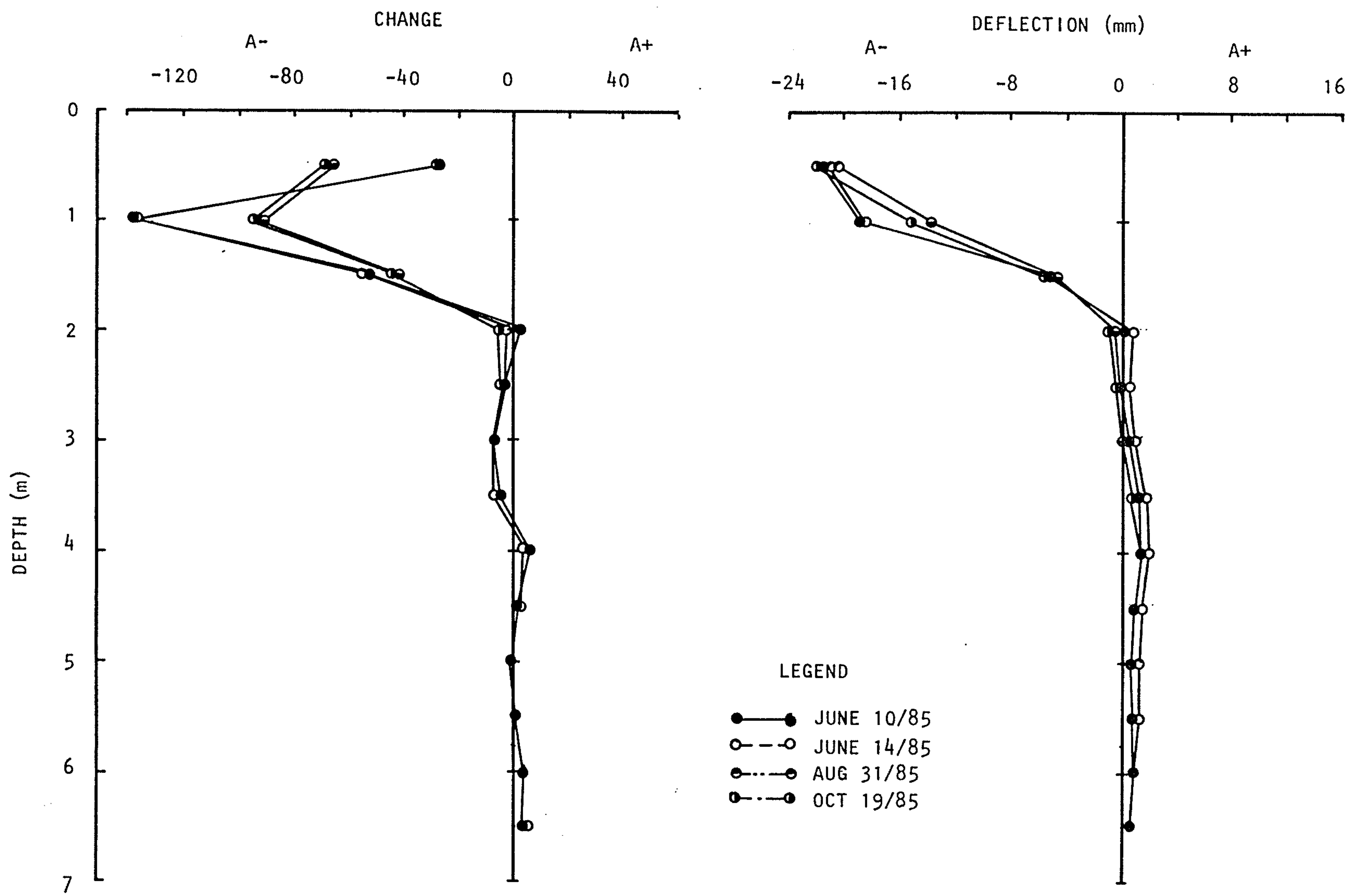

FIG. 2-8 SLOPE INDICATOR READINGS FOR SI-1

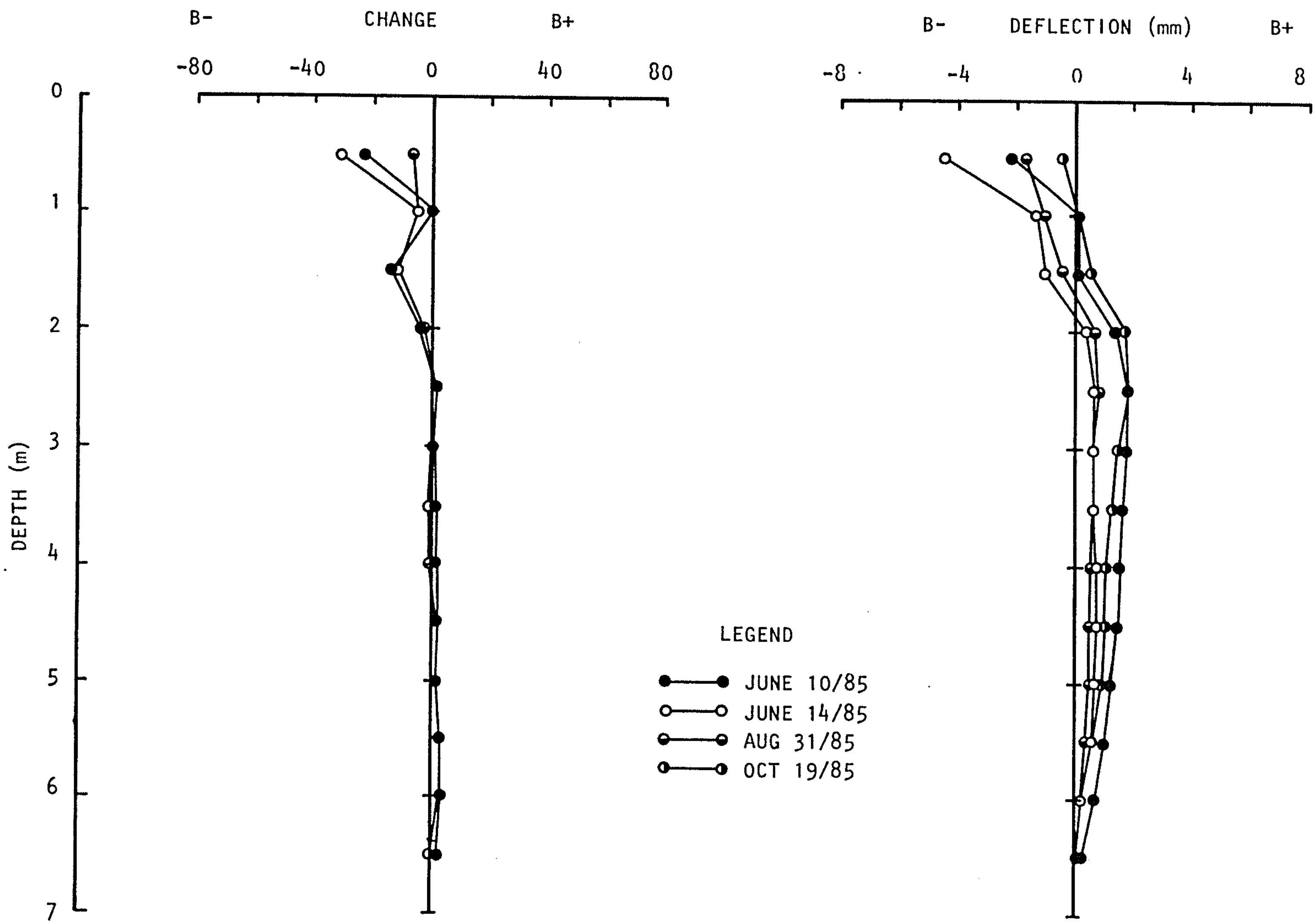

FIG. 2-8 (cont'd) SLOPE INDICATOR READINGS FOR SI-1

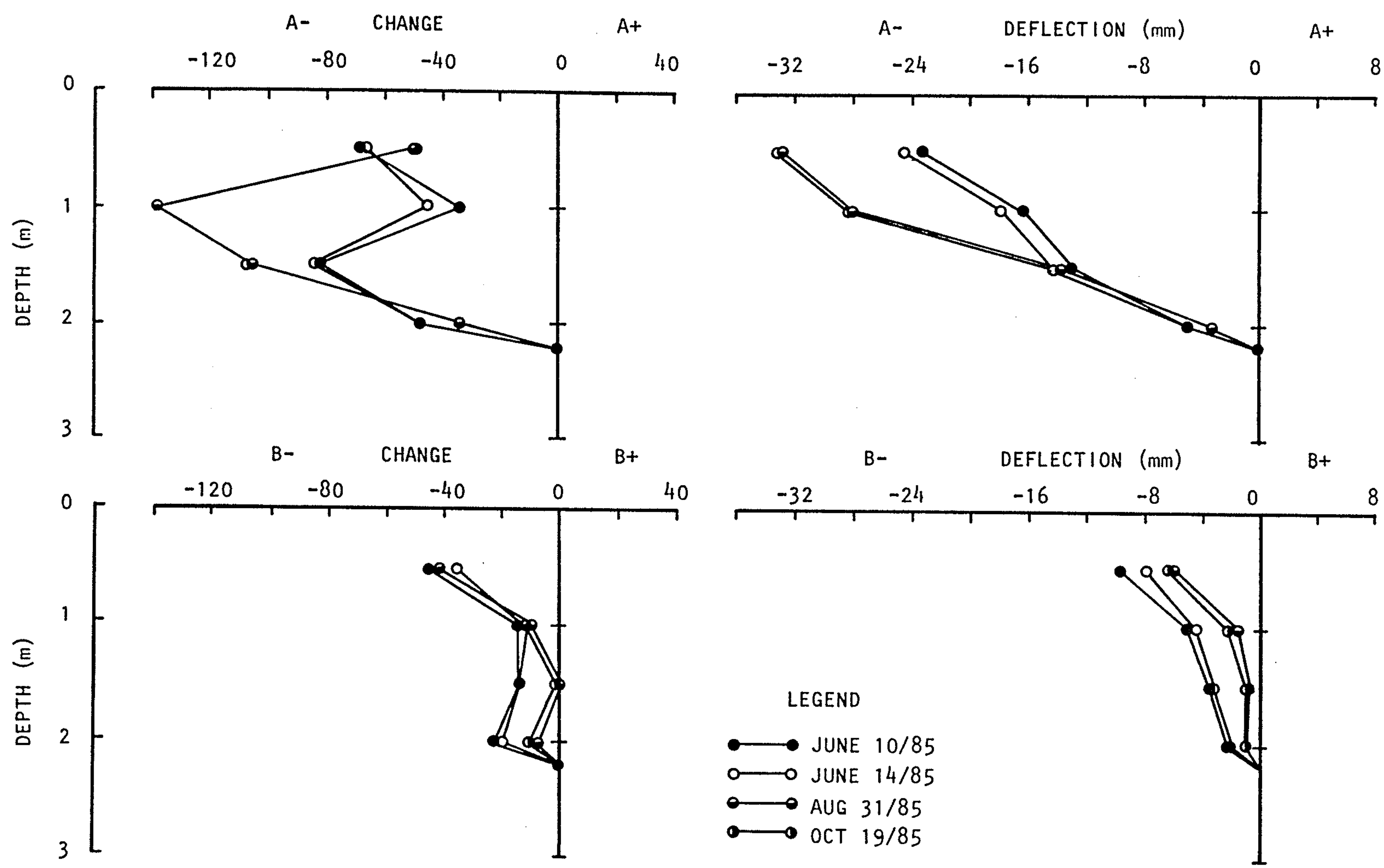

FIG. 2-9 SLOPE INDICATOR READINGS FOR SI-2

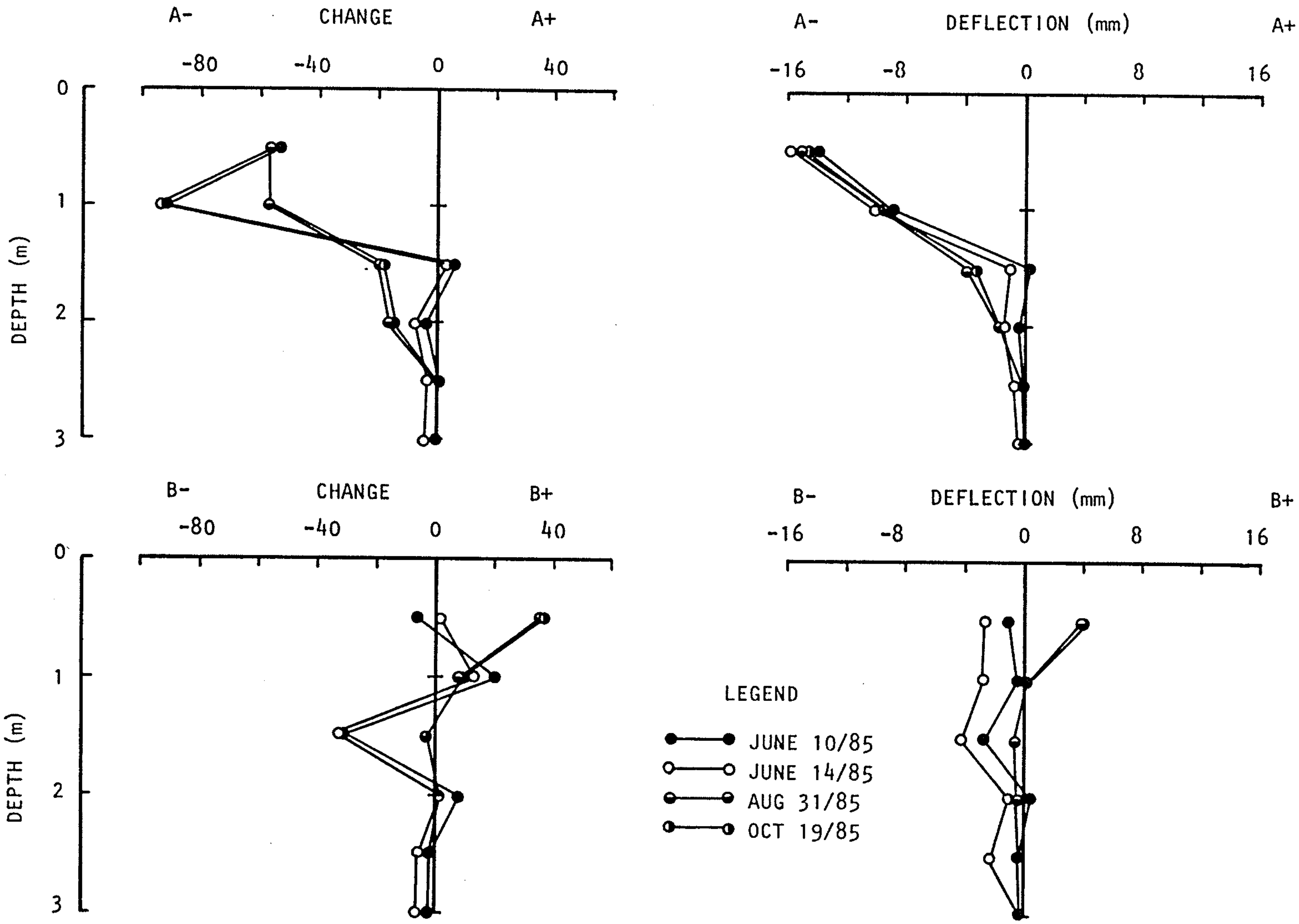

FIG. 2-10 SLOPE INDICATOR READINGS FOR SI-3

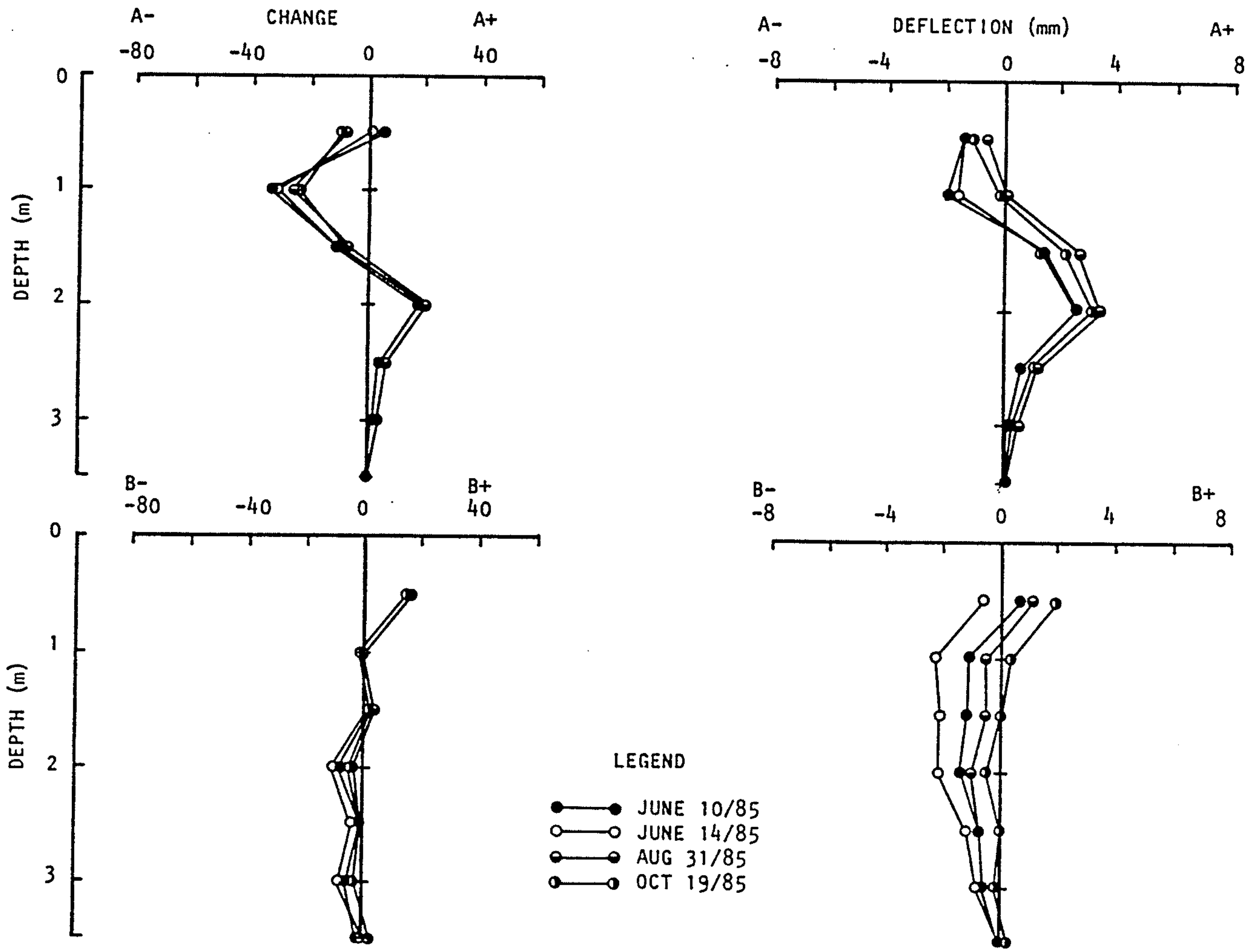

FIG. 2-11 SLOPE INDICATOR READINS FOR SI-4

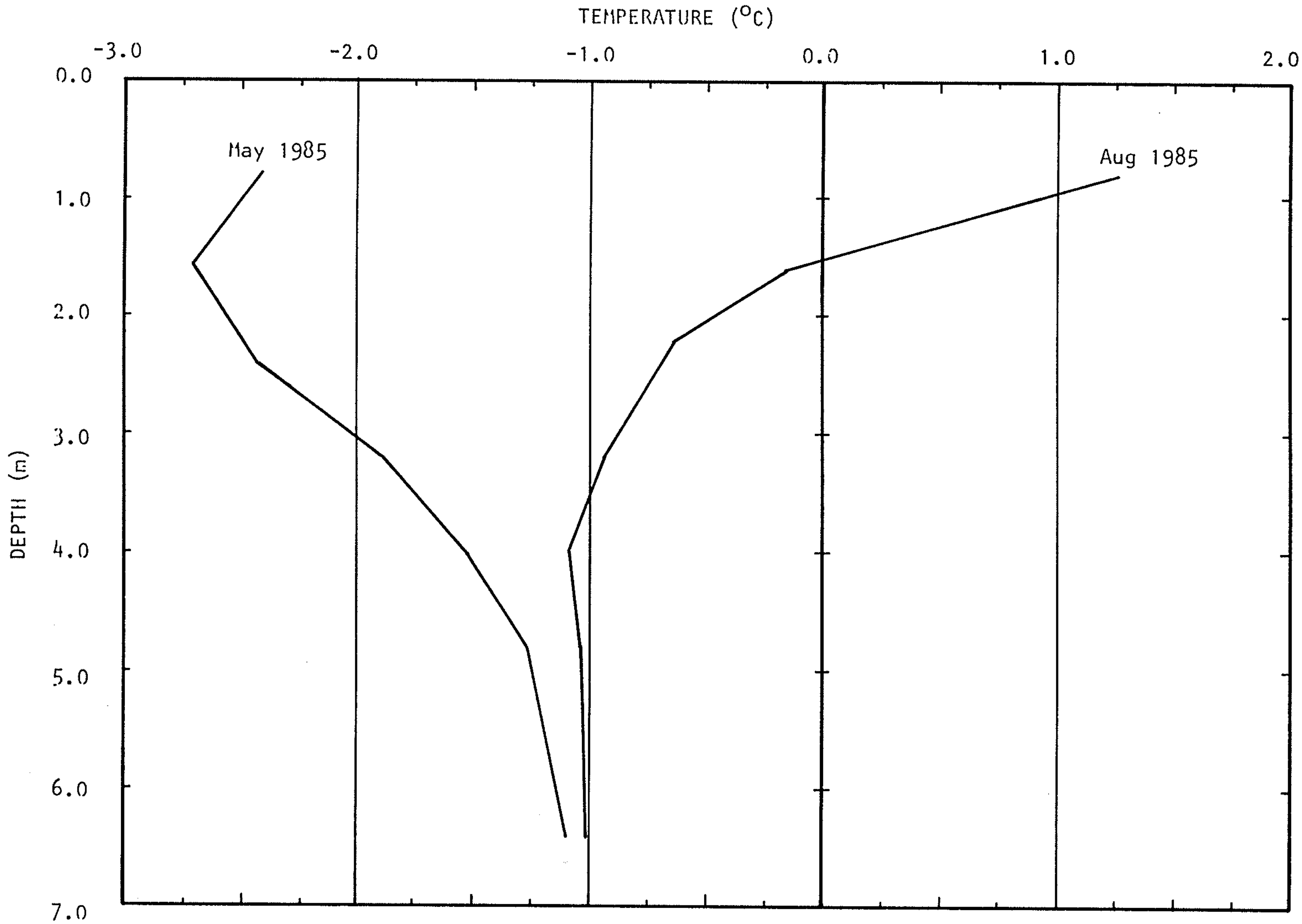

FIG. 2-12 GROUND TEMPERATURE EXTREMES FOR TH-1

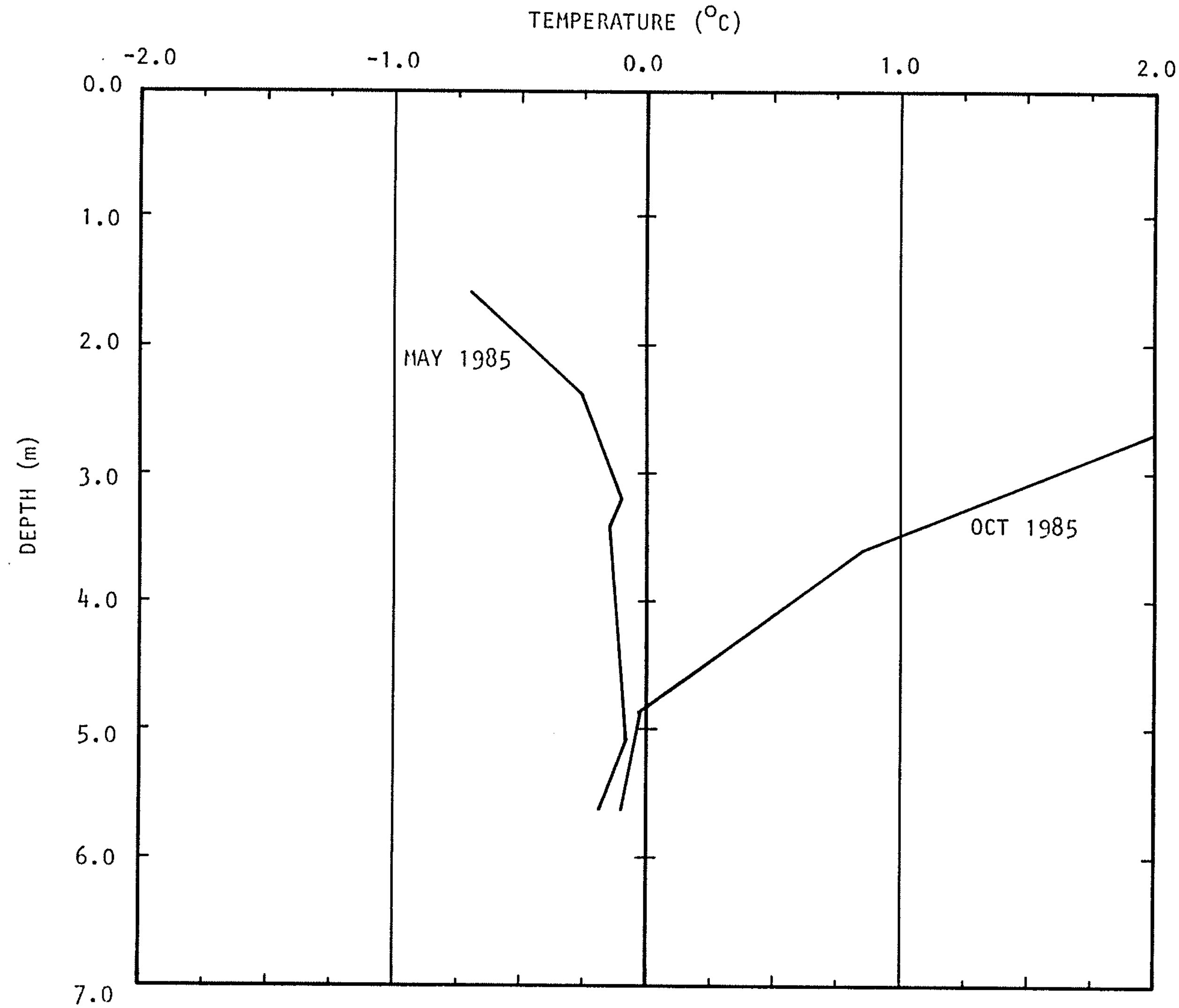

FIG. 2-13 GROUND TEMPERATURE EXTREMES FOR TH-2

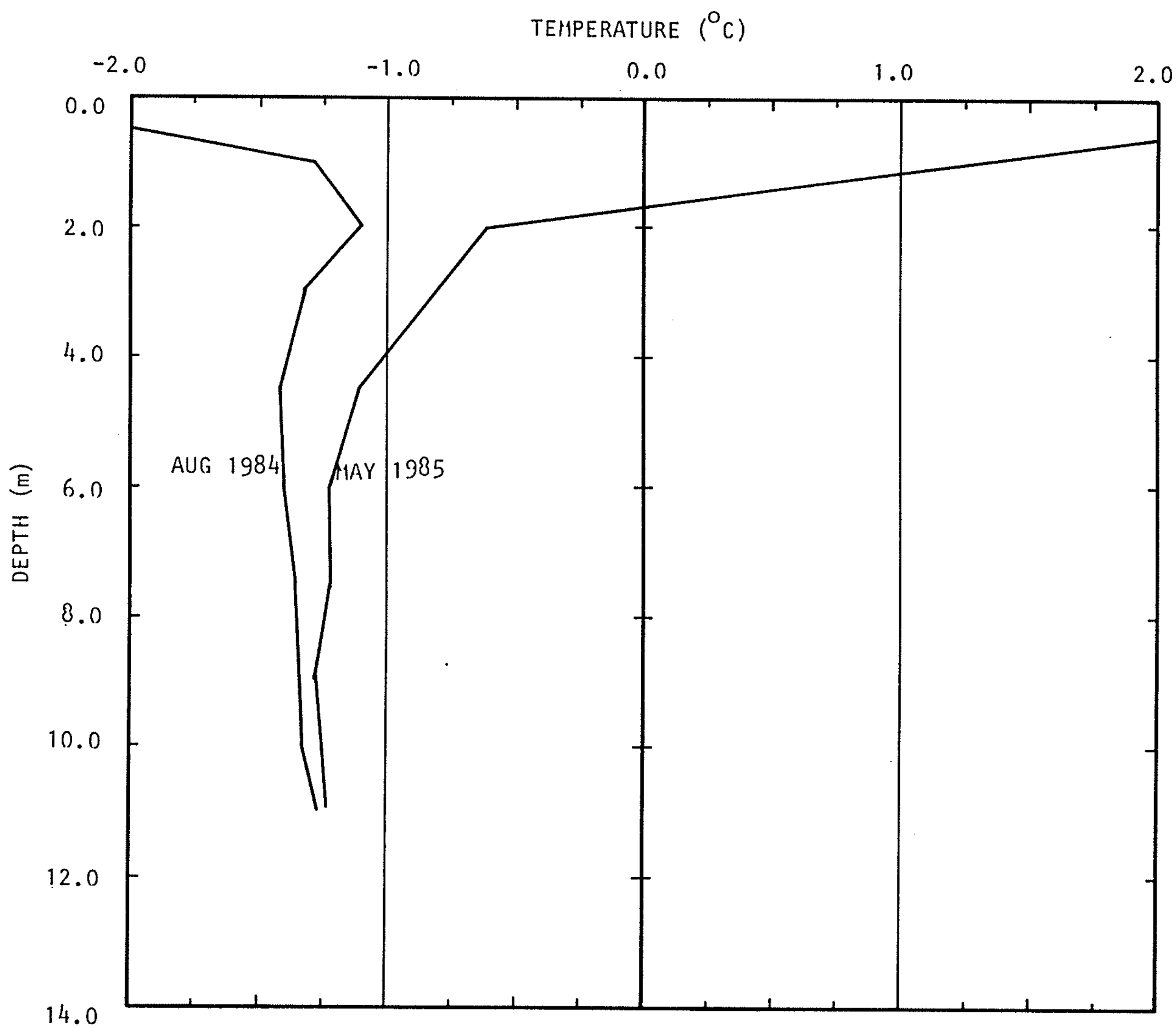

FIG. 2-14 GROUND TEMPERATURE EXTREMES FOR TH-3

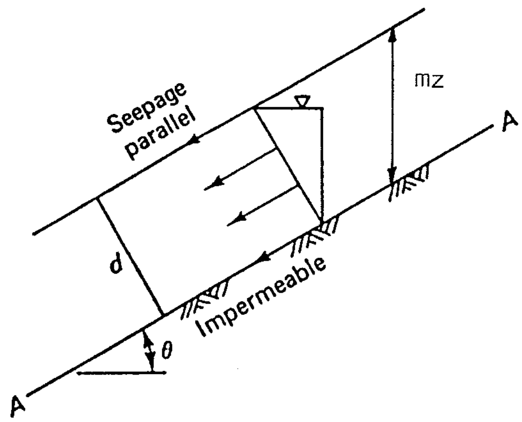

(a)

(a) Case 1: seepage slope. On plane A-A, pore pressure = $\gamma_w d \cos\theta$, total stress = $\gamma d \cos\theta$, effective stress = $(\gamma - \gamma_w) d \cos\theta = \gamma' d \cos\theta$, $F_s = (\gamma' \tan\phi')/(\gamma \tan\theta)$.

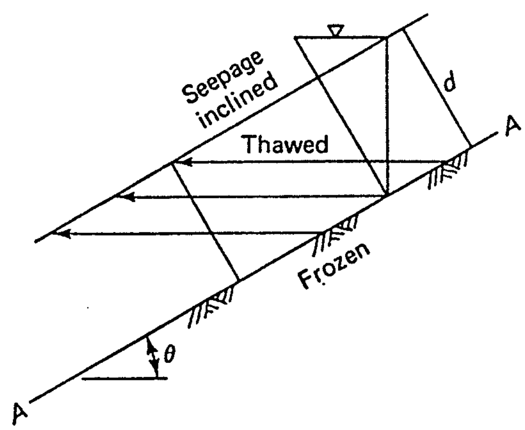

(b)

(b) Case 2: thaw slope. On plane A-A, pore pressure = $\gamma_w d \cos\theta + \gamma' d \cos\theta[1/(1 + 1/2R^2)]$

effective stress = $\gamma d \cos\theta - \gamma_w d \cos\theta - \gamma' d \cos\theta\,[1]/(1 + 1/2R^2)]$,

$$F_s = \frac{\gamma'}{\gamma}\left(1 - \frac{1}{1 + 1/2R^2}\right)\frac{\tan\phi'}{\tan\theta} \qquad \text{where } R = \frac{a}{2(c_v)^{1/2}}$$

(*After McRoberts and Morgenstern, 1974a.*)

FIG. 2-15 INFINITE SLOPE ANALYSES

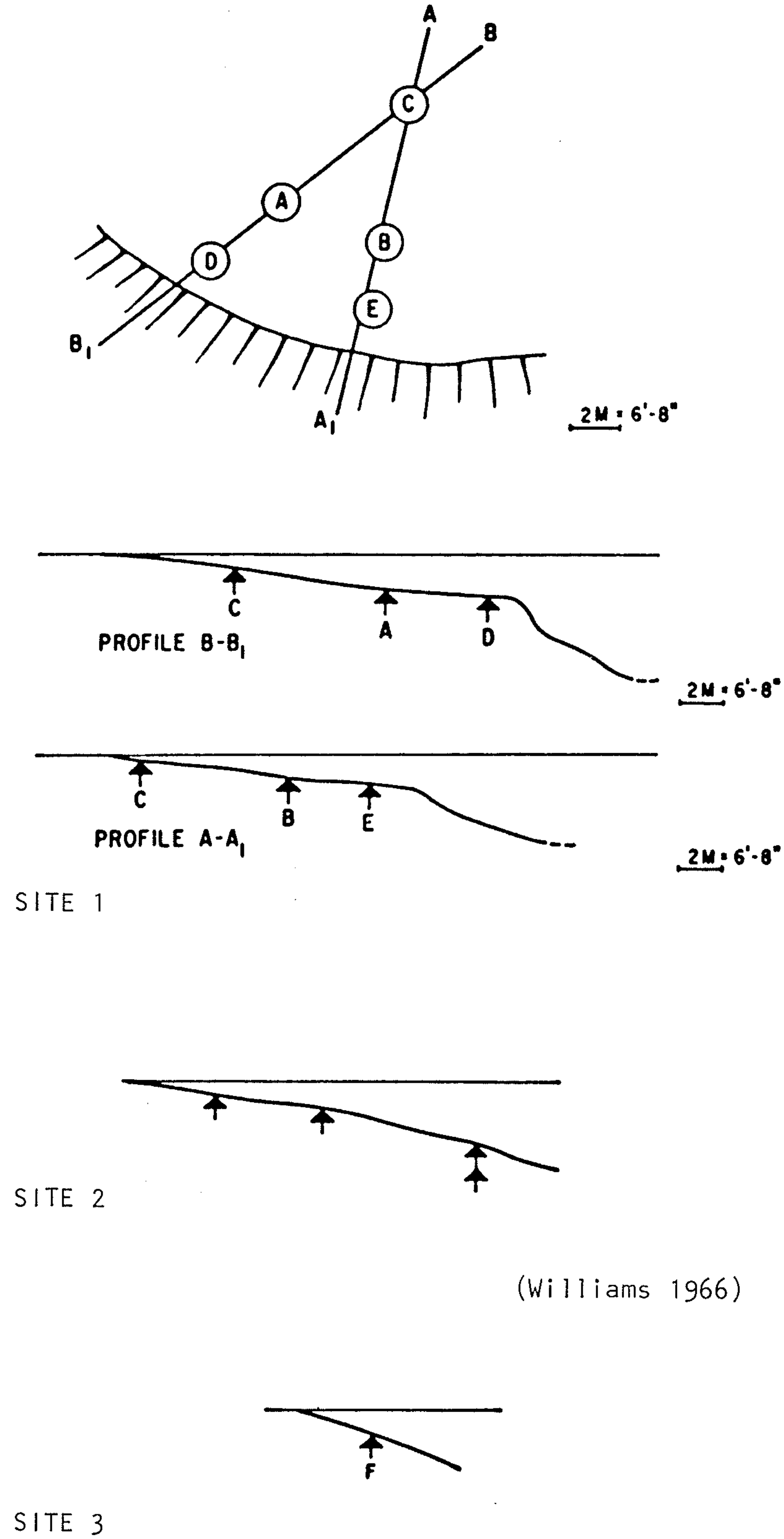

FIG. 3-1 LAYOUT OF TUBES AT SITE 1, AND SLOPE PROFILES FOR SITES 1,2 and 3

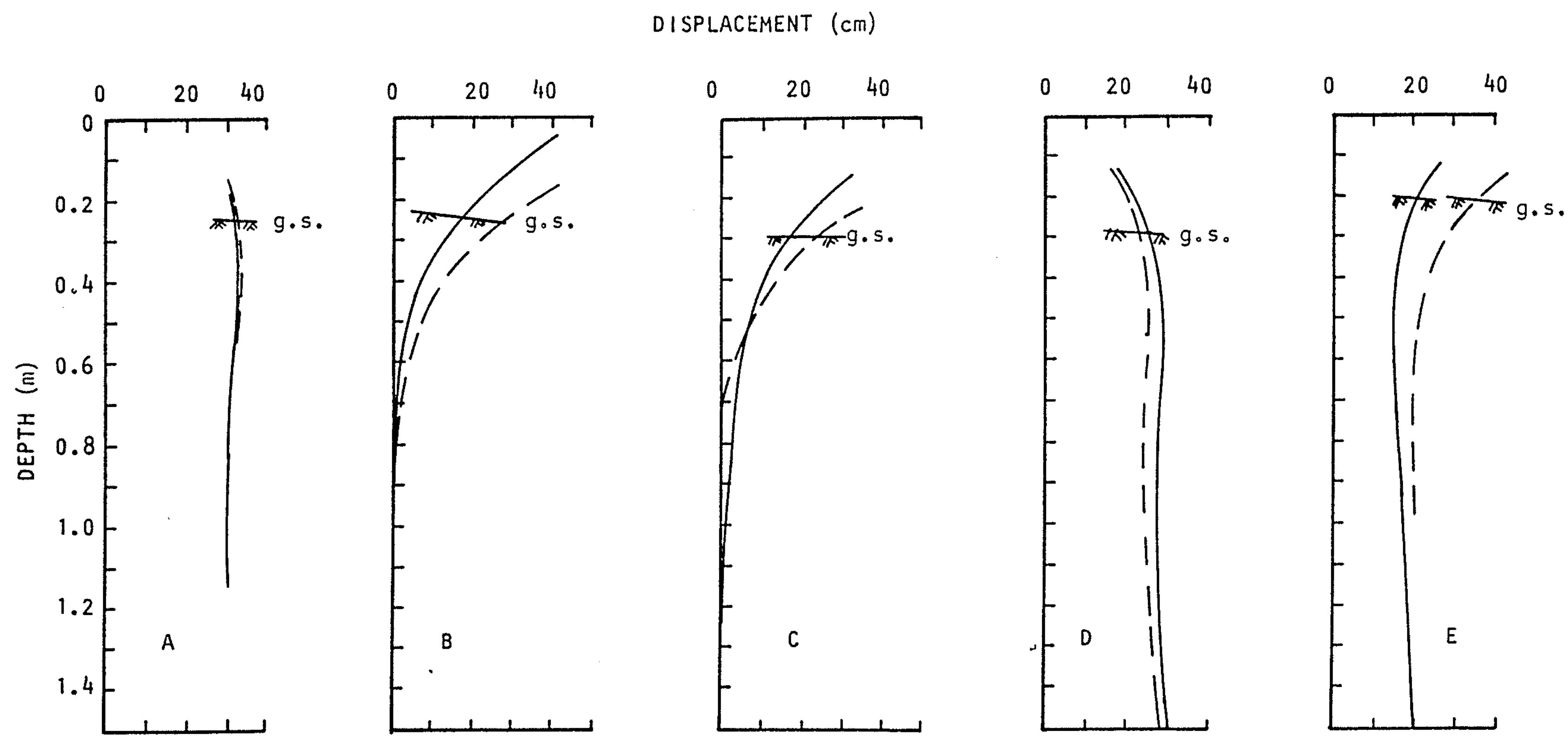

g.s. - ground surface

FIG. 3-2 SHAPES OF BURIED TUBES AT SITE 1 OVER ONE YEAR PERIOD
(Williams 1966)

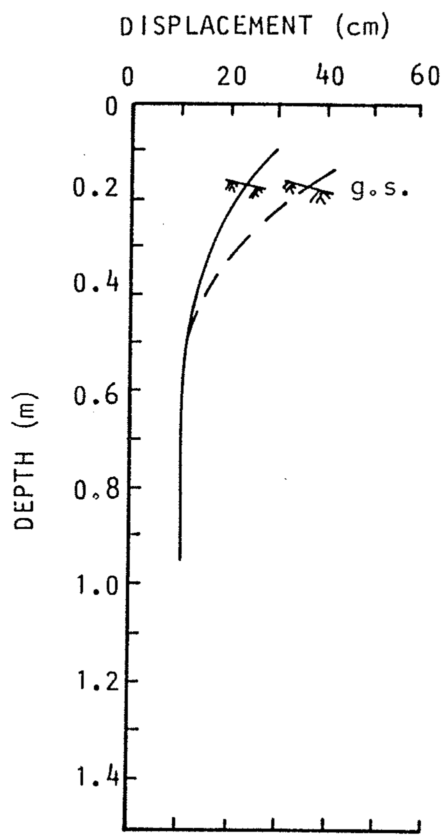

FIG. 3-3 SHAPE OF TUBE AT SITE 3 OVER ONE YEAR PERIOD
(Williams 1966)

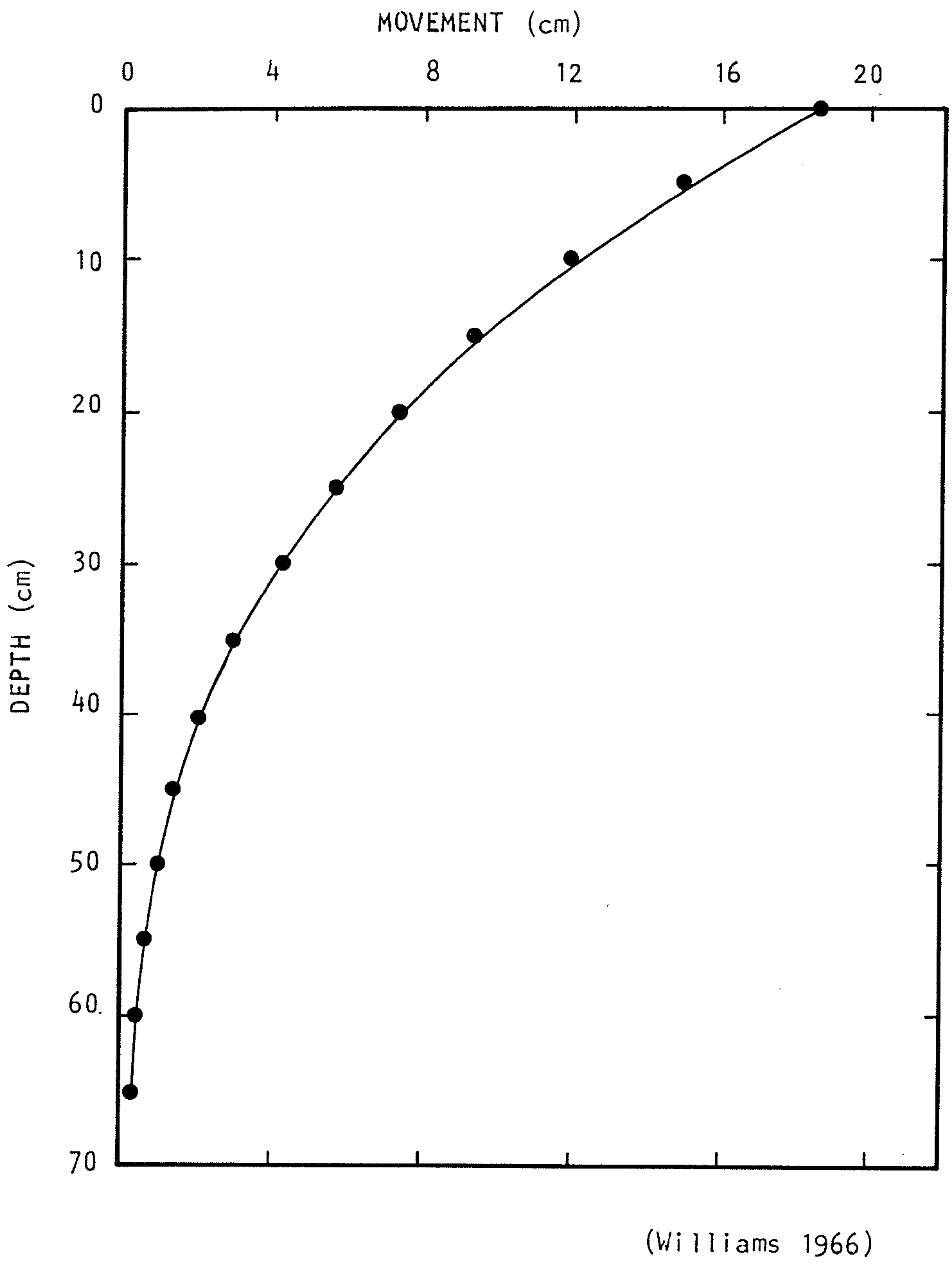

FIG. 3-4 TOTAL DISPLACEMENT OF TUBE C AT SITE 1 FOR A ONE YEAR PERIOD

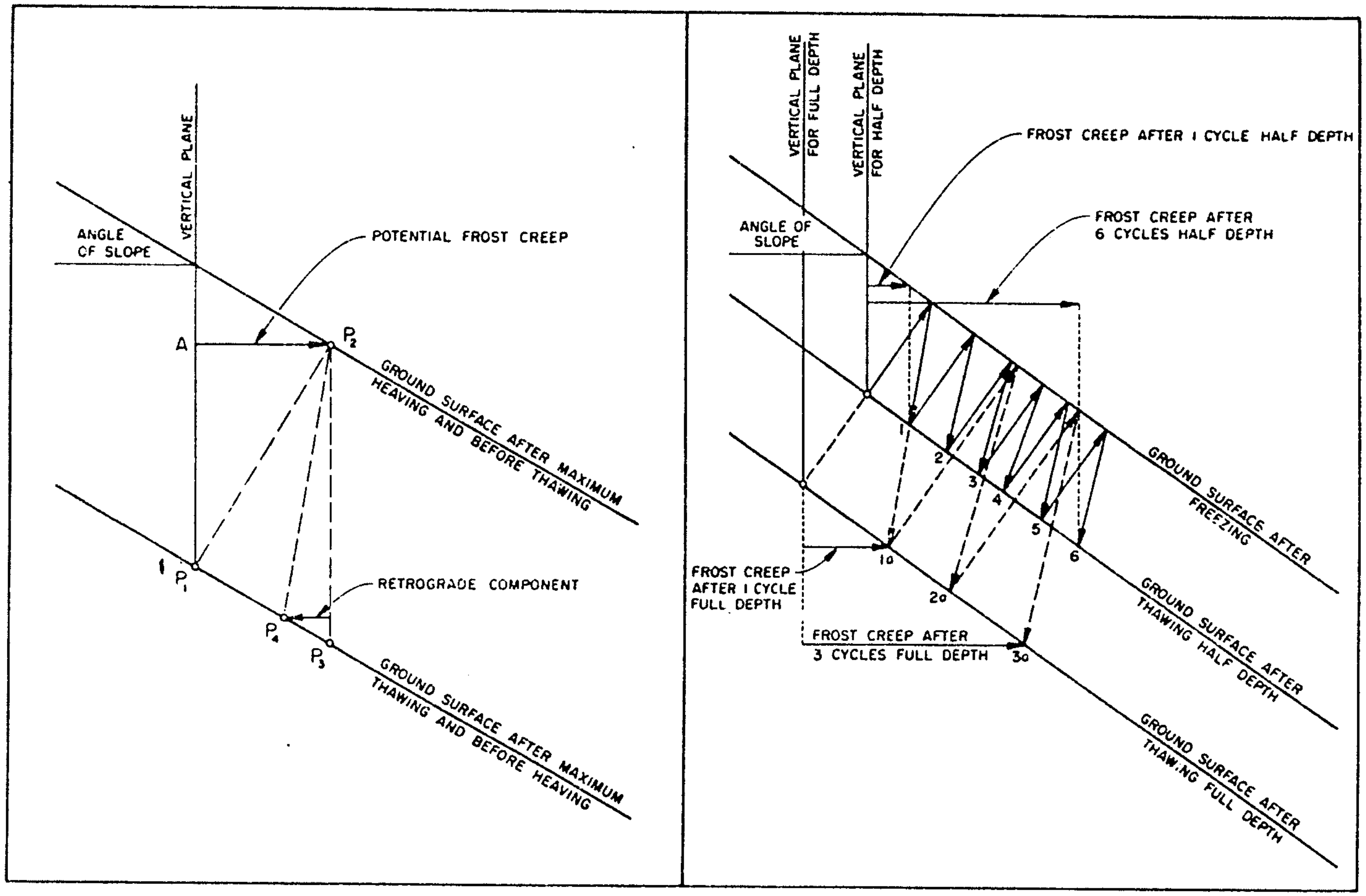

FIG. 3-5 SCHEMATIC OF FROST CREEP MECHANISM (Washburn 1973)

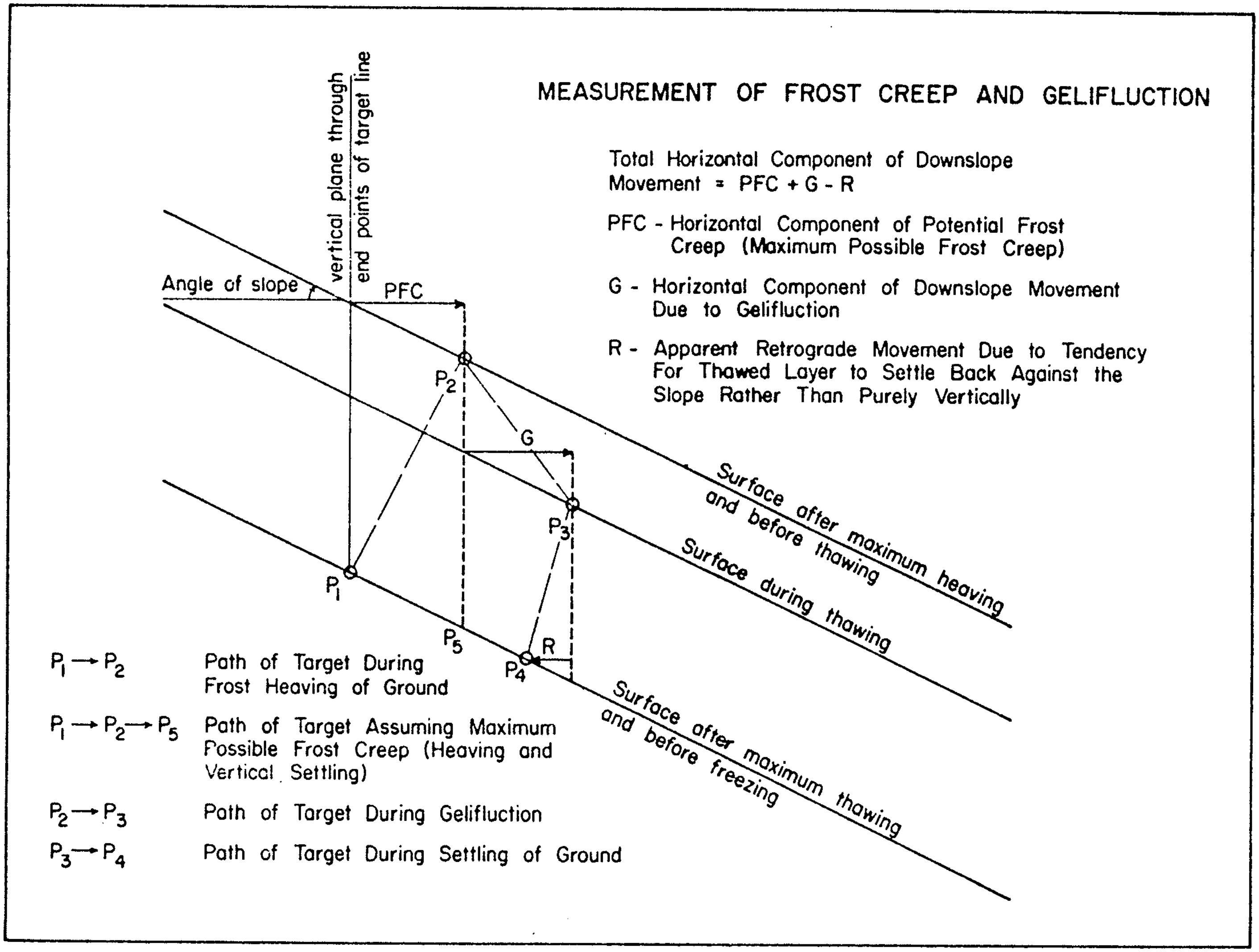

FIG. 3-6 SCHEMATIC OF COMBINATION OF FROST CREEP AND GELIFLUCTION MECHANISM (Washburn 1973)

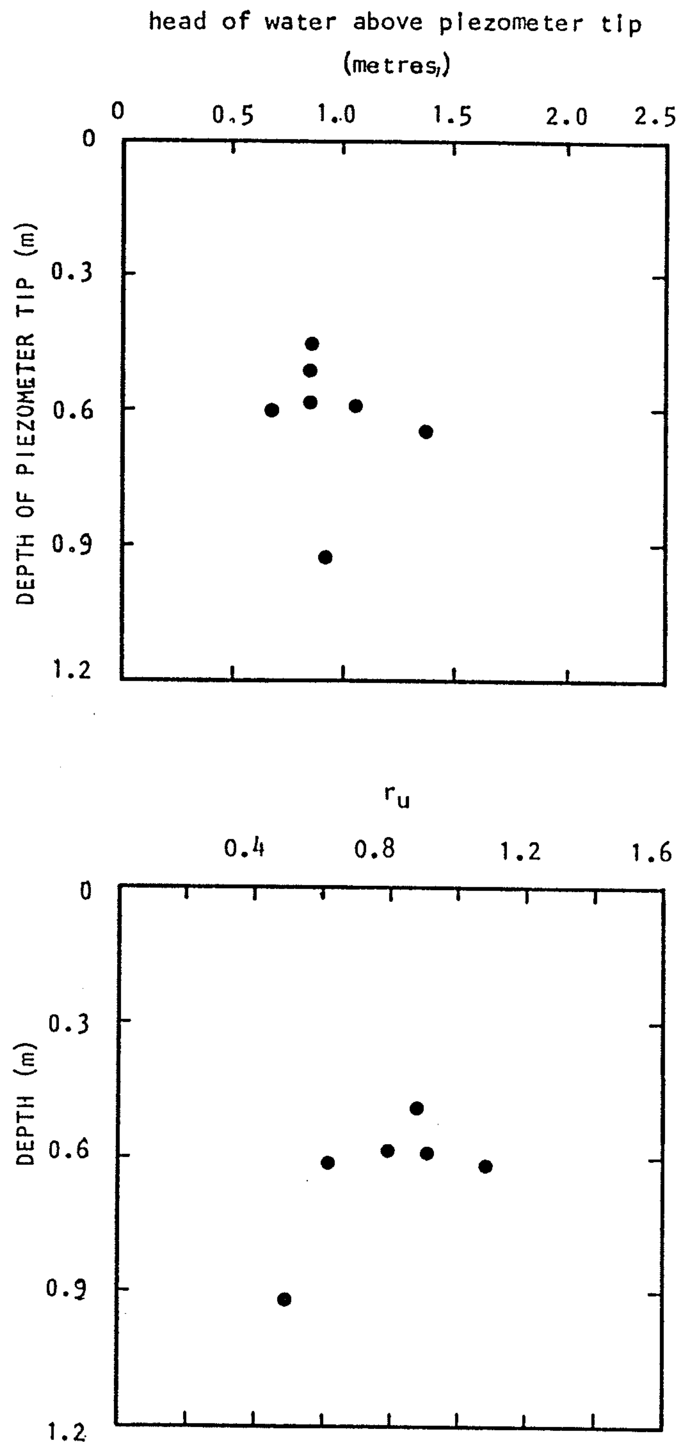

FIG. 3-7 PORE PRESSURE READINGS IN A THAWING SLOPE
(McRoberts and Morgenstern 1974)

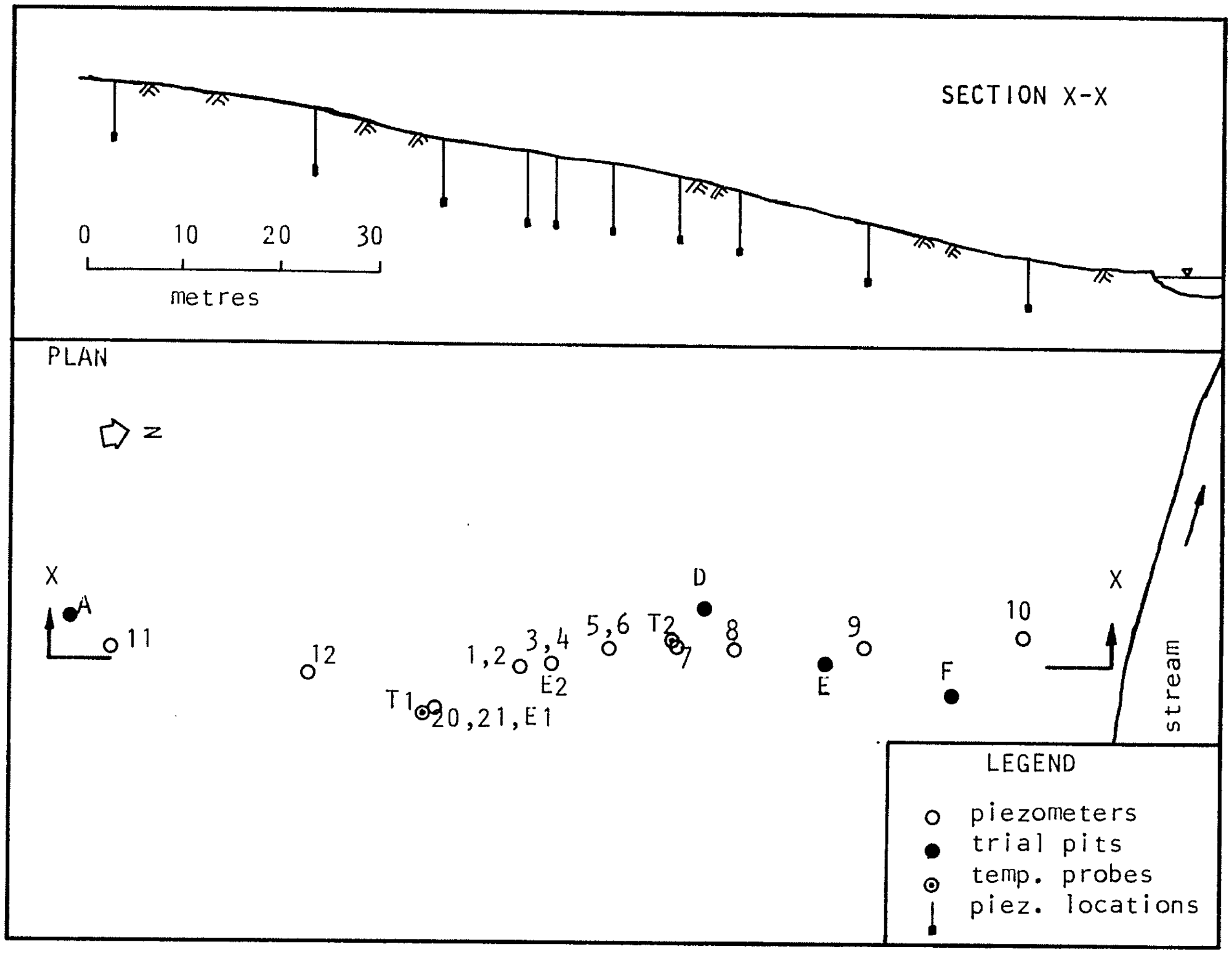

FIG. 3-8 SITE LAYOUT FOR SLOPE 2 (Chandler 1972)

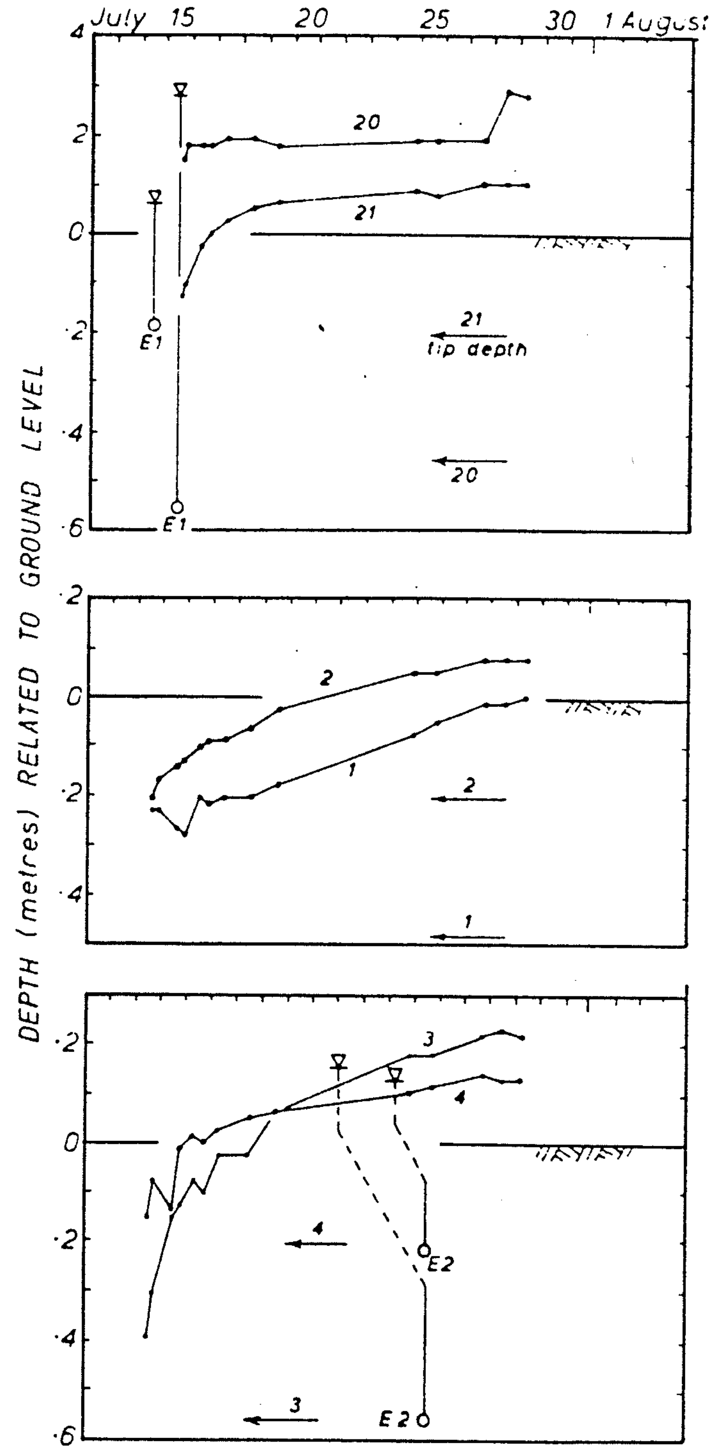

FIG. 3-9 PIEZOMETER READINGS PLOTTED AGAINST TIME FOR LOCATION 2 (Chandler 1972)

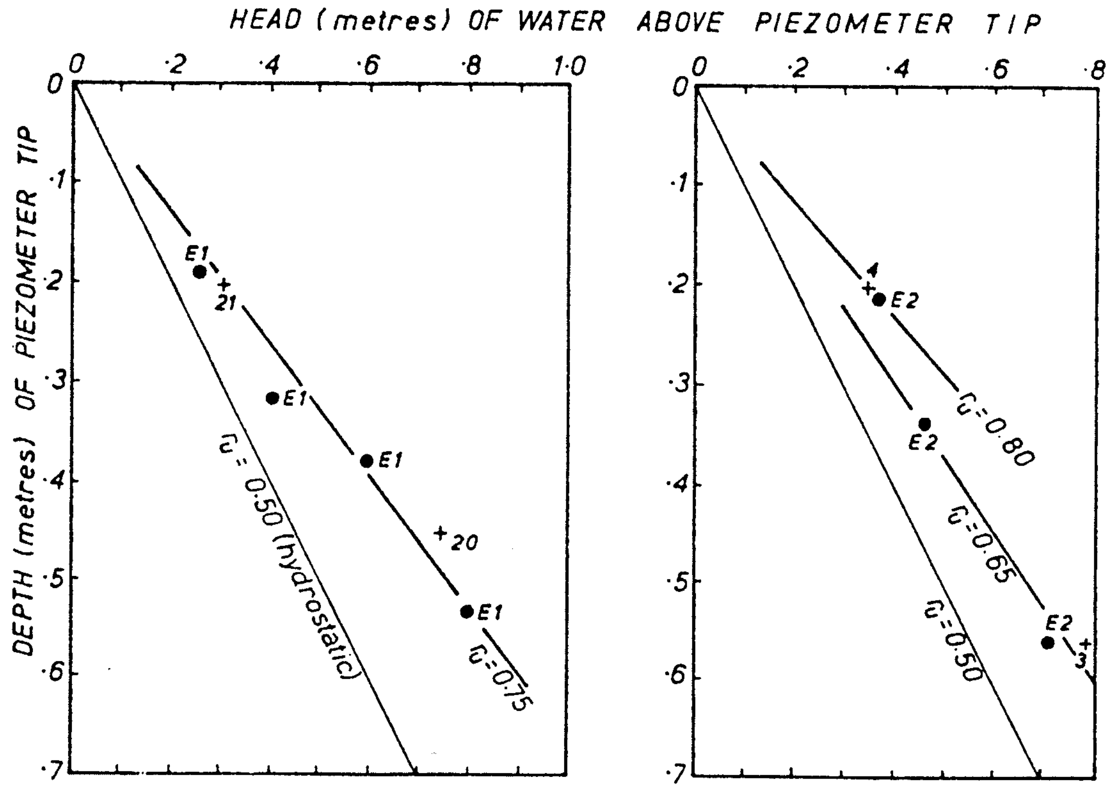

FIG. 3-10 SUMMARY OF MAXIMUM PIEZOMETER READINGS, LOCATION 2 (Chandler 1972)

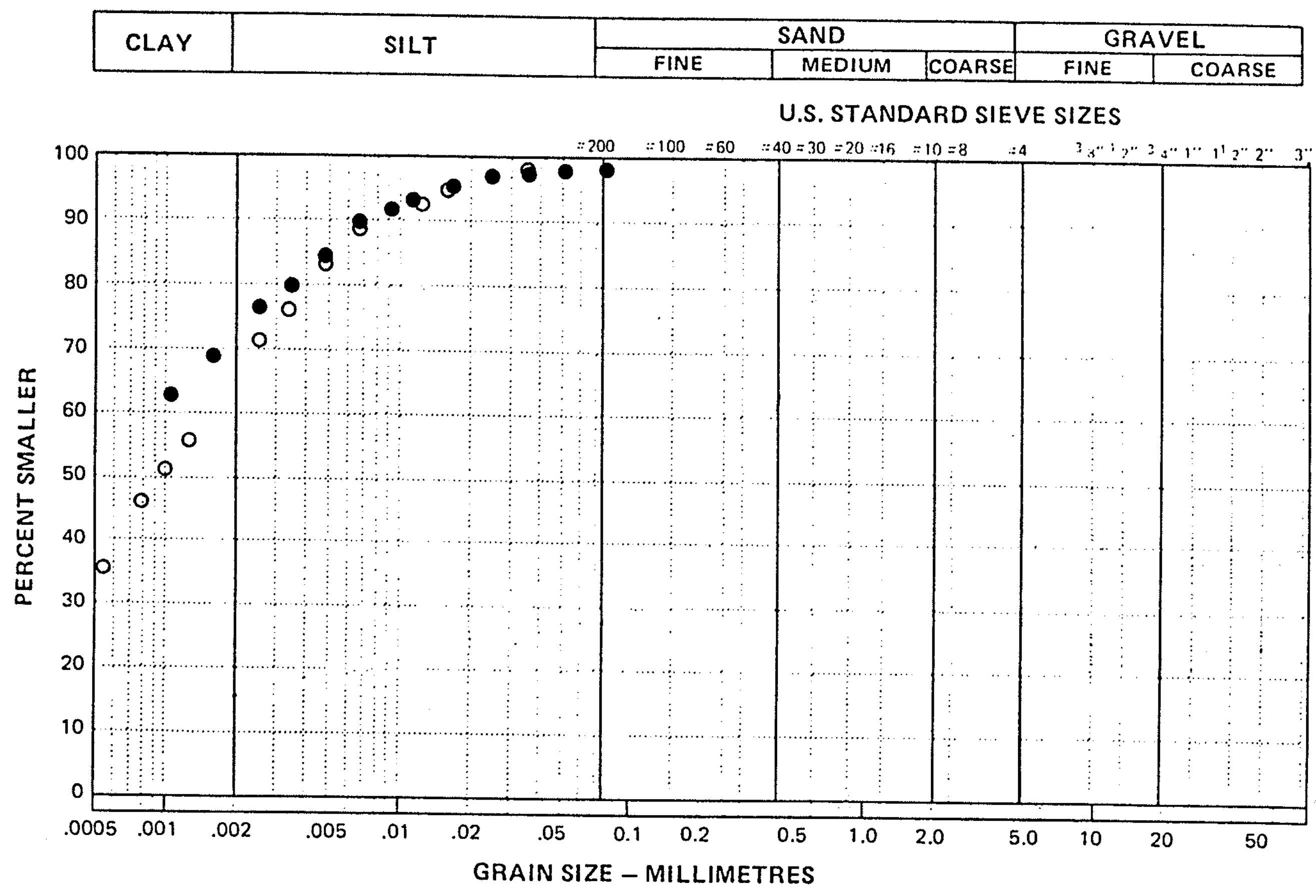

FIG. 4-1 RESULTS OF GRAIN SIZE ANALYSES (Block Sample - 1.8m)

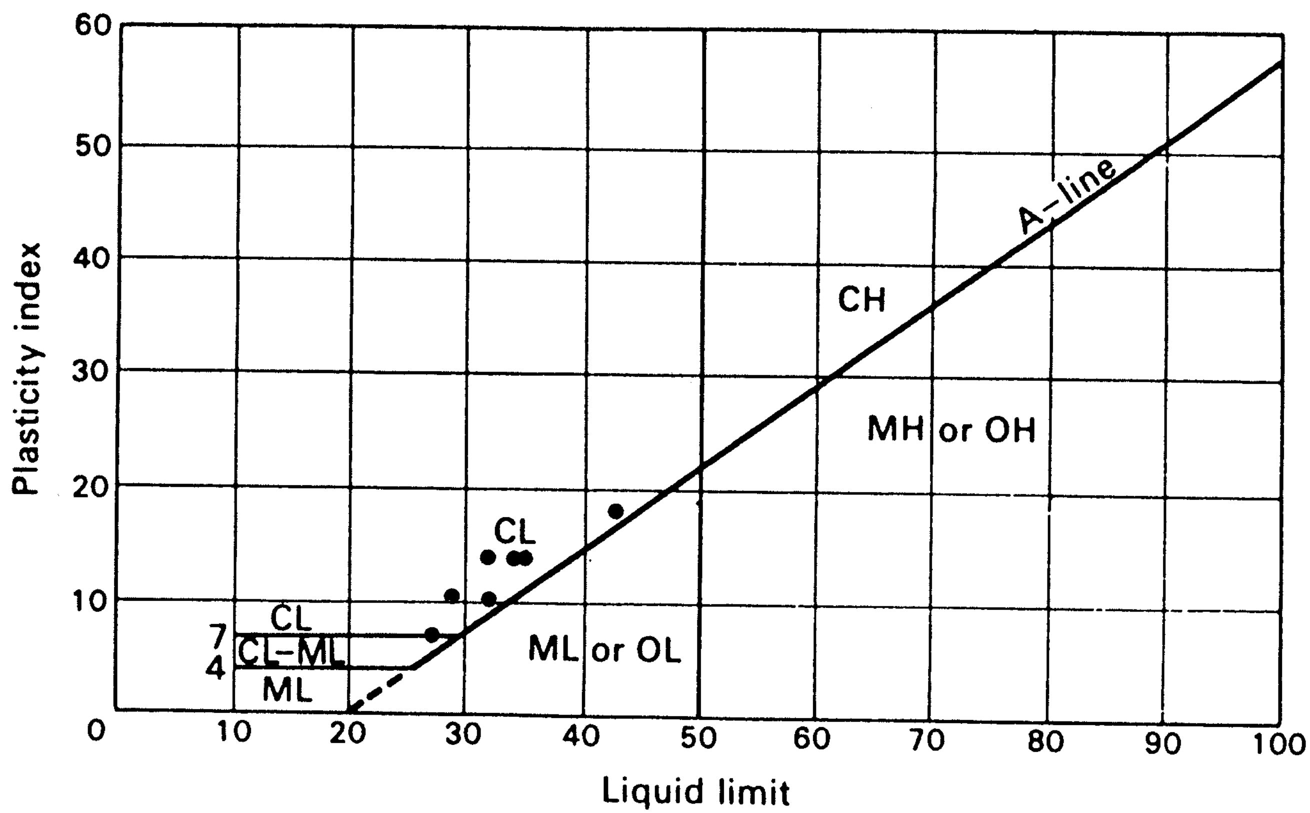

FIG. 4-2 PLASTICITY CHART (Unified Classification System)

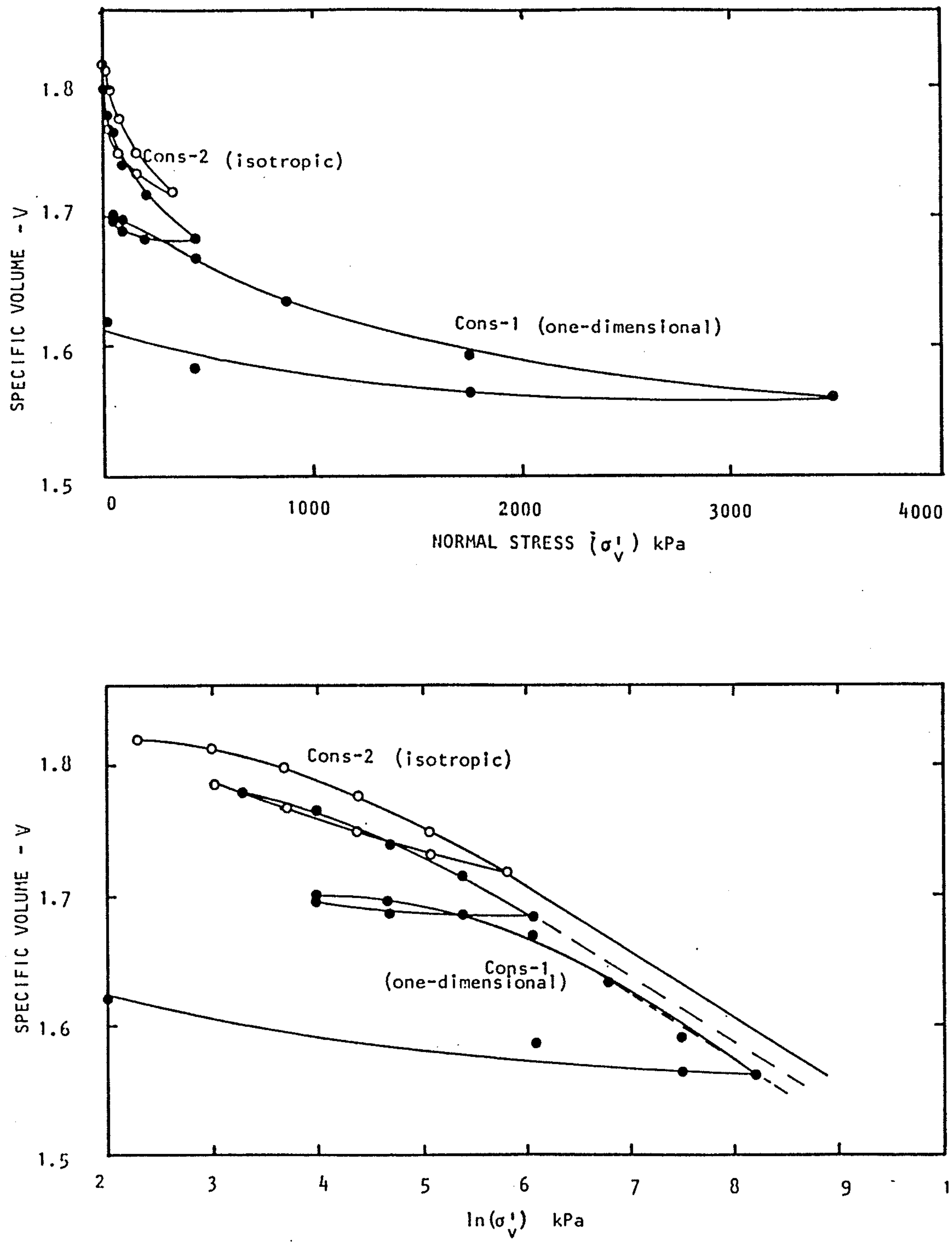

FIG. 4-3 COMPRESSION TEST RESULTS

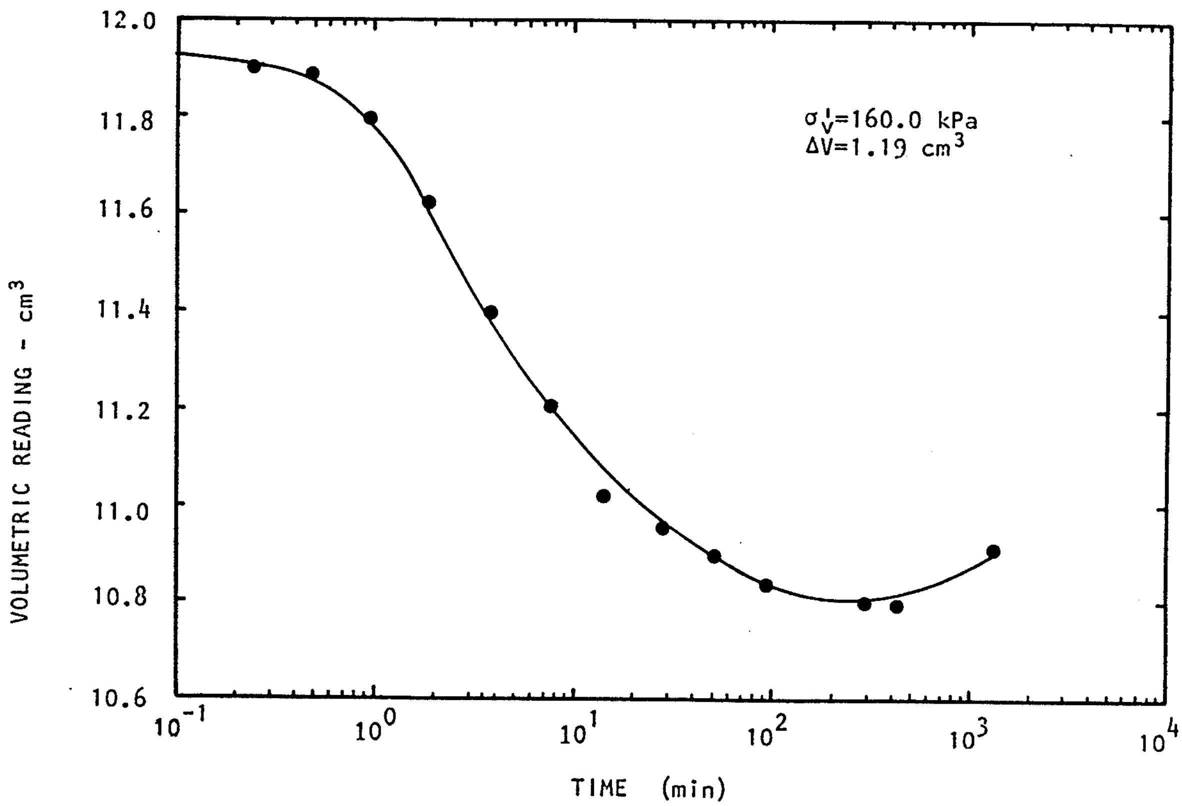

FIG. 4-4 ISOTROPIC CONSOLIDATION CURVE

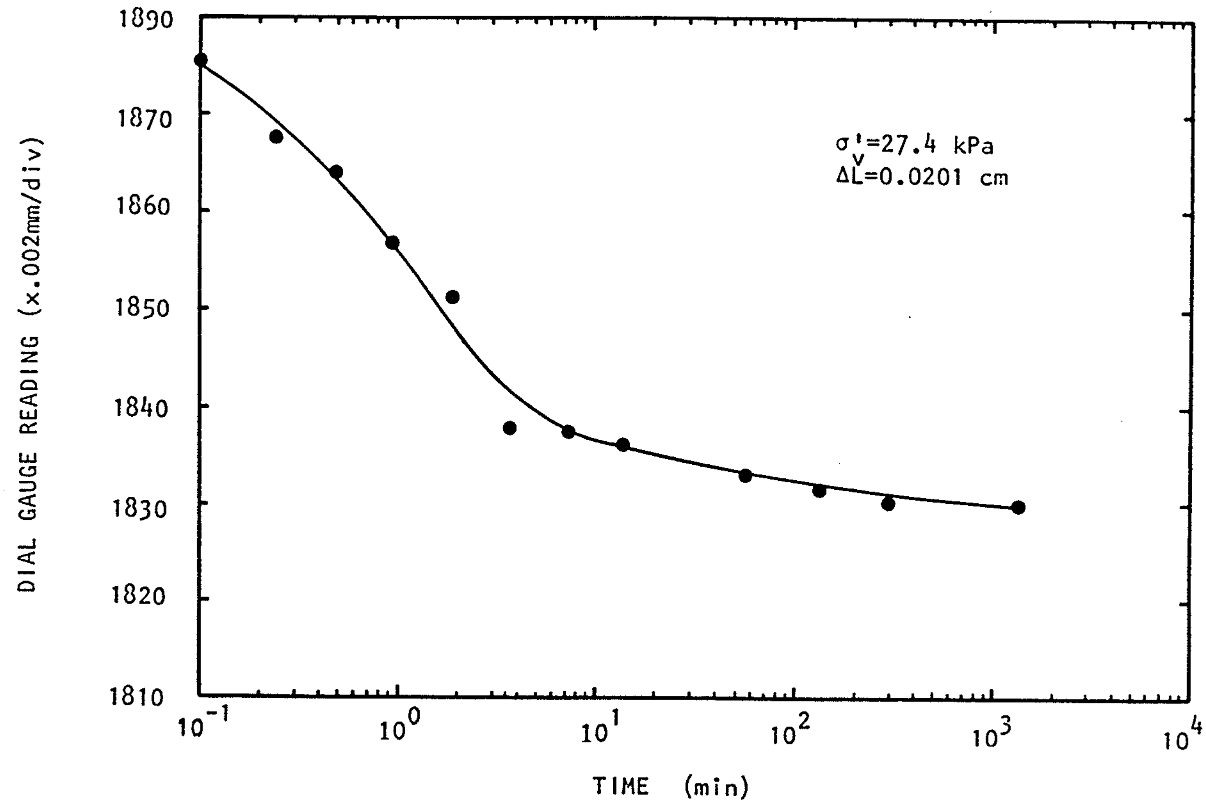

FIG. 4-5 ONE-DIMENSIONAL CONSOLIDATION CURVE

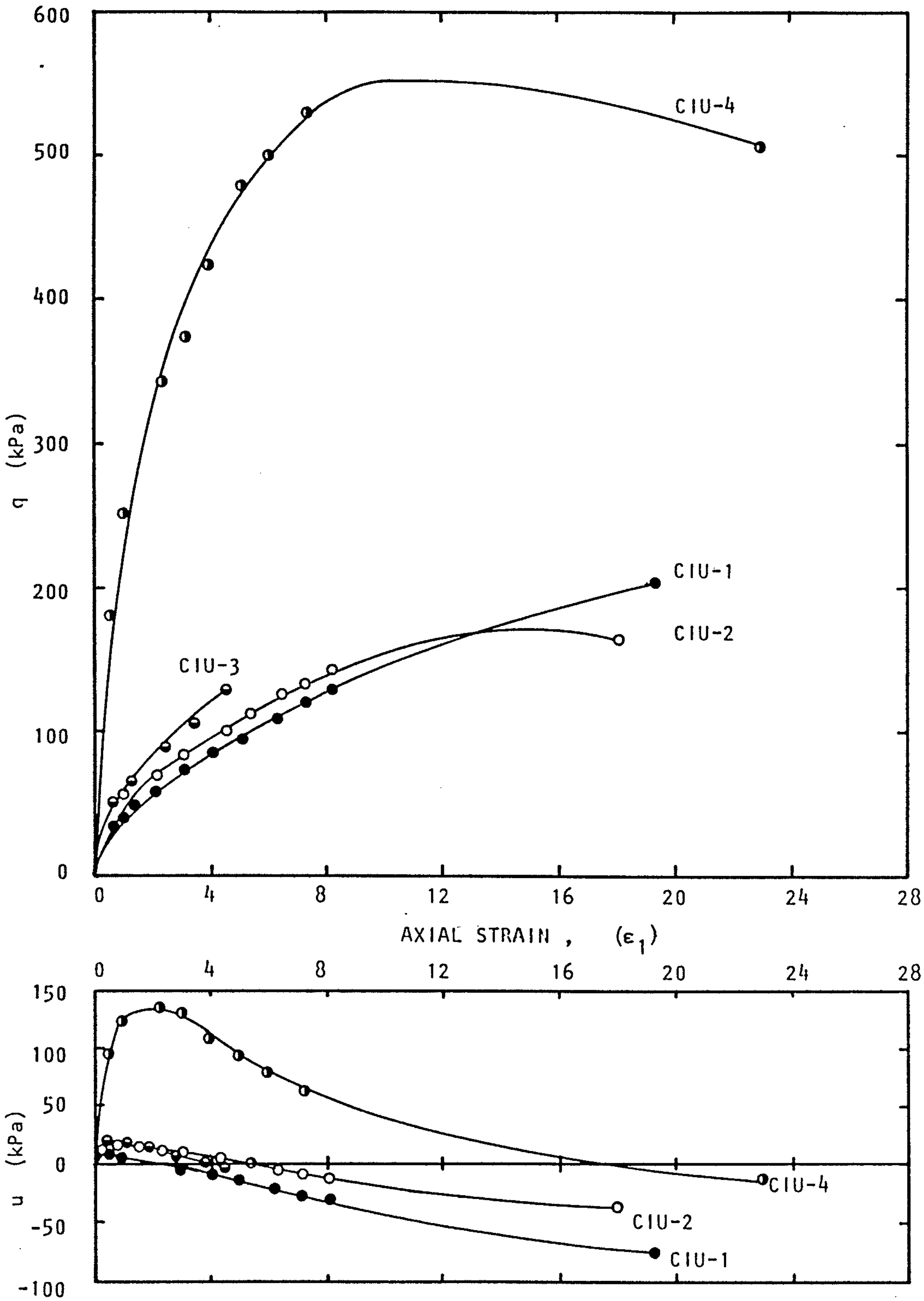

FIG. 4-6 CIU TEST RESULTS - q vs ε_1

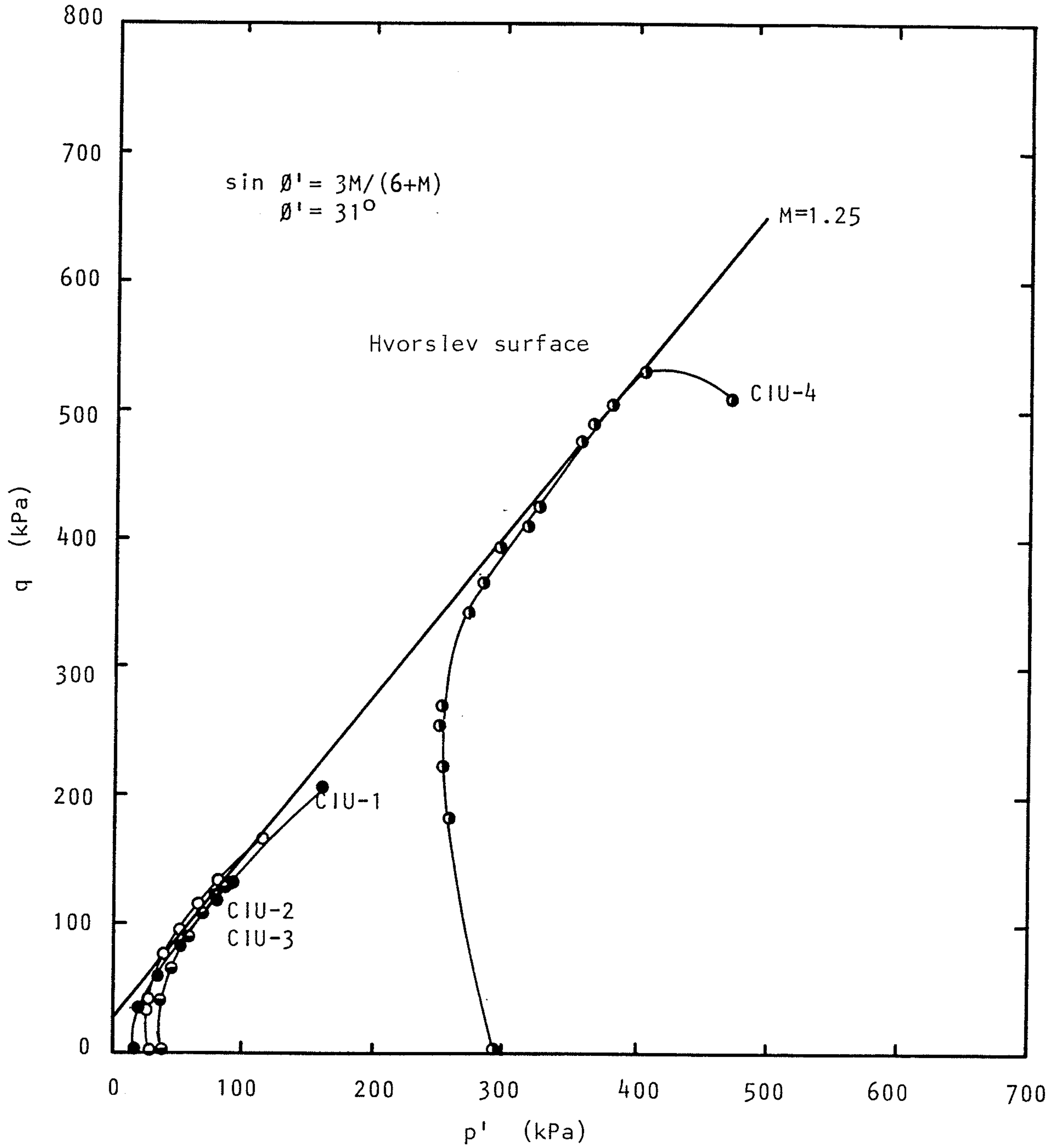

FIG. 4-7 CIU TEST RESULTS - q vs. p'

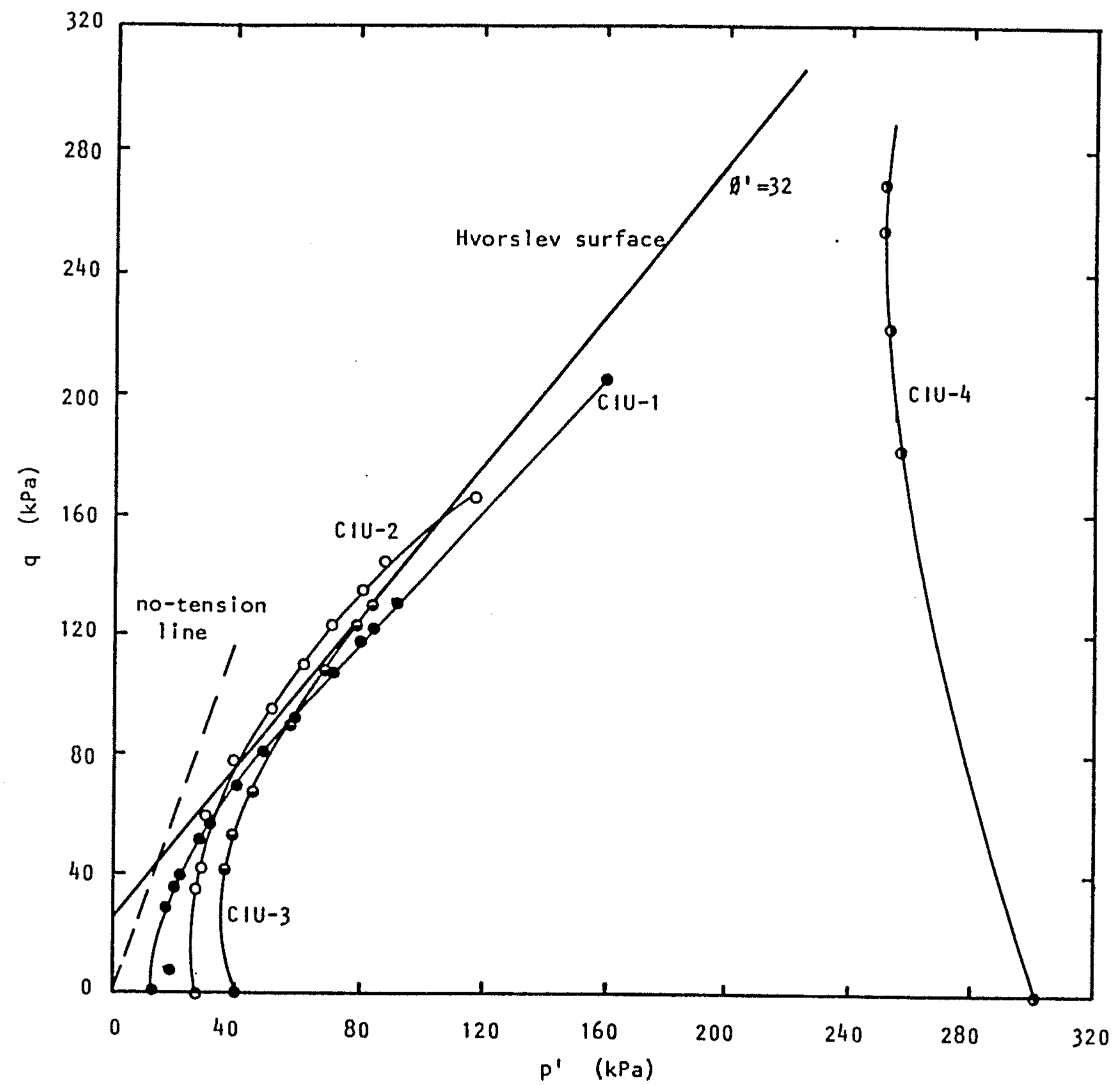

FIG. 4-8 CIU TEST RESULTS - q vs. p' - LOW STRESS RANGE

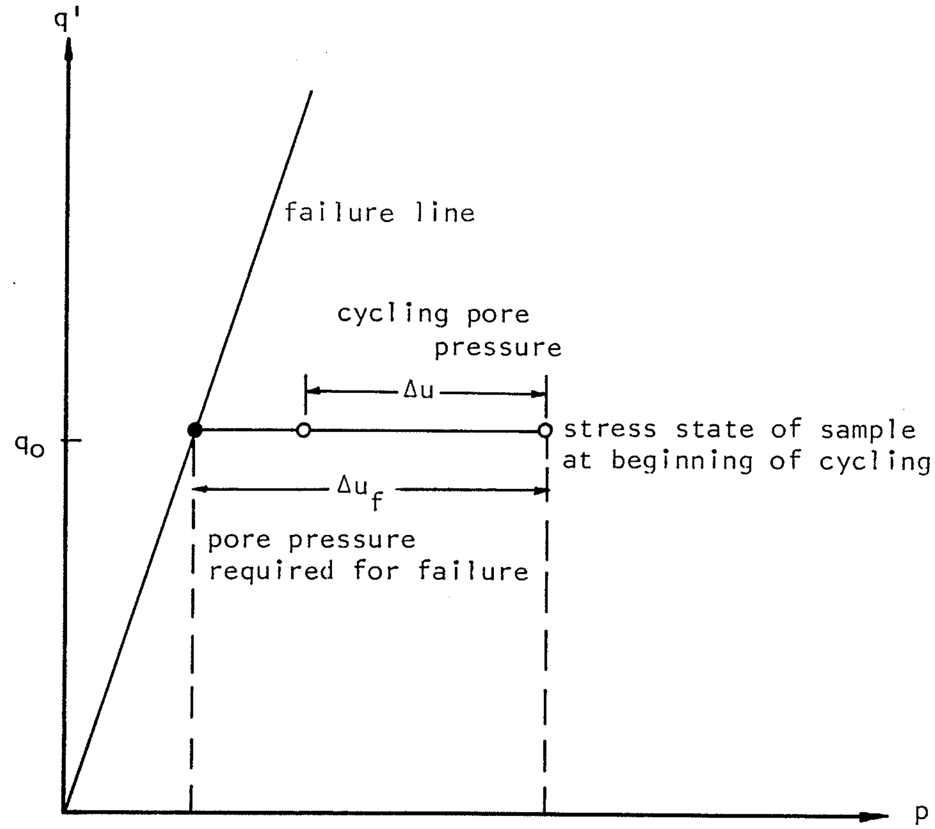

FIG. 4-9 SCHEMETIC OF DEFINITION FOR $\Delta u/\Delta u_f$

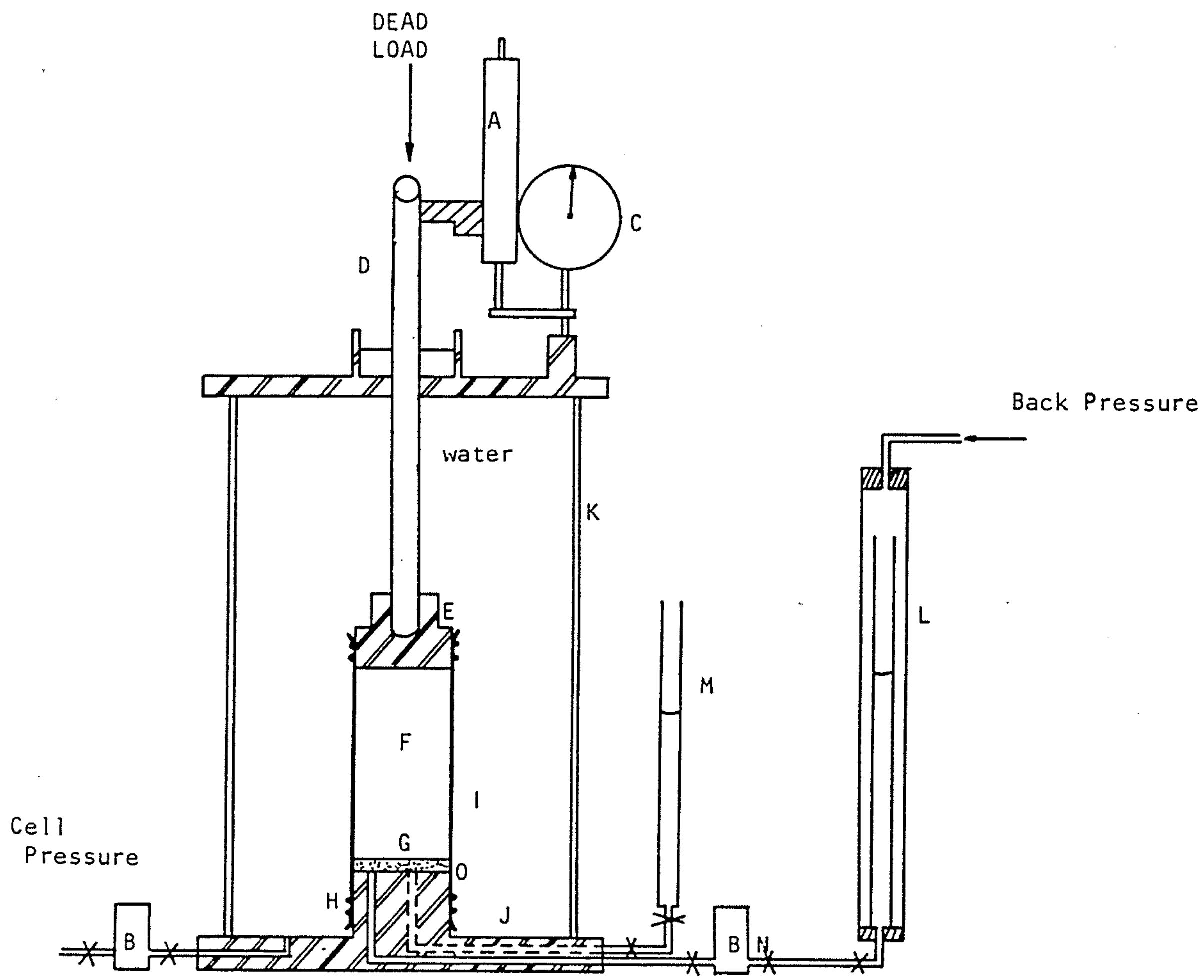

LEGEND

A Displacement Transducer
B Pressure Transducer
C Dial Gauge
D Loading Ram
E Perspex Top Cap
F Clay Sample
G Filter Stone
H O-Rings
I Rubber Membranes
J Cell Base
K Triaxial Cell
L Back Pressure Burette
M Burette (for de-airing)
N Valve
O Pedestal

FIG. 4-10 EQUIPMENT SET-UP

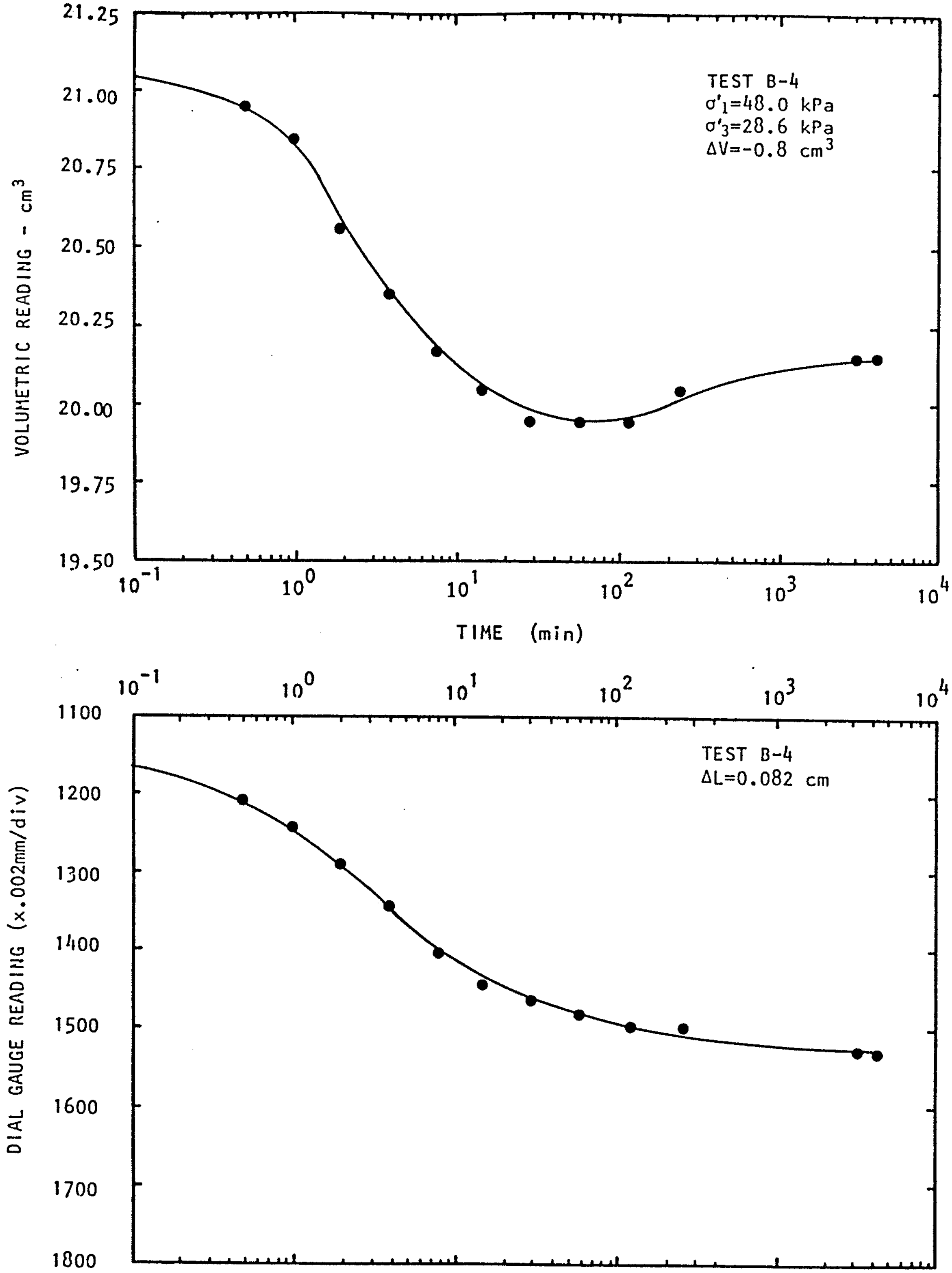

FIG. 5-1 TYPICAL CONSOLIDATION CURVES FROM DTTCP TEST

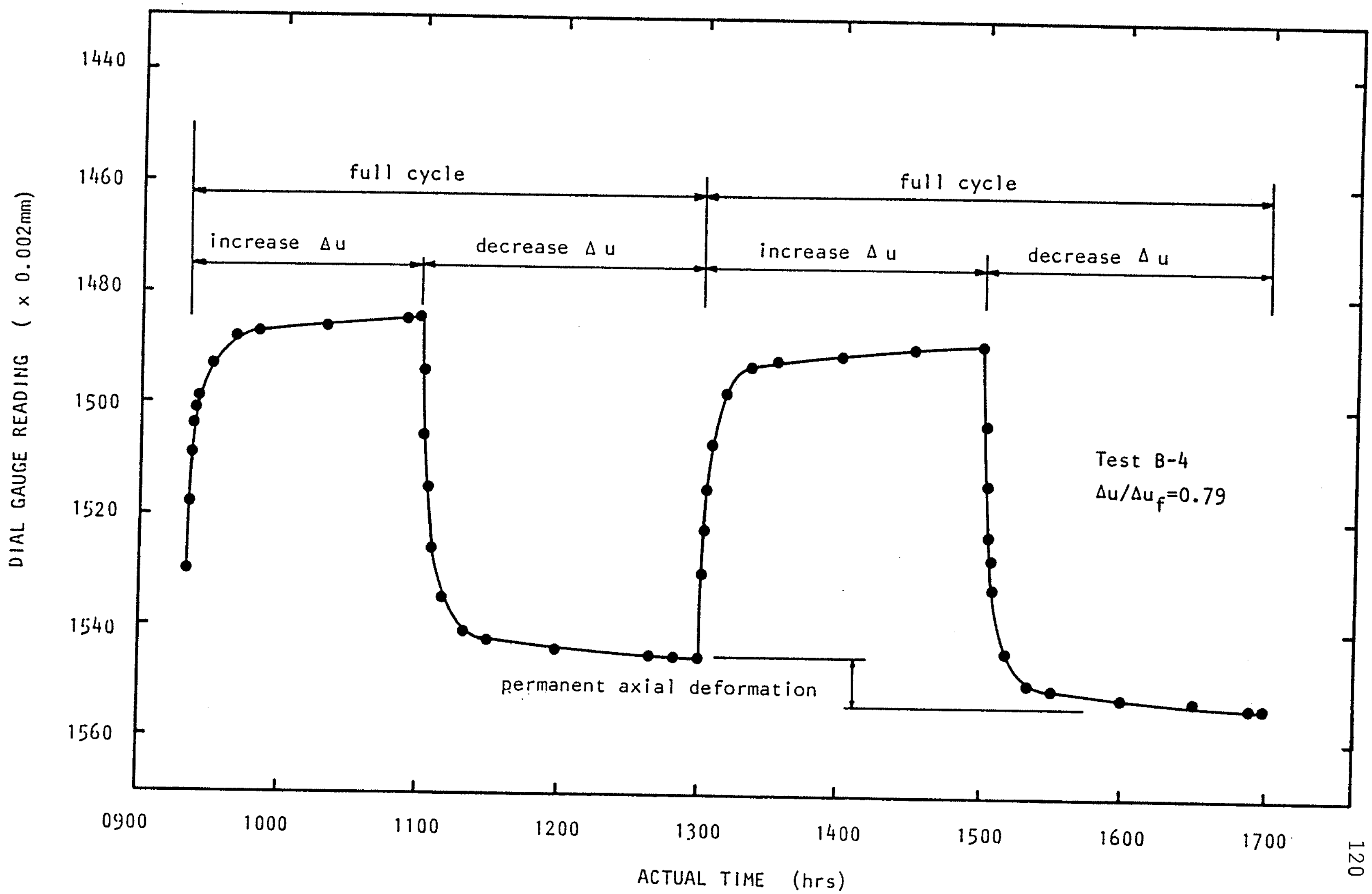

FIG. 5-2 DETAILED SAMPLE BEHAVIOR OVER TWO COMPLETE CYCLES

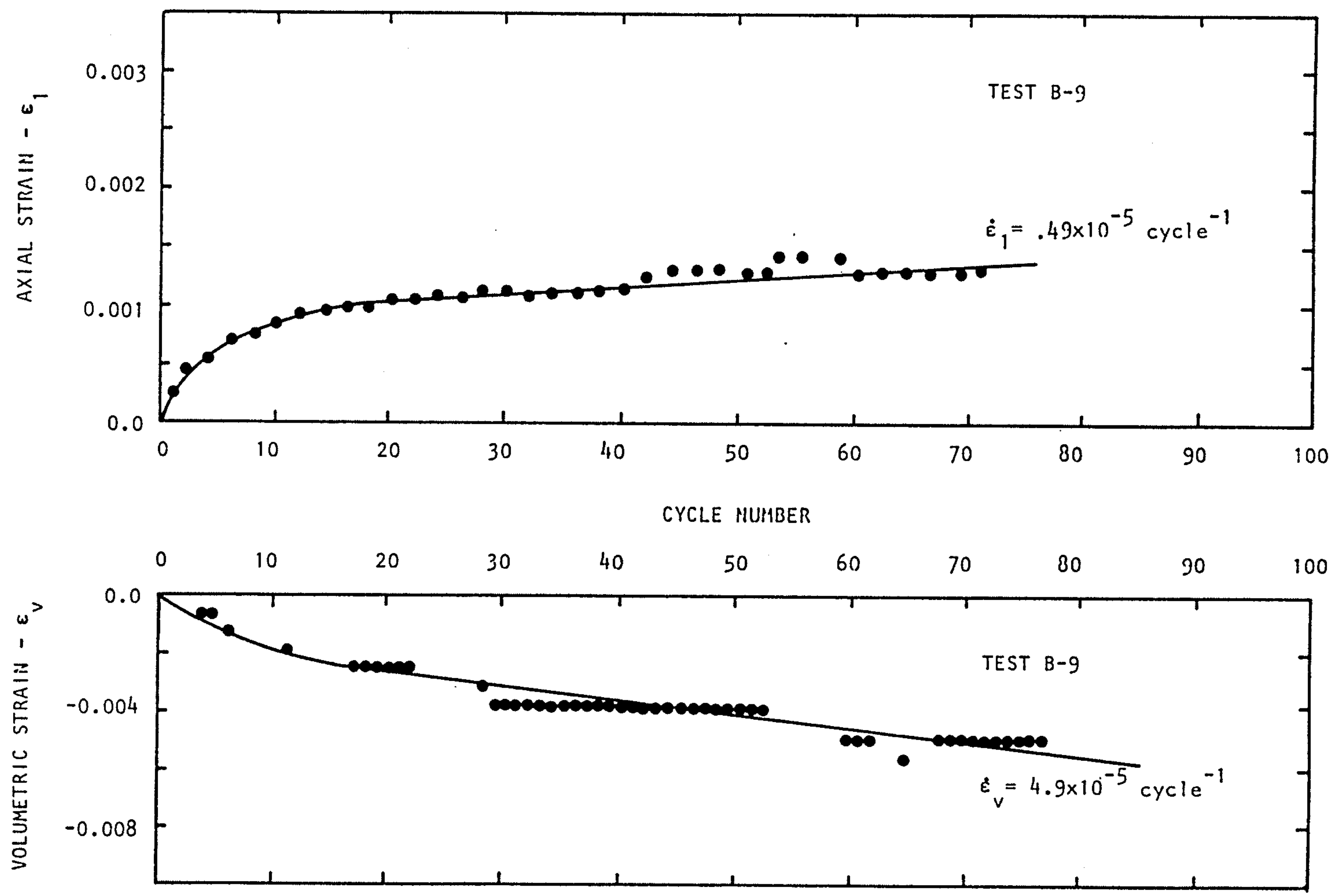

FIG. 5-3 TYPICAL DTTCP TEST RESULT - ε_1 and ε_v vs. cycle number

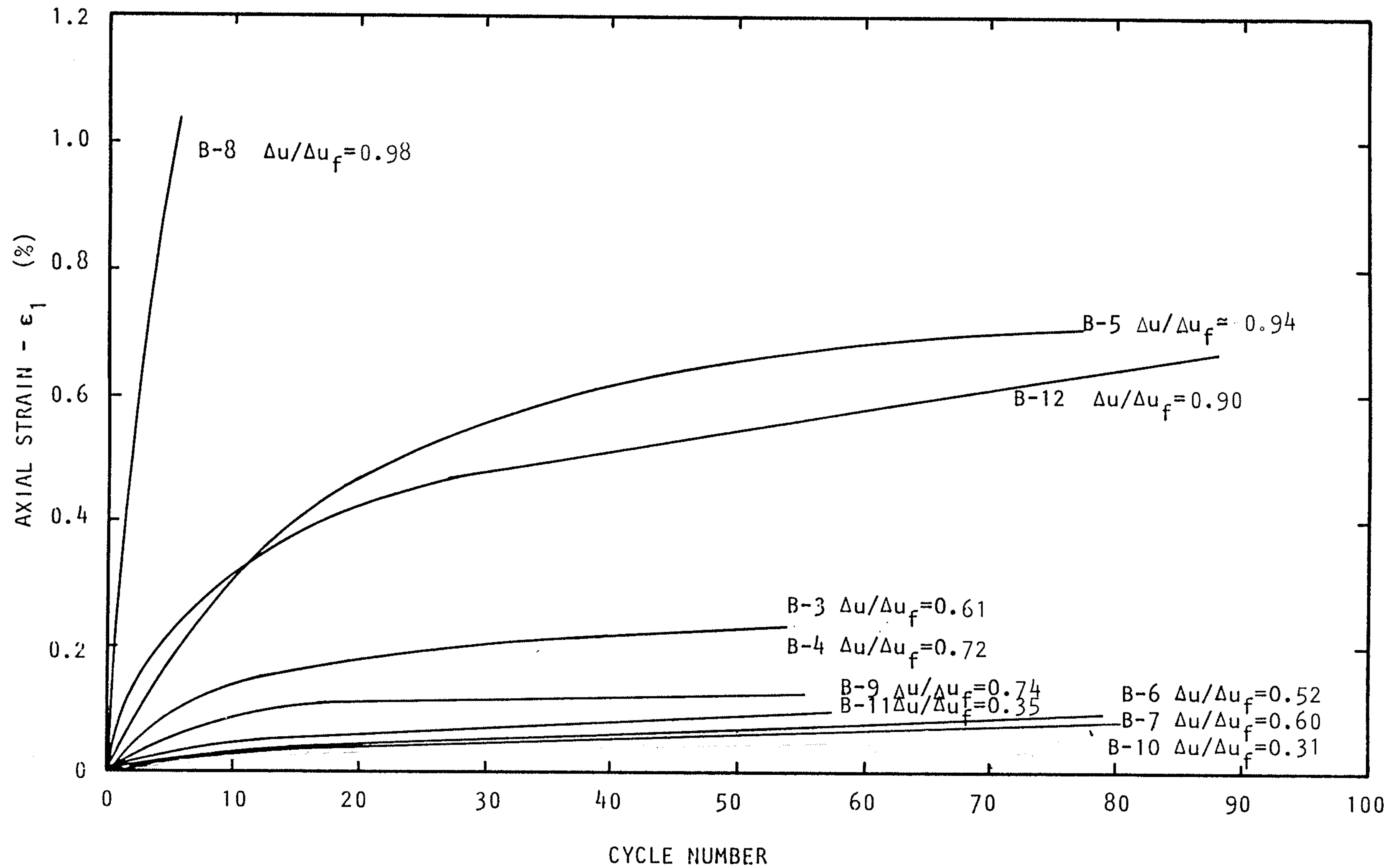

FIG. 5-4 COMPOSITE PLOT OF ε_1 vs. CYCLE NUMBER FOR ALL DTTCP TESTS

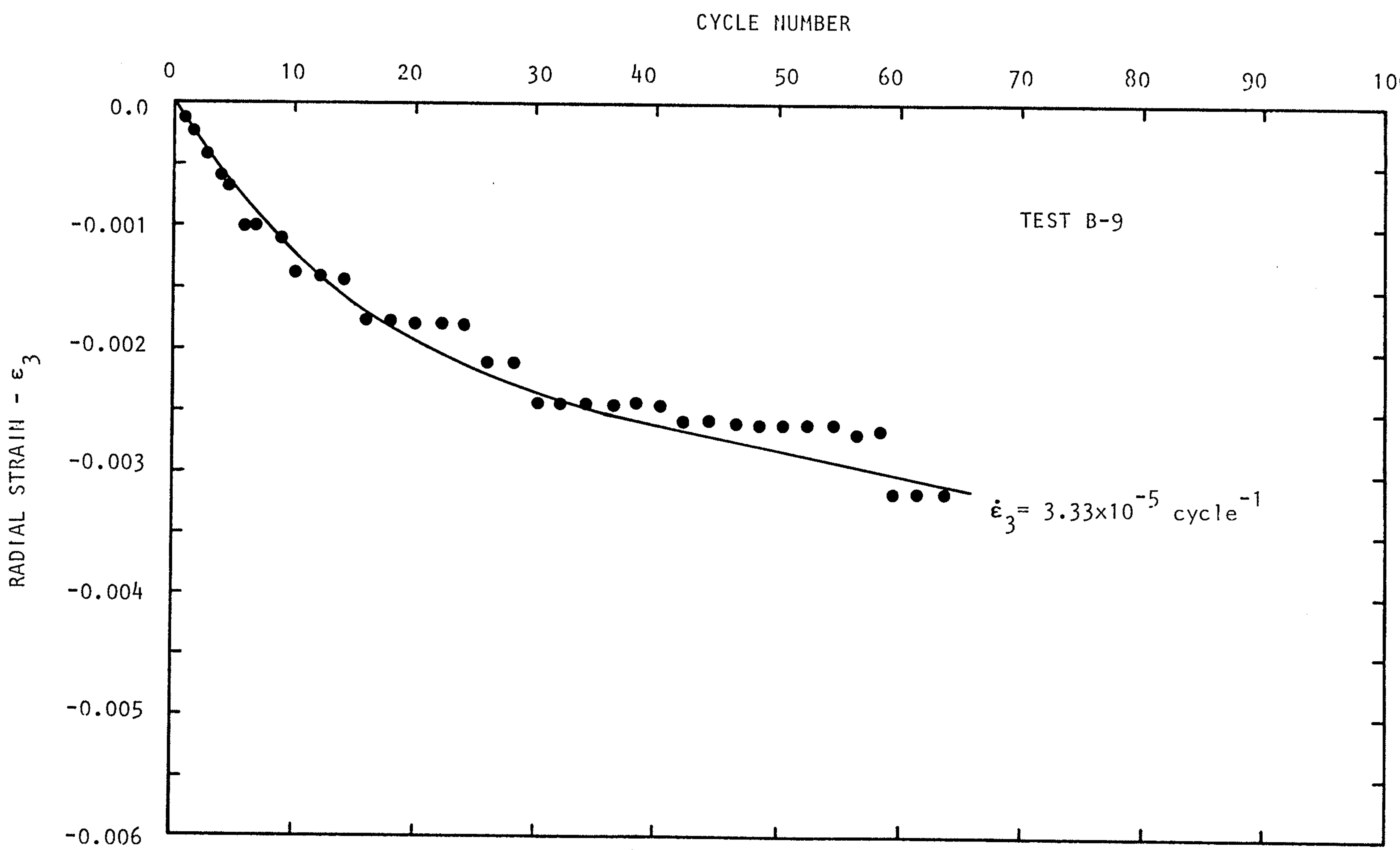

FIG. 5-5 TYPICAL DTTCP TEST RESULT SHOWING ε_3 vs. CYCLE NUMBER

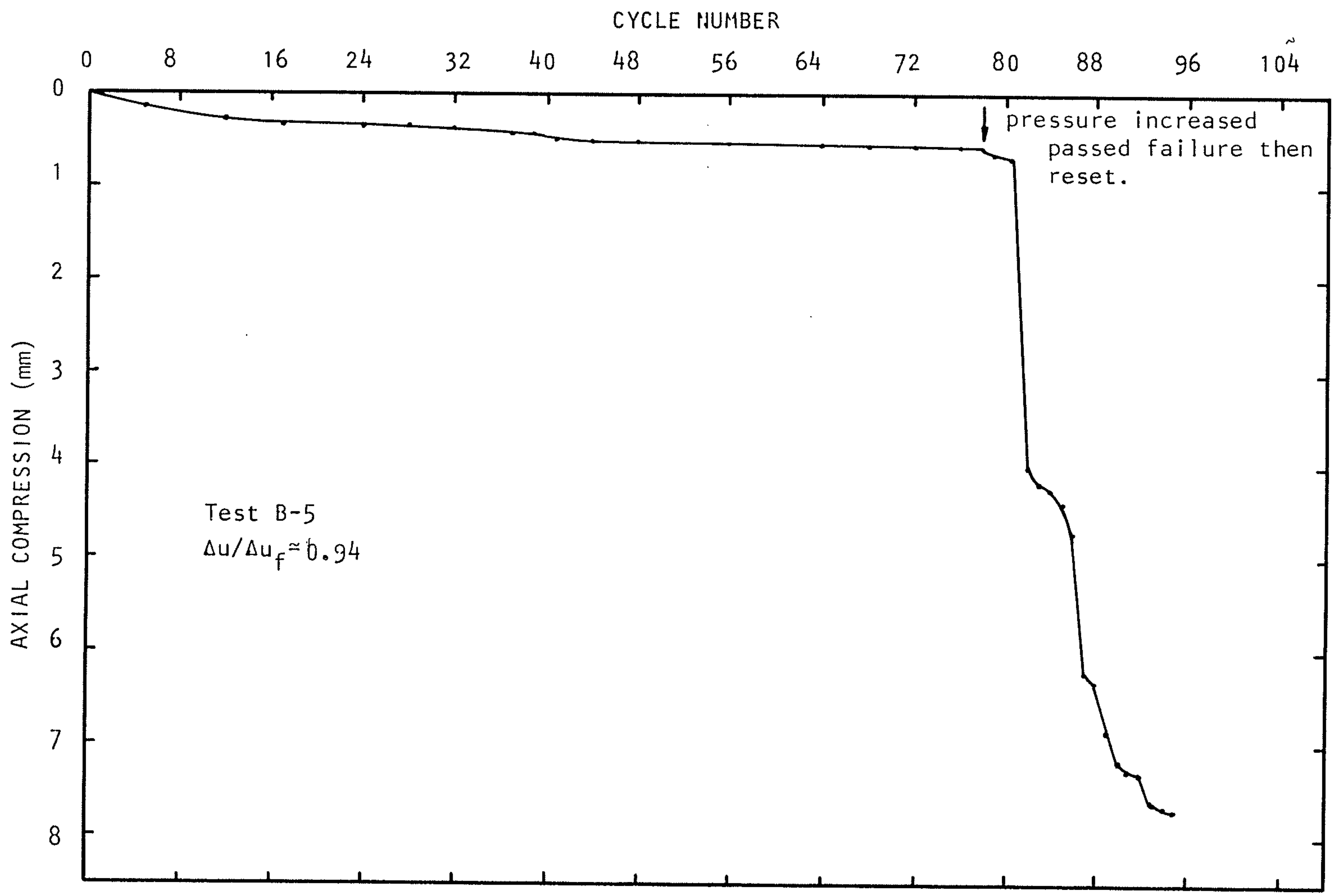

FIG. 5-6 BEHAVIOR OF SAMPLE B-5 DURING CYCLING AND FAILURE

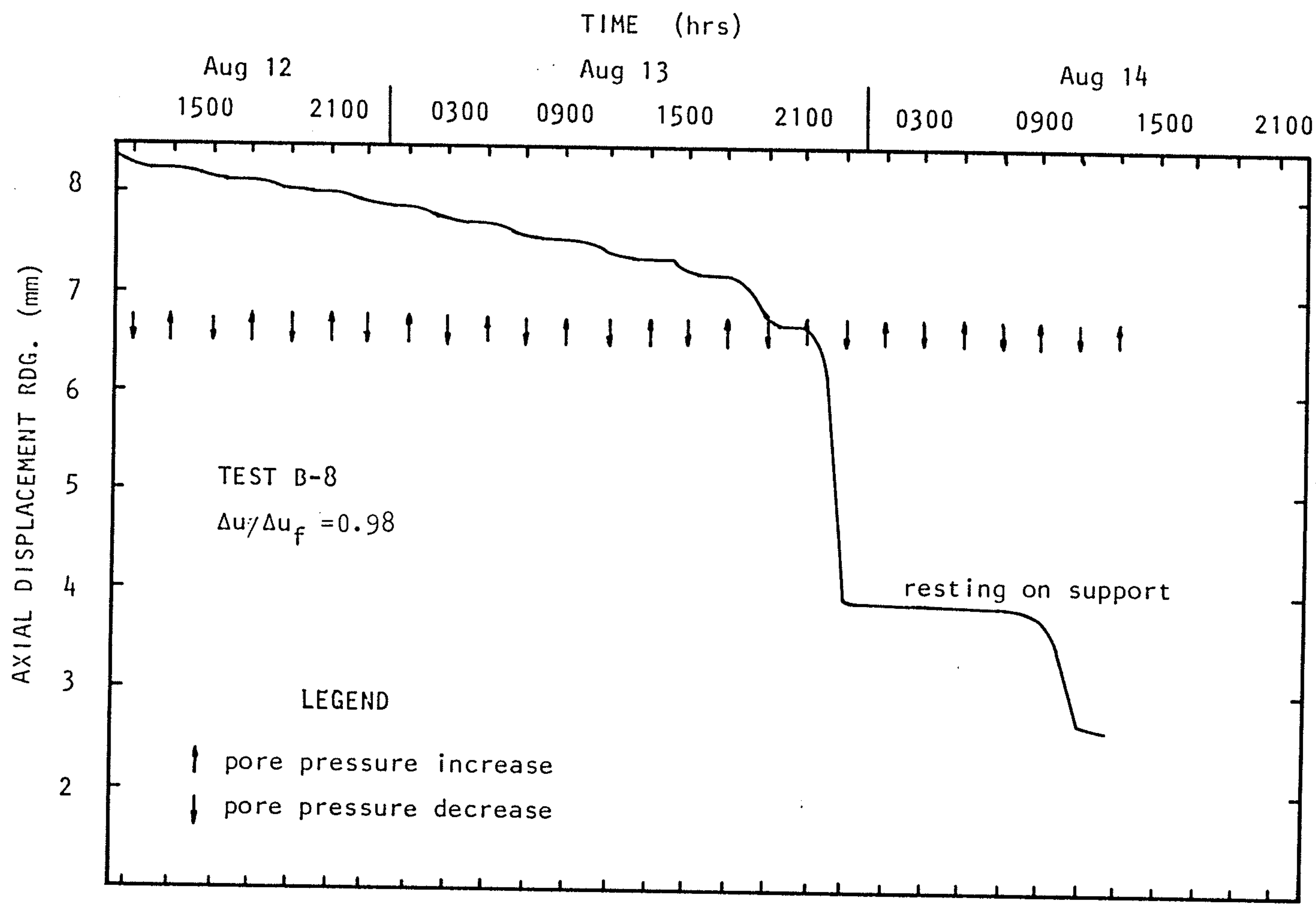

FIG. 5-7 BEHAVIOR OF SAMPLE B-8 DURING CYCLING AND FAILURE

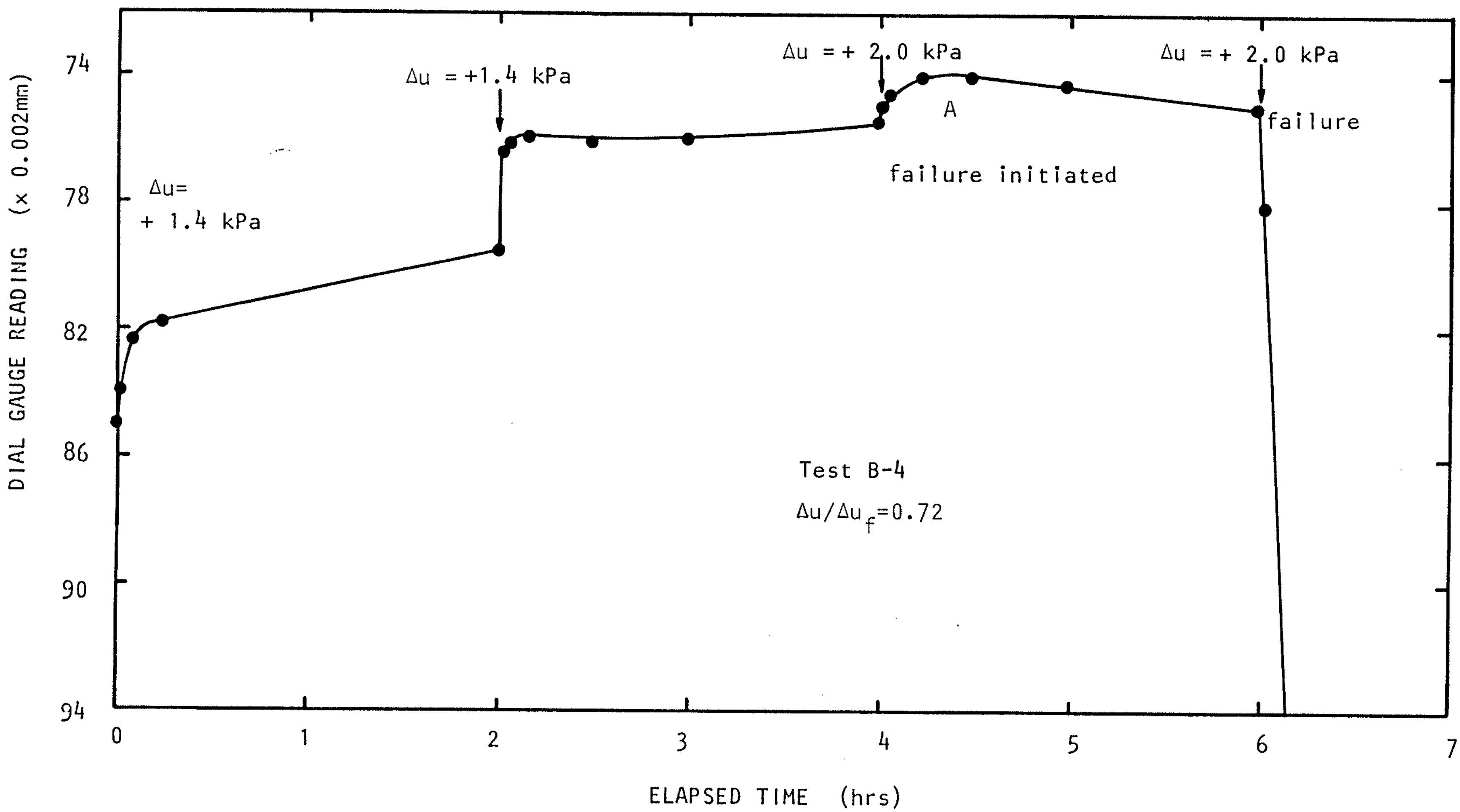

FIG. 5-8 BEHAVIOR OF SAMPLE B-4 DURING INCREMENTAL PORE PRESSURE INCREASES TO FAILURE

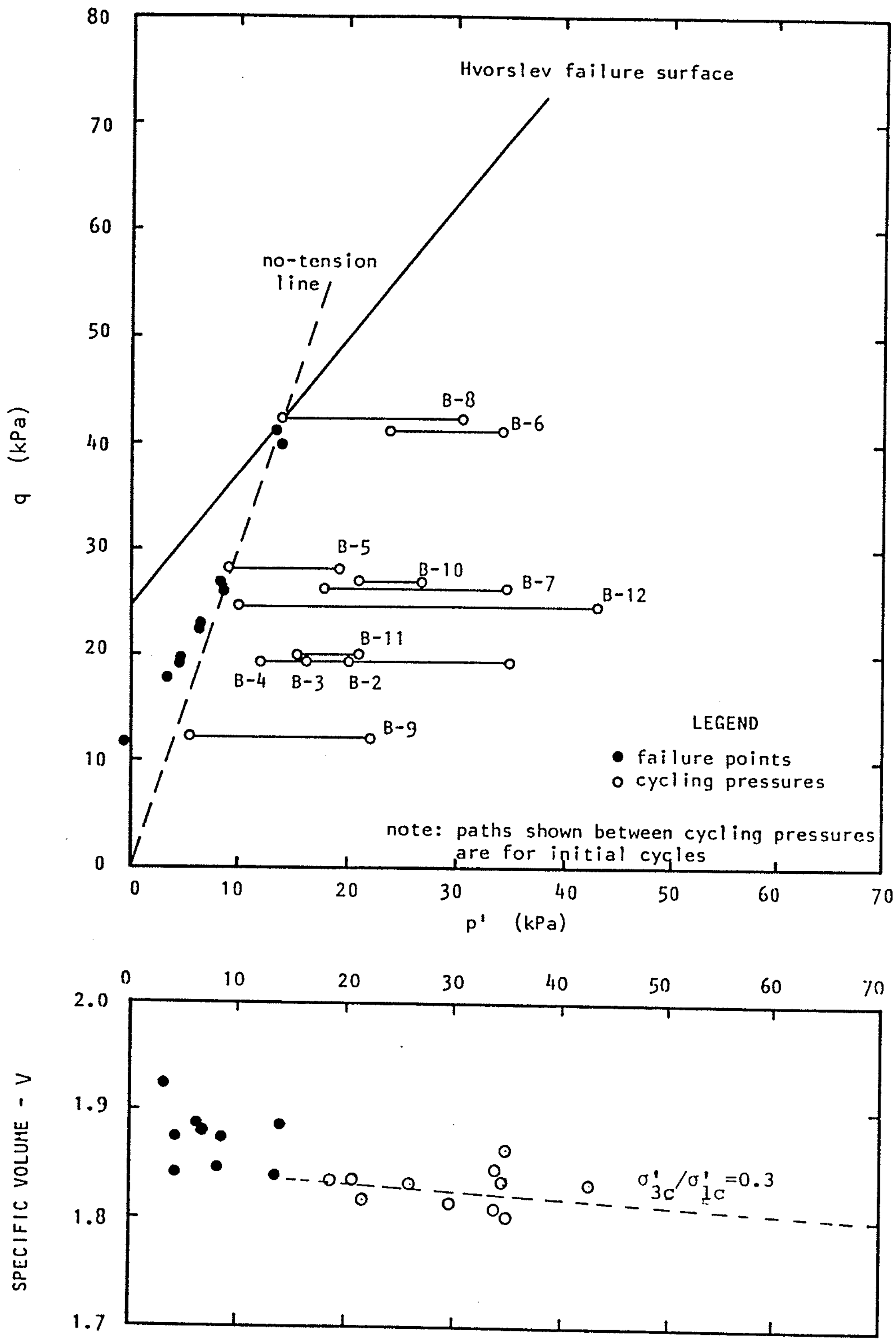

FIG. 5-9 COMPOSITE PLOT OF DTTCP TEST IN q,V,p' STRESS SPACE

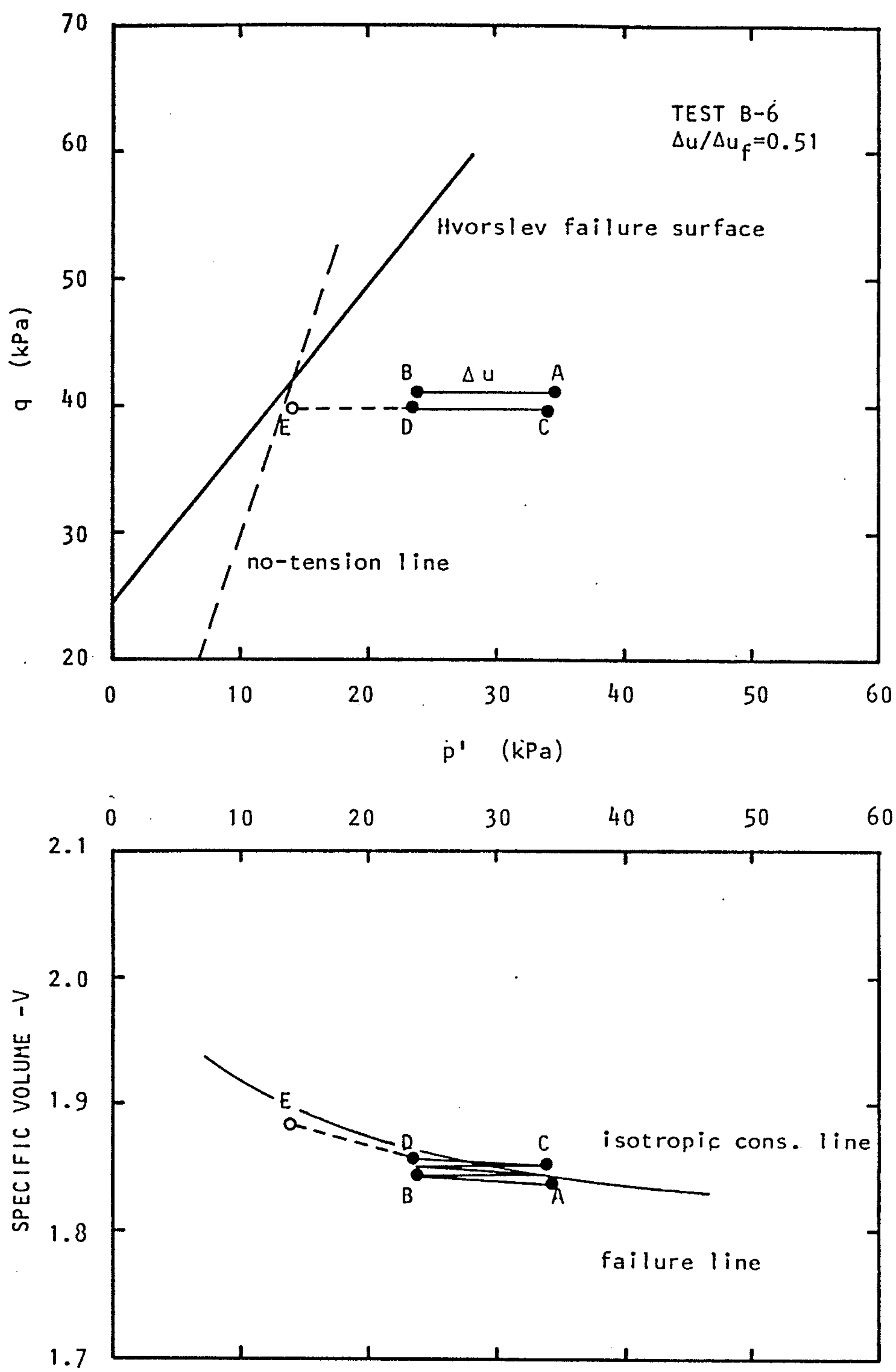

FIG. 5-10 TYPICAL STRESS PATH FOLLOWED IN DTTCP TEST

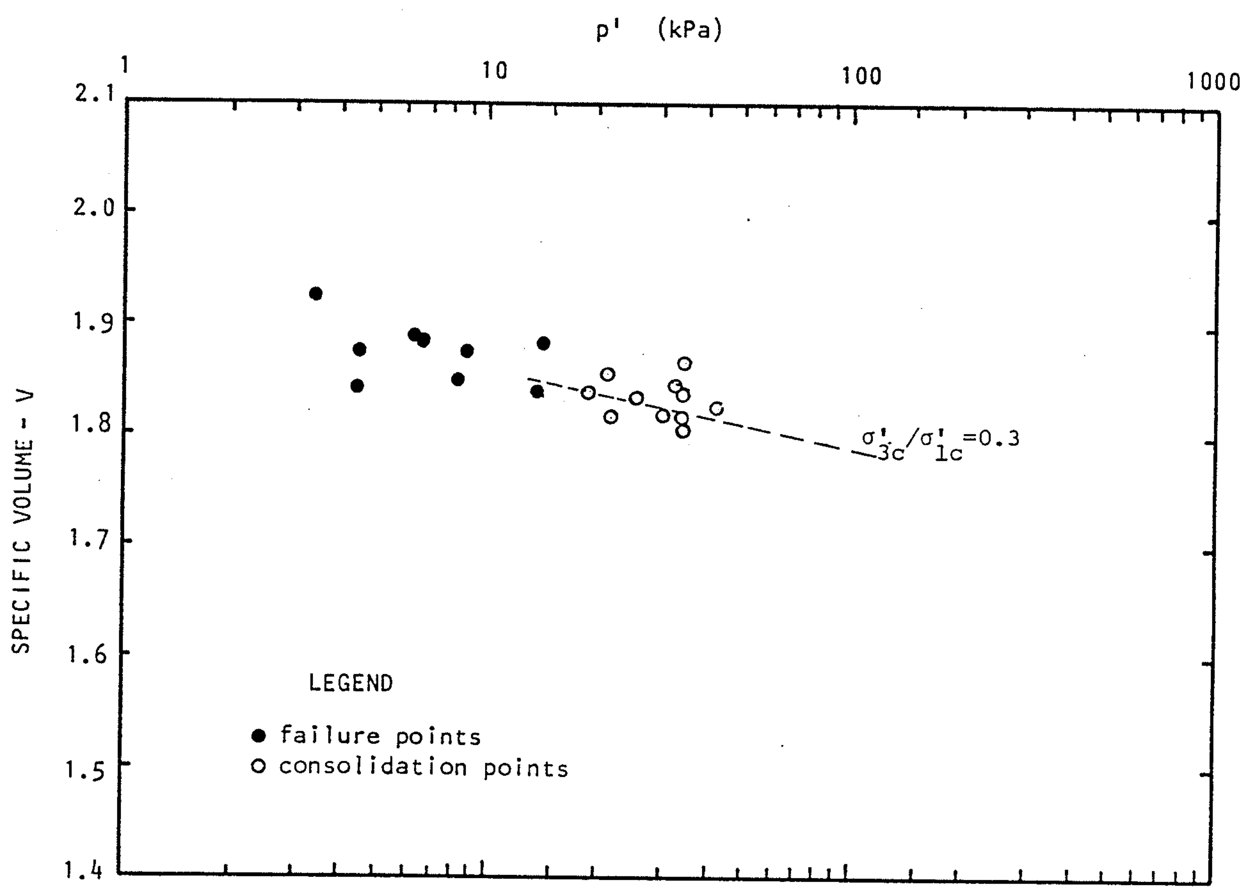

FIG. 5-11 V log p' PLOT OF DTTCP FAILURE CONDITIONS

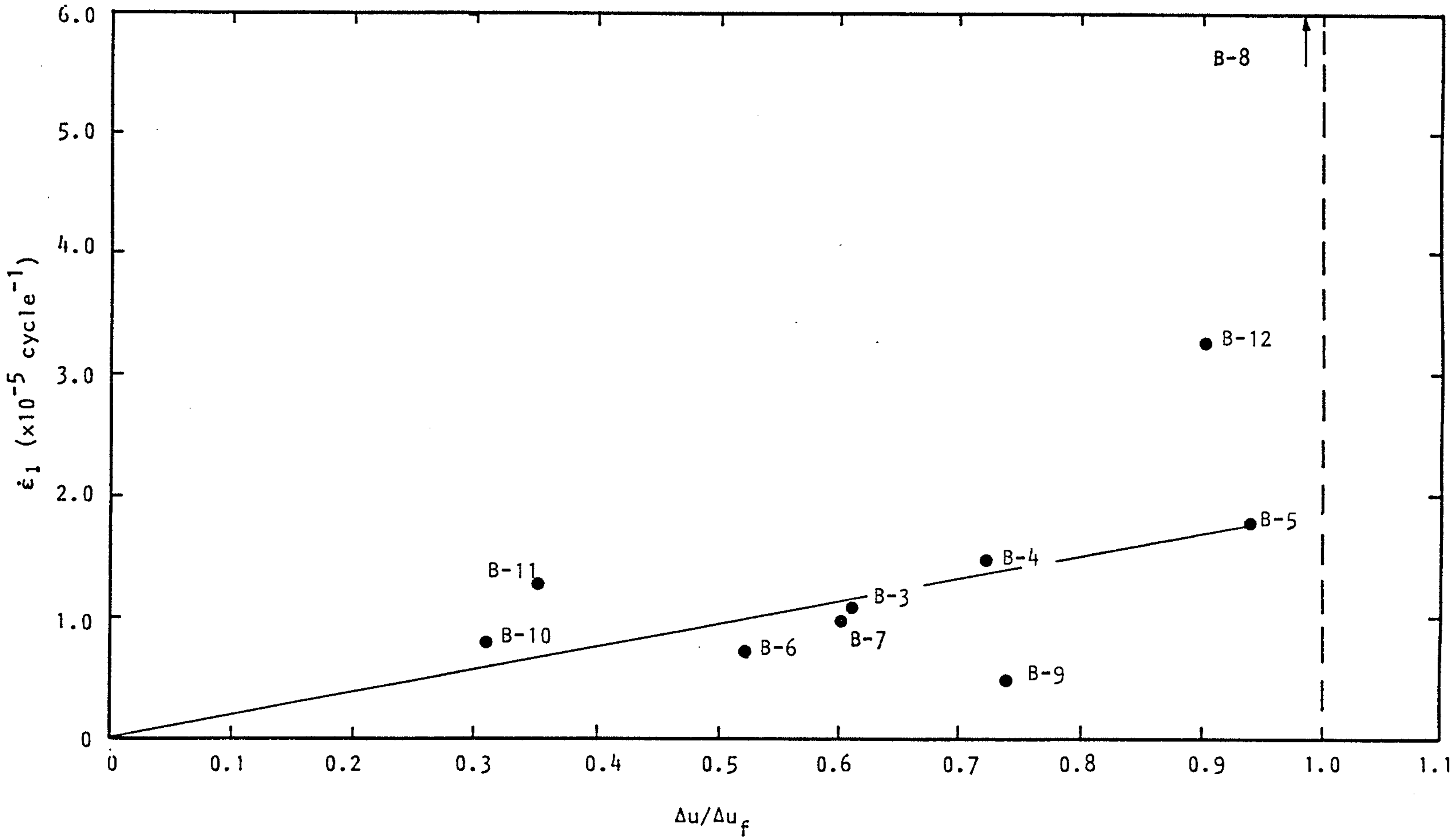

FIG. 5-12 $\dot{\varepsilon}_1$ vs. $\Delta u/\Delta u_f$ FOR DTTCP TESTS

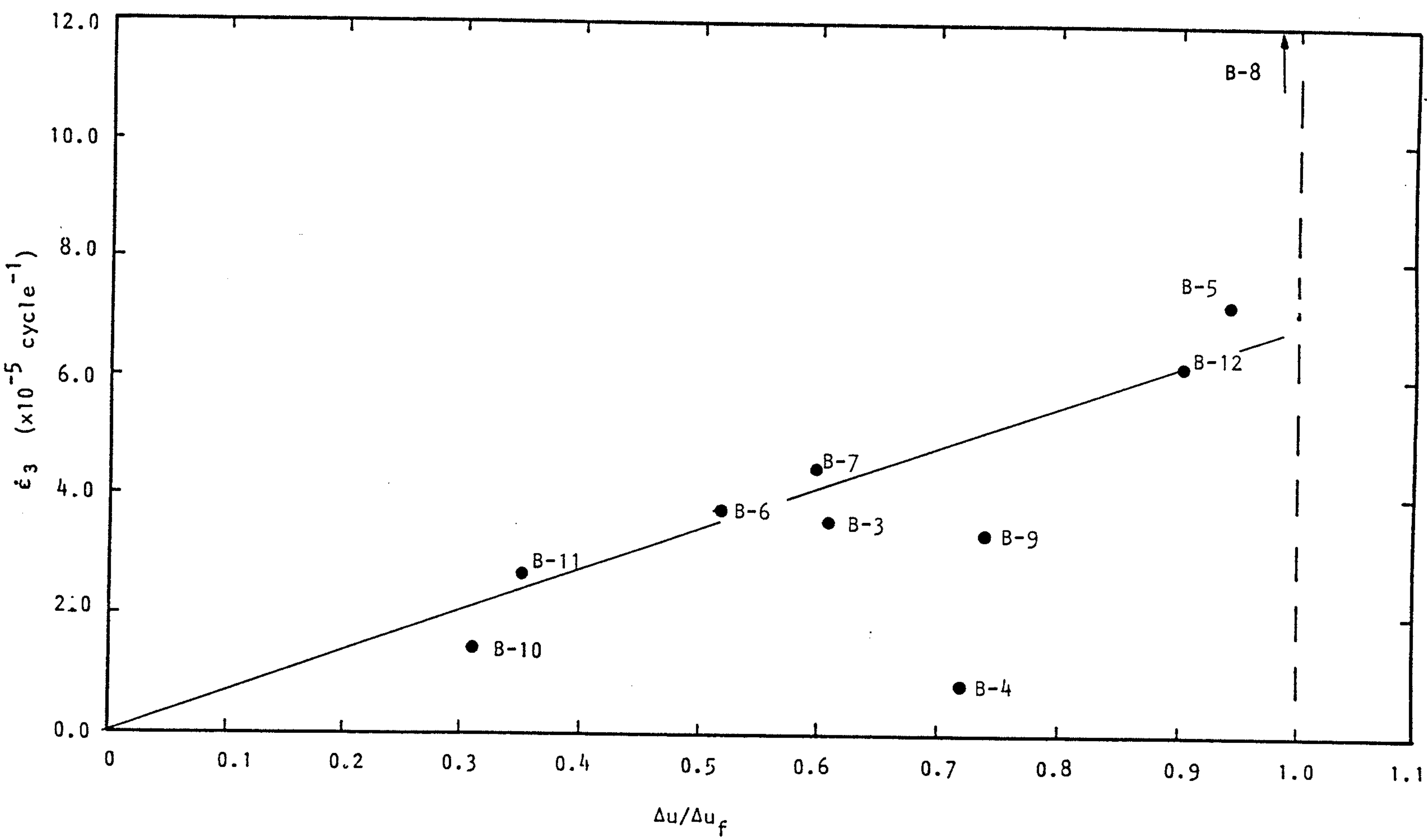

FIG. 5-13 $\dot{\varepsilon}_3$ vs. $\Delta u/\Delta u_f$ FOR DTTCP TESTS

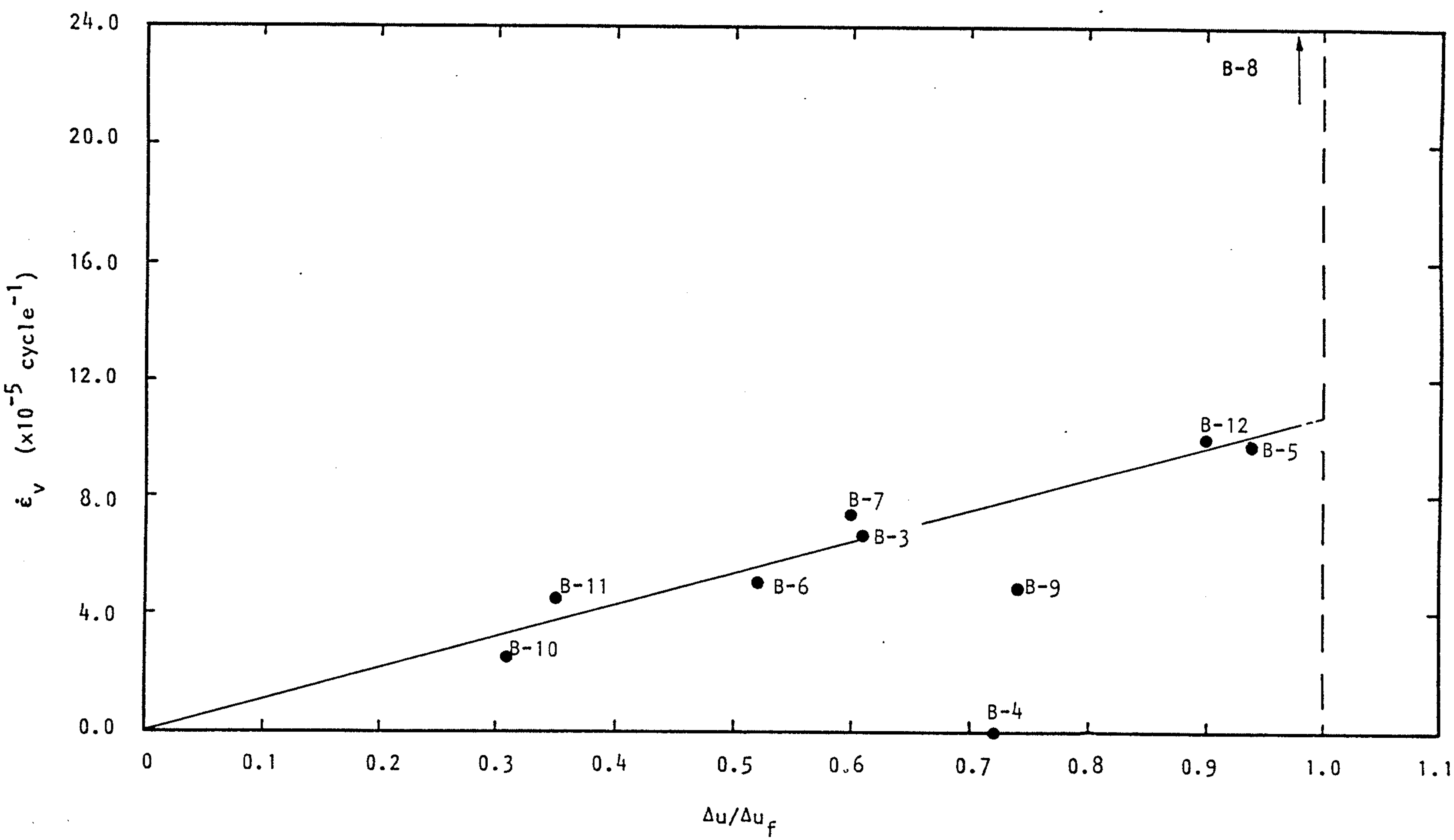

FIG. 5-14 $\dot{\varepsilon}_v$ vs. $\Delta u/\Delta u_f$ FOR DTTCP TESTS

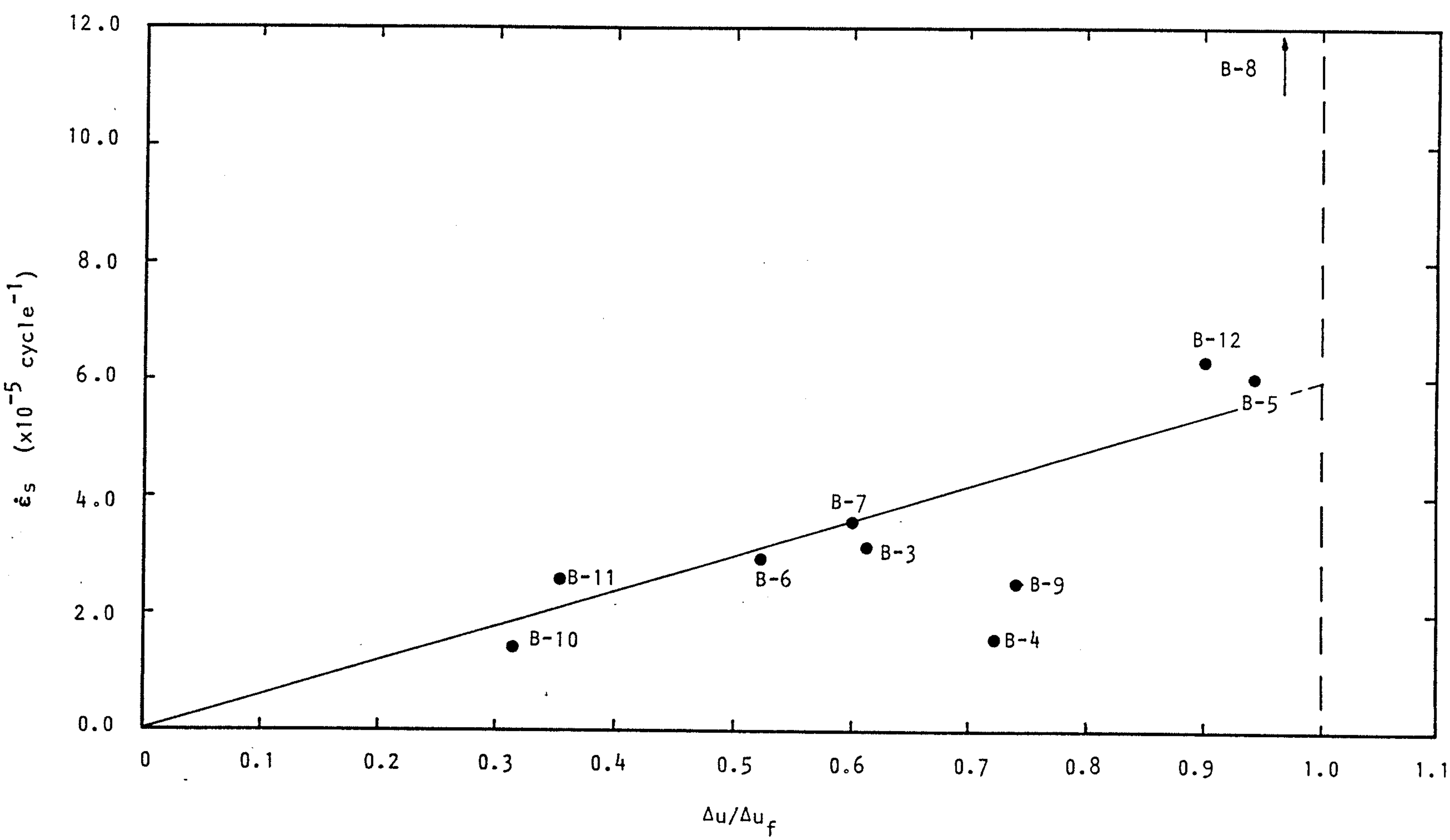

FIG 5-15 $\dot{\varepsilon}_s$ versus $\Delta u/\Delta u_f$ FOR DTTCP TESTS

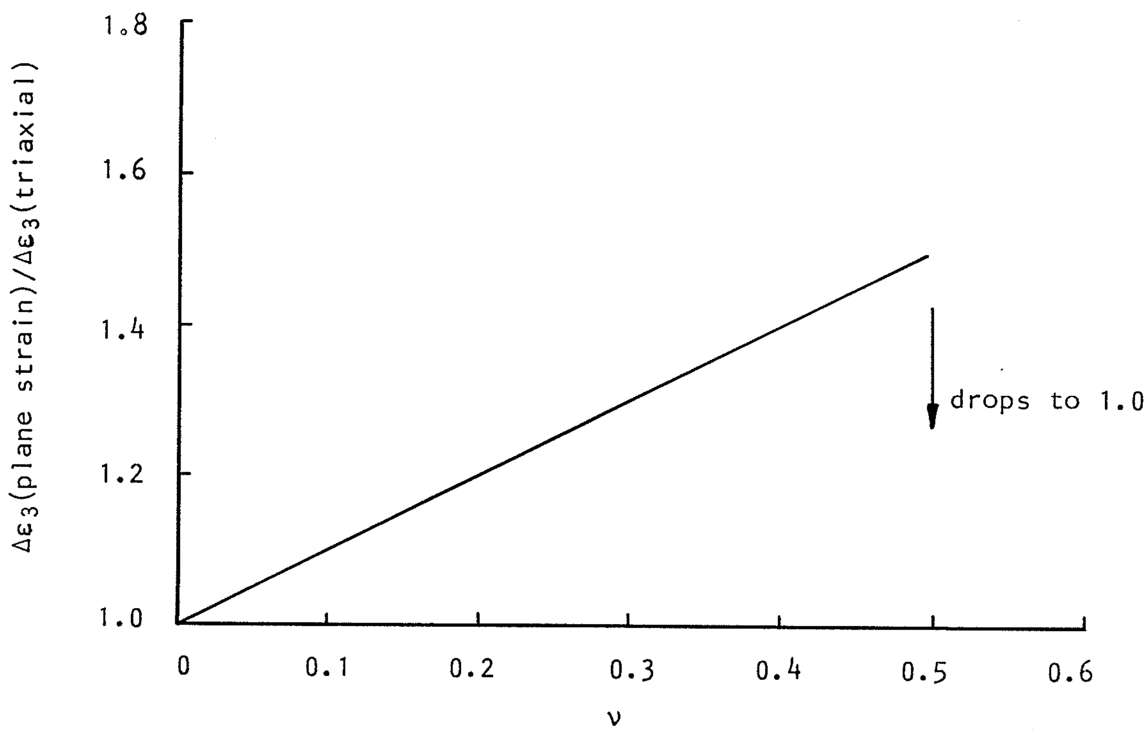

FIG 6-1 RELATIONSHIP BETWEEN $\Delta\varepsilon_3$(plane strain) AND $\Delta\varepsilon_3$(triaxial)

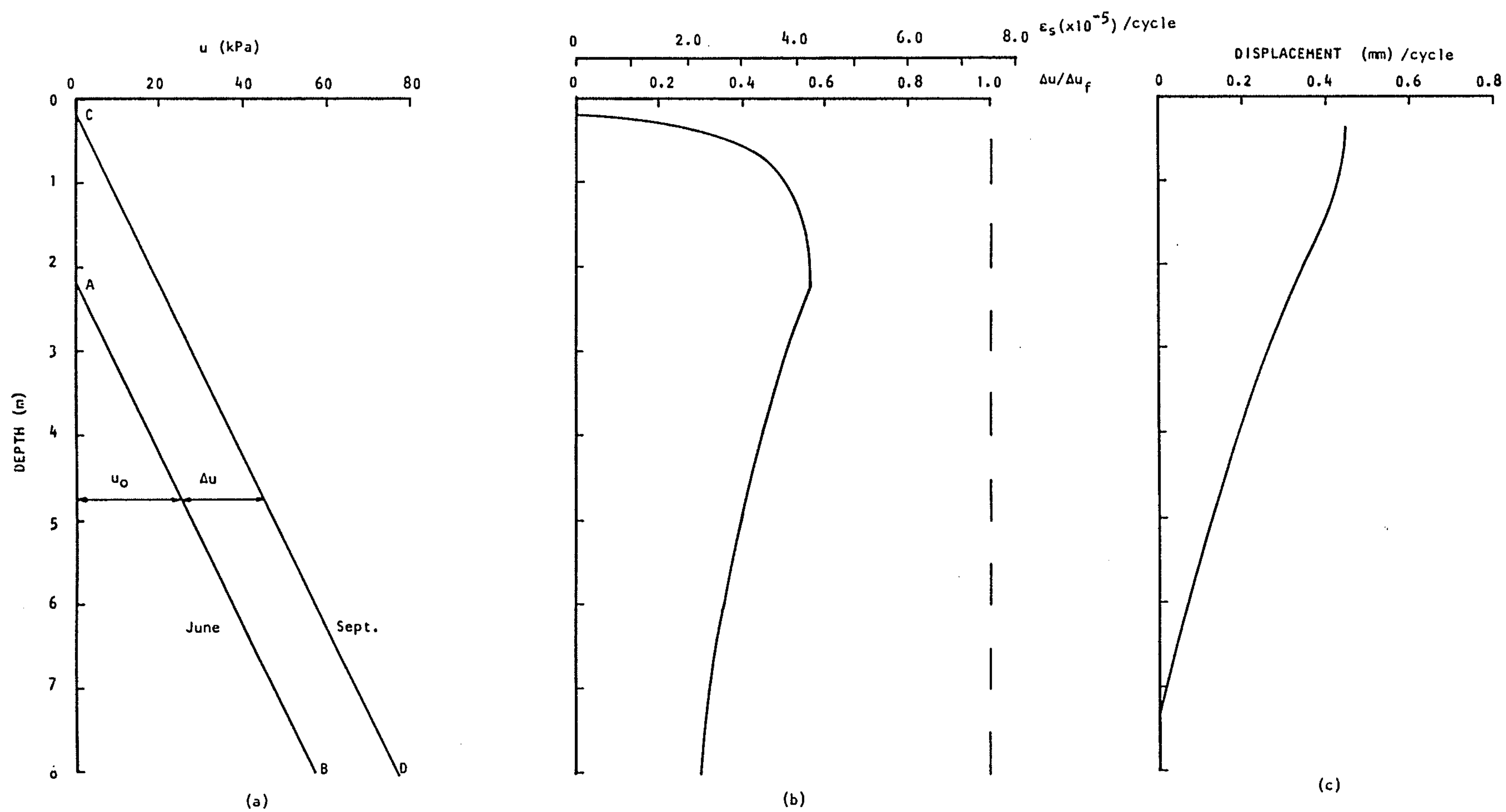

FIG 6-2 PORE PRESSURE VARIATION, SHEAR STRAIN AND DISPLACEMENT PROFILES FOR LOCATION SI-1 DUE TO GROUNDWATER FLUCTUATIONS

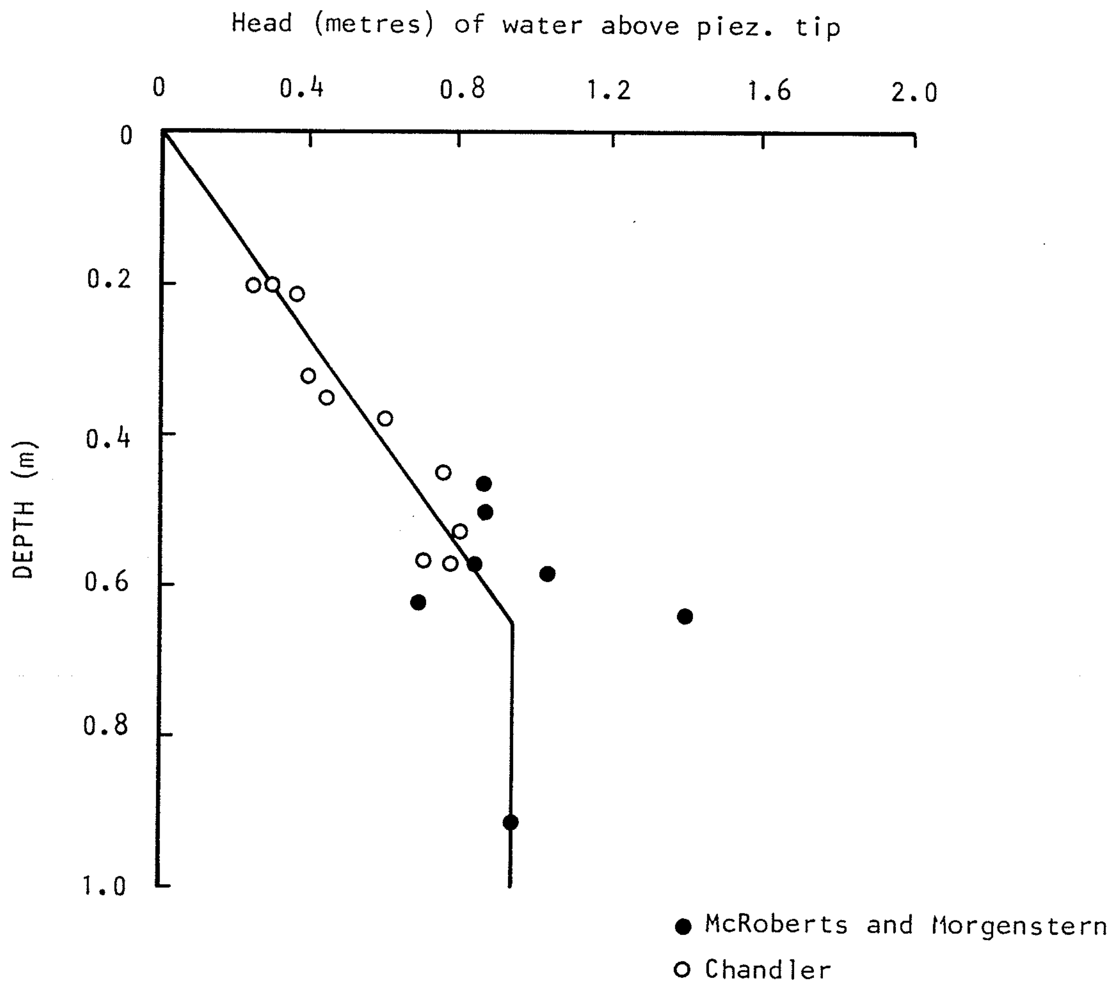

FIG 6-3 RECORDED PORE PRESSURES IN THAWING SLOPES

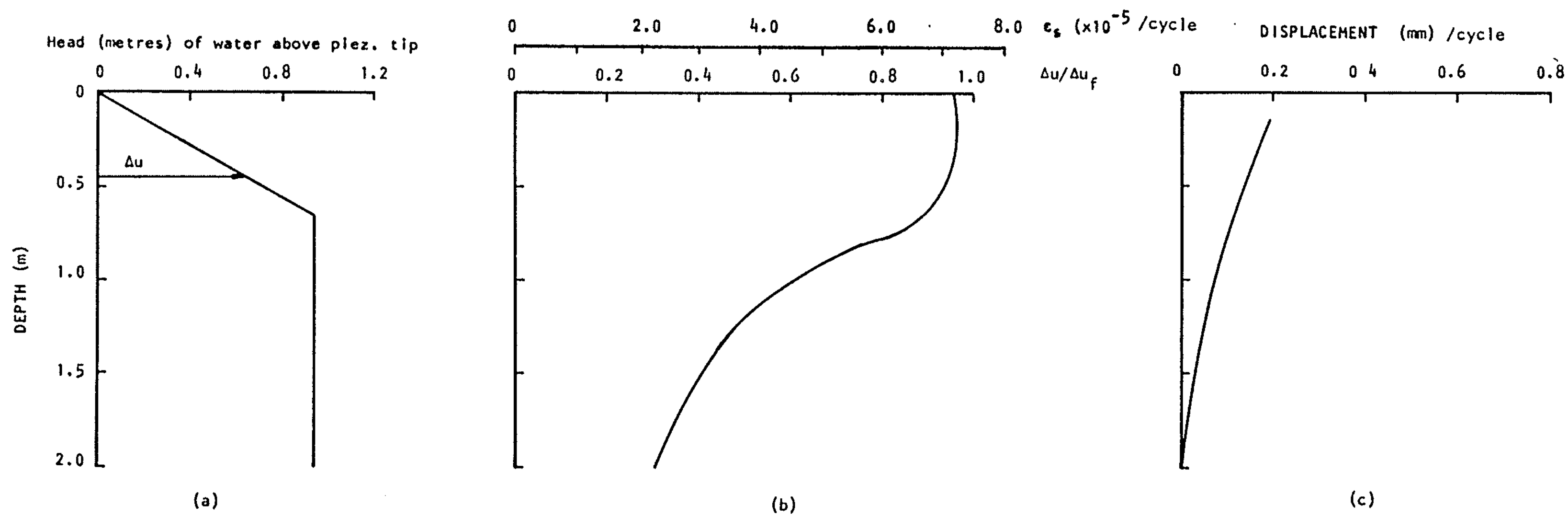

FIG 6-4 PORE PRESSURE VARIATION , SHEAR STRAIN AND DISPLACEMENT PROFILES FOR LOCATION SI-1 DUE TO THAWING

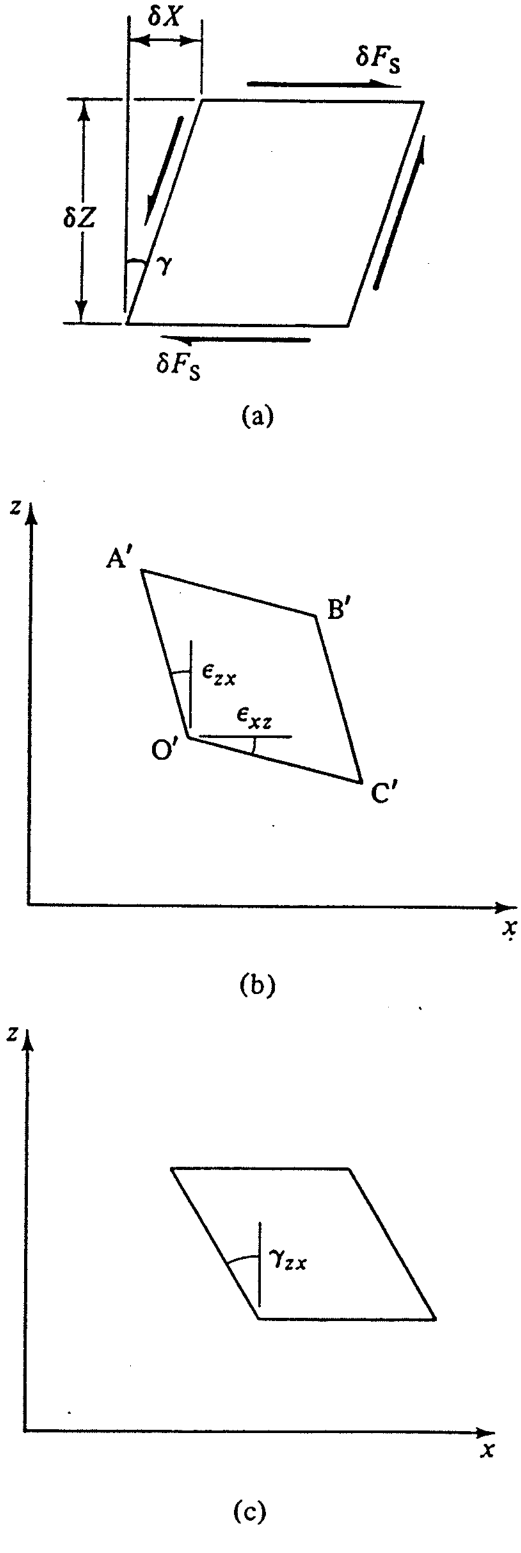

FIG 6-5 RELATIONSHIP BETWEEN PURE SHEAR STRAIN AND ENGINEERS' SHEAR STRAIN

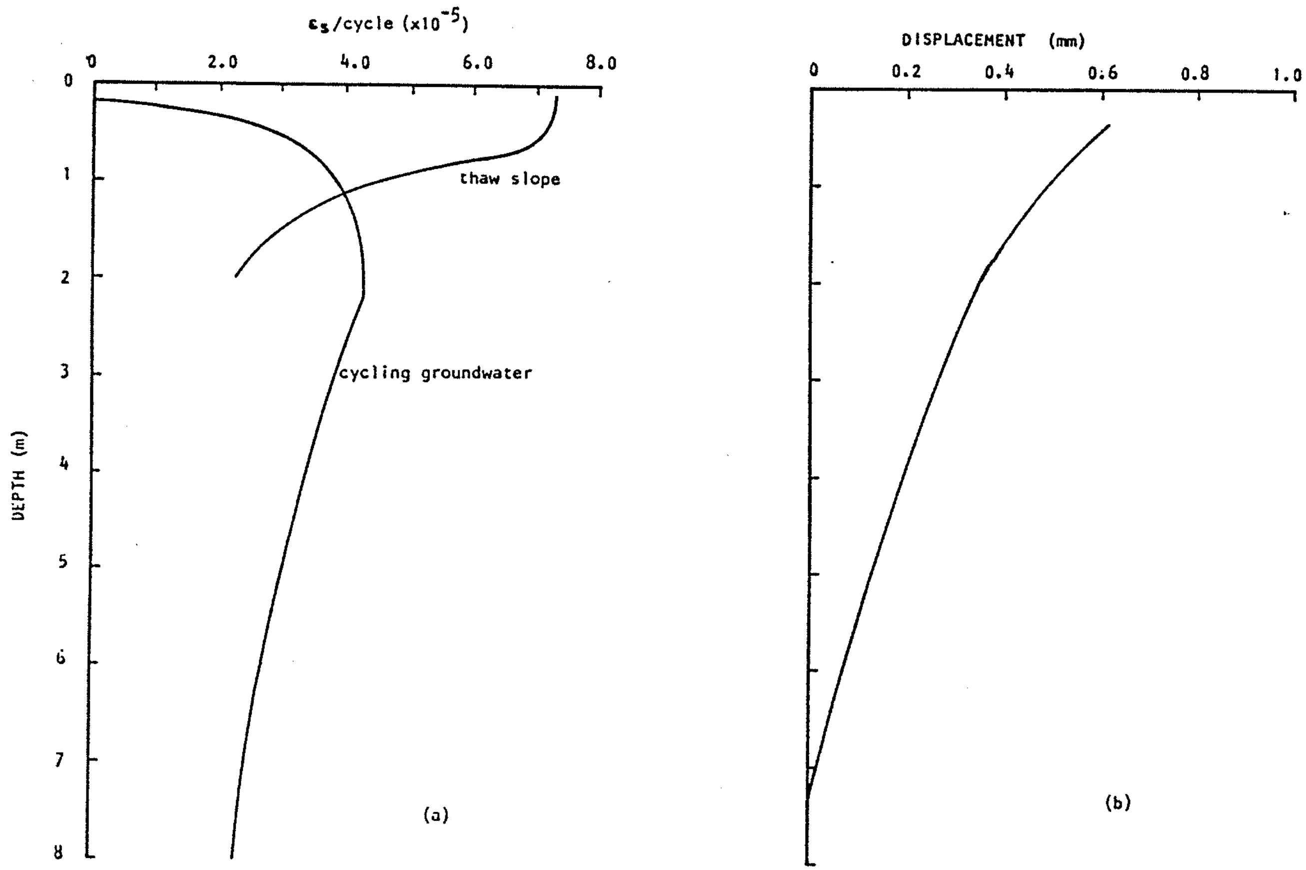

FIG 6-6 COMBINED DISPLACEMENT PROFILE FOR ONE-YEAR PERIOD FOR LOCATION SI-1

APPENDIX A - ADDITIONAL NOTES

REGARDING LABORATORY TESTING PROCEDURES

Table of Contents

A.1 Sample Preparation

A.1.1 Sample Trimming and Handling

A 2" x 2" x 6" piece of clay was cut from the block sample obtained at the 1.8m depth from TP1 and placed into a trimming frame between two end platens which rotated as well as held the sample in place. With a wire saw, thin slices were cut off the sample while the sample was rotated, until the final diameter of 1.4" (3.6 cm) was reached.

Care had to be taken when rotating the sample as well as during trimming. When rotating the sample, both the top platen as well as the bottom platen had to be turned at the same time to prevent any twisting of the sample. An alternate method would be to use a frame which rotated while the sample remained stationary. When lowering the top platen onto the sample care also had to be taken so no excess pressure would be exerted which would consolidate the sample or disturb it.

When trimming, the wire saw was run in an upward direction (bottom towards top) while being moved back and forth in a sawing motion. This had to be done slowly, otherwise, because of the fissured structure, the clay would tear off and leave an uneven surface with pits and holes in it. The trimming was done in an upward motion to prevent consolidation of the sample. However, in order to prevent upward tearing and distortion, the sample was held gently with two fingers immediately over the area being trimmed. This provided a force equal to that created by the saw and prevented further disturbance.

Because of the care which had to be taken during the trimming process, the total trimming time ranged from one-half to one hr. No surface, though, was exposed longer than 10 minutes, since thin slices were removed as the sample was rotated.

Once trimmed to an even diameter, the sample was removed from the trimming frame and the ends were trimmed off to provide a sample length of approximately 3". The sample was then wrapped in plastic foil and stored in a moist room till needed for the testing program.

A.1.2 Sample Set-Up

Initially,the cell pedestal and attached valves were deaired by flushing water through the lines by means of burettes attached to the pedestal drainage leads (L&M on Fig. 4-9). Water was flushed through the pedestal until no more air was detected (evidenced by bubbles).

A saturated porous stone disc was then slid on to the pedestal after which filter paper was placed on the porous stone to protect the porous disc from fines of the soil sample. The sample was weighed and measured for its length and diameter then placed on the pedestal. A thin coat of silicone grease was applied to the sides of the pedestal and the load cap (subsequently placed on the top of the sample) to reduce the possibility of leaks. Water saturated filter paper drains were carefully placed in position around the specimen, ensuring overlapping of the porous disc to provide adequate drainage. A thin rubber membrane was placed over the sample using a membrane stretcher, and the lower section sealed against the pedestal using one o-ring.

The space between the sample and the membrane was deaired by raising the wash burette (on Fig. 4-9), creating a small hydrostatic head sufficient for the water to flow upwards in this space. A small, plastic coated wire was inserted between the membrane and the top cap in order to allow the water and air to escape while the sample was gently stroked with an upward motion.

A layer of silicone oil was then applied to the outside of the first membrane, and again using the membrane stretcher, a second membrane was placed to reduce the possibility of leaks during the long duration of the tests.

The second membrane was sealed at both the base and top with 2 o-rings each.

A thin coat of silicone grease was applied to the cell base before the cell top was fitted to the base and screwed down. Water was then placed into the cell until nearly full. In order to reduce leakage along the load piston, a layer of oil (about 10mm) was poured into the cell from the top. The loading ram, with displacement transducer and dial gauge already attached, was then slowly lowered until it just made contact with the sample. After the loading ram was locked in place, filling of the cell was continued until no more air was evident.

Subsequently, the drainage lead to the wash burette was sealed off and the level in the back pressure burette was set at midheight of the sample (during calibration the water level in both the cell and the back-pressure burette was set at this height and these readings taken as the 'zero' readings). The back presssure was then hooked up to the air supply line, and the hanger placed on the piston with the correct amount of weight applied. The hanger which was used to apply constant axial loads was allowed to hang freely and was protected against disturbances. The weights were added to the hanger while the piston was supported by an arm to prevent any uncontrolled load applications. With the valves to the cell base in the off position, both the cell and back pressures were applied.

The test specimen was then ready for the first stage of testing which was the anisotropic consolidation.

A.2 Load Application

During the anisotropic consolidation of the samples, the water level in the back pressure burette (for volume changes) was recorded manually whereas, the height of the sample was recorded manually using a dial gauge as well as automatically using a displacement transducer connected to the data acquisition centre. Two tests were run simultaneously, both utilizing the same backpressure line and subsequently the same pore pressure variations.

At the beginning of the consolidation stage, initially, it was difficult to apply all three stresses simultaneously; σ_3, σ_1 and back pressure. Originally, when the piston and weight were not supported by an arm, a second person was required to add the weights onto the hanger while the pore pressure and the cell pressure were applied. This method was found to be awkward and unsatisfactory because when the cell pressure was added, the piston was forced upwards and lost contact with the sample. Subsequently, when the weights were added, the piston was forced back into contact with the sample, sometimes causing a slight jolt to the sample.

This method was modified during the early stages of the test series: the piston, and hanger with weights applied, were supported by an arm with the piston just making contact with the sample. At the start of the test the cell pressure was applied shortly before the back pressure, and immediately after, the arm supporting the axial load was released and slowly lowered, thus transferring the weight onto the sample. This procedure had the additional advantage that only one person was required to perform it. The two tests could not be initiated exactly at the same time but had to be started about one hour after each other. The cycling of the pore pressure however, occurred simultaneously.

A.3 Calibration Procedure

The final calibrations for both the cell and pore pressure transducer was accomplished by filling the triaxial cell with water to approximately mid-height sample depth. Pressure lines from an air pressure source were connected to the top of the triaxial cell as well as to one end of a mercury monometer (Fig.A-1). Air pressure was applied in steps of 5 psi and the voltage readings from the pressure transducers was recorded, by opening values A and B while keeping valves C and D closed, along with the corresponding height difference in the mercury monometer. This gave a relationship between pressure as determined by the height of mercury, and voltage output for each transducer which was subsequently used in the data logger. This calibration, however, had to be completed twice for each test, because the transducers had a tendency to 'drift' during the testing. In order to determine the exact pressures at failure, the calibration was performed immediately after the sample was brought to failure. From this calibration, it was possible to determine the condition at failure by back calculations using the previous calibration to determine the voltage output, then inputing this voltage reading into the new calibration to obtain the correct pressure reading. The transducer used for the second cell drifted considerably and was subsequently not used in the latter tests. The cell pressure was determined using the pore pressure transducer which was connected to the same cell. Once this pressure was set, the line was switched back to the cell access valve.

The displacement transducer was calibrated using a triaxial loading frame and a dial gauge connected to the transducer. The platform of the loading frame was raised manually, with the known displacement measured off the dial gauge. The corresponding voltage output was recorded for each movement and a calibration formula was determined from this. The displacement transducers were found not to drift at all but remained stable throughout the testing program.

A.4 Failure Criteria for CIU Tests

The criteria for selecting the failure points for the CIU Tests were based on the condition for overconsolidated clays that the stress path, when plotted in q-p' stress space, will approach the Hvorslev surface and then proceed along the surface until critical state is reached. Atkinson and Bransby (1978) state that "...there is the possibility that failure of a triaxial sample occurs prematurely, probably soon after the sample reaches the Hvorslev surface...". This is considered to be the result of inhomogeneities within the sample.

Using this, all the values for the failure conditions were obtained by approximating when the stress path of each of the tests intercepted the Hvorslev surface, or when the stress path at least continued at a slope approximately parallel to the surface. A summary of these values are presented in Table A-1 for each test and the individual test data are presented in Appendix C.

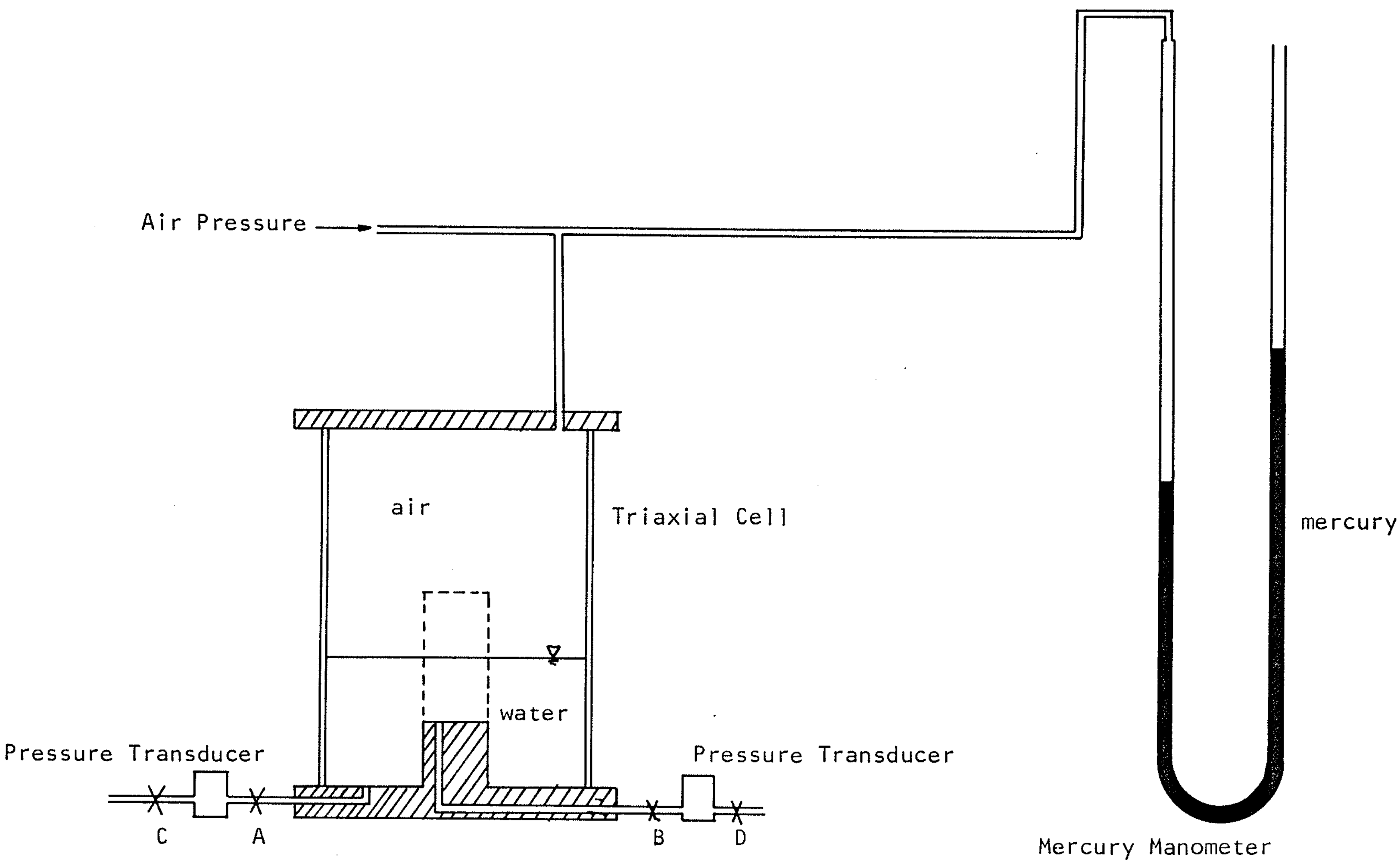

FIG. A-1 EQUIPMENT SET-UP FOR TRANSDUCER CALIBRATION

TABLE A-1 SUMMARY OF FAILURE CONDITIONS FOR CIU TESTS

TEST	CIU-1	CIU-2	CIU-3	CIU-4
σ'_{1c} (kPa)	15	27	40	300
σ'_{3c} (kPa)	15	27	40	300
ε_f (%)	4.53	5.84	4.22	5.05
σ'_{1f} (kPa)	121.5	153.0	162.0	676.8
σ'_{3f} (kPa)	29.0	30.0	38.0	198.0
q_f (kPa)	92.5	123.0	124.0	478.8
p'_f (kPa)	59.0	71.0	79.3	357.6
u_f (kPa)	196.0	204.0	201.0	302.0
A_f	-0.15	-0.02	0.01	0.19

A.5 Method for Determining σ'_{vc}

The value for the preconsolidation pressure cannot be easily determined, since due to the lack of clarity in the curvature, the Casagrande method cannot be applied. According to Graham, Pinkney, Lew and Trianor (1981) "Unthinking application of the Casagrande construction can apparently produce values for σ'_{vc} even though the samples do not yield in the sense that the compressibility increases at some identifiable limit stress." It was further stated that "...care should be taken that the plotting technique does not imply behavior that is absent from the original data." For this reason, results from both consolidation tests were plotted on an arithmetic scale, in a ln scale for σ'_v and in a ln scale for p'. The values for p' for the one-dimensional consolidation were determined by estimating K_o using the correlation $K_o = 1 - \sin\phi'$. From the V-lnσ'_v diagram, σ'_{vc} was estimated to be between $\ln\sigma'_v = 5.25$ to 5.50, resulting in a $\sigma'_{vc} = 190$ kPa to 245 kPa. This selection was also based on observations on the effect of sample disturbance presented in Holtz and Kovacs (1981).

A.6 Method for Calculating the Change in Sample Diameter

The method used for calculating the change in diameter is shown below, with the assumption that the sample diameter changes are uniform throughout the length of the sample.

Starting with the formula for volume of a cylinder,

$$V = \frac{\pi D^2}{4} \times H$$

any increase in both diameter and height will reflect an increase in volume.

Therefore

$$V + \Delta V = \pi(D+\Delta D)^2(H+\Delta H)/4 \qquad (1)$$

rearranging,

$$\Delta D = 2\sqrt{\frac{V+\Delta V}{(H+\Delta H)\pi}} - D \qquad (2)$$

This is for a cylinder increasing in size. In soil mechanics, it is common to assign compression values as positive, therefore, Eq. 2 changes to

$$\Delta D = D - 2\sqrt{\frac{V+\Delta V}{(H+\Delta H)\pi}} \qquad (3)$$

in which a positive value of D denotes a reduction in sample diamter.

A.7 DTTCP Stress Paths

The stress paths presented on the following pages were obtained using the stress conditions from each test as well as the average initial moisture content calculated for the block sample and the samples' actual unit weight. Using the relationship

$$\frac{\gamma}{\gamma_w} = (1-\frac{1}{V})(\frac{1}{w} + 1)$$

where γ = unit weight of the soil

γ_w = unit weight of water (9.81 kN/m^3)

V = specific volume ($V = 1 + e$)

w = water content (31%)

the value for V was obtained for the sample prior to consolidation. From the volume readings taken during the consolidation and DTTCP testing, and the stress conditions on the sample, it was possible to calculate the samples' position in q-p'-V space at any time during the testing. For the plots on the following pages, q, p' and V were determined for the first and the last cycles as well as for the condition just prior to failure.

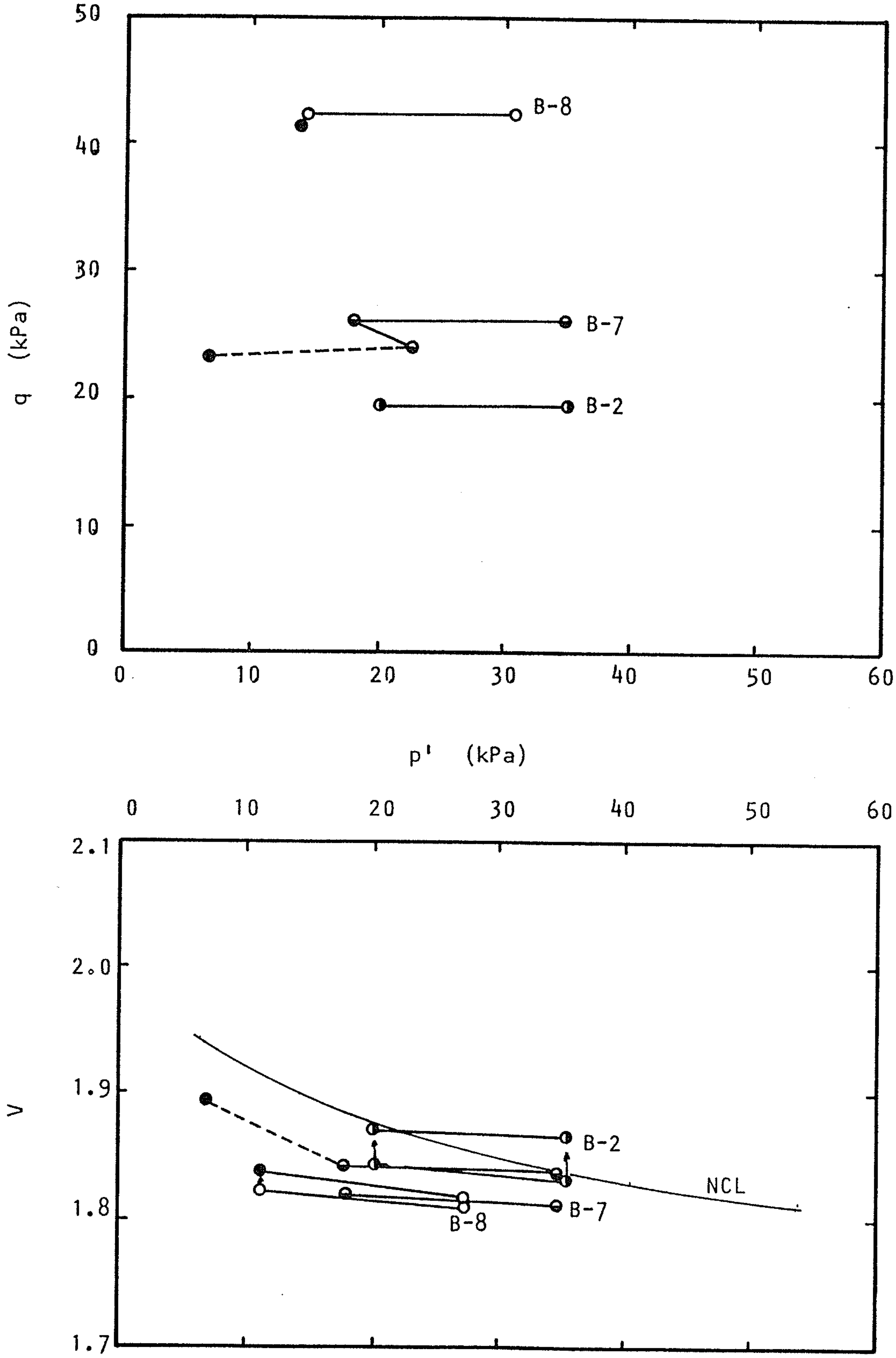

FIG. A-2 DTTCP STRESS PATHS

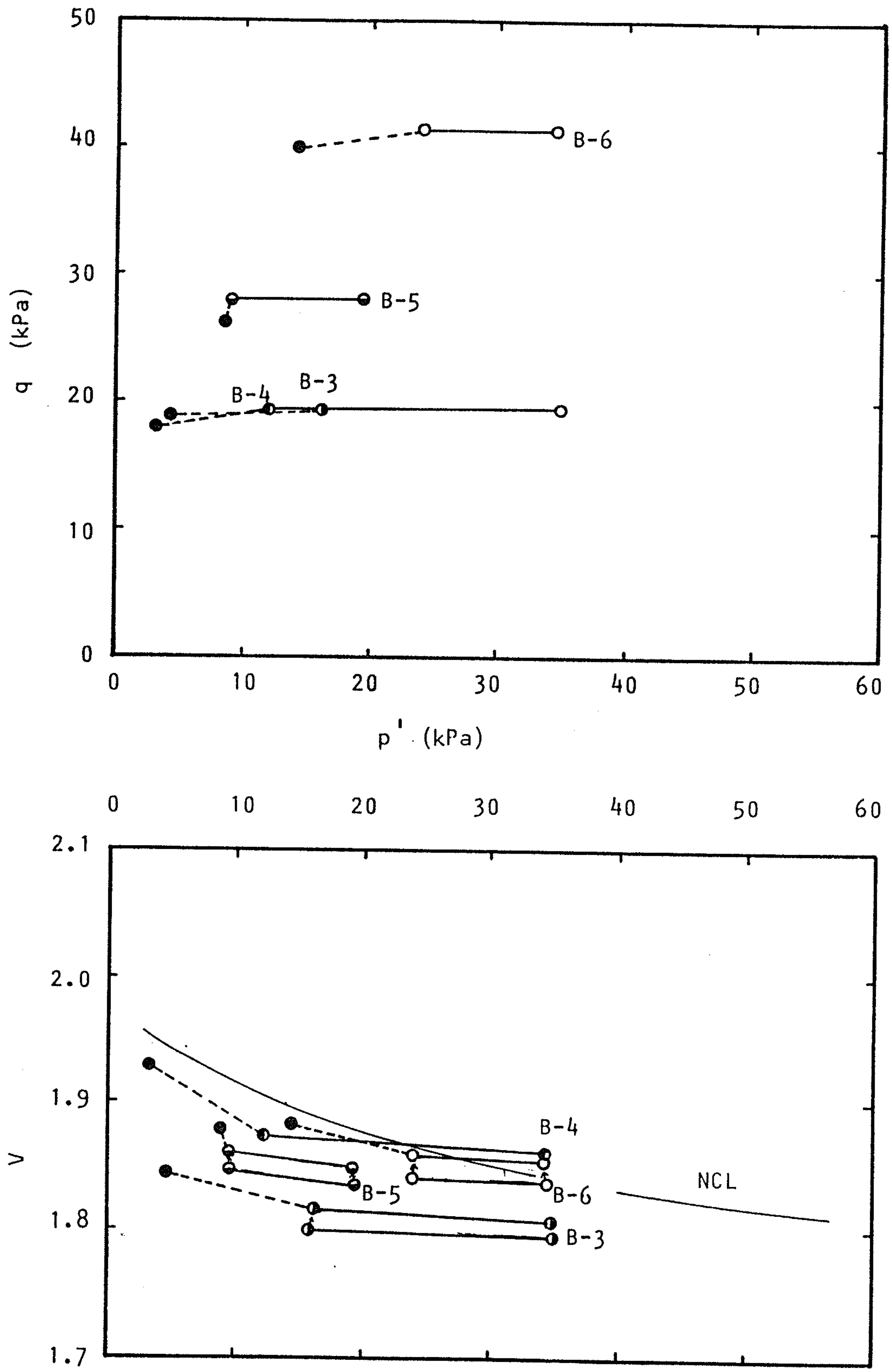

FIG. A-2 (con't) DTTCP STRESS PATHS

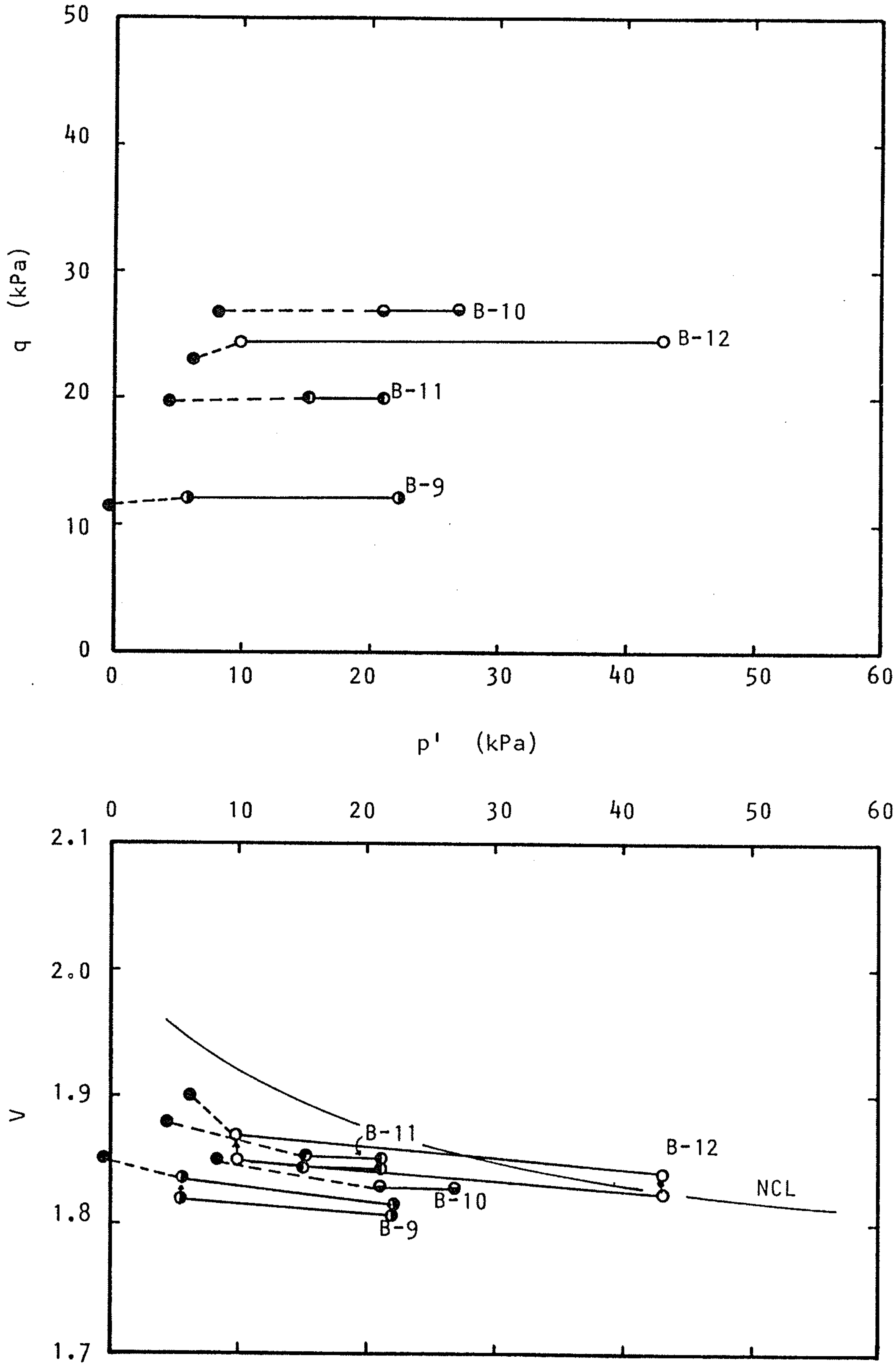

FIG. A-2 (con't) DTTCP STRESS PATHS

A.8 Strain Rates versus $\Delta u/\Delta u_f$ using Δu_f as Pore Pressure Change Required to Produce Failure on the Theoretical No-Tension Line.

This section presents the individual plots of $\dot{\varepsilon}_1$, $\dot{\varepsilon}_3$, $\dot{\varepsilon}_s$ and $\dot{\varepsilon}_v$ versus $\Delta u/\Delta u_f$ in which the ratio $\Delta u/\Delta u_f$ represents the change in pore pressure, Δu, as a fraction of the total pore pressure required to produce failure at the theoretical failure line, at the respective stress level q_o (see Fig. A-3. The total pore pressure required to produce failure is expressed as the difference between p'_{cons} and p'_{nt} where p'_{cons} is the octahedral stress at which the sample was consolidate to and p'_{nt} is the octahedral stress at the no tension line which corresponds to the stress level q_o. Table A-2 presents the summary of all the DTTCP tests using this ratio and the following figures show the composite plot of ε_1 versus cycle number as well as the respective plots of $\dot{\varepsilon}_1$, $\dot{\varepsilon}_3$, $\dot{\varepsilon}_s$ and $\dot{\varepsilon}_v$ versus $\Delta u/\Delta u_f$.

TABLE A-2 SUMMARY OF DTTCP TESTS

TEST	σ_{1c} (kPa)	σ_{3c} (kPa)	k_{cons}	q (kPa)	p' (kPa)	Δu (kPa)	Δu_f (kPa)	$\Delta u/\Delta u_f$	$\dot{\varepsilon}_1$ ($cycle^{-1}$)	$\dot{\varepsilon}_3$ ($cycle^{-1}$)	$\dot{\varepsilon}_v$ ($cycle^{-1}$)	$\dot{\varepsilon}_s$ ($cycle^{-1}$)
B-2	48.0	28.6	0.60	19.4	35.1	15.0	28.6	0.52	0.5×10^{-5}	-8.04×10^{-5}	-15.83×10^{-5}	5.69×10^{-5}
B-3	48.0	28.6	0.60	19.4	35.1	18.7	28.6	0.65	1.09×10^{-5}	-3.57×10^{-5}	-6.70×10^{-5}	3.11×10^{-5}
B-4	48.0	28.6	0.60	19.4	35.1	22.9	28.6	0.80	1.48×10^{-5}	-0.86×10^{-5}	-0.0	1.56×10^{-5}
B-5	38.2	10.1	0.26	28.1	19.5	10.1	10.13	1.00	1.77×10^{-5}	-7.27×10^{-5}	-9.84×10^{-5}	6.03×10^{-5}
B-6	62.0	20.7	0.33	41.3	34.5	10.5	20.7	0.51	0.70×10^{-5}	-3.80×10^{-5}	-5.10×10^{-5}	3.00×10^{-5}
B-7	52.2	26.0	0.50	26.2	34.7	16.7	26.0	0.64	1.00×10^{-5}	-4.44×10^{-5}	-7.40×10^{-5}	3.63×10^{-5}
B-8	59.2	16.8	0.28	42.4	30.9	16.7	16.8	1.00	-	-.150000	-	-
B-9	30.4	18.3	0.60	12.1	22.3	16.7	18.3	0.91	0.49×10^{-5}	-3.33×10^{-5}	-4.90×10^{-5}	2.55×10^{-5}
B-10	44.9	18.0	0.40	26.9	27.0	5.8	18.0	0.32	0.80×10^{-5}	-1.40×10^{-5}	-2.50×10^{-5}	1.45×10^{-5}
B-11	34.5	14.5	0.42	20.0	21.2	5.8	14.5	0.40	1.30×10^{-5}	-2.69×10^{-5}	-4.50×10^{-5}	2.66×10^{-5}
B-12	59.6	35.0	0.58	24.6	43.2	33.0	35.0	0.94	3.30×10^{-5}	-6.20×10^{-5}	-10.0×10^{-5}	6.33×10^{-5}

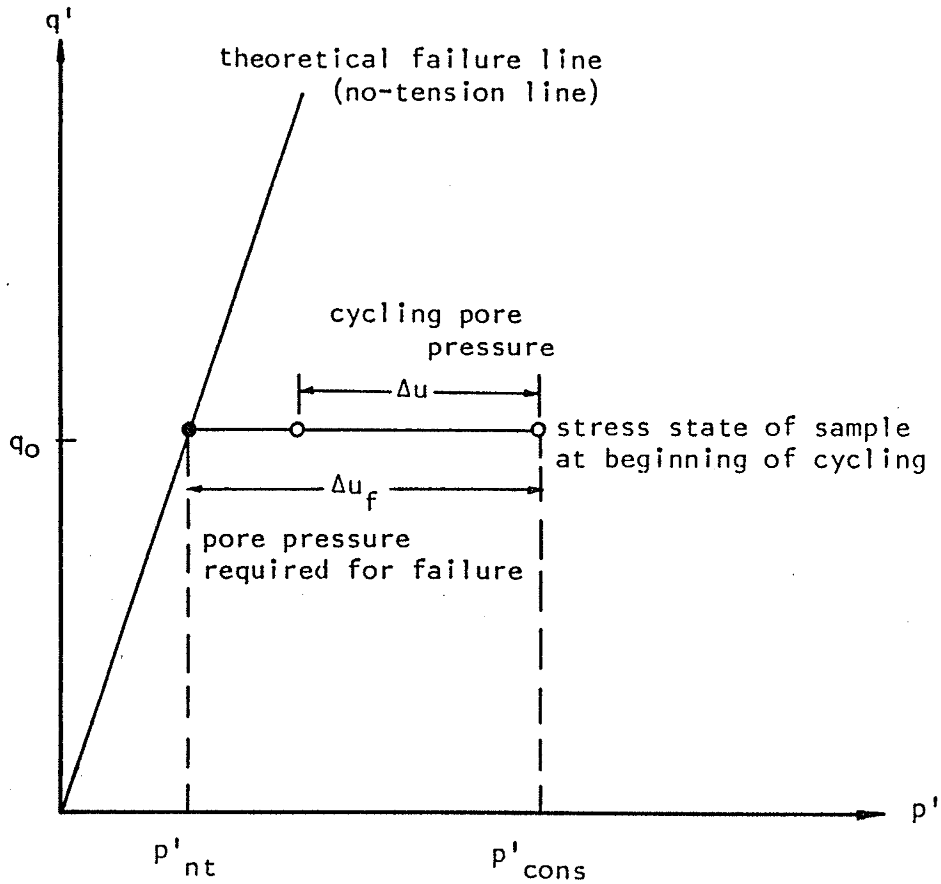

FIG. A-3 DEFINITION OF $\Delta u/\Delta u_f$

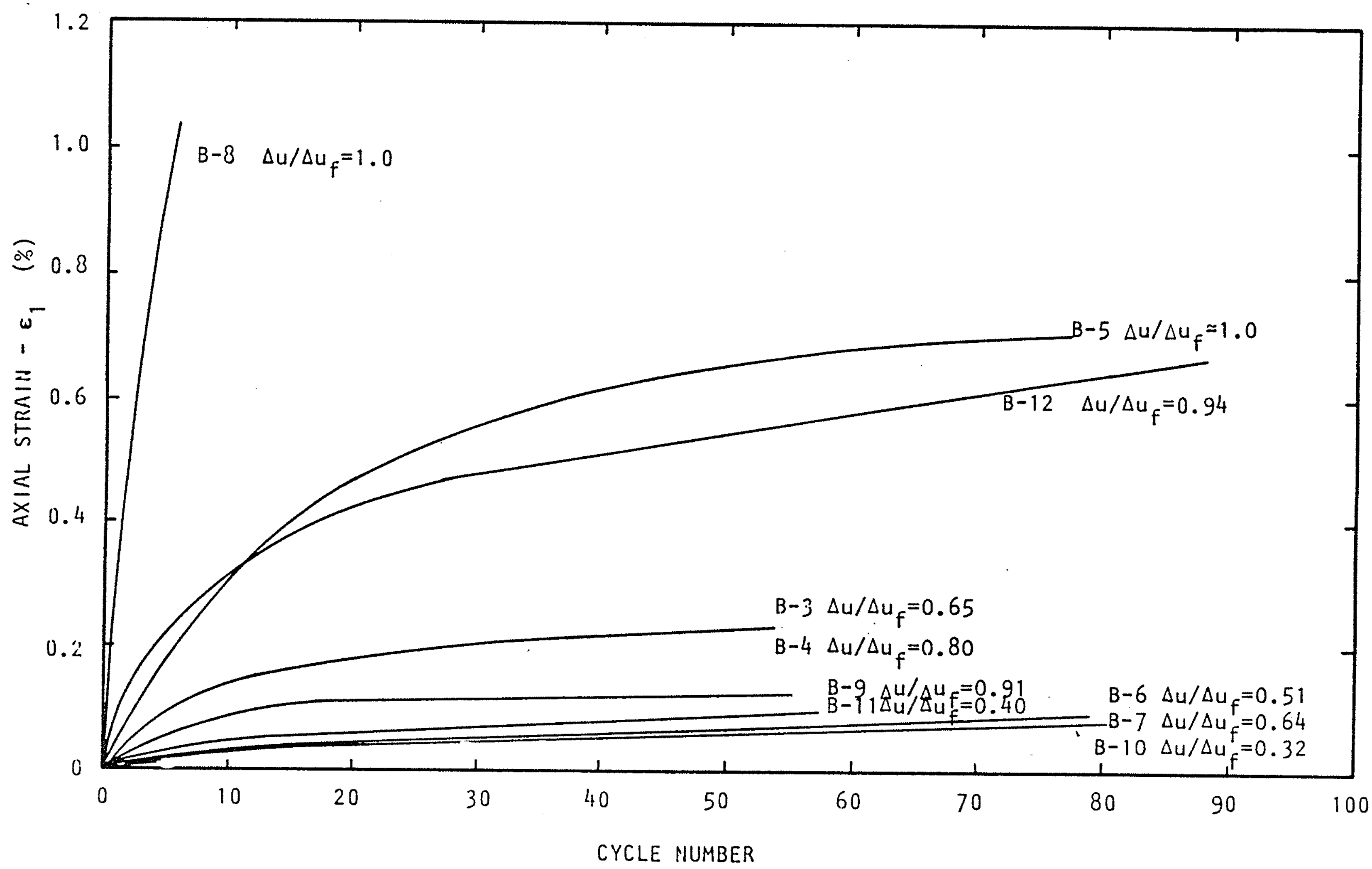

FIG. A-4 ε_1 versus CYCLE NUMBER

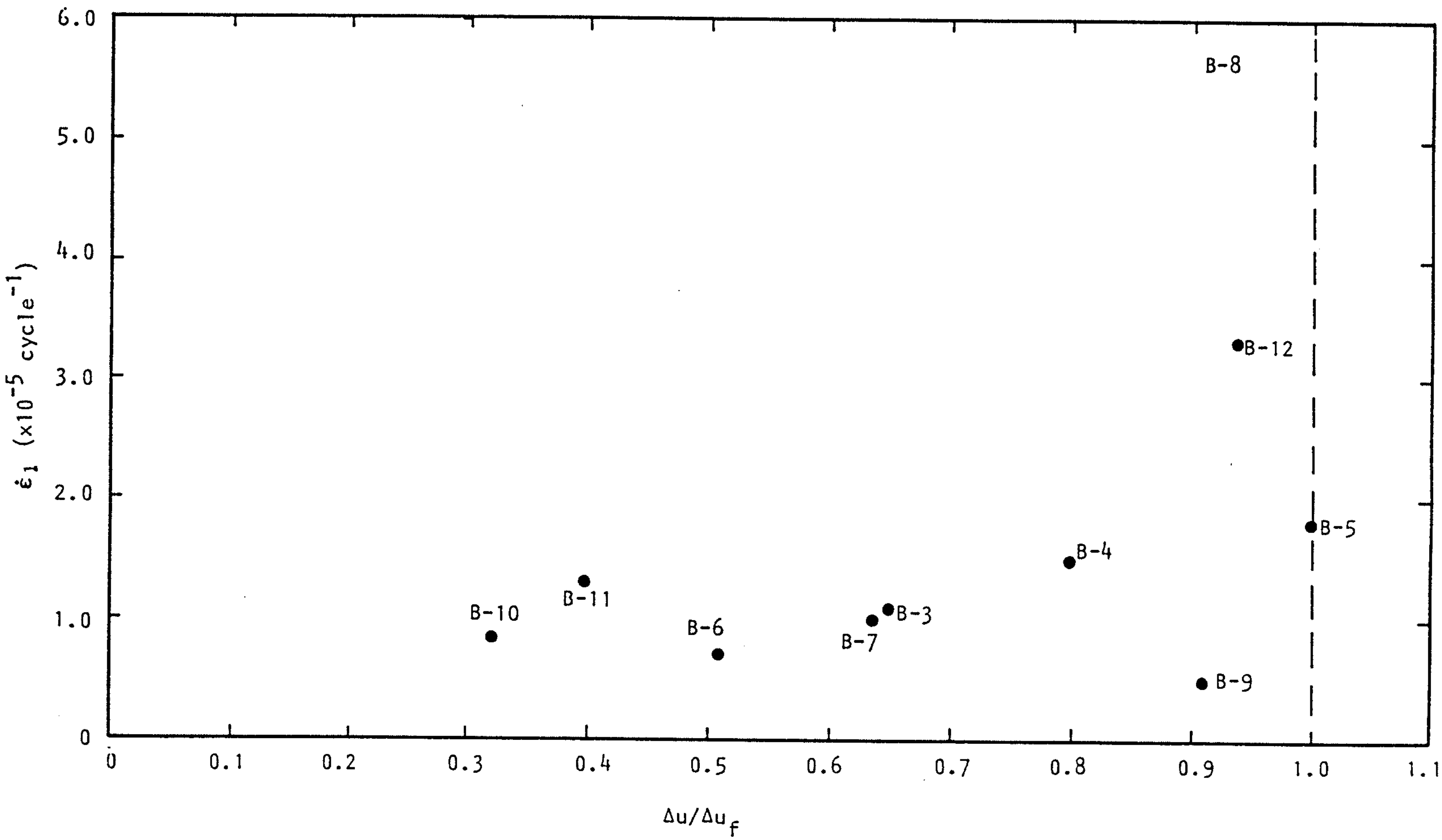

FIG. A-5 $\dot{\varepsilon}_1$ vs. $\Delta u/\Delta u_f$

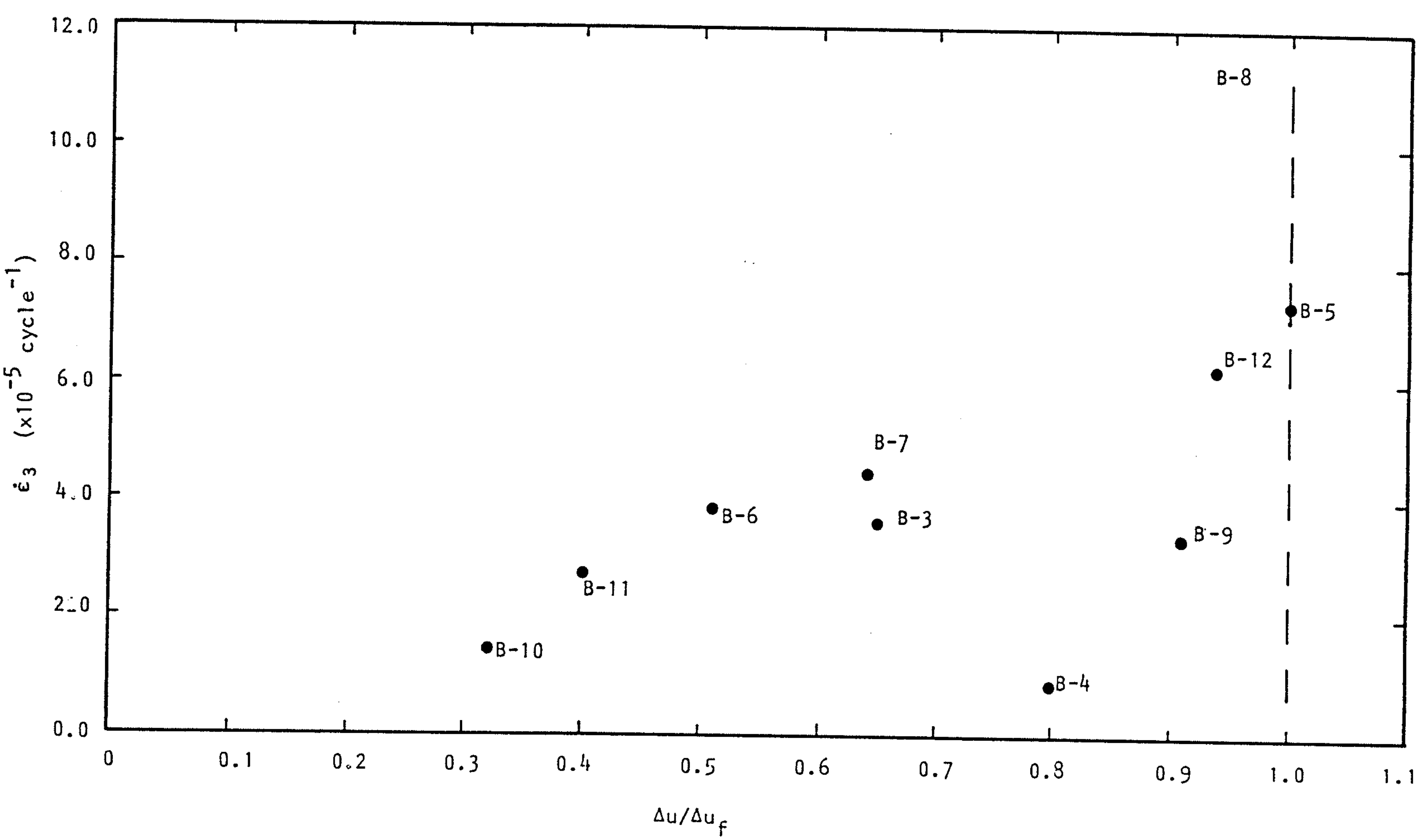

FIG. A-6 $\dot{\varepsilon}_3$ vs. $\Delta u/\Delta u_f$

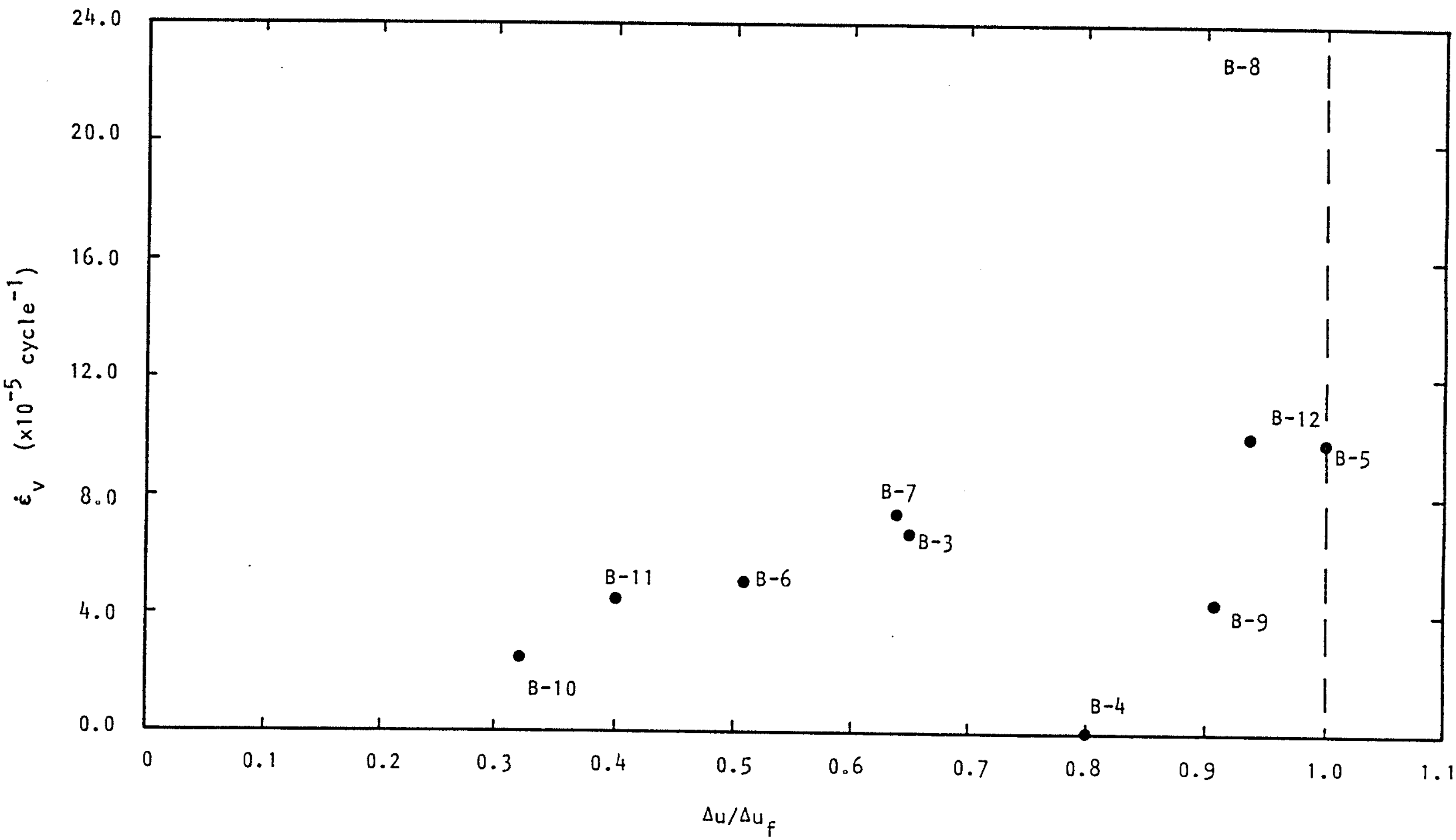

FIG. A-7 $\dot{\varepsilon}_v$ vs. $\Delta u/\Delta u_f$

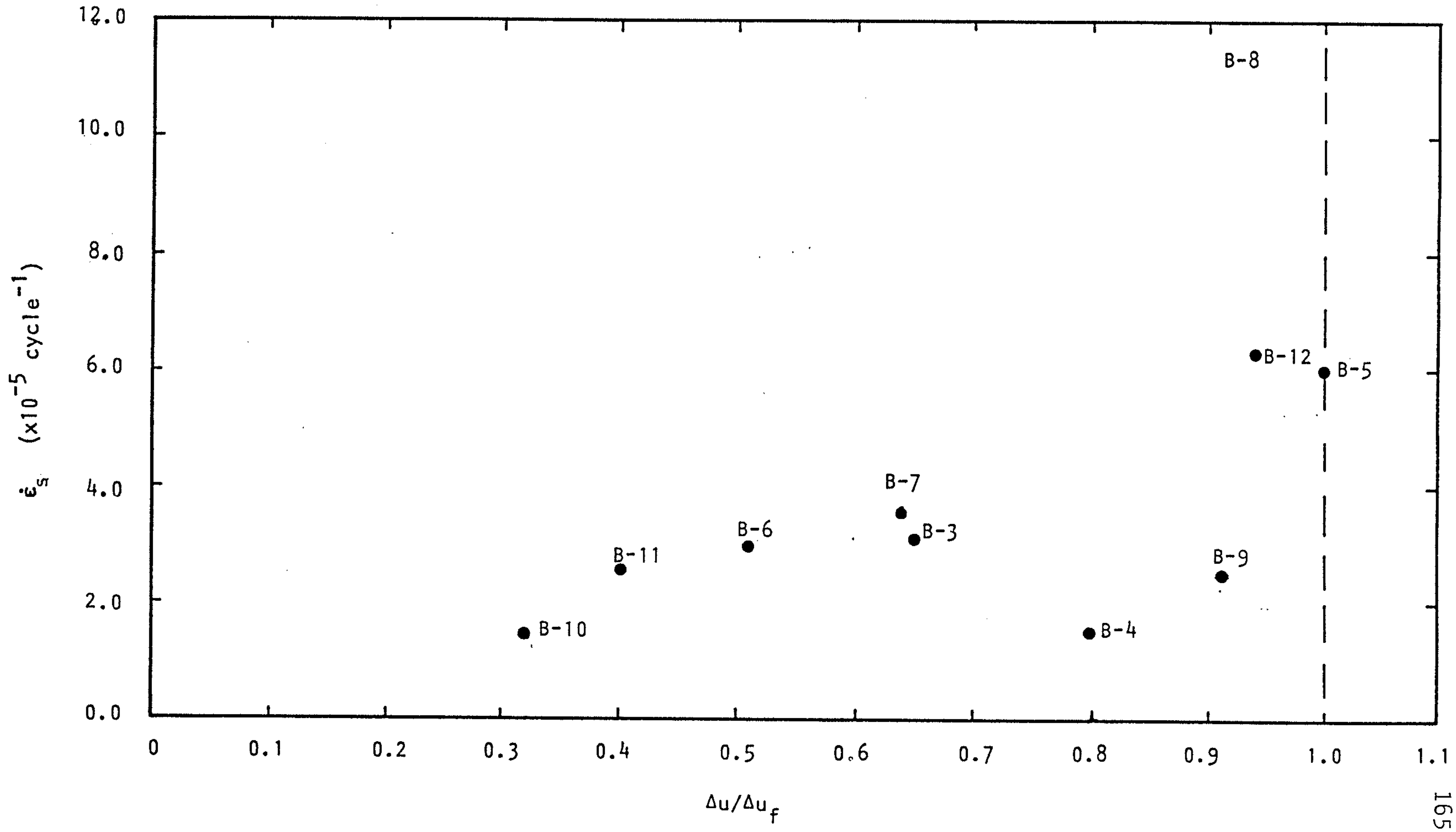

FIG. A-8 $\dot{\varepsilon}_s$ vs. $\Delta u/\Delta u_f$

A.9 IDENTIFICATION OF SOIL MINERALS BY X-RAY DIFFRACTION *

OBJECT: To identify the minerals present in samples of soil by using X-ray diffraction techniques.

THEORY: Most soils consist primarily of fragments of mineral matter which are highly crystalline in nature. Crystals have orderly arrangements of atoms in their structure. Because of the orderly arrangement of the atoms, the atoms in a crystal can be considered to lie in families of planes having interplanar spacing of 'd'. These planes are responsible for the diffraction of X-rays when a ray strikes a plane at an incident angle θ. The ray will leave the plane (be diffracted) in a manner similar to light rays reflected from a mirror, at an angle equal to the incident angle.

Other X-rays will penetrate into deeper planes of the same family, and also be diffracted. The intensity of all the diffracted rays will be a maximum, when the diffracted rays are all in phase. When this happens, the interplanar spacing 'd' of that family of planes can be determined from Bragg's law:

$$d = \frac{\lambda}{2 \sin\theta}$$

where: λ is the wave length of the particular X-ray used. (For a copper target X-ray tube $\lambda = 1.54050$ Å)

By rotating a crystal in a goniometer, so that the incident and diffracted angles are varied, it is possible to get several 'd' distances for a given mineral. The 'd' distances so obtained and the corresponding relative intensities of the diffracted rays constitute a unique "fingerprint" by which the mineral can be identified.

Bragg's law applies to single crystals and to powders of crystals. A fine powder with particles in statistical random orientation, contains sufficient particles in any given orientation to produce the diffraction intensities corresponding to given 'd' distances.

When a powder contains more than one mineral, the families of 'd' distances and relative intensities are superimposed. They can, however, be separated by inspection using a simple trial and error procedure, and the various minerals identified.

With clay minerals, different treatments of the powder, are required to distinguish between clays having similar 'd' distances and intensities. These treatments include:

(1) Using specimens where the particles are oriented by sedimentation on a glass slide.

(2) Using heat treatment of oriented samples on glass slides, to cause identifying changes in 'd' distances.

* taken from the University of Manitoba laboratory manual.

(3) Using organic solvents, e.g. ethelene glycol to cause identifying changes in 'd' distances.

SAMPLE PREPARATION: About 50 gm of air-dried sample are crushed to a fine powder using an agate mortar and pestel. Samples should not be oven-dried as heating can cause mineral changes.

PREPARING A POWDER MOUNT:

(1) Take a powder mount holder and cover the back of the windows with cellulose (Scotch) tape, so as to form a container. (The back side is without the center notch).

(2) Fill the container, open side up, with the powder sample, and strike-off the excess powder with a straight edge. Clean-off any excess powder that may be around the edge of the window.

(3) Place the flat face of a glass slide over the open window containing the powder. With fingers, gently squeeze the sample between the cellulose tape and glass slide so as to press the powder against the glass slide. This will smooth the top surface of the powder. Gently slide the glass slide off the container. Again clean off any excess powder that may be around the window.

(4) The powder mount is now ready for placing in the goniometer. The center notch (on the top side) goes in first. Press the sample holder so as to open the spring retaining clips. Push the holder in sufficiently to hold the powder mount but not to cover the window.

PREPARING AN ORIENTED (GLASS SLIDE) MOUNT:

(1) Standard microscope glass slides, 25 x 75 mm, are scored with a glass cutter and cut into two equal lengths. The halves are then wiped clean with cleaning tissue moistened in alcohol. (The alcohol removes any grease which could later interfere with the sample sticking to the slide).

(2) Prepare a thin slurry of the ground-up soil by adding distilled water to the sample ground-up in the agate mortar. (The slurry should be thin enough so that clay particles can sediment and orient flat side onto the glass, when the slurry is applied onto a glass slide). Mix the soil and water with a spatula until the slurry is smooth and free of any lumps.

(3) Immediately after mixing the slurry, place some slurry on a prepared glass slide to form a dab about 5 mm by 10 mm, centered on the slide. Repeat the procedure on three more glass slides to make a total of 4 slides. Keep the slides horizontal.

(4) Allow the slurry to dry. Drying may be hastened by gentle heat by shining an electric lamp on the sample, or alternatively by placing it in a vacuum oven at a setting of about 40°C. While drying, care should be taken to prevent dust, etc. from falling on the sample.

(5) Once dry, the oriented (glass slide) mount is ready for placing in the goniometer, or for further treatment. The glass slide, with dried slurry side up is inserted into the goniometer. Press the glass slide so that the edge pushes open the spring retaining clips of the goniometer. Push the glass slide in sufficiently to hold the slide, but not to cover the dried dab of slurry.

TREATMENT OF ORIENTED MOUNTS:

(a) Glycolation

Take one of the oriented mounts that has been dried. Place a drop at a time, of ethelene glycol on the glass slide along the perimeter of the dab of dried soil. As the glycol is adsorbed by the dab, add more glycol until no further adsorption takes place. Keep the sample in a covered dish for 1 hour. It is then ready to be inserted in the goniometer.

(b) Heat Treatment

1. Place the oriented mount, with soil dab up, onto an oven tray, and insert into heat treatment oven.

2. Heat the oriented mount in oven at required temperature (325°C) for at least one hour.

3. Remove tray with mount from oven, and place in covered desiccator to cool.

4. Once cool, the oriented mount is ready for insertion in the goniometer.

5. Repeat with a second oriented mount. Use an increased temperature of 550°C. (It is possible to re-use the oriented mount previously heated to 300°C after that mount has been scanned in the goniometer).

OPERATING THE GONIOMETER;

The following instructions are for a Philips PW1096/10 Goniometer attached to a Philips PW1011/80 X-ray Generator. It is assumed that the X-ray equipment has been set with the goniometer ready to operate. It is also assumed that an X-ray tube with a copper target is being used in conjunction with a Flow Counter detector. Reference should be made to the equipment manual to confirm the above before commencing. If changes are necessary follow manual procedures carefully or ask for assistance.

1. Make sure the goniometer is attached to X-ray, Port 1.Rotate the filter selector over Port 1 so that the Ni. filter covers the port. Check that Ports 2,3 and 4 are closed.

2. Turn on water supply. Valve is on wall.

3. Switch wall mounted electric main switch to ON.

4. On generator front panel, turn rotary switches marked volts and amps to lowest position. Press ON switch and allow 10 to 15 minutes warm-up time. Proceed with following steps while warm-up is taking place.

5. Check that the appropriate slits are inserted in the goniometer. For routine testing, a 1° divergence slit, a 0.2° receiving slit and 1° scatter slit, may be used. Goniometer switches should initially be set at:

   Step scan - off
   Line - off
   Limit - OSC. (Oscillate)
   Clutch - disengaged (to right)
   Initial 2θ - 3°

6. Select appropriate goniometer gears for controlling 2θ scanning rate. A satisfactory speed for 2θ is 1° per min for routine work. See table on goniometer for gears to be used.

7. Check recorder. Initially the chart motor should be disengaged. Check that there is sufficient paper on roll. (Place new roll if required. See equipment manual for instructions). Similarly check ink supply for two recording pens. Suitable settings on the recording equipment are as follows. Asterisks indicate settings which may require re-setting. The other settings are normally <u>not</u> altered.

   (a) PW1375 High Voltage Supply
   ∿ - On
   Flow counters - 1700, and 70

   (b) PW4237 Counter - Timer
   ∿ - On
   Present count - 1 x ∞
   Present time - 1 x ∞
   Start - Ext.
   Operate - Up

   (c) PW1362 Ratemeter
   * Range - select suitable range to maintain chart peats on graph
   - 4×10^2 cps usually satisfactory for oriented slides
   - 2×10^3 cps may be required for powder mounts
   *Time constant - 4 sec usually satisfactory for scan speed 1° of 2θ per min
   Goniometer supply - ON.
   Aut. Mains switch - inc. gen.

   (d) PW4280 Amplifier/Analyser
   Attenuation - z = 3
   Lower level - 0.50
   Window - 1.30 x Thr.
   Switch to - FLC

8. Remove cover plate from goniometer sample holder. Insert sample. Make sure sample is centered and soil not covered by holder. Replace cover plate. (Note safety switch which will turn off X-ray if cover plate removed during a test. X-rays used for diffraction work are dangerous, and no part of the body should be exposed to the radiation).

9. By this time the warm-up of X-ray Generator should be completed. Voltage should read 20 KV.
First turn voltage slowly to 40 KV.
Then turn Amps slowly to 20 ma.
(Note at no time should voltage x amps be permitted to exceed 1000).
Turn AB switch for Port 1, to ∿ and KV to 1.
Press Port 1 button.

10. Switch Goniometer Line to ON.

11. Simultaneously engage goniometer drive clutch and chart drive. A suitable chart speed is 300 mm/hr, when a 2θ scan of $1°$/min is used. Mark starting angle on the chart.

12. Allow goniometer to turn through required 2θ angle. For the powder mount use a 2θ range from $3°$ to $63°$. For the oriented mounts, the changes caused by glycolation and heat treatments can be observed in the range of 2θ $3°$ to $21°$.

13. When the goniometer has turned through the angles noted in Step 12, turn Port 1, AB switch to OFF. Disengage goniometer drive clutch, turn chart drive OFF. Sample may then be removed.

14. Manually rotate goniometer crank to initial $2\theta = 3°$. At this time another sample may be inserted in the goniometer and steps 11 to 14 inclusive repeated for as many times as there are samples. Between samples, the paper in the chart may be manually advanced to give some space between diffractograms. If testing is complete, proceed to step 15 to turn equipment off.

15. First turn Amps to lowest setting.
Then turn Volts to lowest setting.
Wait at least 10 sec. before pressing red OFF button.

16. Switch wall switch to OFF.
Turn off water.

<u>NOTE</u>: During the operation of the X-ray equipment, the power may automatically trip off. This may be caused by:

(a) The goniometer reaching the high or low limits. Should this happen, the goniometer will operate in reverse direction when the equipment is next turned on.

(b) A safety switch has been tripped. Switches on the X-ray ports will turn the equipment off if for example the cover is removed from the sample holder, or the door is opened to the high voltage supply during operation.

(c) The water pressure drops.

If the power automatically trips off, check to determine the cause. If this can be corrected, recommence at Step 4. If the equipment automatically trips off again, follow steps 15 and 16. Notify the technician.

ANALYSIS

A. The following analysis is made on the diffractogram of the power mount or oriented slide scanning the range 2θ = 3° to 62°.

1. Mark the 2θ angle opposite each peak obtained on the chart. Convert the angle to 'd' spacing using Bragg's Law, and record these opposite each peak. Conversion tables may be used or computations made with a calculator.

2. Examine the peaks for quartz. Often 6 of the 10 or more prominent peaks are visible. When less than 10% quartz is present, only 2 peak may show at 4.26Å and 3.343Å. This peak is an excellent one to check the calibration of the 2θ angles. Mark the quartz peaks.

3. Examine and mark the peaks for other more common non-clay minerals including: feldspar; amphibole 8.4Å and 3.12Å; pyroxene 2.9Å, 2.94Å, and 1.62Å; calcite 3.03Å; dolomite 2.89Å; and gypsum 7.56Å. To verify the pressure of these minerals two or more secondary peaks should also be checked. Refer to Table I, or diffraction tables edited by Brown (1972).

4. The remaining peaks may be checked using Table I and mineral present confirmed by reference to diffraction tables.

B. Identification of the clay minerals requires comparison of diffractograms of the treated and non-treated specimens.

The following analysis is made by comparing treated and non-treated oriented mounts, and powder mounts.

1. If the untreated oriented mount shows increased 14Å, 10Å or 7Å peaks (relative to quartz peaks) when compared to the powder mount, the effect is due to the orientation of clay particles.

2. A 15Å peak that shifts to 17Å on glycolation, and collapses to 9Å on heating to 300°C indicates smeatite (montmorillonite group).

3. A 14Å peak that does not change on glycolation, and becomes slightly to noticeably more intense on heating to 550°C indicates chlorite.

4. A 14Å peak that is unaffected by glycolation, and dehydrates in steps when heated indicates vermiculite. Further heat treatment (1 hour at 700°C) causes collapse of the 14Å peak to broad 9Å peak.

5. A 10Å peak that does not change on glycolation, and becomes more intense on heating indicates illite. Mica reacts similarly but shows a 5Å peak as well.

6. Peaks at 7.15Å and 3.75Å which do not change on glycolation or heat to 300°C indicate kaolinite. Kaolinite becomes amorphous (no peaks) when heated to 550-600°C.

For further identification, the procedures of Warshaw and Roy (1961), and Carroll (1970) may be used.

CONCLUSION

Make sure all the identifying data; sample description, sample number, type of mount and treatment used, are shown on the diffractogram. Include data on X-ray radiation used, filter, slits, Volts, Amps, 2θ° and paper speed used. Include data of tests, name of person testing, and acknowledge University of Manitoba facilities.

List the minerals present. A rough quantitative comparison of the clay minerals present can be made by reference to the following relationship of peak intensities for oriented mounts:

(a) For equal amounts of illite and chlorite, the 14Å chlorite peak approximately equals the 10Å illite peak.

(b) For equal amounts of illite and chlorite, the 7Å chlorite peak is 2 to 3 times larger than the 10Å illite.

(c) For equal amounts of illite and kaolinite, the 7Å kaolinite peak is 2 to 3 times larger than the 10Å illite peak.

(d) For equal amounts of kaolinite and chlorite, the 7Å and 3.5Å kaolinite peaks are about equal to 7Å and 3.5Å chlorite peaks.

(e) For equal amounts of illite and smectite, the 14Å smectite peak is 3 to 4 times larger than the 10Å illite peak.

(f) For equal amounts of illite and smectite after heat treatment at 300°C, the 10Å smectite peak equals the 10Å illite peak.

A comparison of the actual peak height ratios, can be used to estimate the relative quantities of the clay minerals present. If the percentage of clay is known from a hydrometer analysis, the percentage of the total sample for each clay mineral may be estimated.

Swelling, shrinking, etc. characteristics can be predicted for the soil sample considering the properties of the minerals present.

REFERENCES

Brown, G. (Editor) 1972. X-ray identification and crystal structure of clay minerals. Mineral Soc. London.

Carroll, D. 1970. Clay Minerals: A guide to their X-ray identification. Geol. Soc. Amer., Special Paper 126.

Klug & Alexander, 1954. X-ray diffraction procedures. John Wiley & Sons, New York.

Mitchell, James K. 1976. Fundamentals of Soil Behaviour. John Wiley & Sons, pp. 87-94.

Warshaw, C.M. and Roy, R. 1961. Classification and a scheme for the identification of layer silicates. Geol. Soc. Amer. Bull. 72(10) pp. 1455-1492.

DIAGNOSTIC d (Å) SPACINGS, AND 2θ° FOR COMMON SOIL MINERALS
X-RAY DIFFRACTION, COPPER TARGET

d spacing Angstrom	I	2 theta Degrees	Mineral	Notes
15.0-12.5	vs	5.9-7.1	Smectites	varying degrees of hydration
14.5-13.5	vs	6.1-6.5	Chlorites	
14.5-13.5	vs	6.1-6.5	Vermiculite	fully hydrated
12.5-12.0	vs	7.0-7.4	Vermiculite	partially hydrated
10.5	vs	8.4	Attapulgite	(Palygorskite)
10.1	s	8.8	Illite	
10.1-9.9	vvs	8.8-8.9	Micas	Muscovite, Biotite, Phlogopite
9.3	s	8.9	Talc	
8.5-8.4	vs	10.4	Amphibole	Hornblende, Actinolite
7.56	vs	11.7	Gypsum	
7.36	vs	12.0	Serpentine	Antigorite, Chrysotile
7.5-7.2	mw	11.8-12.3	Halloysite	Metahalloysite ($2H_2O$)
7.15	s	12.4	Kaolinite	
7.2-7.0	vs	12.3-12.6	Chlorite	
7.2-6.8	vs	12.3-13.0	Chlorites	iron rich
6.65	m	13.3	Orthoclase	"high" K-feldspar
6.46	m	13.7	Microcline	"low" K-feldspars
6.55-6.38	m	13.5-13.9	Plagioclase	Anorthite to Albite
5.61-5.57	mw	15.8-15.9	Analcite	
4.85	s	15.9	Gibbsite	
4.79-4.69	ms	18.5-18.9	Chlorite	
4.50-4.45	m	19.7-19.9	Clays	Kaolinite and Smectites
4.37	m	20.3	Gibbsite	
4.27	s	20.8	Gypsum	
4.26	s	20.8	Quartz	
4.24-4.21	s	20.9-21.1	K-feldspar	
4.18	vs	21.2	Goethite	
4.04	vs	22.0	Cristobalite	
4.04-4.02	mw	22.0-22.1	Plagioclase	
3.97-3.84	mw	22.4-23.1	Feldspars	
3.83-3.79	s	23.2-23.5	K-feldspars	Microline & Orthoclase
3.77-3.74	ms	23.6-23.8	Plagioclase	
3.66-3.61	ms	24.3-24.6	Plagioclase	
3.66-3.64	s	24.3-24.4	Serpentine	
3.57	ms	24.9	Kaolinite	
3.59-3.52	s	24.8-25.3	Chlorite	
3.48-3.46	m	25.6-25.7	Feldspar	
3.43	s	26.0	Analcite	
3.37-3.36	vvs	26.4-26.5	Micas	Muscovite and Biotite
3.343	vvs	26.64	Quartz	
3.33	vs	26.8	Orthoclase	
3.23	vvs	27.5-27.6	Microline	and Orthoclase
3.21-3.19	vvs	27.8-28.0	Plagioclase	Albite to Anorthite
3.18	vvs	28.0	Plagioclase	only Albite & Oligclase
3.17-3.16	s	28.1-28.22	Plagioclase	only Andesine to Anorthite

DIAGNOSTIC d (Å) SPACINGS, AND 2θ° FOR COMMON SOIL MINERALS
X-RAY DIFFRACTION, COPPER TARGET

d spacing Angstrom	I	2 theta Degrees	Mineral	Notes
3.13-3.11	wm	28.5-28.7	Plagioclase	only Andesine to Anorthite
3.13-3.09	s	28.5-28.9	Amphibole	Horneblende & Actinolite
3.10	vs	28.8	Talc	
3.09	vs	28.0	Jarosite	
3.06	s	19.2	Gypsum	
3.03-3.02	vvs	29.5-29.6	Calcite	
3.01	vs	29.7	Alunite	
3.01-2.95	ms	29.7-30.3	Feldspars	131 peak
2.99	s	29.9	Augite	
2.94-2.91	mw	30.4-30.7	Feldspars	
2.89	vs	30.9	Dolomite	
2.87-2.82	mw	31.1-31.7	Chlorite	
2.86-2.82	mw	31.3-31.7	Feldspars	131 peak
2.82	vs	31.7	Halite	
2.75	s	32.5	Ilmenite	
2.74	vs	32.7	Magnesite	
2.71-2.69	s	33.0-33.3	Amphibole	Hornblende & Actinolite
2.69	sb	33.3	Hematite	and Goethite
2.56	s	35.0	Augite	
2.56-2.51	md	35.0-35.7	Feldspars	and Micas
2.53	s	35.45	Magnetite	
2.51	s	35.7	Augite	and Hematite
2.50-2.44	mw	35.8-36.8	Feldspars	Albite to Labradorite
2.48	m	36.2	Cristobalite	
2.458	mw	36.52	Quarta	
2.33	m	38.6	Kaolinite	
2.282	mw	39.45	Quartz	and Calcite
2.19	ms	41.2	Dolomite	
2.10	mw	43.0	Calcite	
2.01-1.99	m	45.1-45.5	Micas	Muscovite & Biotite
1.99	s	45.5	Halite	
1.91	mw	45.6	Calcite	
1.87	mw	48.7	Calcite	
1.817	mw	50.16	Quartz	and Dolomite
1.82-1.80	mw	50.1-50.7	Feldspars	
1.78	mwb	51.3	Dolomite	
1.62	mw	56.8	Magnetite	
1.56	ms	59.2	Septichlorites	especoally Chamosite (060)
1.55-1.53	w	59.6-60.5	Chlorites	060 peak
1.541	mw	59.98	Quarta	211 peak
1.54	mw	60.0	Biotite	060 peak
1.54-1.53	w	60.0-60.45	Vermiculite	and trioct. Smectite (060)
1.53	mw	60.5	Serpentintes	and talc (060)
1.53-1.52	w	60.5-60.9	Phlogopite	060 peak
1.52-1.49	w	60.9-62.3	Smectite	dioct.(060)
1.50	m	61.8	Muscovite	& Illite & Attpulgite (060)
1.49	m	62.3	Kaolinite	& Halloysite (060)

APPENDIX B - Field Program

Table of Contents

B.1 Instrumentation Installations

B.1.1 Open Standpipe Installation

Four open standpipes were installed in the sand and gravel (see Fig.2 -2), in order to confirm the observations obtained from the piezometers and therefore are alternately located between them.

A typical standpipe installation is illustrated in Fig. B-1(a). The tip was covered with a filter cloth in order to prevent fines from plugging up the tube. After being lowered into the borehole, Ottawa sand was placed around the standpipe tip. Above the sand, a clay seal was formed by pouring bentonite balls down the borehole. This seal was generally 30-40cm thick. The rest of the boring around the tube was subsequently backfilled with available fill on the site.

The standpipes above the penstock were installed without the use of a drill casing as the soil stood open long enough to allow complete installation. The one standpipe (STP-1) below the penstock however, had to be installed through the annulus of the hollow stem drill rod because of the tendency of the hole to slough in before the standpipe was installed. A bentonite plug was formed approximately 6m above the tip and above this, clay backfill was placed.

B.1.2 Piezometer Installation

Three semiconductor type electrical piezometers were installed on the site (Model 45005 of Geokon Inc.)

The piezometer installation is similar to that used for the standpipe. The piezometer was lowered into the borehole and Ottawa sand then poured till it was 20 cm above the piezometer. Bentonite pellets were then placed above this to form a seal of about 40cm thick. The remainder of the borehole was then backfilled with clay. A typical installation is also presented in Fig. B-1(b).

B.1.3 Slope Indicator Installation

Four slope indicator casings were installed, three uphill from the penstock and one downhill of it, using ABS plastic 84.8 mm OD x 72.9 mm ID x 3.05 m long casing.

Once the borehole was completed, the casing was lowered into the hole, with each joint being glued as the lowering commenced. Once in position, cement grout was poured into the borehole (around the SI casing) and allowed to set while the SI casing was held down to counter the bouyancy.

A schematic of the installation is shown in Fig. B-1(c).

B.1.4 Thermistor Cable Installation

Two thermistor cables were installed to record the temperature regime of the ground. An earlier installation completed by EBA Engineering (1982) indicated a permafrost area downslope of the penstock. All three installations are shown on Fig. 2-2.

Installation of a thermistor cable involved inserting the cable inside a 50 mm diamter PVC access tube which had been placed in the borehole. This access tube was then filled with dry Ottawa sand and the borehole was backfilled with available fill material. Because the thermistor cables were manufactured to predetermined lengths, both had to be folded back in order to conform to the borehole depths limited by the depth of bedrock in each location. A typical installation is shown in Fig. B-1(d).

B.1.5 Earth Pressure Cell

Two earth pressure cells were installed against the pier support on the west side of the penstock in Test Pit No. 1, whose location is shown in Fig. 2-2. They were installed to depths of 1.45m and 1.70m. The pressure cells used were manufactured by Geokon Inc. and consist of two circular stainless steel plates (23 cm dia.) welded together around their periphery, with a cavity between them. This cavity is filled with anti-freeze, which transfers the soil pressure to a pressure transducer. The pressure transducer is of the semi-conductor type and the accuracy of the system is 0.25% of the full scale. Further specifications are presented at the end of this Appendix.

The earth pressure cells were placed against a 3/4" piece of plywood which again was supported by 8" x 8" blocks of wood against the pier in order to balance out the difference between the pier and the pile cap. Both cells were then covered with fine sand in order to protect them from damage by the gravel fill which was used for backfilling the excavation. The fill was placed carefully in layers of 10cm thickness till the cells were completely covered. The remainder of the pit was backfilled with the excavated clay material. Figure B-2 shows schematically backfilling and installation details. Both pressure cells were eventually connected to the continuous data logger.

B.1 SUMMARY OF 1984 FIELD DRILLING PROGRAM

BOREHOLE	DEPTH (m)	INSTRUMENT INSTALLED	DEPTH OF INSTALLATION (m)
TH-1	6.7	Thermistor String	6.7 (1.3m foldback)
TH-2	5.6	Thermistor String	5.6 (2.3m foldback)
P-1	5.0	Electro - Piezometer	4.8
SI-1	8.5	Slope Indicator Casing	7.3
STP-1	7.9	Standpipe	7.8
STP-2	2.1	Standpipe	2.0
SI-2	2.4	Slope Indicator Casing	2.4
P-2	4.8	Electro - Piezometer	4.7
SI-3	4.0	Slope Indicator Casing	3.4
SI-4	3.7	Slope Indicator Casing	3.65
STP-3	4.0	Standpipe	4.0
P-3	2.9	Electro - Piezometer	2.4
STP-4	2.4	Standpipe	2.3

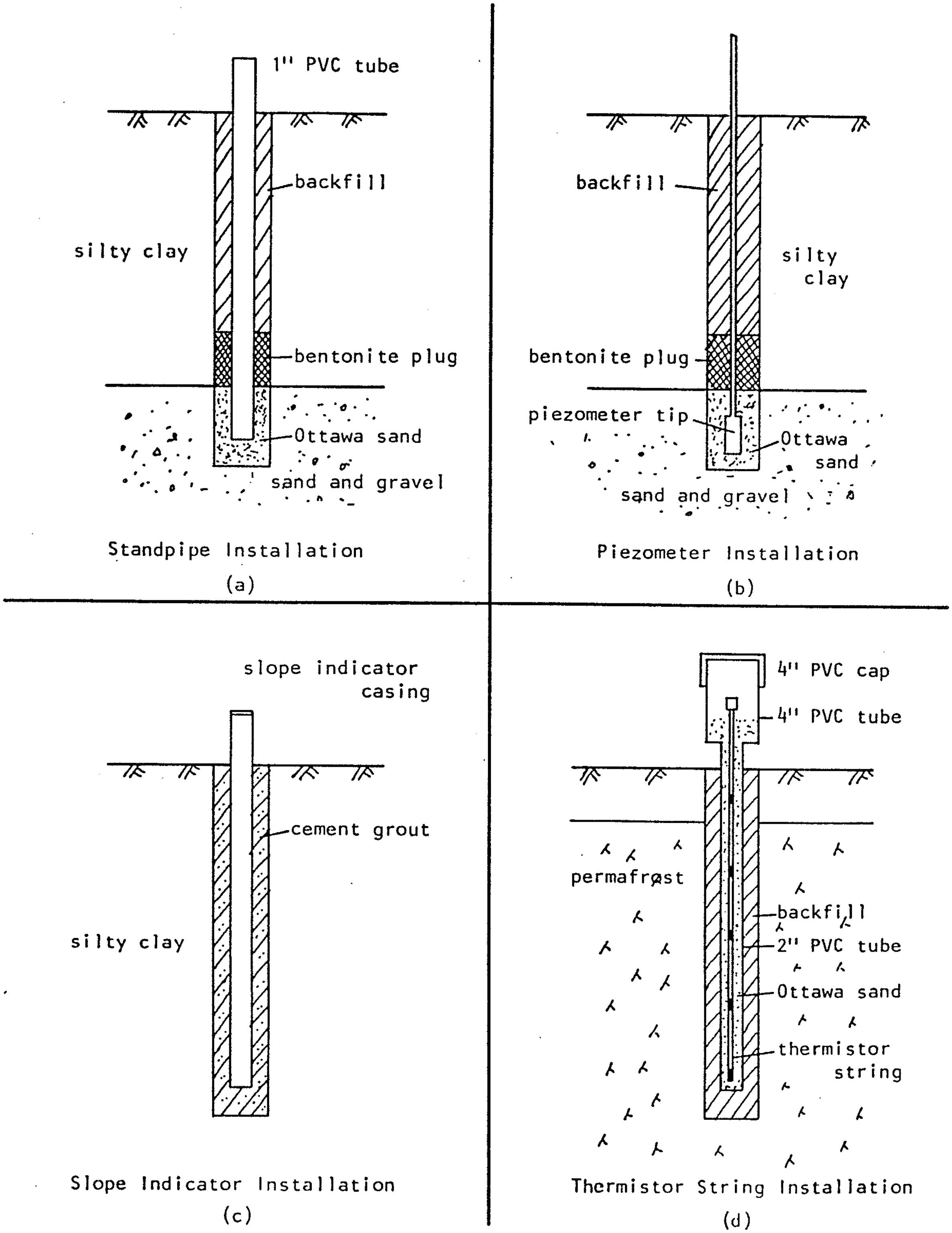

FIG. B-1 INSTRUMENTATION INSTALLATIONS

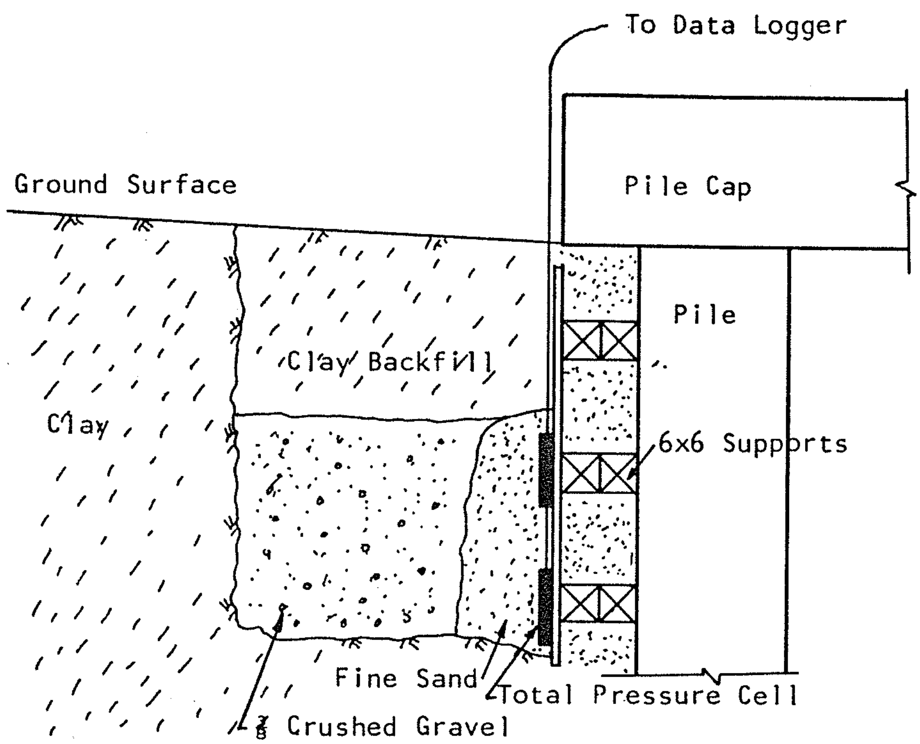

FIG. B-2 TOTAL PRESSURE CELL INSTALLATION

B.3 Temperature Profiles

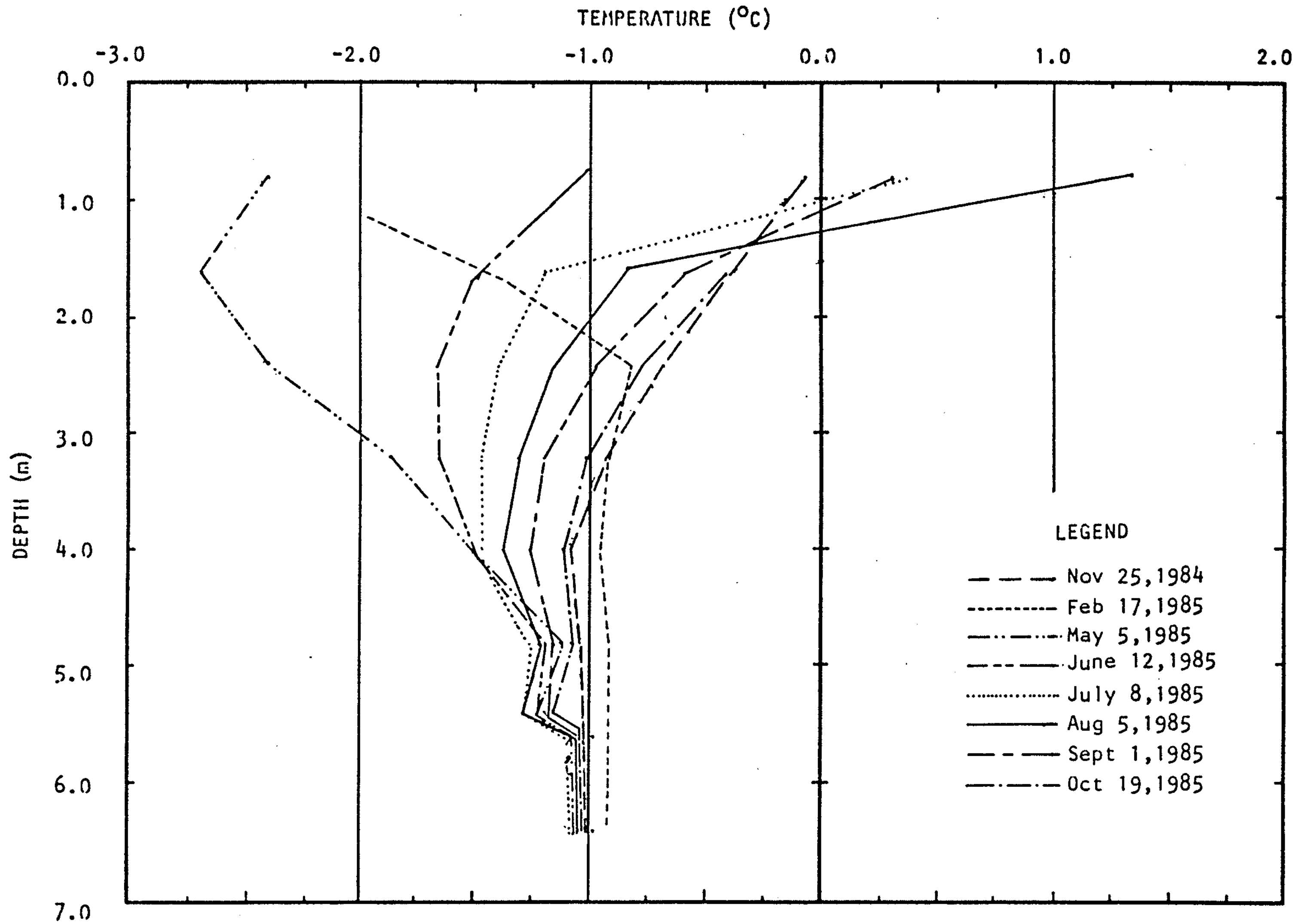

FIG. B-3 TEMPERATURE PROFILES FOR THERMISTOR NO.1

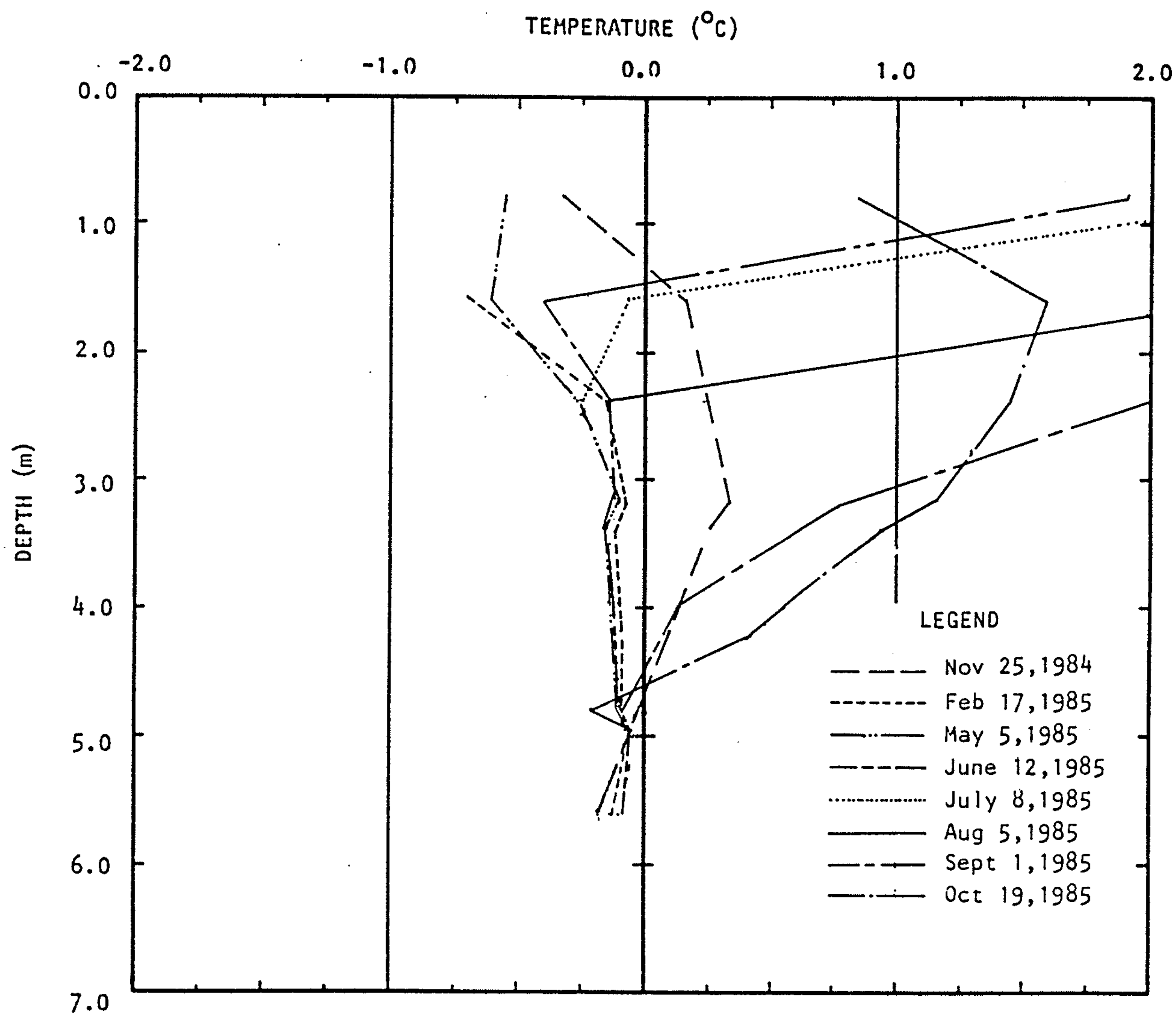

FIG. B-4 TEMPERATURE PROFILES FOR THERMISTOR NO.2

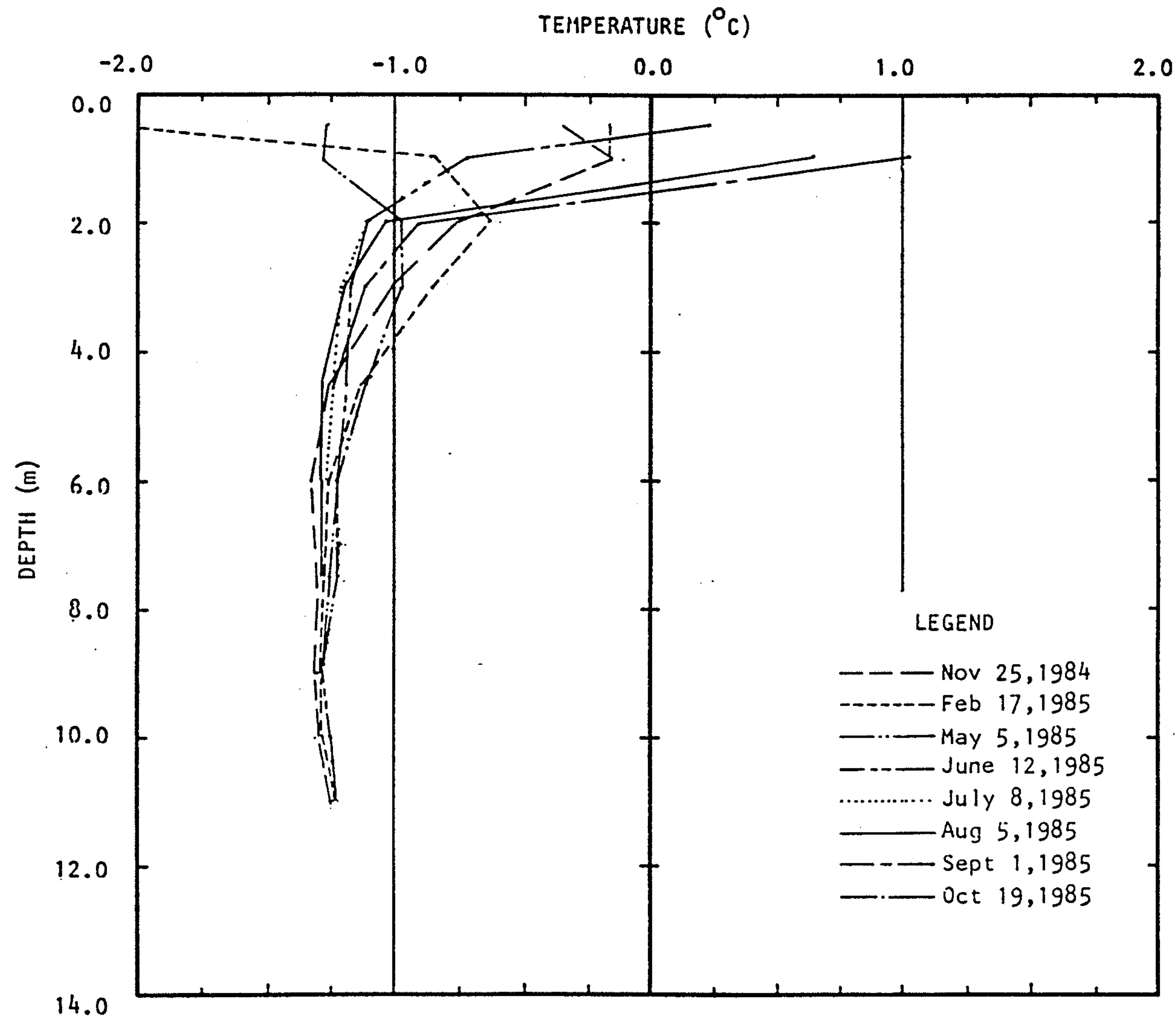

FIG. B-5 TEMPERATURE PROFILES FOR THERMISTOR NO.3

B.4 Borehole Logs

DEPTH (metres)	SOIL DESCRIPTION	SAMPLE	COMMENTS	MOISTURE CONTENT P_L (%) W (%) L_L (%) 10 20 30 40 50
	SILT - clayey, organics, grey		unfrozen	
1	CLAY - silty, lt. brown			
2			frozen Vx 20%	
3				
4				
5				
6				
	BEDROCK End of hole 6.7m			
7	Thermistor no.1 installed (1.3m foldback)			

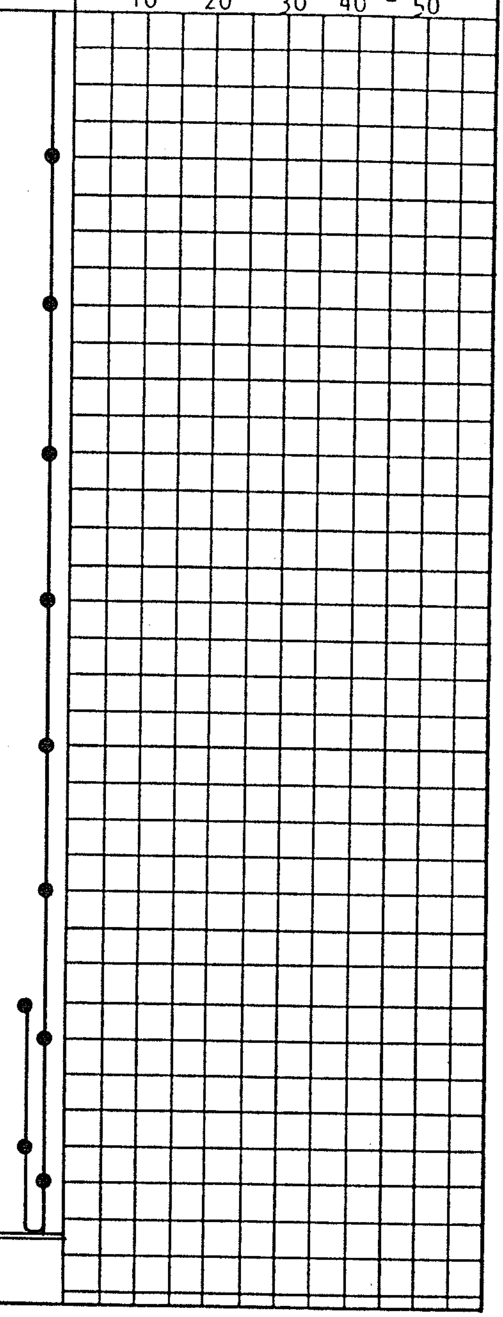

SFC. ELEVATION (m) 164.555	DATE DRILLED Aug 8,1984	BOREHOLE NO. TH-1
COMPLETION DEPTH (m) 6.7	LOGGED BY JPB	
DRILLING RIG	LOCATION Bluefish Lake	PAGE 1 of 1

DEPTH (metres)	SOIL DESCRIPTION	SAMPLE	COMMENTS
	CLAY - silty, lt.brown		unfrozen
1			
2			frozen?
3			
4			
5			
	SAND & Gravel		
	BEDROCK		
	End of hole 5.6m Thermistor no.2 installed (2.3m foldback)		
6			
7			

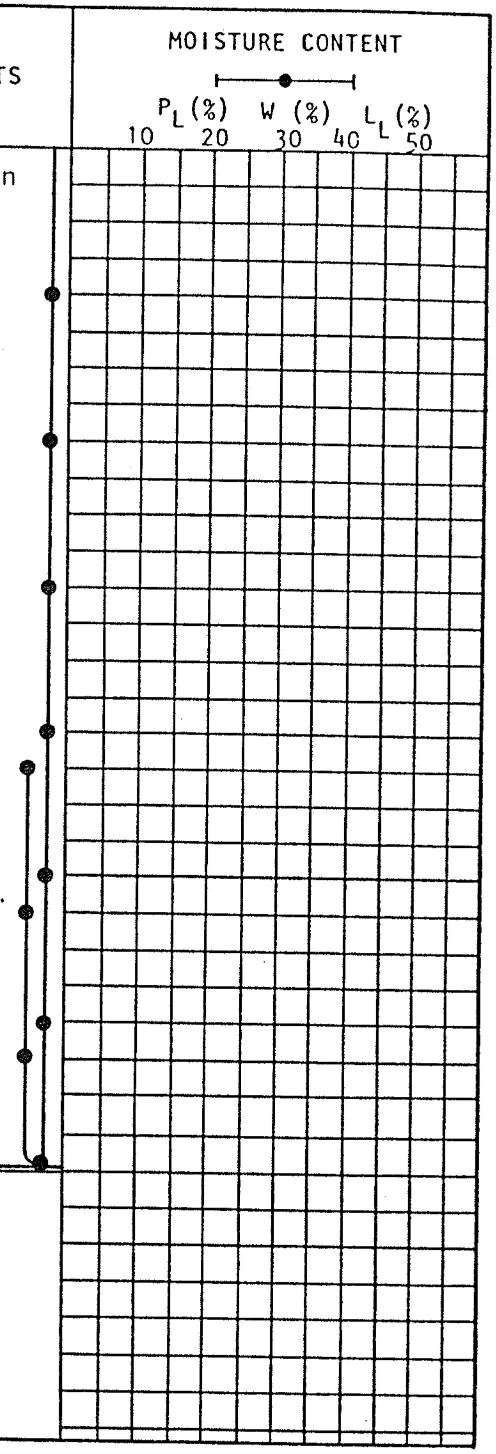

SFC. ELEVATION (m) 165.235	DATE DRILLED Aug 8,1985	BOREHOLE NO.	TH-2
COMPLETION DEPTH (m) 5.6	LOGGED BY JPB		
DRILLING RIG	LOCATION Bluefish Lake	PAGE 1 of 1	

DEPTH (metres)	SOIL DESCRIPTION	SAMPLE	COMMENTS	MOISTURE CONTENT P_L (%) W (%) L_L (%) 10 20 30 40 50
	GRAVEL and BOULDERS - some silt and clay		unfrozen	
	CLAY TILL - silty,br.grey			
1				
2	tr. gravel			
3				
4			84/08/16	
	tr. sand and gravel			
	BEDROCK			
5	End of hole 5.0m Install electro-piezo to 4.8m			
6				
7				

SFC. ELEVATION (m) 165.410	DATE DRILLED Aug 10,1984	BOREHOLE NO. P-1
COMPLETION DEPTH (m) 5.0	LOGGED BY JPB	
DRILLING RIG	LOCATION Bluefish Lake	PAGE 1 of 1

DEPTH (metres)	SOIL DESCRIPTION	SAMPLE	COMMENTS	MOISTURE CONTENT P_L (%) W (%) L_L (%) 10 20 30 40 50
	CLAY - silty,soft,wet,br. grey		unfrozen	
1				
2				
3				
4				
5				
6				
	SAND and GRAVEL overlying BEDROCK at 8.2m Slope Indicator casing installed to 7.3m			
7				

SFC. ELEVATION (m) 166.32	DATE DRILLED Aug 10-11,1984	BOREHOLE NO. SI-1
COMPLETION DEPTH (m) 8.5	LOGGED BY JPB	
DRILLING RIG	LOCATION Bluefish Lake	PAGE 1 of 1

DEPTH (metres)	SOIL DESCRIPTION	SAMPLE	COMMENTS	MOISTURE CONTENT P_L (%) W (%) L_L (%) 10 20 30 40 50
	CLAY - silty, soft, wet, br.grey		not frozen	
1				
2				
3				
4				
5				
6				
	SAND and GRAVEL			
7	BEDROCK at 7.9m standpipe installed			

SFC. ELEVATION (m) 166.675	DATE DRILLED Aug 11,1984
COMPLETION DEPTH (m) 7.9	LOGGED BY JPB
DRILLING RIG	LOCATION Bluefish Lake

BOREHOLE NO. STP-1
PAGE 1 of 1

DEPTH (metres)	SOIL DESCRIPTION	SAMPLE	COMMENTS	MOISTURE CONTENT P_L (%) W (%) L_L (%) 10 20 30 40 50
	CLAY - silty,organics, br.grey,surface covered with organics			
1				
2	SAND and GRAVEL - silty			
	BEDROCK			
	End of hole 2.4m Standpipe installed to 2.3m			
3				
4				
5				
6				
7				

SFC. ELEVATION (m) -	DATE DRILLED Aug 14,1984	BOREHOLE NO. STP-4
COMPLETION DEPTH (m) 2.4	LOGGED BY JPB	
DRILLING RIG	LOCATION Bluefish Lake	PAGE 1 of 1

DEPTH (metres)	SOIL DESCRIPTION	SAMPLE	COMMENTS	MOISTURE CONTENT P_L (%) W (%) L_L (%) 10 20 30 40 50
	CLAY - silty,moist to wet, soft,br.grey		not frozen	
2	tr. gravel	T		
		G		
3	sand sloughed up to 3.0m while installing piezometer			
			84/08/16	
	BEDROCK			
5	End of hole 4.8m Electro-piez. no.103 installed to 4.7m			

SFC. ELEVATION (m) 168.225	DATE DRILLED Aug 13,1984
COMPLETION DEPTH (m) 4.8	LOGGED BY JPB
DRILLING RIG	LOCATION Buefish Lake

BOREHOLE NO. P-2

PAGE 1 of 1

DEPTH (metres)	SOIL DESCRIPTION	SAMPLE	COMMENTS	MOISTURE CONTENT P_L (%) W (%) L_L (%) 10 20 30 40 50
0–3	CLAY - silty,moist,soft to firm,br.grey		not frozen	
3–4	SAND and GRAVEL End of hole 4.0m			
4–7	BEDROCK Slope Indicator casing installed to 3.4m			

SFC. ELEVATION (m) 168.018	DATE DRILLED Aug 13,1984
COMPLETION DEPTH (m) 4.0	LOGGED BY JPB
DRILLING RIG	LOCATION Bluefish Lake

BOREHOLE NO. SI-3
PAGE 1 of 1

DEPTH (metres)	SOIL DESCRIPTION	SAMPLE	COMMENTS	MOISTURE CONTENT P_L (%) W (%) L_L (%) 10 20 30 40 50
	CLAY - silty,moist,br.grey		not frozen	
1				
2				
3				
	End of hole 3.7m			
	BEDROCK			
4	Slope Indicator casing installed to 3.65m			
5				
6				
7				

SFC. ELEVATION (m) 168.45	DATE DRILLED Aug 13,1984	BOREHOLE NO. SI-4
COMPLETION DEPTH (m) 3.7	LOGGED BY JPB	
DRILLING RIG	LOCATION Bluefish Lake	PAGE 1 of 1

DEPTH (metres)	SOIL DESCRIPTION	SAMPLE	COMMENTS	MOISTURE CONTENT P_L (%) W (%) L_L (%) 10 20 30 40 50
0	CLAY - silty,br.grey		not frozen	
1				
2			84/08/16	
3	SAND and GRAVEL - wet			
4	End of hole 4.0m			
	BEDROCK Standpipe installed to 4.0m			
5				
6				
7				

SFC. ELEVATION (m) 168.41	DATE DRILLED Aug 13,1984	BOREHOLE NO. STP-3
COMPLETION DEPTH (m) 4.0	LOGGED BY JPB	
DRILLING RIG	LOCATION Bluefish Lake	PAGE 1 of 1

DEPTH (metres)	SOIL DESCRIPTION	SAMPLE	COMMENTS	MOISTURE CONTENT P_L (%) W (%) L_L (%) 10 20 30 40 50
0	CLAY - silty,br.grey boulders on surface		not frozen	
2	SAND and GRAVEL ?			
2.9	End of hole 2.9m		no rdg. 84/08/16	
3	BEDROCK Electro-piezo no.102 installed to 2.4m			

SFC. ELEVATION (m) -	DATE DRILLED Aug 13,1984	BOREHOLE NO. P-3
COMPLETION DEPTH (m) 2.9	LOGGED BY JPB	
DRILLING RIG	LOCATION Bluefish Lake	PAGE 1 of 1

DEPTH (metres)	SOIL DESCRIPTION	SAMPLE	COMMENTS
	CLAY - some silt and sand, moist,br,grey		not frozen
1			pp=2.5 tsf tv=0.9 tsf
	laminations of clay and sil some ice-rafted pe-bles,max size 12mm,some organics, breaks along laminations	T	
2	End of hole 2.1m	T G	pp=3.3 tsf tv=0.6 tsf
	BEDROCK Standpipe installed to 2.0m		
3			
4			
5			
6			
7			

MOISTURE CONTENT

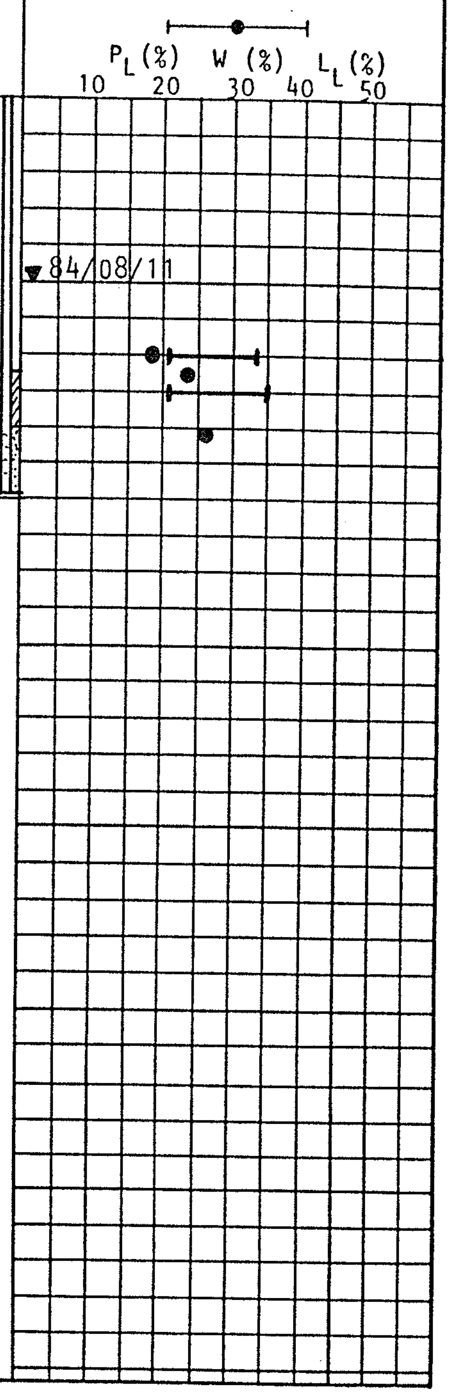

SFC. ELEVATION (m) 167.67	DATE DRILLED Aug 11,1984	BOREHOLE NO. STP-2
COMPLETION DEPTH (m) 2.1	LOGGED BY JPB	
DRILLING RIG	LOCATION Bluefish Lake	PAGE 1 of 1

DEPTH (metres)	SOIL DESCRIPTION	SAMPLE	COMMENTS	MOISTURE CONTENT
	CLAY - silty, some gravel and cobbles, br. grey		not frozen	
1				
	silt. tr. clay and pebbles, max. size 25mm, moist to wet, some organics, iron oxide stains, horz. laminations of silt and clay, soft	T	pp=2.0 tsf	
2		T		
	sandy and gravelly			
	End of hole 2.4m			
	BEDROCK			
	Slope Indicator casing installed to 2.4m			
3				
4				
5				
6				
7				

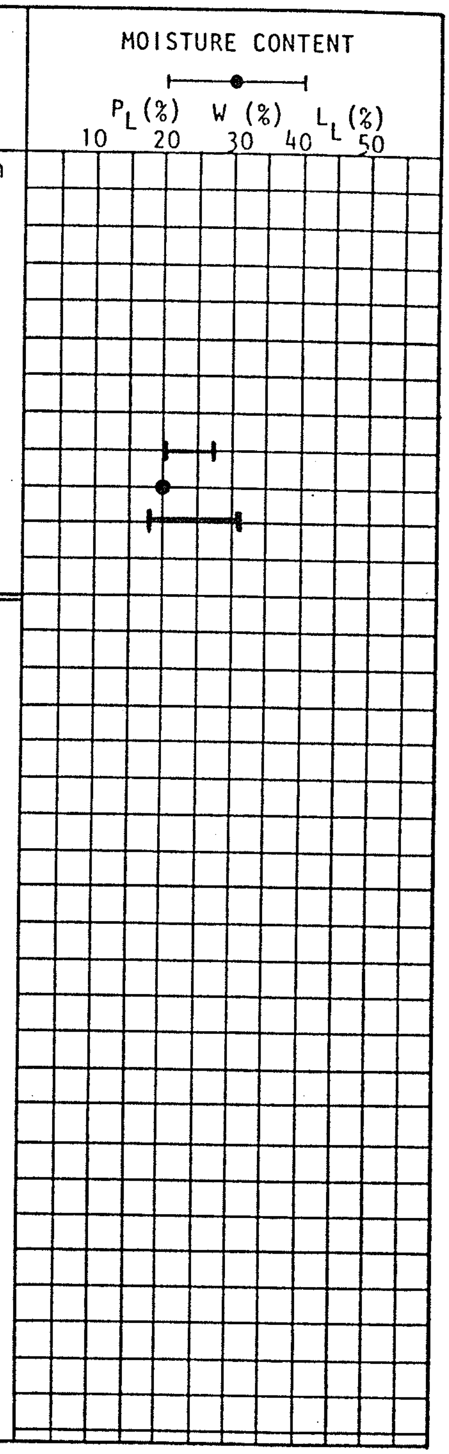

SFC. ELEVATION (m) 168.107	DATE DRILLED Aug 13, 1984	BOREHOLE NO. SI-2
COMPLETION DEPTH (m) 2.4	LOGGED BY JPB	
DRILLING RIG	LOCATION Bluefish Lake	PAGE 1 of 1

DEPTH (metres)	SOIL DESCRIPTION	SAMPLE	COMMENTS	MOISTURE CONTENT: P_L (%), W (%), L_L (%) — 10, 20, 30, 40, 50
	CLAY TILL - some large rocks max.size 30 cm.,rootlets throughout. - blocky clay,greyish		pp=3.0 tsf tv=0.9 tsf	
1	- wet layer of silt - dk.grey clay,some silt high plastic		pp=1.0 tsf tv=0.3 tsf pp=2.0 tsf tv=0.7 tsf	
	- CLAY TILL - tr.gravel, dk.grey,iron oxide dep. - slickensides,blocky structure,block sample obtained.	B		
2				
	TPC 102 installed at 1.7m TPC 101 installed at 1.45m			
3				
4				
5				
6				
7				

SFC. ELEVATION (m) -	DATE DRILLED Aug 9-11,1984
COMPLETION DEPTH (m) 1.8	LOGGED BY JPB
DRILLING RIG	LOCATION Bluefish Lake

BOREHOLE NO. TP-1
PAGE 1 of 1

DEPTH (metres)	SOIL DESCRIPTION	SAMPLE	COMMENTS	MOISTURE CONTENT P_L (%) W (%) L_L (%) 10 20 30 40 50
	CLAY TILL - silty,weathered organics throughout			
1	SILT - greyish,very wet		frozen 06/13/85	
2	End of hole 2.0m			
3				
4				
5				
6				
7				

SFC. ELEVATION (m) -	DATE DRILLED Oct 19,1985	BOREHOLE NO. TP-2
COMPLETION DEPTH (m) 2.0	LOGGED BY JPB	
DRILLING RIG	LOCATION Bluefish Lake	PAGE 1 of 1

B.5 Instrumentation Specifications

geokon

GEOTECHNICAL INSTRUMENTATION

Models 2510, 3500, 3650, 4800E and 4800EC

Earth Pressure Cells

and

Models 2520, 3600, 3660 and 4800C

Concrete Stress Cells

FEATURES

- Long-term stability.
- High sensitivity.
- High pressure range.
- Post-stressing tube for re-inflation in concrete.
- Low volumetric displacement.
- Suitable for remote monitoring over long time periods.

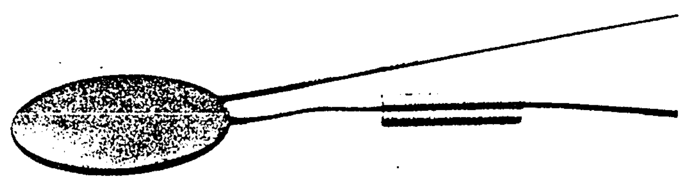

Geokon Earth Pressure Cells are designed to measure total pressure in earth fills and embankments as well as pressures on the surface of retaining walls, buildings, bridge abutments, sheet pilings, tunnel linings etc. Concrete stress cells are designed to measure stress in mass concrete.

All cells consist of two circular stainless steel plates welded together around their periphery and spaced apart by a narrow cavity filled with either an antifreeze solution (Earth Pressure Cells) or mercury (Concrete Stress Cells). A length of high-pressure stainless steel tubing connects the cavity to a pressure transducer. External pressures acting on the cell are balanced by an equal pressure induced in the internal fluid. This pressure is converted by the pressure transducer into an electrical signal which is transmitted by a four-conductor shielded cable (direct burial type) to the readout location. A readout box is used to read the cells, and calibrations are provided to enable the observed readings to be converted to units of pressure or stress. (Models 2510 and 2520 have a pneumatic transducer which connects to the readout location by means of polyethylene twin tubes in an outer PVC wrap).

In all systems the internal fluid is degassed to a maximum dissolved gas content of 2.0 ppm. This ensures that the volumetric displacement of the cells is a minimum and that their response characteristics are linear and highly sensitive. Concrete stress cells have a 24-inch long "pinch" or "post-stressing" tube to allow mercury to be forced back into the cell after the concrete cures. This ensures good physical contact between the cell and the surrounding concrete. Concrete stress cells may be pre-encapsulated in concrete to simplify the post-stressing operation.

Thermistors may be included in the transducer housing to measure temperatures. Cables can be routed inside flex conduit for added mechanical protection.

geokon
[illegible] CENTRAL AVENUE
WEST LEBANON, N.H. 03784
[illegible]

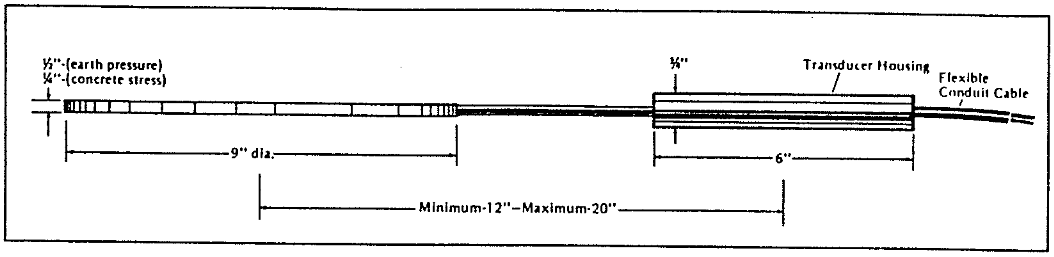

Geokon offers the following four basic types of transducers:

Pneumatic (Models 2510 and 2520). This transducer is a Petur Model P-100 and is connected to the readout location via twin pneumatic tubes (Model T-102). It is read out using the Petur Model C-102 Readout Box.

Semiconductor Strain Gage — Conventional style pressure transducer compatible with many existing dataloggers where 5 volt DC or AC excitation is provided. The signal output is large enough to be scanned directly without further amplification. They may also be read remotely using the Geokon Model RB-101 Readout Box.

Resistance Strain Gage — These transducers are compatible with other resistance strain gage systems such as load cells, borehole deformation gages etc. They may be read out using conventional strain indicator or readout boxes (Vishay P350A, Vishay P3500 etc.).

Vibrating Wire (Model 4500H). This transducer is compatible with the rest of the Geokon line of vibrating wire instruments and is recommended for use with the Model GK-4 Datalogger or GK-401 Readout Box. It incorporates all of the advantages of the vibrating wire system of measurements.

SPECIFICATIONS

Model Number	EP Cell CS Cell	2510 2520	3500 3600	3650 3660	4800E 4800C
Transducer type	—	Pneumatic	Semiconductor strain gage	Resistance strain gage	Vibrating wire
Typical ranges available	psi	15 to 3000*	25,100,500 1000,3000,5000	25,100,500 1000,3000,5000	50,100,500 1000,3000,5000
Over-range capacity	% F.S.	3000 psi max.	200	200	150
Accuracy	% F.S.	0.4*	1	0.5	0.25
Resolution	% F.S.	0.4*	infinite	infinite	0.1
Thermal effect on zero	% F.S./°F	zero	<0.05	<0.02	<0.05
Excitation voltage	V	—	max.6v (DC or AC)	max.10v (DC or AC)	5v sq.wave
Signal output	mv/v	—	20	3	1200-2000Hz frequency
Bridge resistance	ohms	—	150in 115out	350	coil 150
Transducer housing dia.	in.	1.5	1.625	2.25	1
Transducer housing length	in.	6	6	6	6
Weight (less cable	lbs.	5 7	5 7	5 7	5 7
Connecting leads	—	Polyethylene twin tubes	4-cond. shielded	4-cond. shielded	2-cond. shielded
Readout box	—	Petur C-102	Geokon RB-101	Vishay P350A	Geokon GK-401

*Depends on pressure gage in readout box.

Accessories
GK-401 Readout Box.
Thermistor Readout.
RB-101 Readout Box.
P350A Readout Box.
Petur C-102 Readout Box.

Options
Thermistors.
Flex Conduit Cable Protection.

Ordering Information
Specify: 1.Model Number.
2.Range.
3.Cable Length.
4.Accessories Required.
5.Options Required.

For further information contact us . . . . .

geokon incorporated
7 CENTRAL AVENUE
WEST LEBANON. N.H. 03784

603/298-5064

geokon

GEOTECHNICAL
INSTRUMENTATION

Vibrating Wire Piezometers and Pressure Transducers

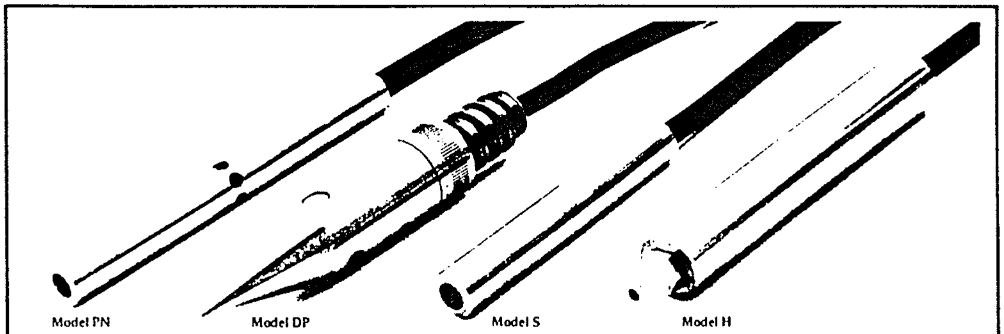

Geokon Vibrating Wire Piezometers and Pressure Transducers are designed to measure fluid pressures (e.g. ground water elevations, pore pressures) in boreholes, embankments, foundations, pipelines, wells and pressure vessels.

- Long term stability in difficult environments.
- Hermetically sealed.
- Small size.
- Stainless steel construction.
- Lightning protected.
- Heavy duty cable.

The transducer employs a sensitive diaphragm, coupled to a vibrating wire, that converts the fluid pressures to be measured into an equivalent frequency signal. Transmitted through a cable to the readout location, the frequency signal is there displayed on a portable readout box. Alternatively, a Datalogger can be used to record the data automatically.

Several different models and options are available. The standard sensor is dimensionally small enough to be installed into fills, embankments, boreholes, standpipes or observation wells. A drive-in version is available for pushing directly into soft ground on the end of diamond drill rods. For use in critical locations another model has been developed with a pneumatic back-up system to provide confirmation of gage accuracy and stability. One model is available for use where fluctuating temperatures are a problem and another for use in typical pressure transducer applications where a hydraulic pressure connection is required to permit easy coupling to pressurized tanks, pipelines, earth pressure cells, etc.

All models of transducers may be obtained with a built-in thermistor for measuring temperatures at the sensor location.

Construction: Geokon piezometers utilize the latest developments in vibrating wire pressure transducer technology. The transducer is fabricated entirely from stainless steel components, selected to minimize temperature effects and welded together to create a hermetically sealed chamber for the vibrating wire element. The ends of the vibrating wire are clamped using a patented swaging technique that ensures high stability while allowing miniaturization of the components.

An electromagnetic coil, located close to the wire, is used to both pluck the wire and to convert the wire vibrations so produced into an electrical output current whose frequency is identical to the natural resonant frequency of the wire. Changing pressure causes deflection of the diaphragm thereby altering the tension of the wire and its resonant frequency of vibration. Thus for each pressure there is a corresponding frequency output.

The cable used to transmit the frequency signals is designed for direct burial in the ground. It has two thick outer wraps of tough high-density polyethylene separated by a metallic armored sheath. The cable is grease filled to discourage water wicking along it in the event that it is cut. Both cable and coil are protected from lightning damage. It should be noted that lead wire resistance changes brought about by water penetration, temperature variations and contact resistance do not affect the frequency of the output signal. This factor, coupled with excellent zero stability, makes the Geokon Vibrating Wire Transducer more preferable than conventional strain gage transducers for long-term measurements in difficult environments.

In geotechnical environments it is necessary to use a filter stone to prevent soil particles from impinging directly on the diaphragm. The standard filter stone is made from sintered stainless steel with a 50 micron pore size. In partially saturated soils, where air is to be excluded from the piezometer cavity, a high air entry filter stone may be specified. Note that negative pressures (suction) can be measured.

geokon incorporated
7 CENTRAL AVENUE
WEST LEBANON, N.H. 03784
603/298-5064

MODELS AVAILABLE

Model 4500S STANDARD MODEL

This model is designed for direct burial in embankments, fills, etc. Also for installation inside boreholes or observation wells. Its small size allows for its installation in conventional standpipe piezometer riser pipe (minimum I.D. is ¾").

Model 4500DP DRIVE POINT MODEL

This transducer is located inside an EW drill rod coupling with a pointed nose cone attached. When screwed onto the end of EW drill rods the unit can be pushed directly into soft ground with the signal cable located inside the drill rod. This model is recoverable at the end of the job.

Model 4500PN VIBRO/PNEUMATIC MODEL

To be used in very critical applications needing verification of readings. A pneumatic transducer packaged in tandem with the vibrating wire transducer permits a second evaluation of the measured pressures. The signal cable is supplemented with two pneumatic tubes.

Model 4500T TEMPERATURE STABLE MODEL

Where temperatures fluctuate markedly this model is useful since it is only minimally affected by these changes (.01% F.S./°F,—compared to 0.1%F.S./°F for standard models). *Note:* All models can be supplied with thermistors built into the transducer to measure the temperature at the transducer location.

Model 4500H PRESSURE TRANSDUCER MODEL

This model is supplied with a ¼" male pipe thread fitting to permit the transducer to be coupled directly into hydraulic or pneumatic pressure lines. For laboratory use a lighter, more flexible signal cable should be specified

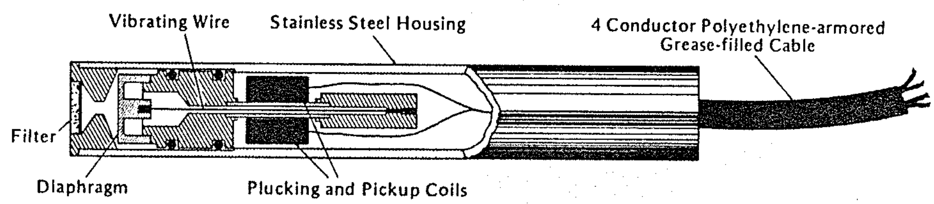

Readout Instrumentation:
All models can be read using the Geokon Model GT1174 Portable Readout Box. The box displays the reading on a 5-digit liquid crystal display (LCD). The displayed readings can be converted into psi by using the calibration data supplied with the piezometer. The pneumatic half of the Model 4500PN Piezometer can be read using the Petur Model C-102 Readout Box. Junction boxes and terminal boxes are available to protect cable splices and electrical connectors. Automatic and remote recording can be accomplished using the Geokon Model GT1172 Portable Datalogger.

GENERAL SPECIFICATIONS

Standard ranges (lbs./sq. in.)	50, 100, 250, 500, 1000, 5000
Over range	2X rated pressure
Resolution	0.1% F.S. minimum
Accuracy	± 0.5 % F.S.
Operating temperature	-20° to 150° F (-29° to 65°C)
Thermal zero shift	0.1%F.S./°F (Model 4500T - 0.01%F.S./°F)
Diaphragm displacement	.01 cc at F.S.
Cable	4 conductor direct burial type — 22 ga.
Filter	standard: 50 micron sintered stainless steel high air entry: Coors Alumina - approx. 2 microns

WEIGHTS AND DIMENSIONS

Model No. 4500		S	DP	PN	T	H
Diameter	in (mm)	0.75 (19)	1.312 (33.3)	0.75 (19)	0.75 (19)	1.0 (25.4)
Length	in (mm)	5.125 (130)	6.75 (171)	7.125 (181)	5.125 (130)	6 (152)
Weight	lbs (kg)	.26 (.12)	1.0(.45)	.5(.23)	.26(.12)	1.0(.45)

Ordering Information

Specify: 1.Model No.
2.Pressure range
3.Cable length
4.Options required

Optional Accessories

Thermistor
High-entry filter stone
Light-duty cable
Terminal boxes
Junction boxes

For further information contact us . . .

geokon incorporated
7 CENTRAL AVENUE
WEST LEBANON, N.H. 03784

603/298-5064

GENERAL PURPOSE PRESSURE TRANSDUCER

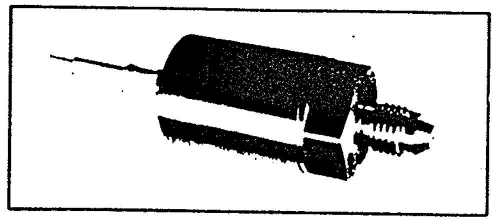

IPT-1100 SERIES

- High Unamplified Output
- Rugged All Welded Construction
- High Overload Capabilities
- Excellent Long Term Stability

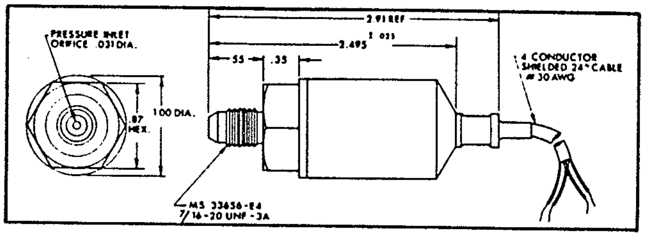

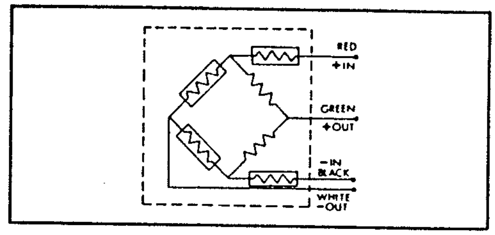

The ingenious application of modern solid state technology to transducer sensing is the main reason for making the IPT-1100 Series the most advanced general purpose pressure transducer available. Designed to measure liquid or gas pressure, the transducers are of all-welded stainless steel construction, with integral pressure port and diaphragm. The IPT-1100 provides an extremely rugged, accurate and inexpensive means for pressure-to-voltage conversion. The IPT-1100 Series are ideally suited for a large number of applications in **Industry, Process Control, Marine, Automation, Hydraulics,** and **Aerospace.**

INPUT	
Pressure Ranges	0-5 10 25 50 100 250 500 1000 2500 5000 PSI 0-0.34 0.68 1.72 3.4 6.9 17.2 34.5 69.0 172.0 345.0 BAR
Operational Mode	Sealed Gauge, Vented Gauge.
Over Pressure	2 Times Rated Pressure Range.
Burst Pressure	5 Times Rated Pressure Range to Max. of 20,000 PSI. (1379 BAR.).
Pressure Media	Any Liquid or Gas Compatible with 17-4PH SS (H 900 Condition).
Rated Electrical Excitation	10 VDC/AC (RMS)
Max. Electrical Excitation	12 VDC/AC (RMS)
Input Impedance	1800 Ohm (Nominal)
OUTPUT	
Output Impedance	650 Ohm (Nominal)
Full Scale Output (FSO)	100 mV (Nominal)
Residual Unbalance	5% FSO
Combined Non-Linearity, Hysteresis, and Repeatability	0.5% FSO Max.
Hysteresis	0.25% FSO Max.
Repeatability	0.1% FSO Max.
Resolution	Infinite
Natural Frequency (Nom.)	12 KHz for 50 PSI Range to 50 KHz for 5000 PSI Range
Insulation Resistance	100 Megohm Min. at 50V DC
ENVIRONMENTAL	
Operating Temperature Range	−40°F to +250°F (−40°C to +120°C).
Compensated Temperature Range	80°F to 180°F (27°C to 80°C).
Thermal Zero Shift	2% FSO/100°F (55°C).
Thermal Sensitivity Shift	2% FSO/100°F (55°C).
Steady Acceleration and Linear Vibration	Not Greater Than 0.02% FSO/g. Frequency Range 0-2000 Hz Max. Acceleration 50g (100g with no damage)
Altitude	−150 ft. to +70,000 ft. Will not Damage Sensor.
Submersion	To 50 ft. Without Damage.
Humidity	100% Relative Humidity.
Mechanical Shock	100g half Sine Wave 1 m. sec. Duration.
PHYSICAL	
Pressure Port	A.-33656/E4 7/16-20 UNF-3A *B.-1/4"-18 NPT Male Available at Extra Cost
Electrical Connection	Sealed Cable Assembly in lengths up to 30 ft. (9 meters)
Weight	110 Grams Approx.

ORDERING INFORMATION: IPT-1100-XXXX-XX-X-XXX
Pressure Range in PSI
Operational Mode (VG or SG)
Pressure Port Thread Size (A or B)
Cable Length

HR SERIES—GENERAL APPLICATIONS

- OPTIMUM PERFORMANCE FOR THE MAJORITY OF APPLICATIONS
- LARGE CORE-TO-BORE CLEARANCE – 1/16 INCH (1.6 mm) RADIAL

The HR high reliability series of LVDT's is suitable for most general applications. The HR series features large core-to-bore clearance, high output voltage over a broad range of excitation frequencies, and a magnetic stainless steel case for electromagnetic and electrostatic shielding.

GENERAL SPECIFICATIONS

Input Voltage . . . . . 3 V rms (nominal)
Frequency Range . . . 400 Hz to 10 kHz
Temperature Range . . -65°F to +300°F (-55°C to +150°C)
Null Voltage . . . . . . Less than 0.5% full scale output
Shock Survival . . . . . 1000 g for 11 milliseconds

Vibration Tolerance . 20 g up to 2 kHz
Coil Form Material . . High density, glass- filled polymer
Housing Material . . . AISI 400 series stainless steel
Lead Wires . . . . 28 AWG, stranded copper, Teflon-insulated, 12 inches (300 mm) long (nominal)

PERFORMANCE SPECIFICATIONS AND DIMENSIONS (2.5 kHz) *METRIC DIMENSIONS IN BLUE*

LVDT MODEL NUMBER	NOMINAL LINEAR RANGE	LINEARITY ±PERCENT FULL RANGE				SENSITIVITY mV Out/ Volt In Per		IMPEDANCE Ohms		PHASE SHIFT	WEIGHT Grams		DIMENSIONS A (Body)		B (Core)	
	Inches	50	100	125	150	.001 In.	mm	Pri.	Sec.	Degrees	Body	Core	Inches	mm	Inches	mm
050 HR	±0.050	0.10	0.25	0.25	0.50	6.3	250	430	4000	–1	32	4	1.13	28.5	0.80	20
100 HR	±0.100	0.10	0.25	0.25	0.50	4.5	180	1070	5000	–5	48	6	1.81	46	1.30	33
200 HR	±0.200	0.10	0.25	0.25	0.50	2.5	100	1150	4000	–4	60	8	2.50	63.5	1.65	42
300 HR	±0.300	0.10	0.25	0.35	0.50	1.4	56	1100	2700	–11	77	10	3.22	82	1.95	50
400 HR	±0.400	0.15	0.25	0.35	0.60	0.90	36	1700	3000	–18	90	15	4.36	111	2.95	75
500 HR	±0.500	0.15	0.25	0.35	0.75	0.73	[illegible]	460	375	–1	109	18	5.50	140	3.45	88
1000 HR	±1.000	0.25	0.25	1.00	1.30•	0.39	16	460	320	–3	126	21	6.63	168	4.00	102
2000 HR	±2.000	0.25	0.25	0.50•	1.00•	0.24	9.6	330	330	+5	168	27	10.00	254	5.30	135
3000 HR	±3.000	0.15	0.25	0.50•	1.00•	0.27	11	115	375	+11	225	28	12.81	325	5.60	142
4000 HR	±4.000	0.15	0.25	0.50•	1.00•	0.22	8.8	275	550	+1	295	36	15.64	397	7.00	178
5000 HR	±5.000	0.15	0.25	1.00•	—	0.15	6.1	310	400	+3	340	36	17.88	454	7.00	178
10000 HR	±10.00	0.15	0.25	1.00•	—	0.08	3.0	550	750	–5	580	43	30.84	783	8.50	216

•Requires reduced core length

ORDERING INFORMATION

(Fold out page 32 for instructions on how to use this chart.)

5.0 kHz LIN. TEST (NOTE 4) / 10.0 kHz LIN. TEST (NOTE 4) / METRIC THREAD CORE (NOTE 1) / TEFLON BORELINER / SMALL DIAMETER CORE (NOTE 2) / 10 FOOT (3m) LEADS / MIL-QLY RADIATION RESISTANT (NOTE 3)

OPTION NO.	002	003	006	010	020	120
MODEL NO.						
050 HR	A	A	N	B	B	F
100 HR	A	A	N	B	B	F
200 HR	A	A	N	B	B	F
300 HR	X	X	N	B	B	F
400 HR	A	A	N	B	B	F
500 HR	A	A	N	B	B	F
1000 HR	X	X	N	C	X	F
2000 HR	X	X	N	C	X	F
3000 HR	X	X	N	C	X	F
4000 HR	X	X	N	C	X	F
5000 HR	X	X	N	C	X	F
10000 HR	X	X	N	C	X	F

Note 1: See outline drawing for metric thread size
Note 2. Consult factory for mass, dimensions, and thread size
Note 3: Withstands 10^{12} NVT total integrated flux
Note 4: See frequency option note on page 32

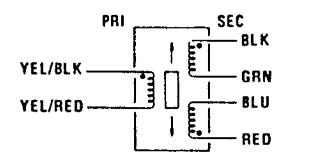

CONNECT GRN TO BLU FOR DIFFERENTIAL OUTPUT

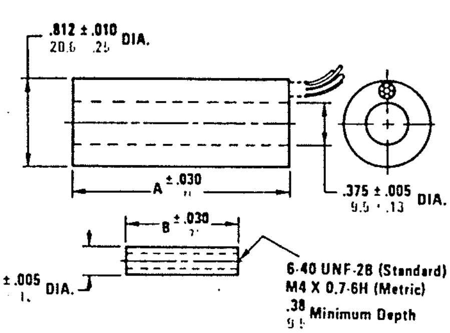

SEE SCHAEVITZ SERIES 70 BULLETINS FOR COMPATIBLE SIGNAL-CONDITIONING AND READOUT EQUIPMENT

APPENDIX C - Test Results

Table of Contents

C.1 Consolidation Test Results

C.1.1 CIU Consolidation Curves

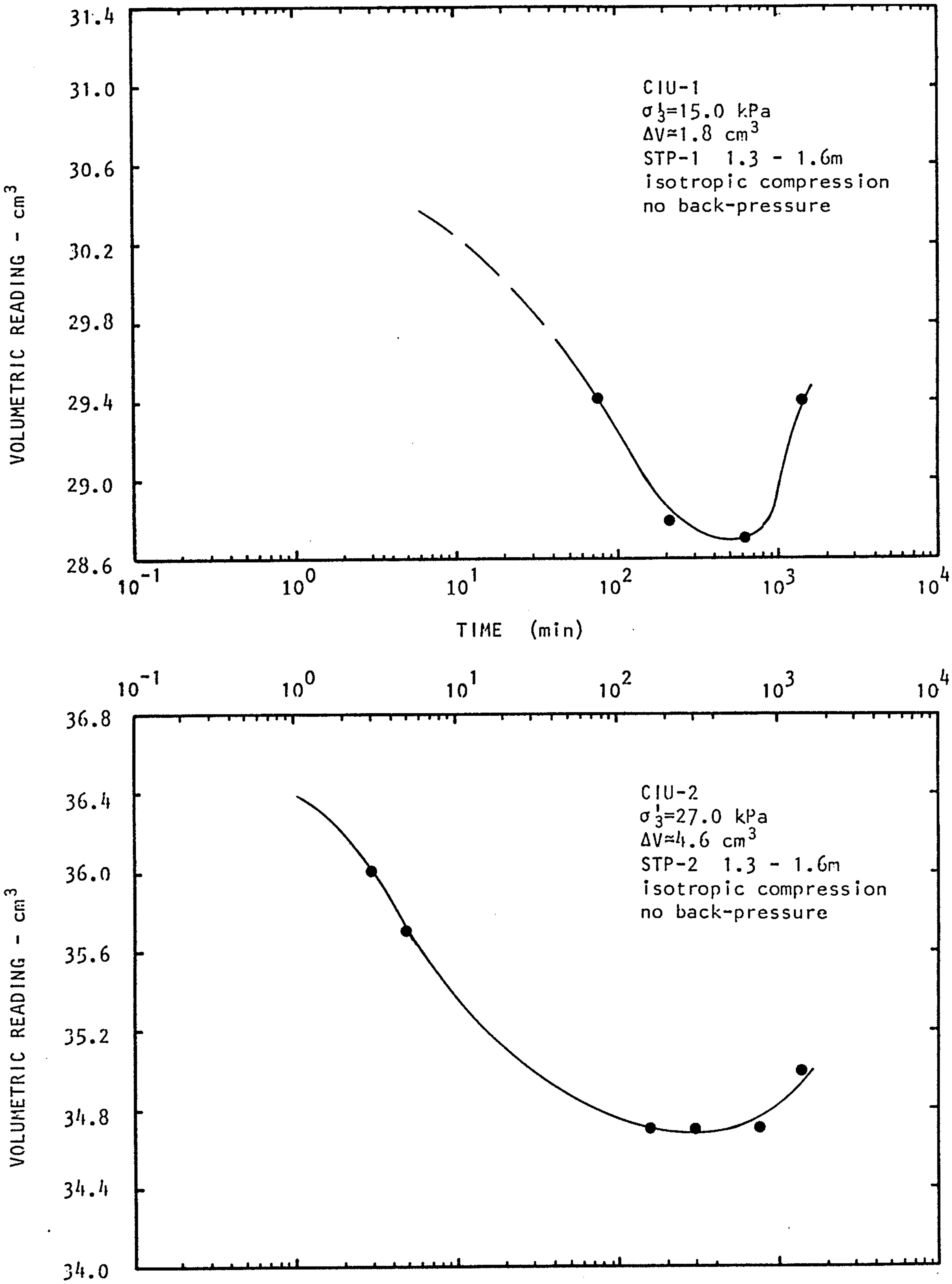

31.4
31.0
30.6
30.2
29.8
29.4
29.0
28.6
VOLUMETRIC READING - cm3
CIU-1
σ'3=15.0 kPa
ΔV≈1.8 cm3
STP-1 1.3 - 1.6m
isotropic compression
no back-pressure
10-1
100
101
102
103
104
TIME (min)
36.8
36.4
36.0
35.6
35.2
34.8
34.4
34.0
VOLUMETRIC READING - cm3
CIU-2
σ'3=27.0 kPa
ΔV≈4.6 cm3
STP-2 1.3 - 1.6m
isotropic compression
no back-pressure

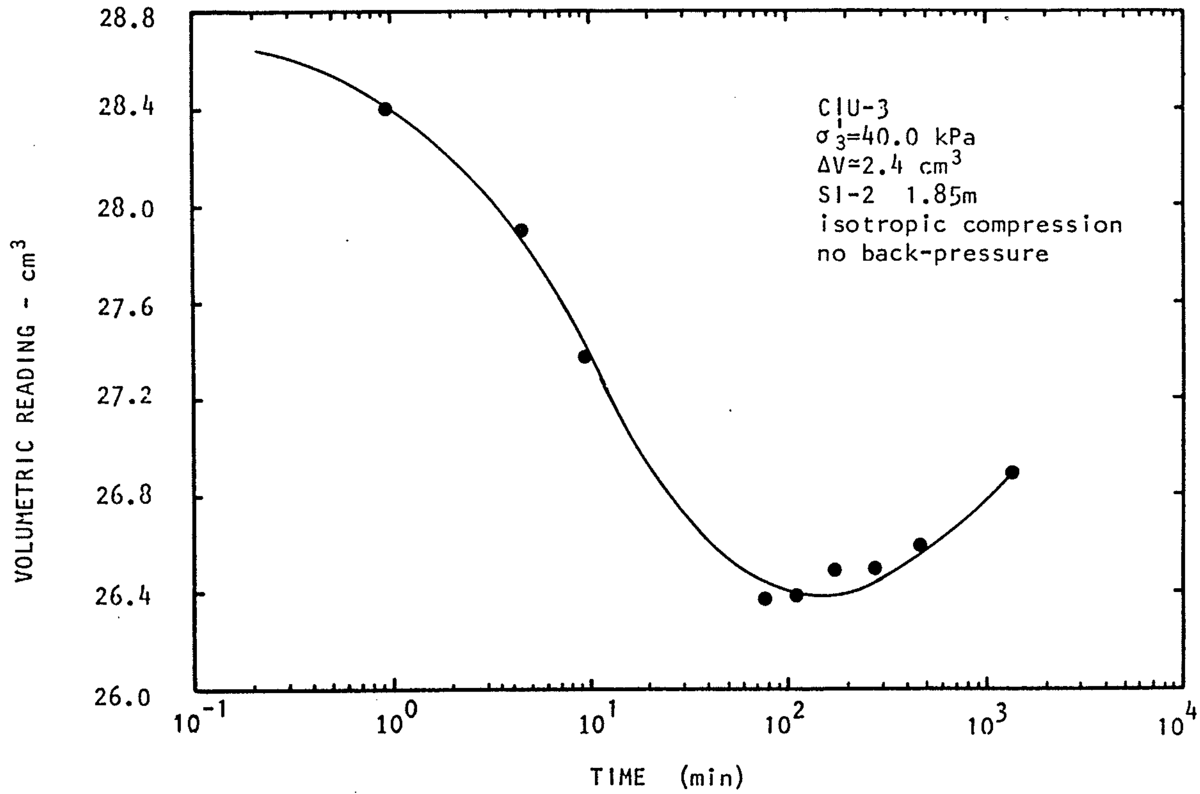

28.8
28.4
28.0
27.6
27.2
26.8
26.4
26.0
VOLUMETRIC READING - cm3
CIU-3
σ'3=40.0 kPa
ΔV≈2.4 cm3
SI-2 1.85m
isotropic compression
no back-pressure
10-1
100
101
102
103
104
TIME (min)

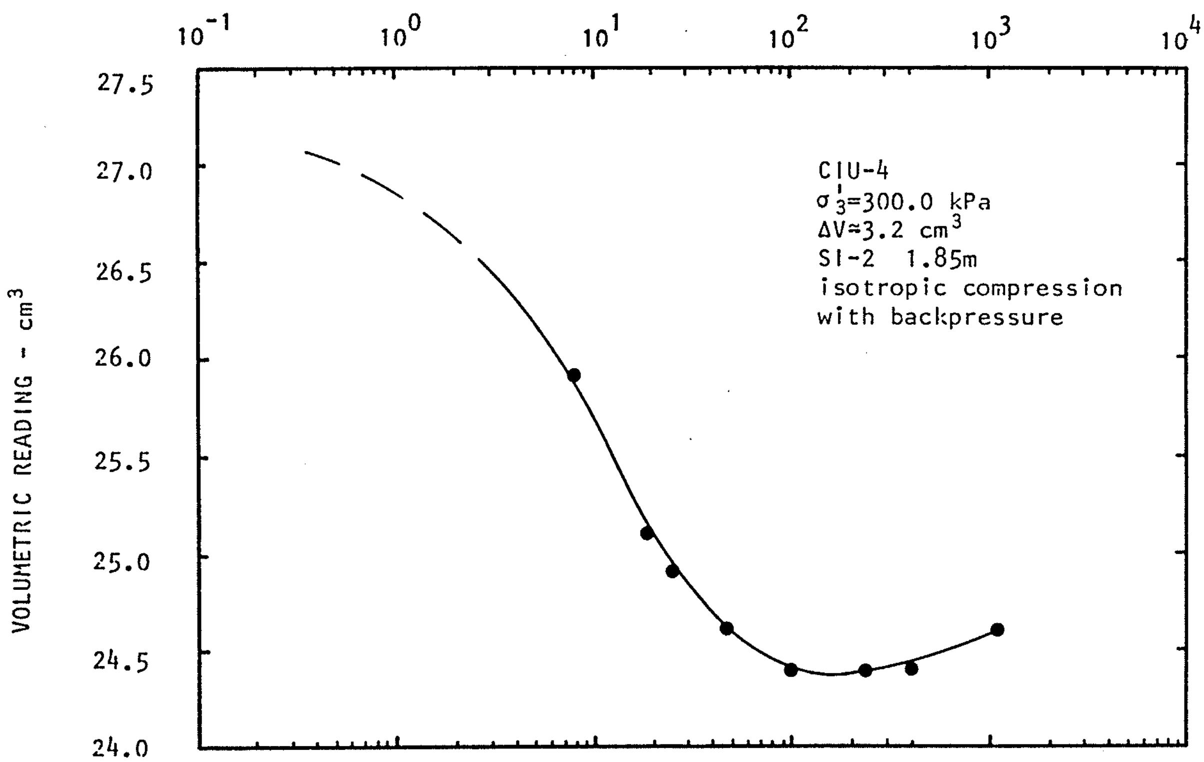

10-1
100
101
102
103
104
27.5
27.0
26.5
26.0
25.5
25.0
24.5
24.0
VOLUMETRIC READING - cm3
CIU-4
σ'3=300.0 kPa
ΔV≈3.2 cm3
SI-2 1.85m
isotropic compression
with backpressure

C.1.2 Isotropic Consolidation Curves

ISOTROPIC CONSOLIDATION TEST DATA

Load inc. no.	Load p' (kPa)	ΔV cm^3	Vv cm^3	e	V
1	10	0.16	34.28	0.8190	1.8190
2	20	0.40	34.04	0.8132	1.8132
3	40	1.05	33.39	0.7977	1.7977
4	80	1.90	32.54	0.7774	1.7774
5	160	3.09	31.35	0.7490	1.7490
6	320	4.35	30.09	0.7189	1.7189
7	160	3.80	30.64	0.7320	1.7320
8	80	3.10	31.34	0.7487	1.7487
9	40	2.30	32.14	0.7678	1.7678
10	20	1.59	32.85	0.7848	1.7848

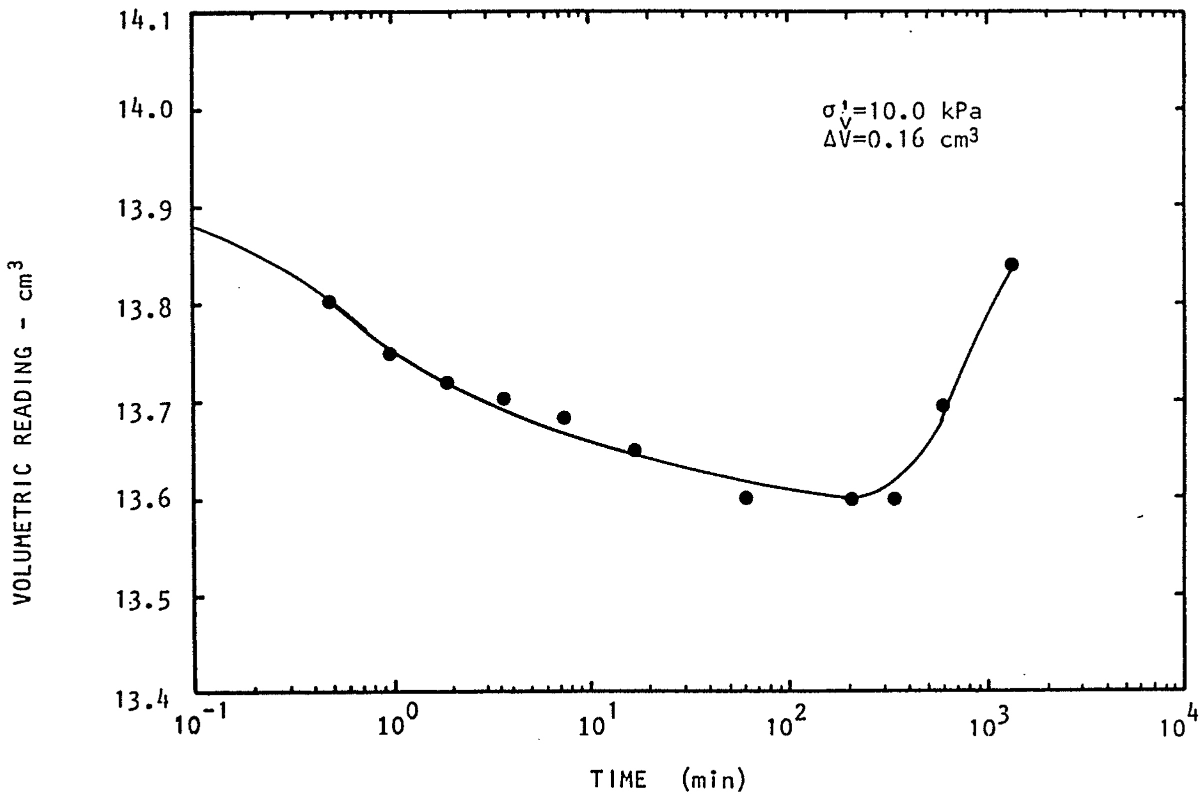

σ'v=10.0 kPa
ΔV=0.16 cm3
VOLUMETRIC READING - cm3
TIME (min)

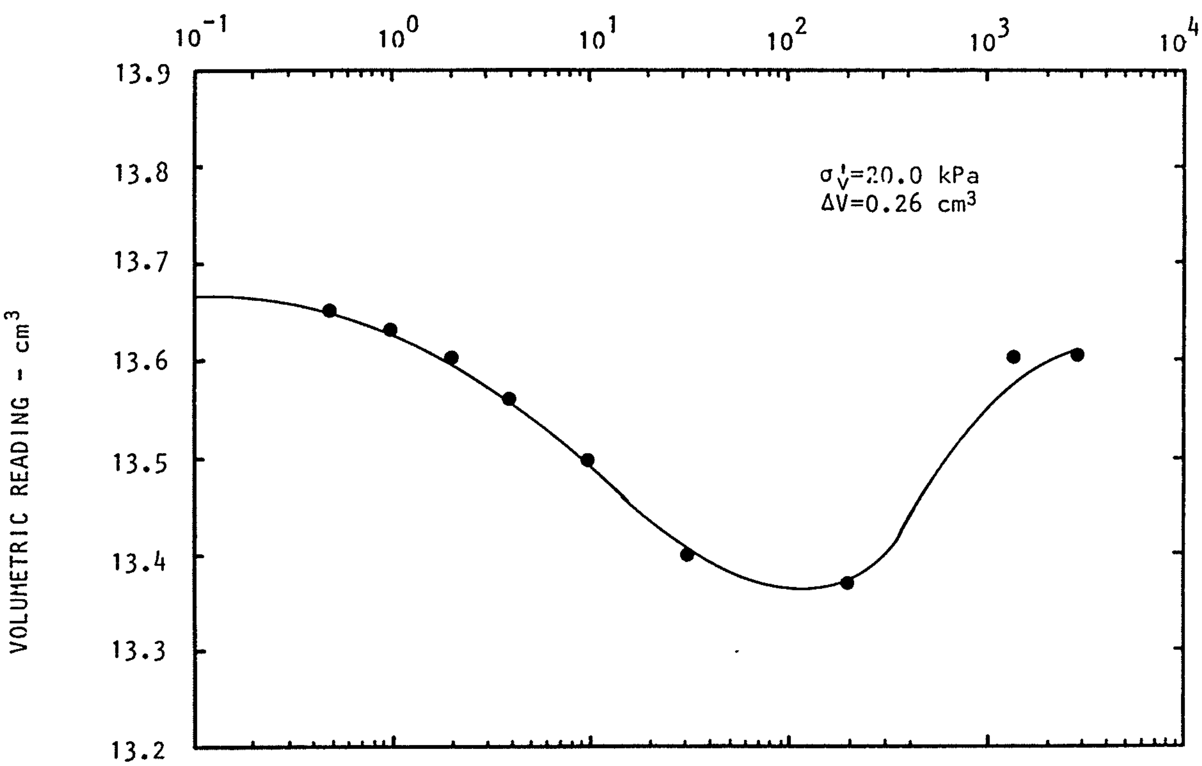

σ'v=20.0 kPa
ΔV=0.26 cm3
VOLUMETRIC READING - cm3

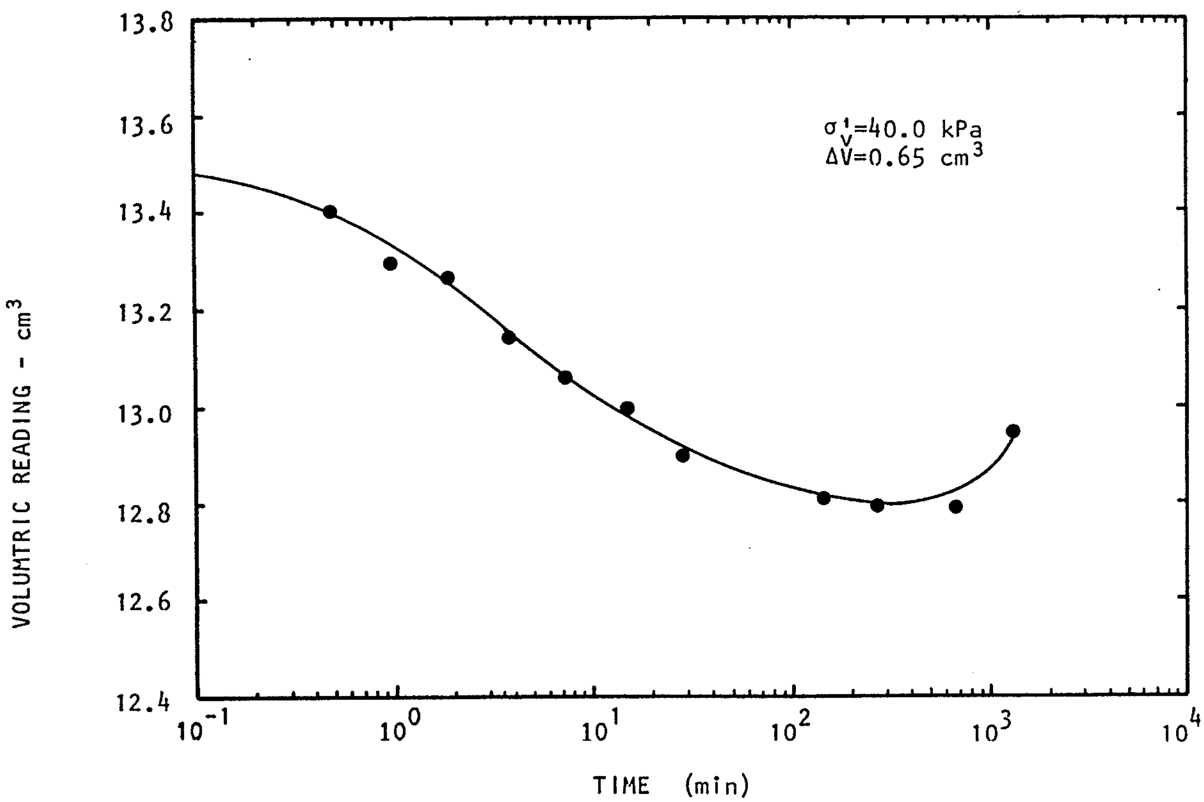

13.8
13.6
13.4
13.2
13.0
12.8
12.6
12.4
VOLUMTRIC READING - cm3
σ'v=40.0 kPa
ΔV=0.65 cm3
10-1
10 0
10 1
10 2
10 3
10 4
TIME (min)

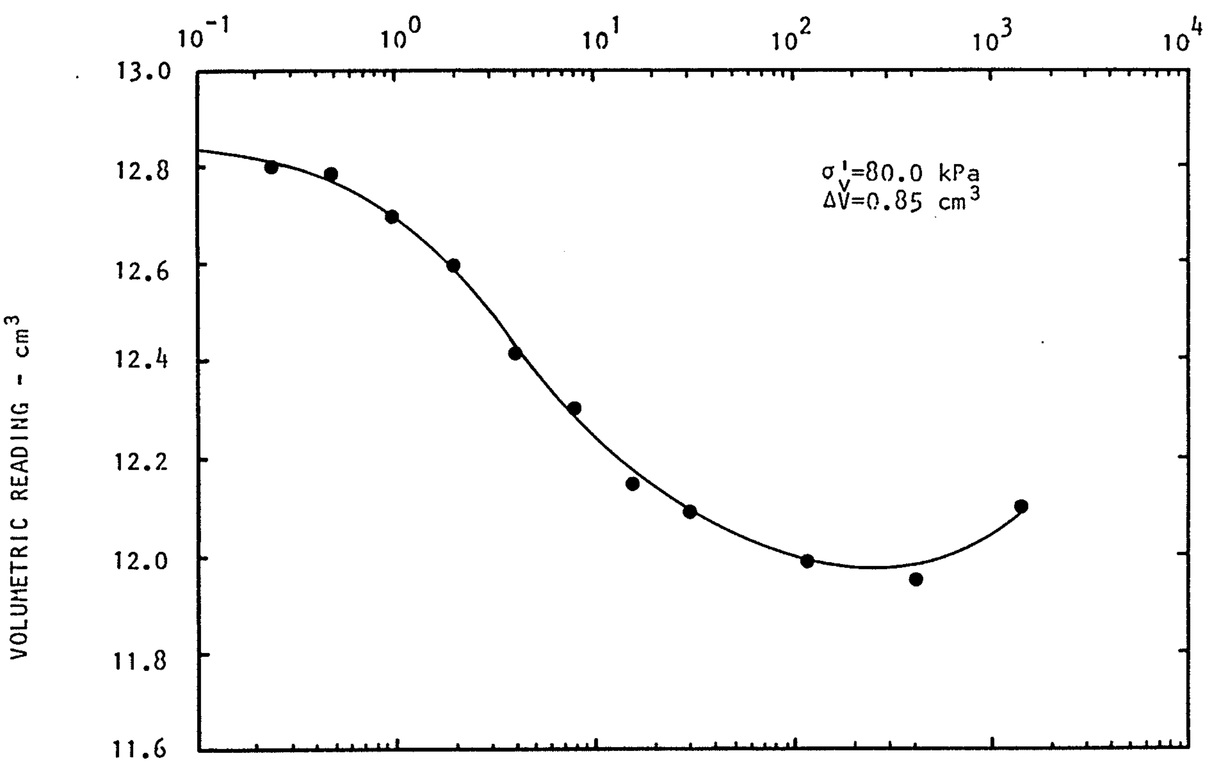

10-1
10 0
10 1
10 2
10 3
10 4
13.0
12.8
12.6
12.4
12.2
12.0
11.8
11.6
VOLUMETRIC READING - cm3
σ'v=80.0 kPa
ΔV=0.85 cm3

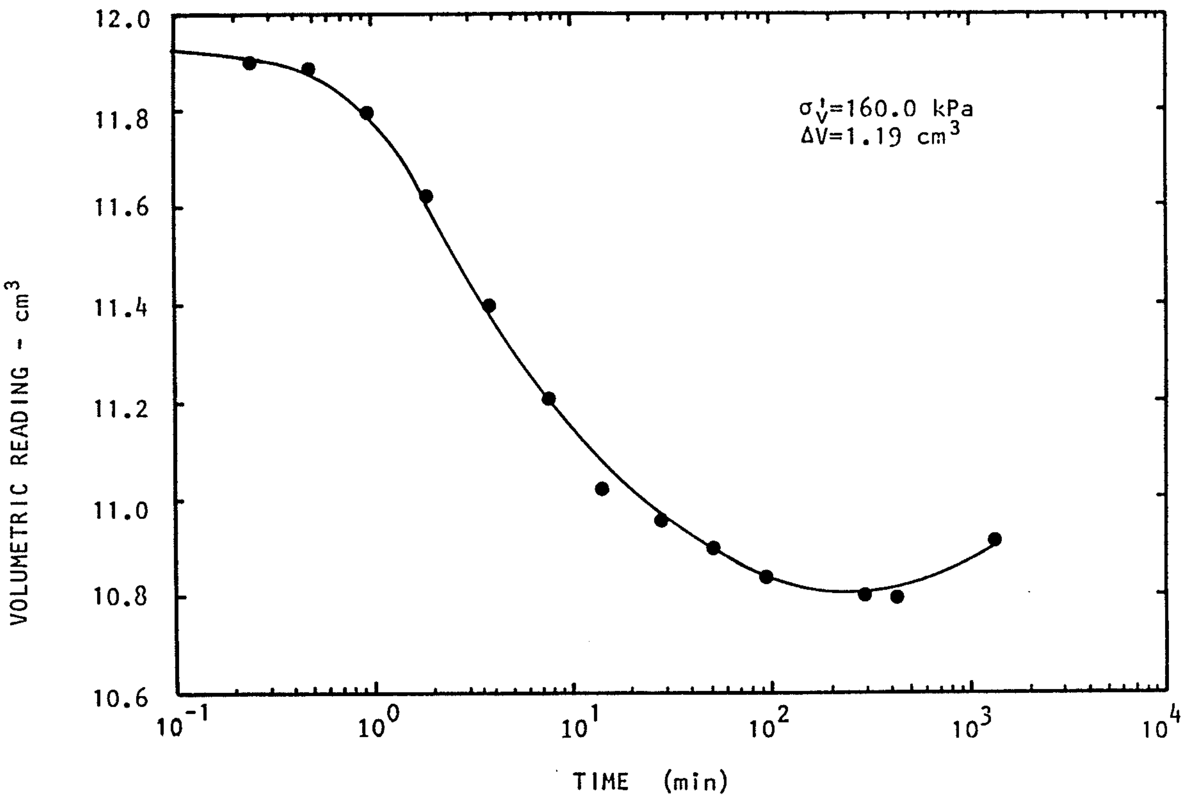

12.0
11.8
11.6
11.4
11.2
11.0
10.8
10.6
VOLUMETRIC READING - cm3
σ'v=160.0 kPa
ΔV=1.19 cm3
10-1
100
101
102
103
104
TIME (min)

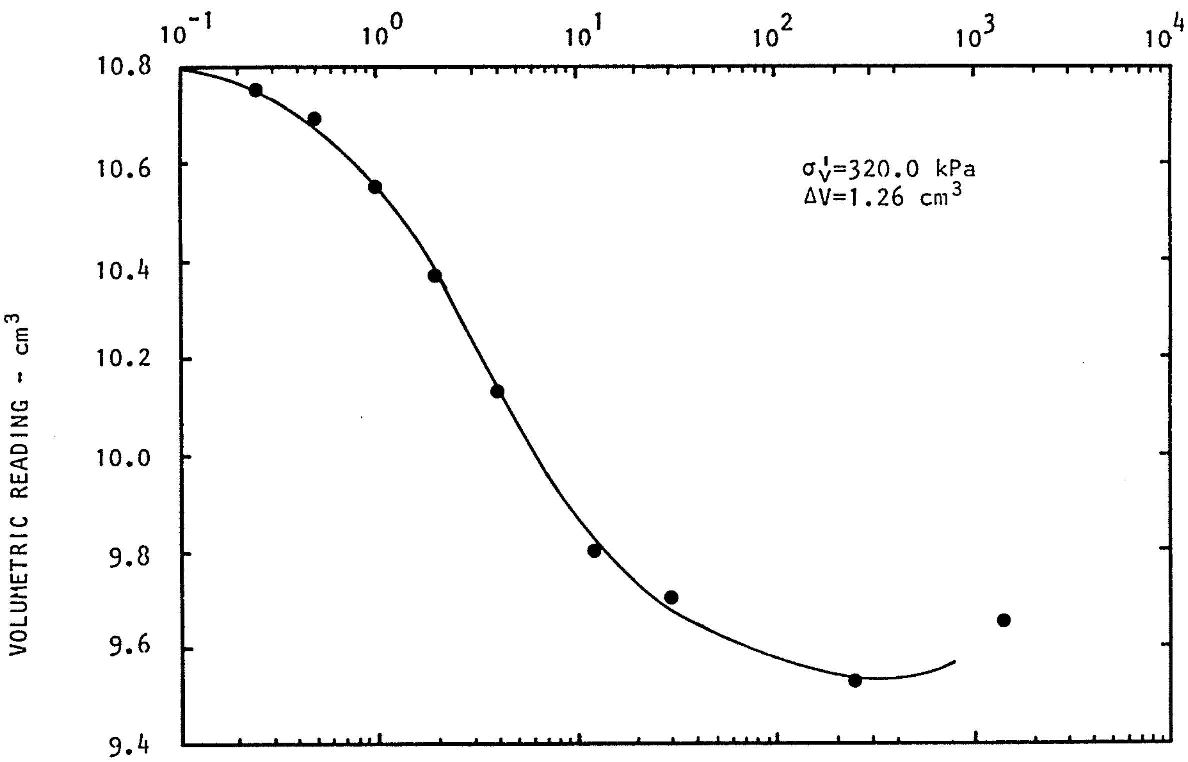

10-1
100
101
102
103
104
10.8
10.6
10.4
10.2
10.0
9.8
9.6
9.4
VOLUMETRIC READING - cm3
σ'v=320.0 kPa
ΔV=1.26 cm3

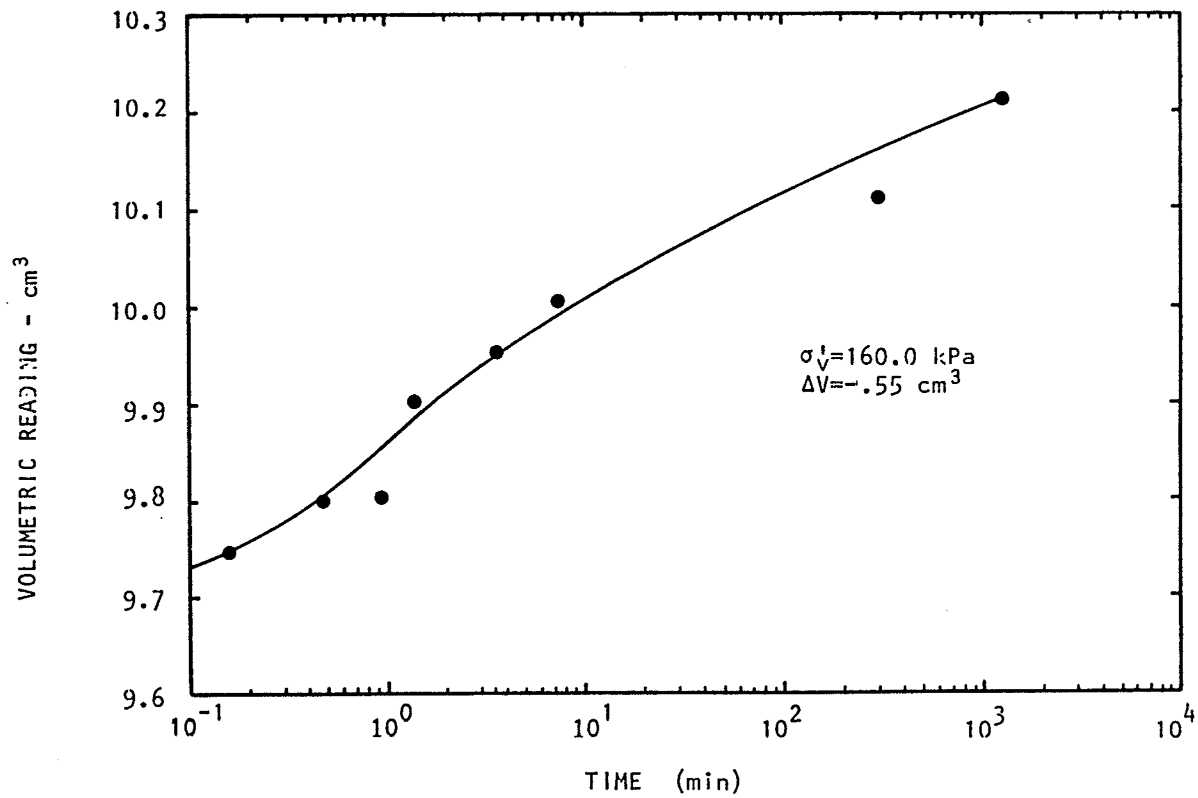
10.3
10.2
10.1
10.0
9.9
9.8
9.7
9.6
VOLUMETRIC READING - cm3
σ'v=160.0 kPa
ΔV=-.55 cm3
10-1
100
101
102
103
104
TIME (min)

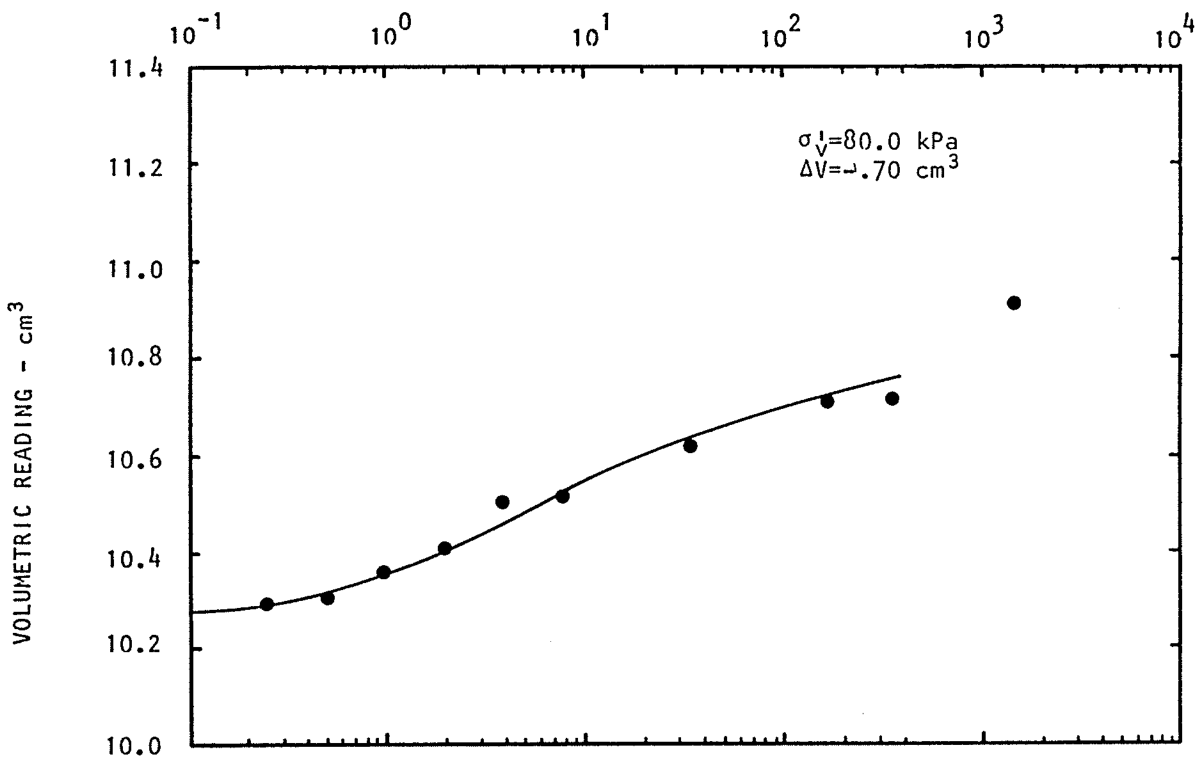
10-1
100
101
102
103
104
11.4
11.2
11.0
10.8
10.6
10.4
10.2
10.0
VOLUMETRIC READING - cm3
σ'v=80.0 kPa
ΔV=-.70 cm3

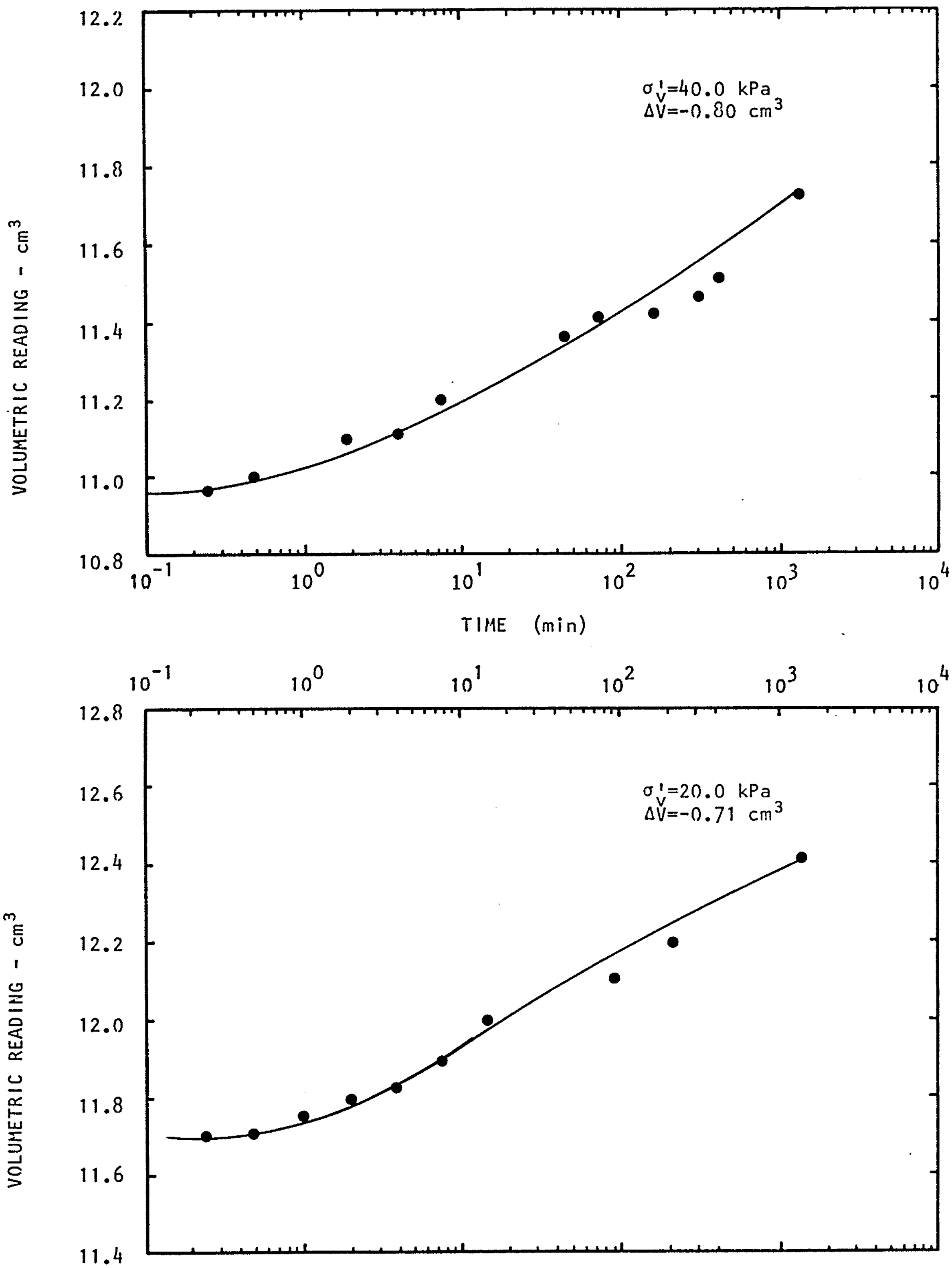
12.2
12.0
11.8
11.6
11.4
11.2
11.0
10.8
VOLUMETRIC READING - cm3
σ'v=40.0 kPa
ΔV=-0.80 cm3
10-1
100
101
102
103
104
TIME (min)
12.8
12.6
12.4
12.2
12.0
11.8
11.6
11.4
VOLUMETRIC READING - cm3
σ'v=20.0 kPa
ΔV=-0.71 cm3

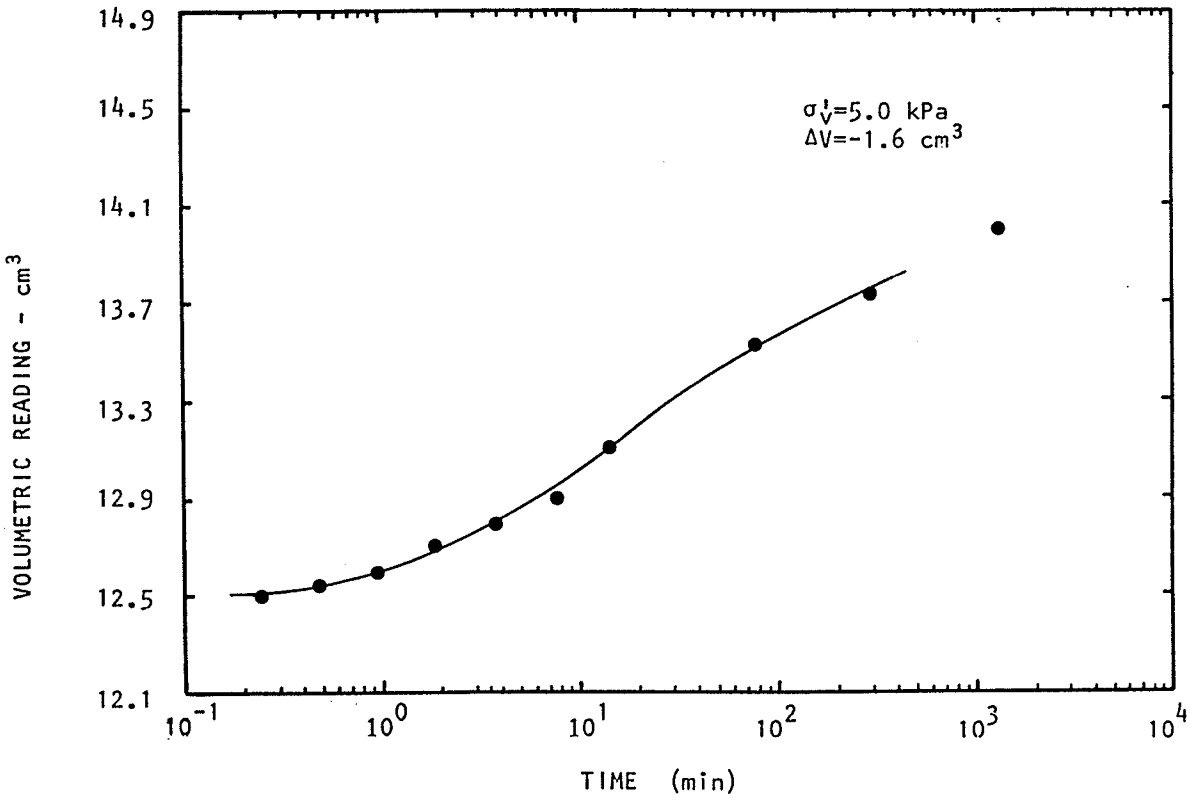

σ'_v=5.0 kPa
ΔV=-1.6 cm^3
VOLUMETRIC READING - cm^3
14.9
14.5
14.1
13.7
13.3
12.9
12.5
12.1
10^{-1}
10^0
10^1
10^2
10^3
10^4
TIME (min)

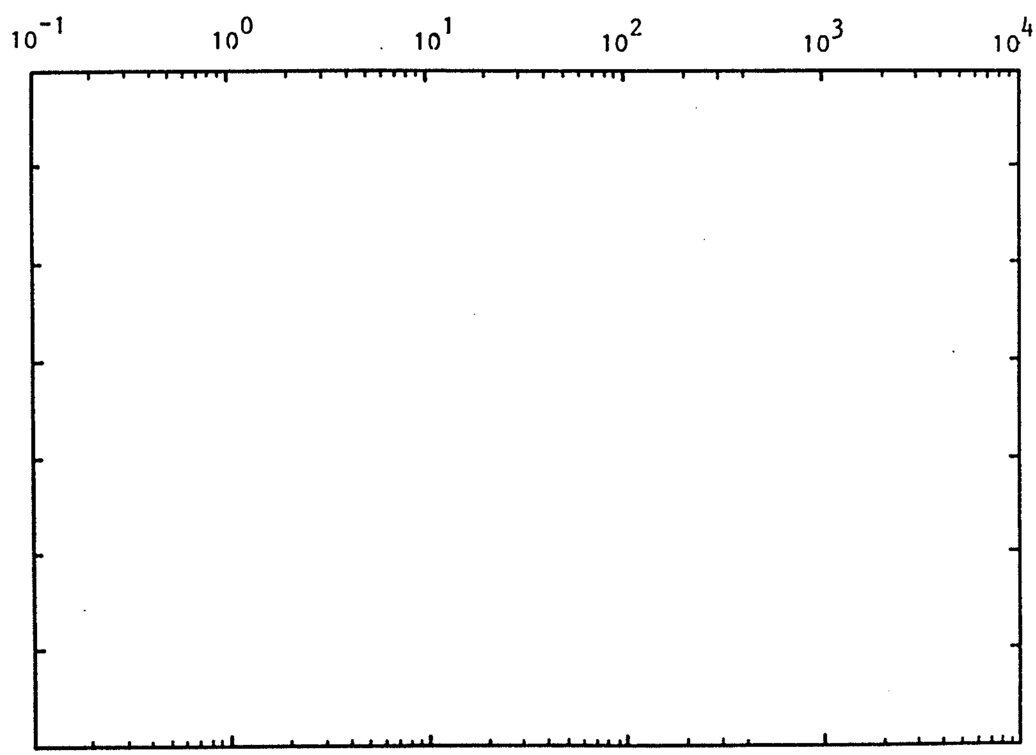

10^{-1}
10^0
10^1
10^2
10^3
10^4

C.1.3 One-Dimensional Consolidation Curves

ONE-DIMENSIONAL CONSOLIDATION TEST DATA

Load inc.	σ_v (kPa)	ΔH cm	Δe	e	V
1	27.4	0.021	0.0191	0.7809	1.7809
2	54.7	0.0366	0.0348	0.7652	1.7652
3	109.5	0.0627	0.0595	0.7405	1.7405
4	219.0	0.0876	0.0832	0.7168	1.7168
5	437.8	0.1226	0.1164	0.6836	1.6836
6	219.0	0.1208	0.1147	0.6852	1.6852
7	109.5	0.1158	0.1100	0.6900	1.6900
8	54.7	0.1002	0.0952	0.7048	1.7048
9	109.5	0.1074	0.1020	0.6980	1.6980
10	219.0	0.1214	0.1153	0.6847	1.6847
11	438.0	0.1392	0.1322	0.6678	1.6678
12	876.0	0.1748	0.1660	0.6340	1.6340
13	1751.0	0.2190	0.2080	0.5920	1.5920
14	3502.0	0.2516	0.2390	0.5611	1.5611
15	1751.0	0.2490	0.2365	0.5635	1.5635
16	438.0	0.2260	0.2146	0.5854	1.5854
17	27.4	0.1900	0.1804	0.6196	1.6196

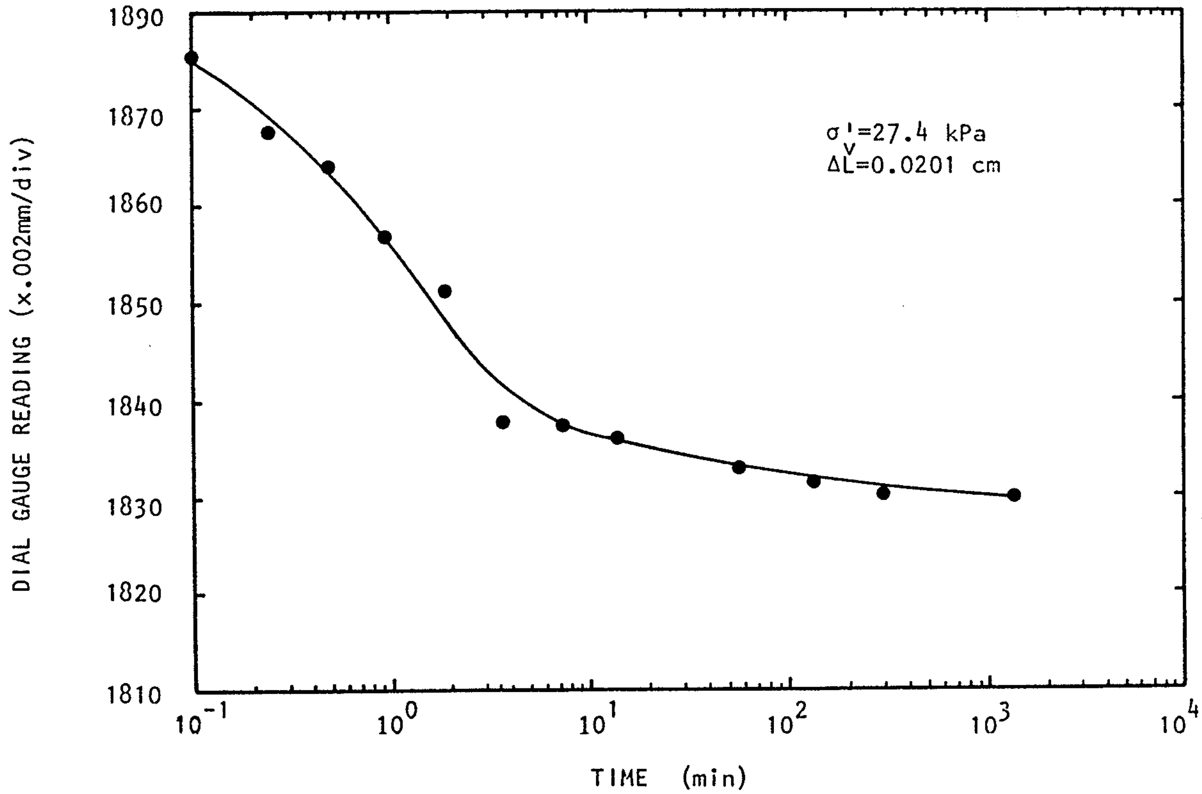

DIAL GAUGE READING (x.002mm/div)
1890
1870
1860
1850
1840
1830
1820
1810
σ'v=27.4 kPa
ΔL=0.0201 cm
10⁻¹
10⁰
10¹
10²
10³
10⁴
TIME (min)

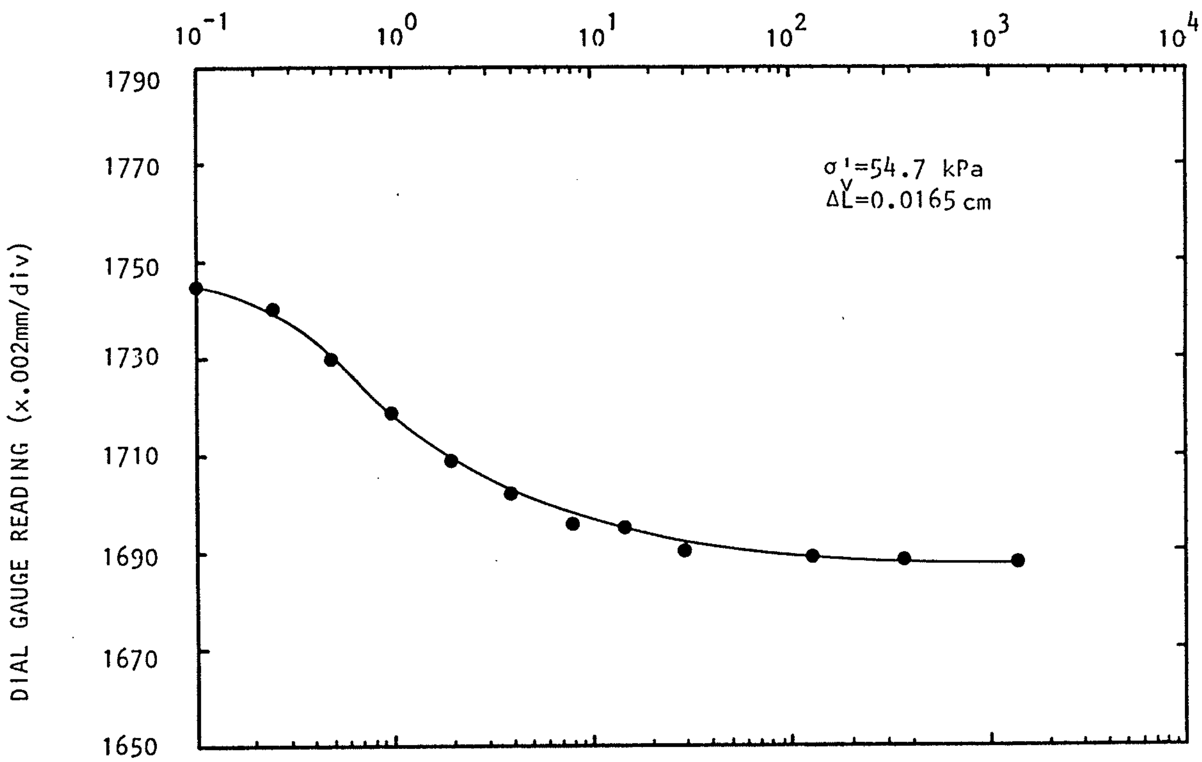

10⁻¹
10⁰
10¹
10²
10³
10⁴
DIAL GAUGE READING (x.002mm/div)
1790
1770
1750
1730
1710
1690
1670
1650
σ'v=54.7 kPa
ΔL=0.0165 cm

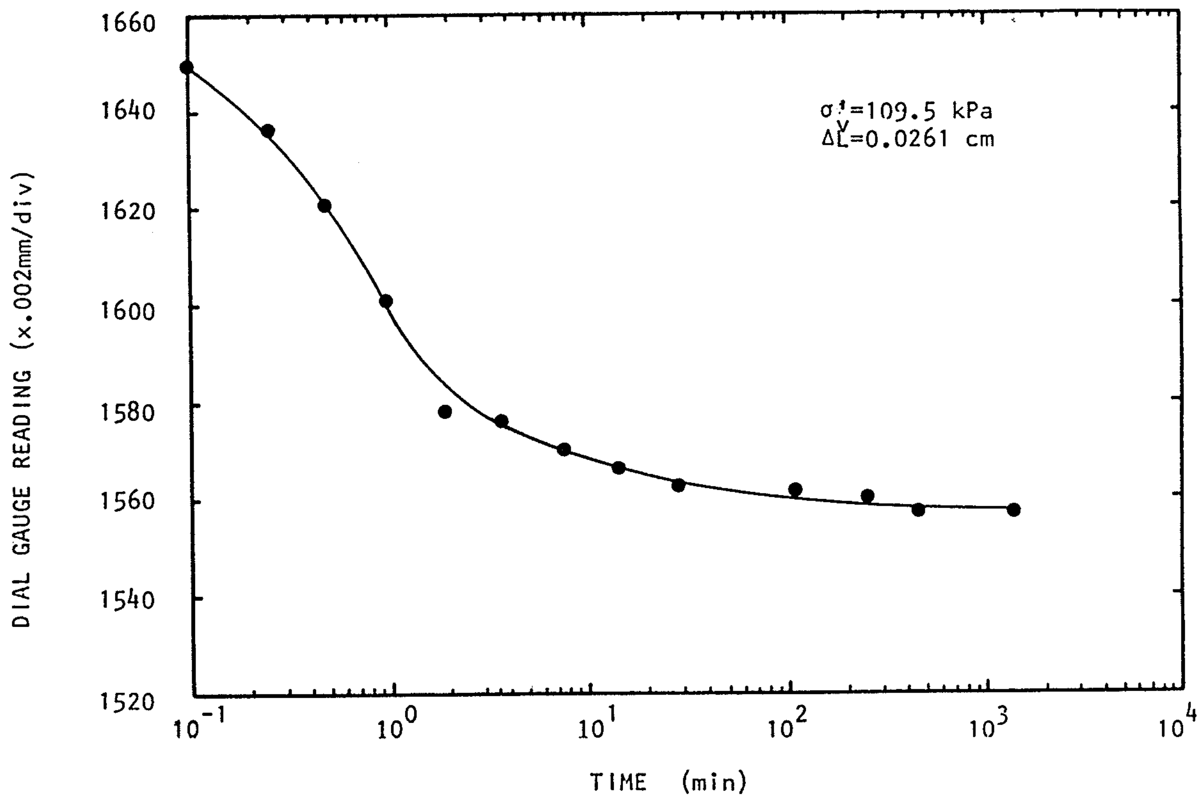
σ'v=109.5 kPa
ΔL=0.0261 cm
DIAL GAUGE READING (x.002mm/div)
1660
1640
1620
1600
1580
1560
1540
1520
10^-1
10^0
10^1
10^2
10^3
10^4
TIME (min)

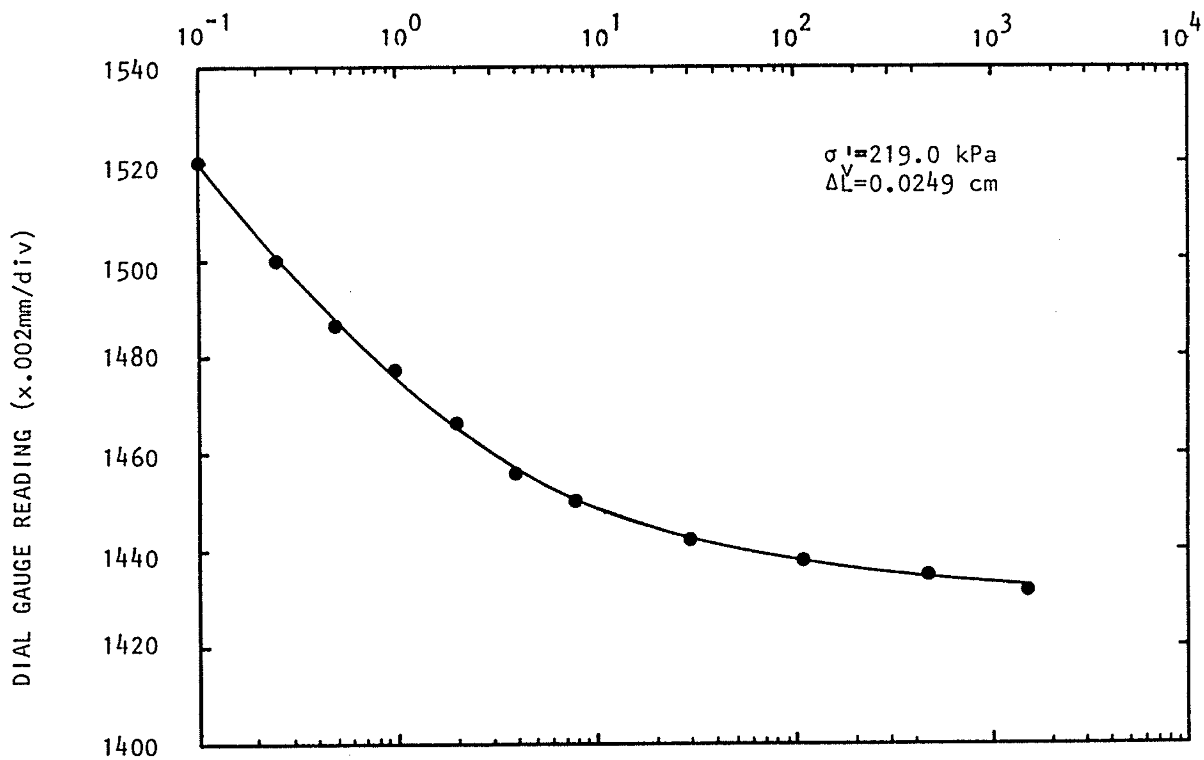
10^-1
10^0
10^1
10^2
10^3
10^4
σ'v=219.0 kPa
ΔL=0.0249 cm
DIAL GAUGE READING (x.002mm/div)
1540
1520
1500
1480
1460
1440
1420
1400

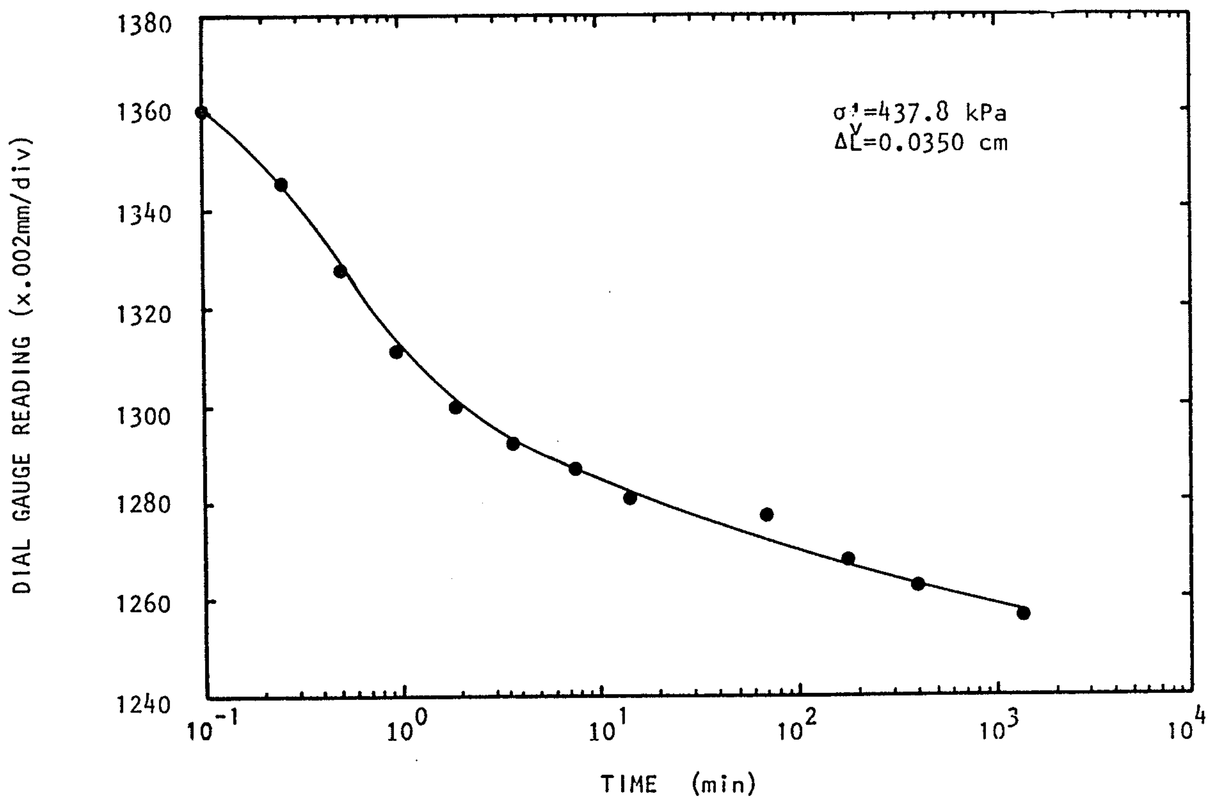
DIAL GAUGE READING (x.002mm/div)
σ'v=437.8 kPa
ΔL=0.0350 cm
TIME (min)

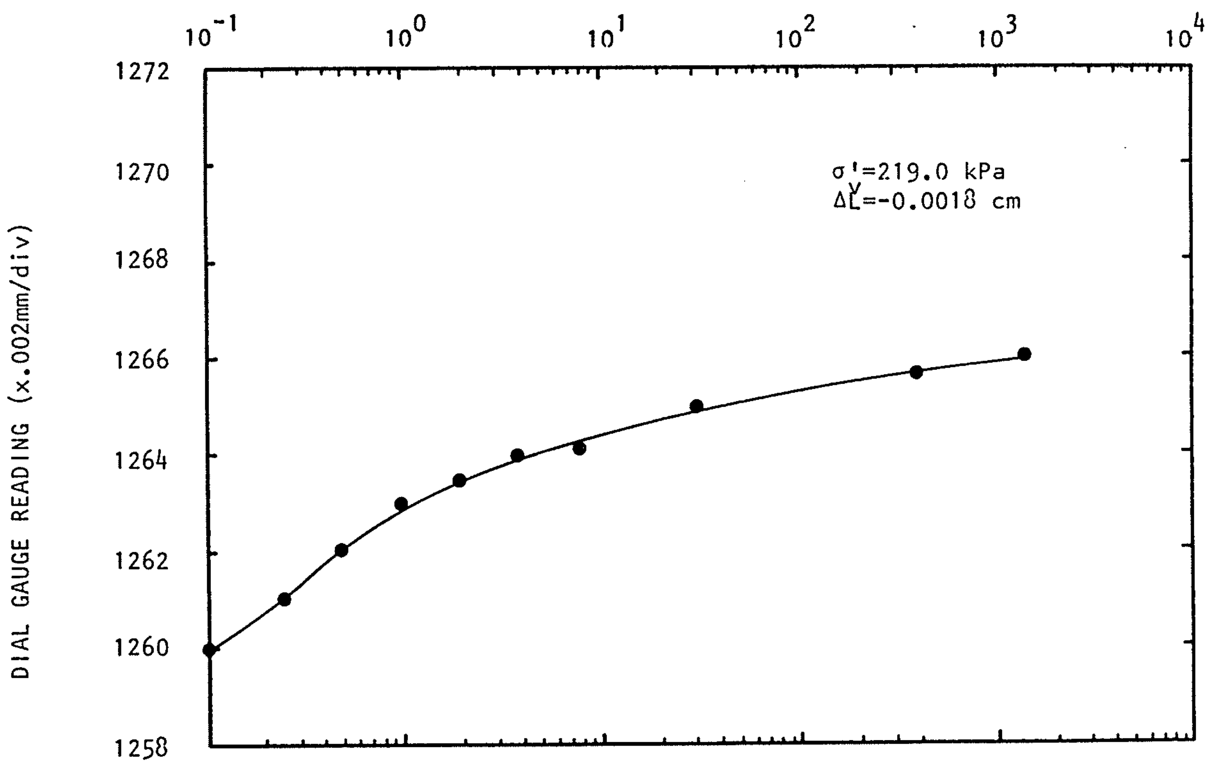
DIAL GAUGE READING (x.002mm/div)
σ'v=219.0 kPa
ΔL=-0.0018 cm

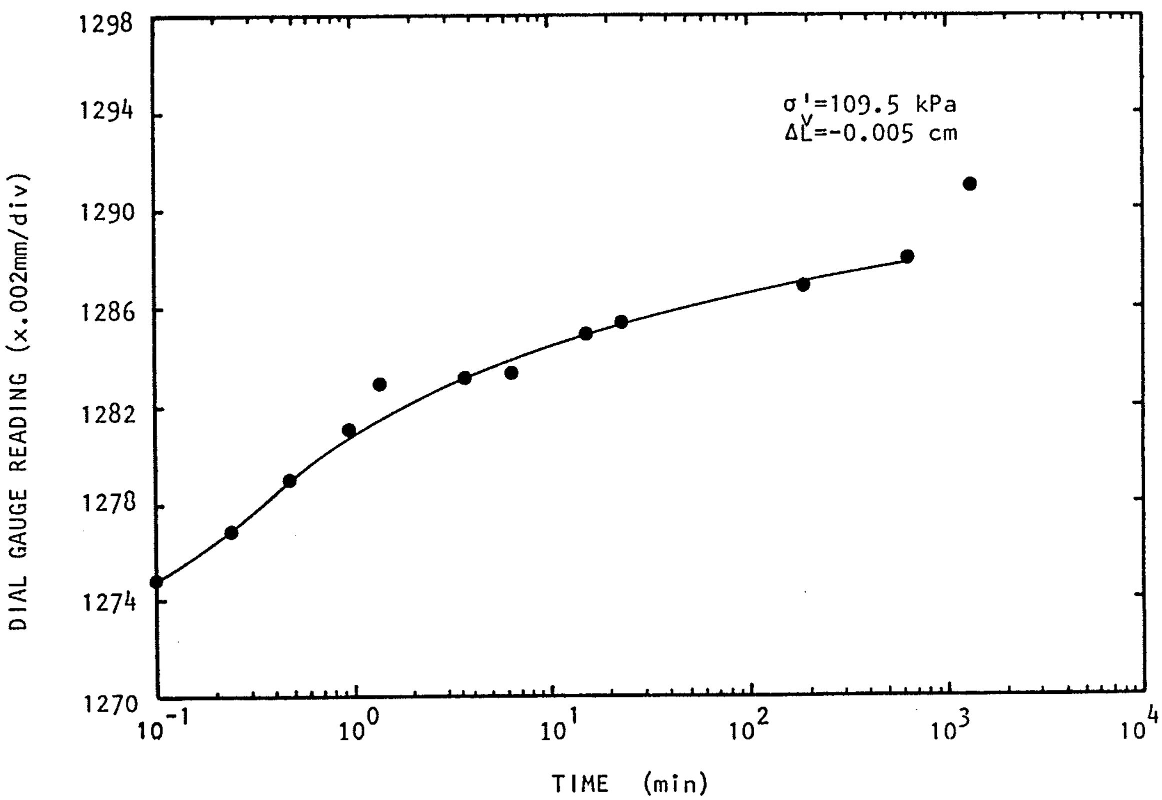

σ'v=109.5 kPa
ΔL=-0.005 cm
DIAL GAUGE READING (x.002mm/div)
1298
1294
1290
1286
1282
1278
1274
1270
10^-1
10^0
10^1
10^2
10^3
10^4
TIME (min)

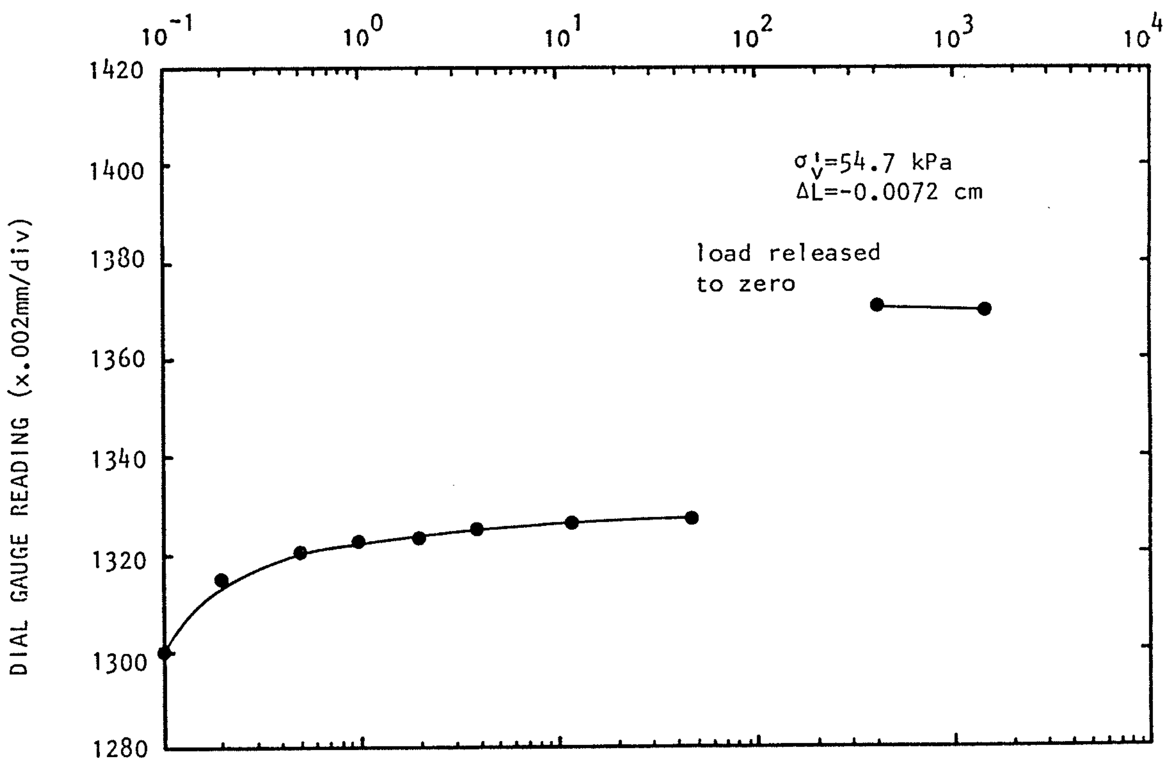

10^-1
10^0
10^1
10^2
10^3
10^4
σ'v=54.7 kPa
ΔL=-0.0072 cm
load released
to zero
DIAL GAUGE READING (x.002mm/div)
1420
1400
1380
1360
1340
1320
1300
1280

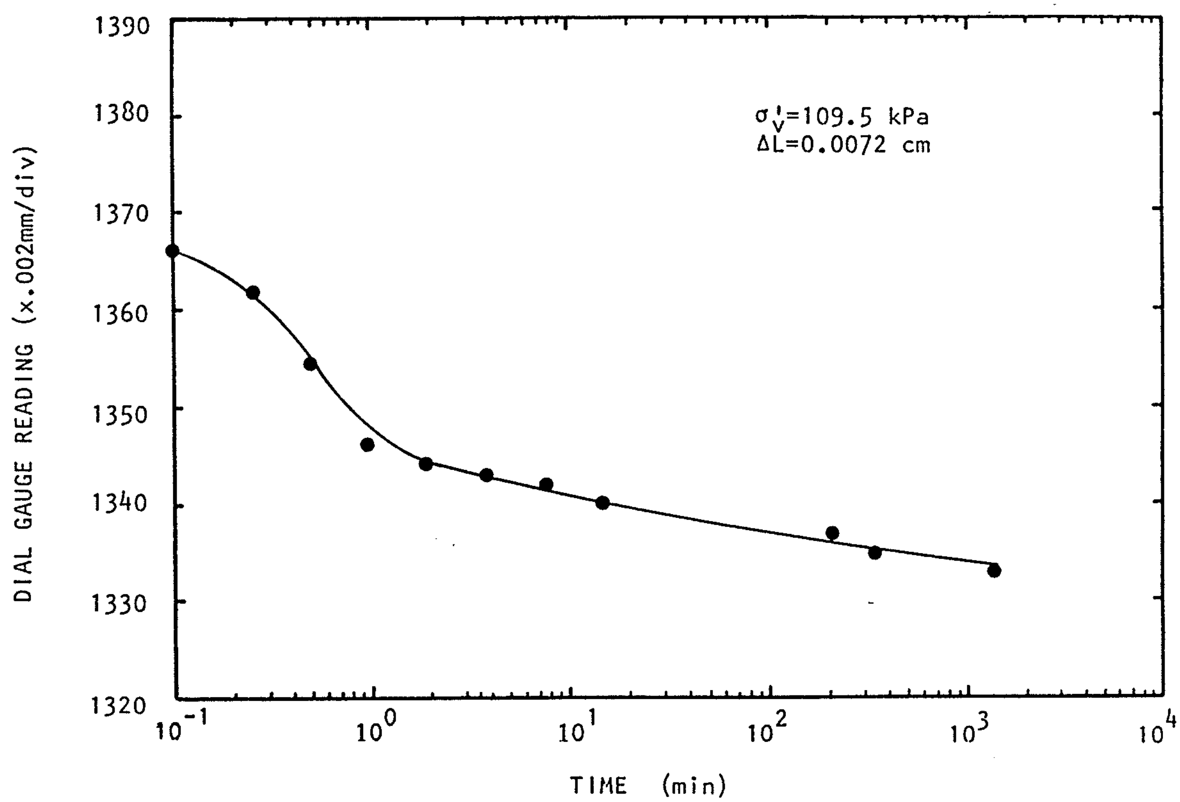

σ'v=109.5 kPa
ΔL=0.0072 cm
DIAL GAUGE READING (x.002mm/div)
1390
1380
1370
1360
1350
1340
1330
1320
10^-1
10^0
10^1
10^2
10^3
10^4
TIME (min)

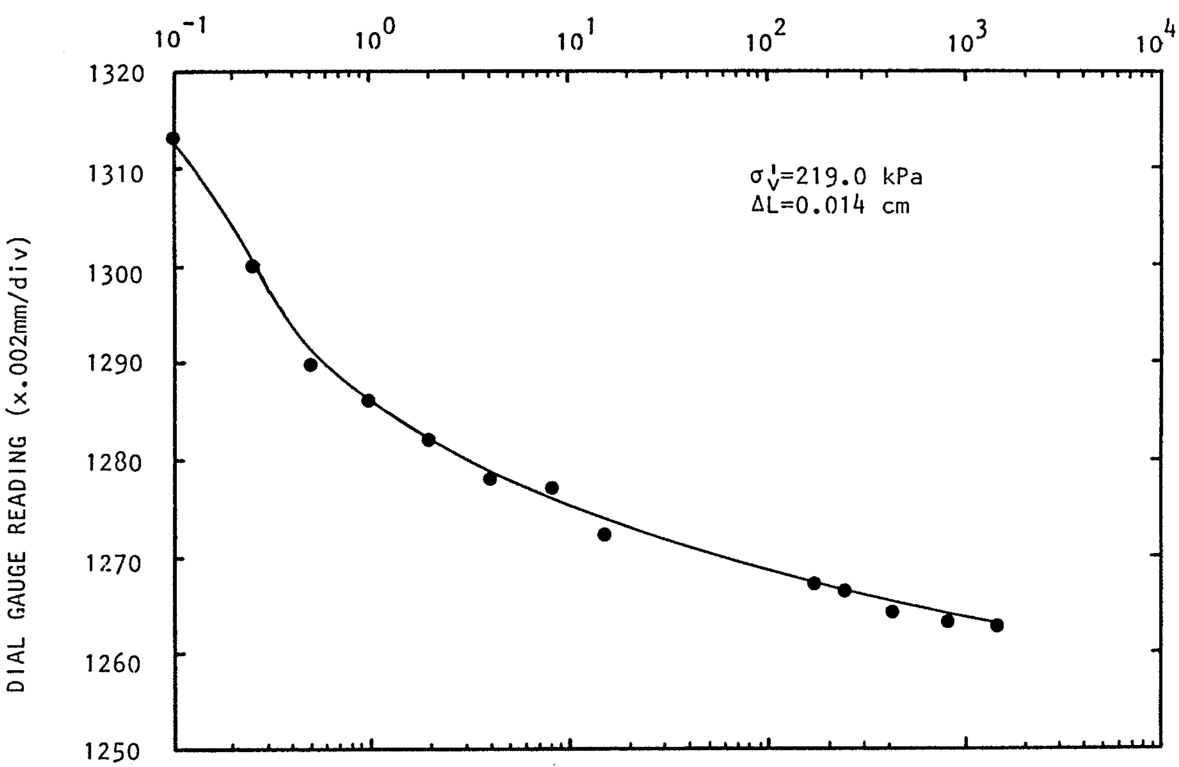

σ'v=219.0 kPa
ΔL=0.014 cm
DIAL GAUGE READING (x.002mm/div)
1320
1310
1300
1290
1280
1270
1260
1250
10^-1
10^0
10^1
10^2
10^3
10^4

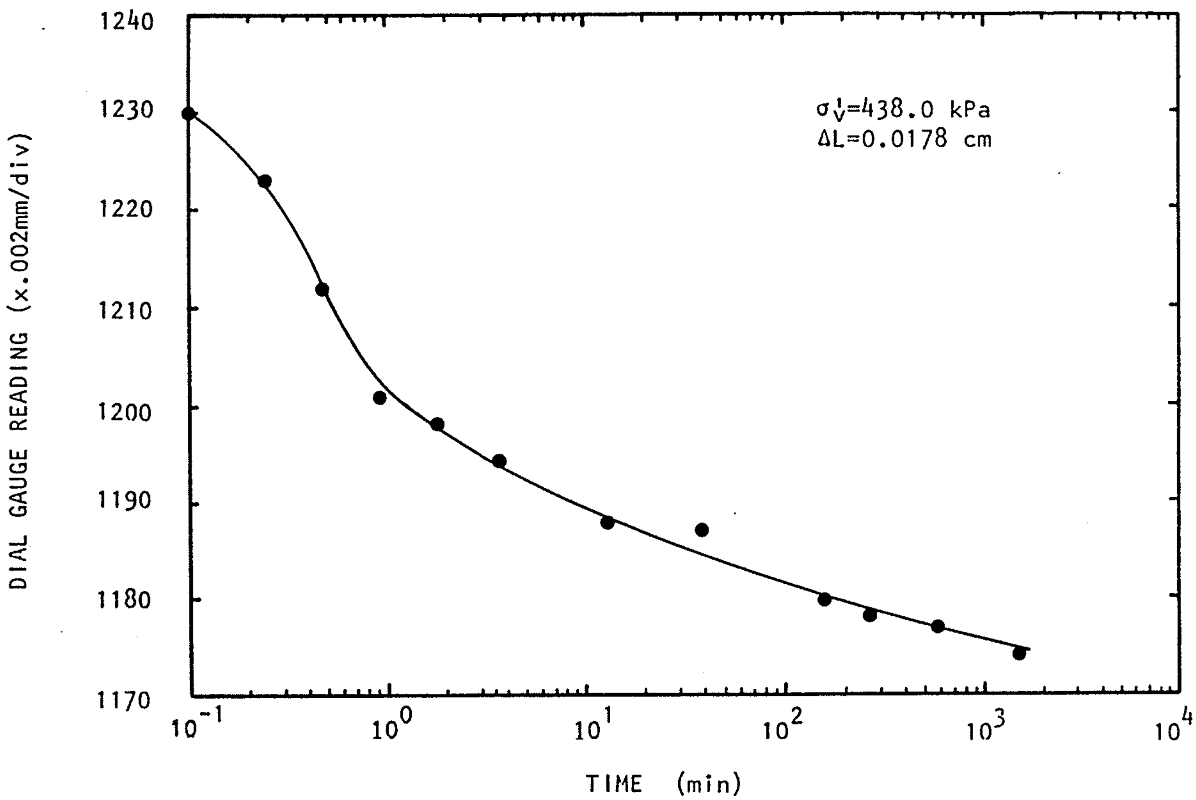
1240
1230
1220
1210
1200
1190
1180
1170
DIAL GAUGE READING (x.002mm/div)
σ'_v=438.0 kPa
ΔL=0.0178 cm
10^{-1}
10^{0}
10^{1}
10^{2}
10^{3}
10^{4}
TIME (min)

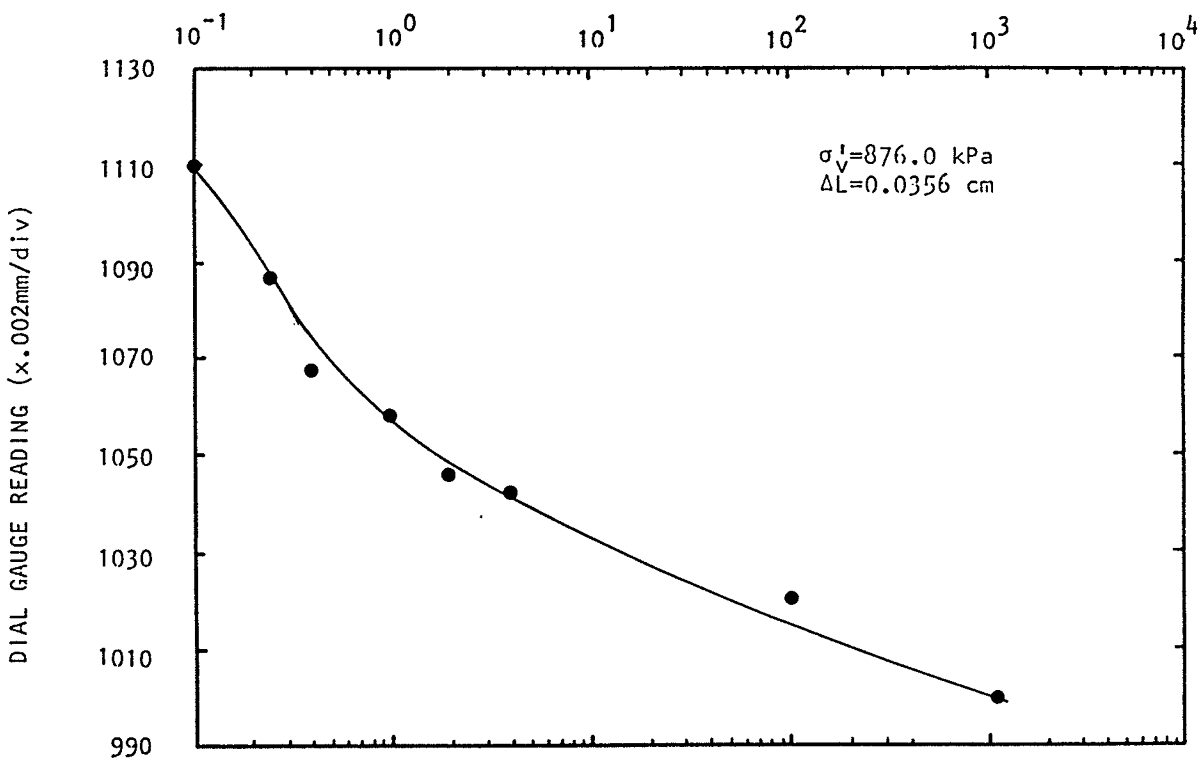
10^{-1}
10^{0}
10^{1}
10^{2}
10^{3}
10^{4}
1130
1110
1090
1070
1050
1030
1010
990
DIAL GAUGE READING (x.002mm/div)
σ'_v=876.0 kPa
ΔL=0.0356 cm

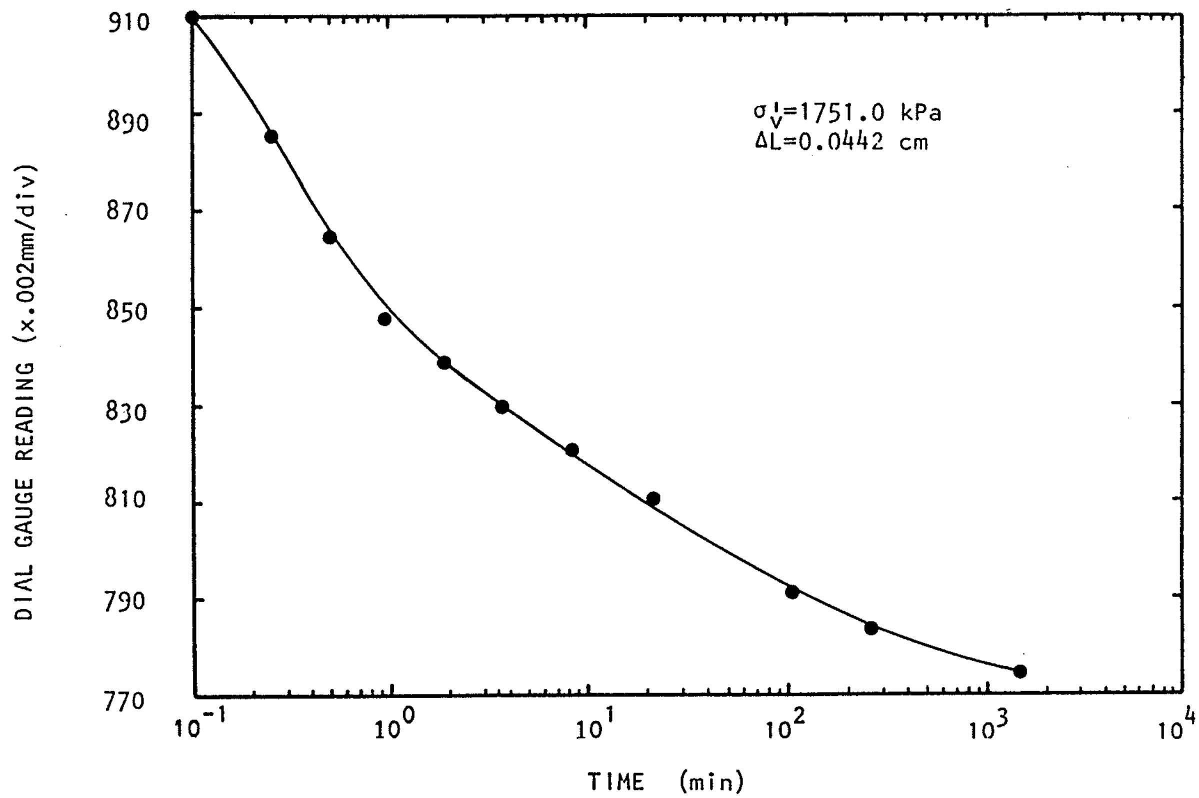

910
890
870
850
830
810
790
770
DIAL GAUGE READING (x.002mm/div)
σ'v=1751.0 kPa
ΔL=0.0442 cm
10-1
10^0
10^1
10^2
10^3
10^4
TIME (min)

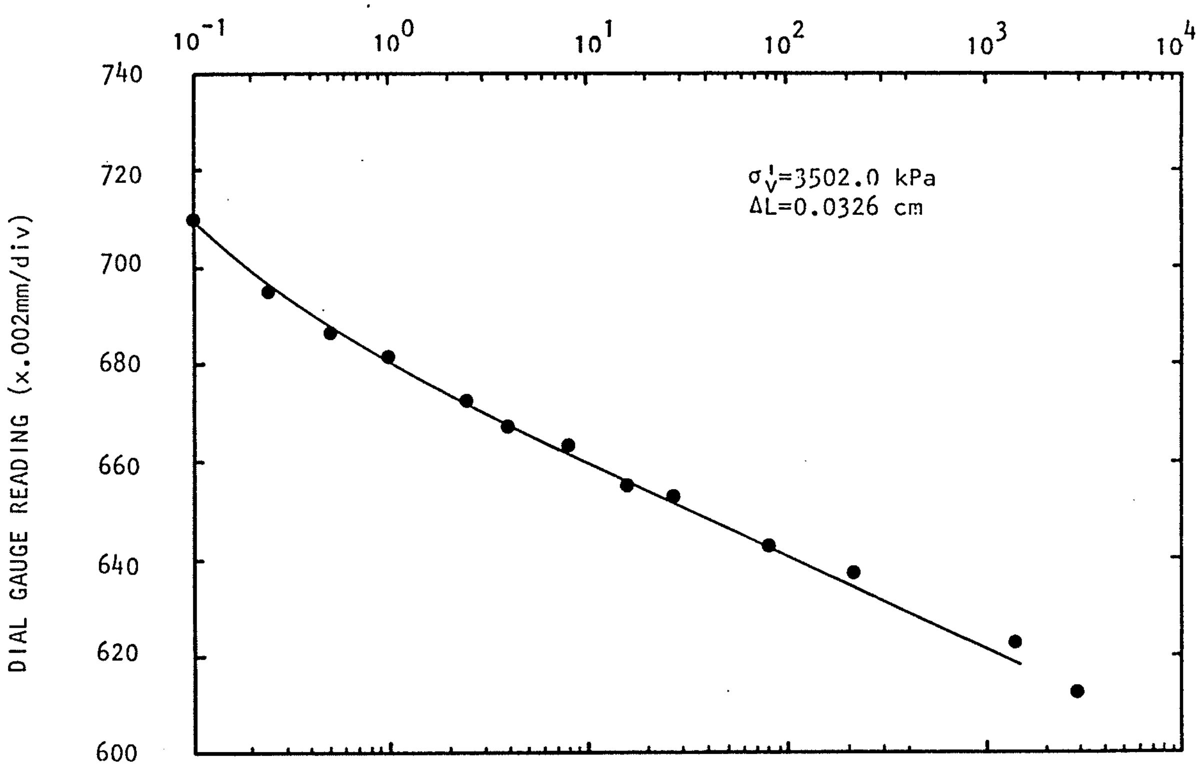

10-1
10^0
10^1
10^2
10^3
10^4
740
720
700
680
660
640
620
600
DIAL GAUGE READING (x.002mm/div)
σ'v=3502.0 kPa
ΔL=0.0326 cm

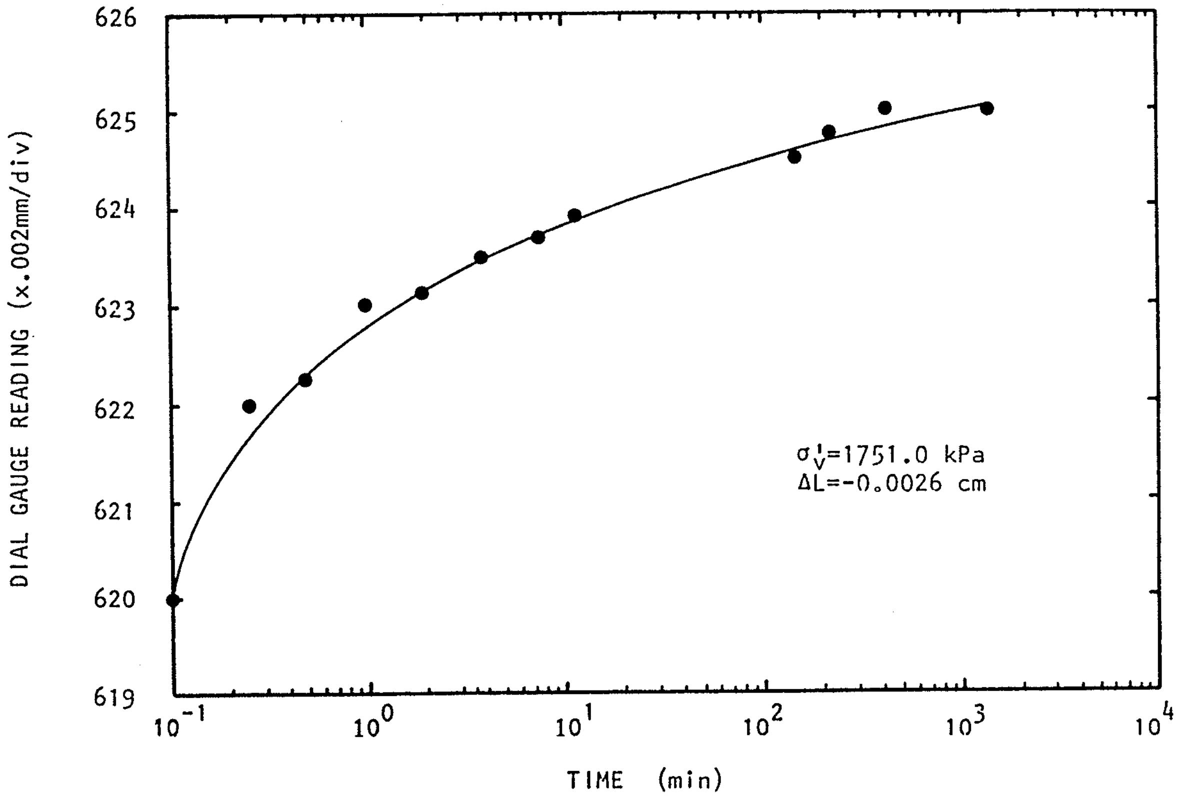

DIAL GAUGE READING (x.002mm/div)
626
625
624
623
622
621
620
619
10^{-1}
10^{0}
10^{1}
10^{2}
10^{3}
10^{4}
σ_v'=1751.0 kPa
ΔL=-0.0026 cm
TIME (min)

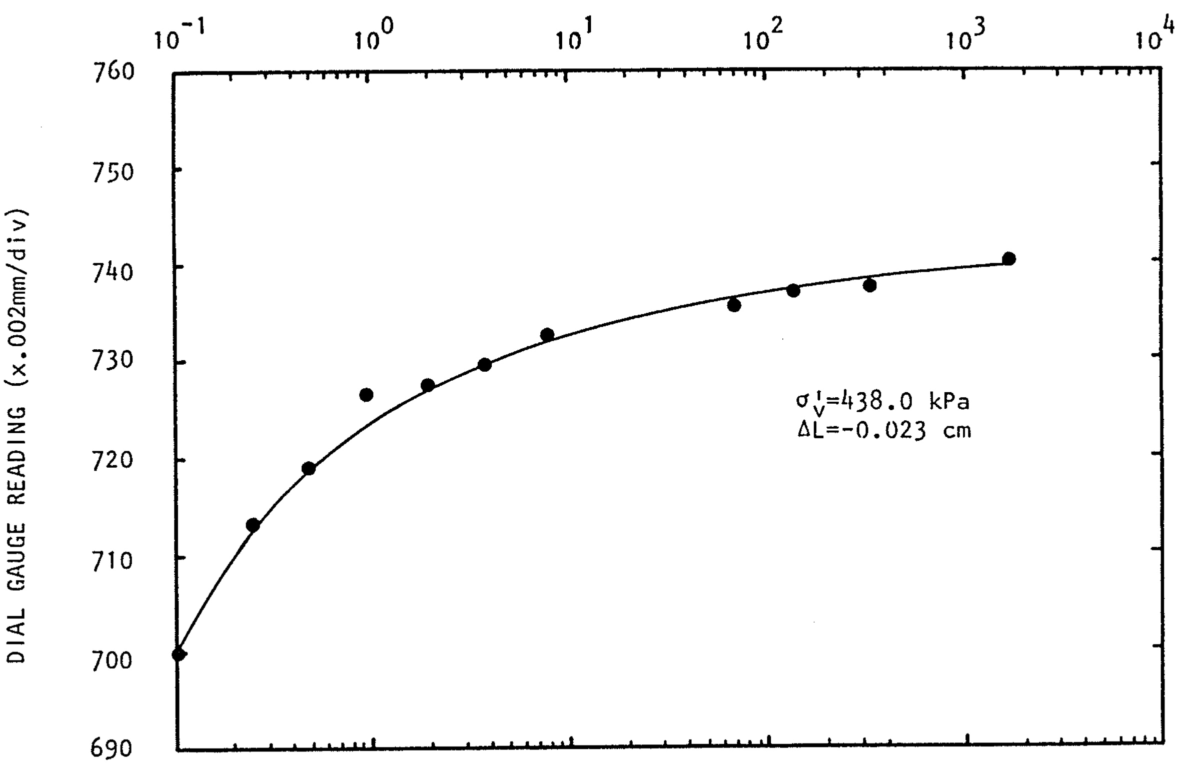

10^{-1}
10^{0}
10^{1}
10^{2}
10^{3}
10^{4}
DIAL GAUGE READING (x.002mm/div)
760
750
740
730
720
710
700
690
σ_v'=438.0 kPa
ΔL=-0.023 cm

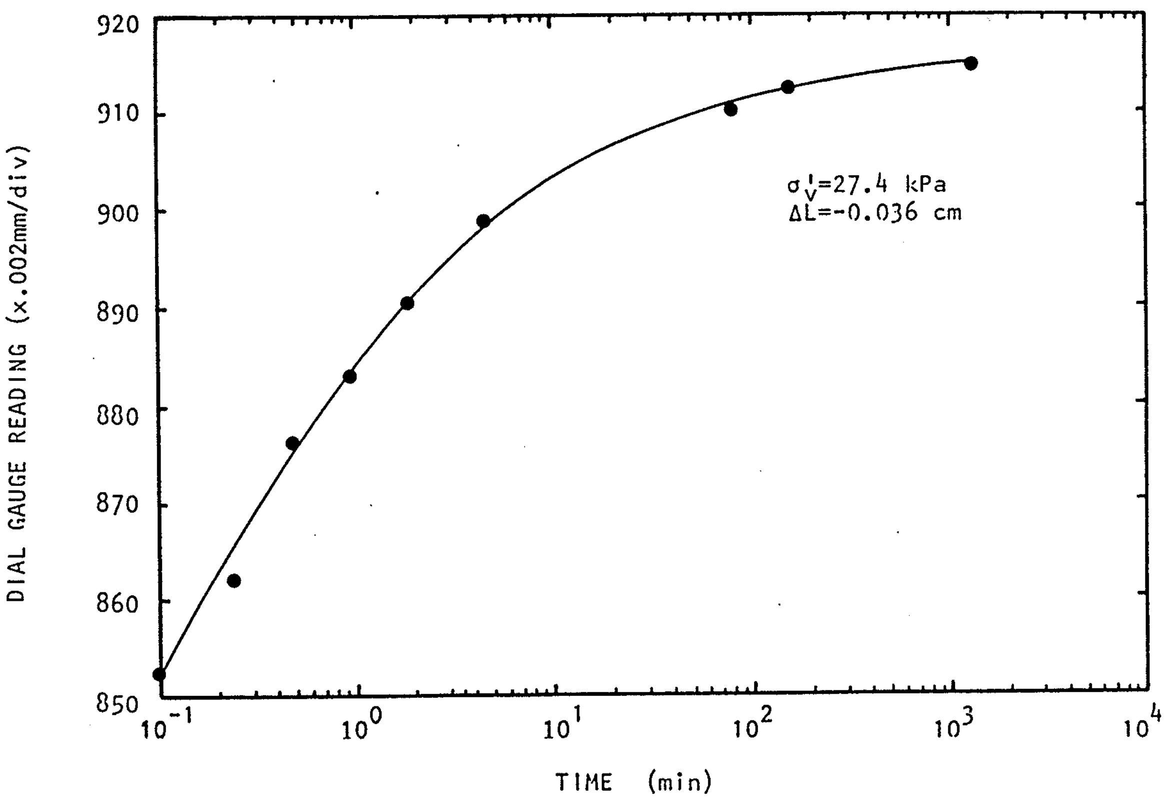
920
910
900
890
880
870
860
850
DIAL GAUGE READING (x.002mm/div)
σ'v=27.4 kPa
ΔL=-0.036 cm
10^-1
10^0
10^1
10^2
10^3
10^4
TIME (min)

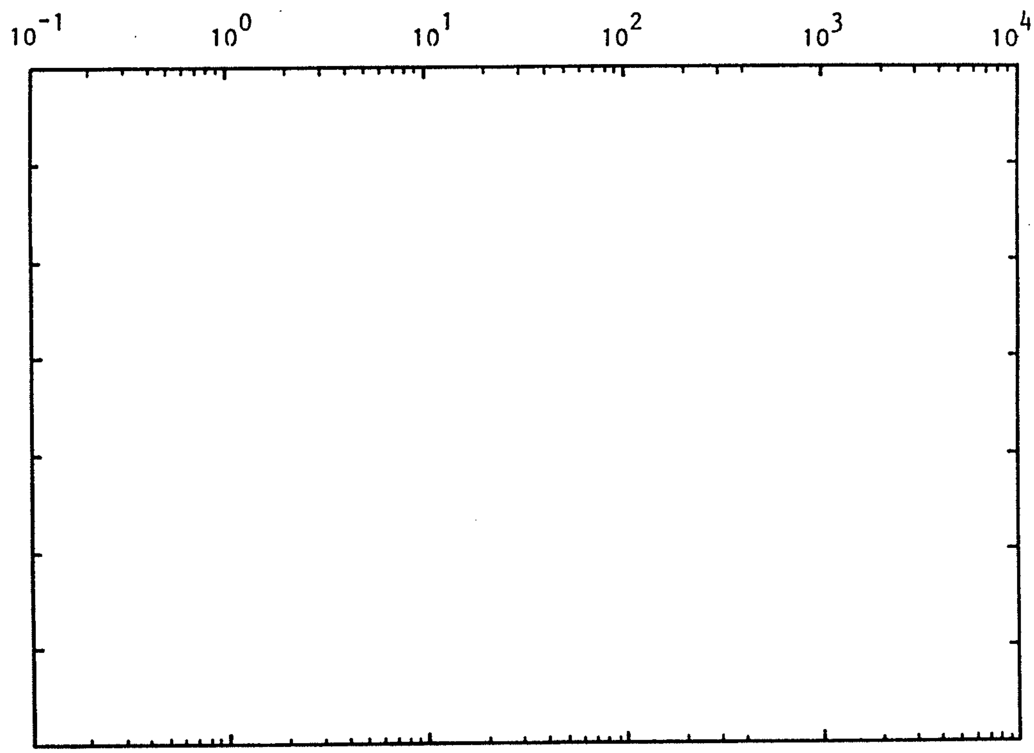
10^-1
10^0
10^1
10^2
10^3
10^4

C.1.4 DTTCP Consolidation curves

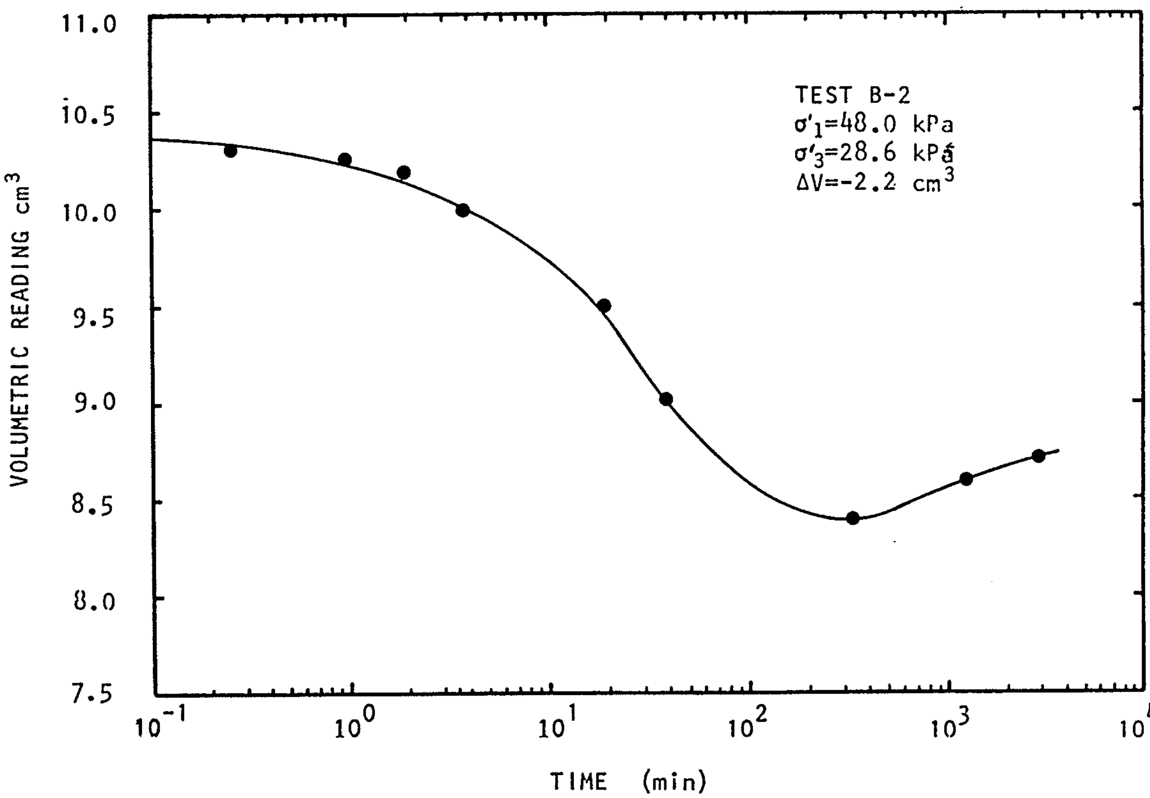
TEST B-2
σ'1=48.0 kPa
σ'3=28.6 kPa
ΔV=-2.2 cm3
VOLUMETRIC READING cm3
11.0
10.5
10.0
9.5
9.0
8.5
8.0
7.5
10-1
100
101
102
103
104
TIME (min)

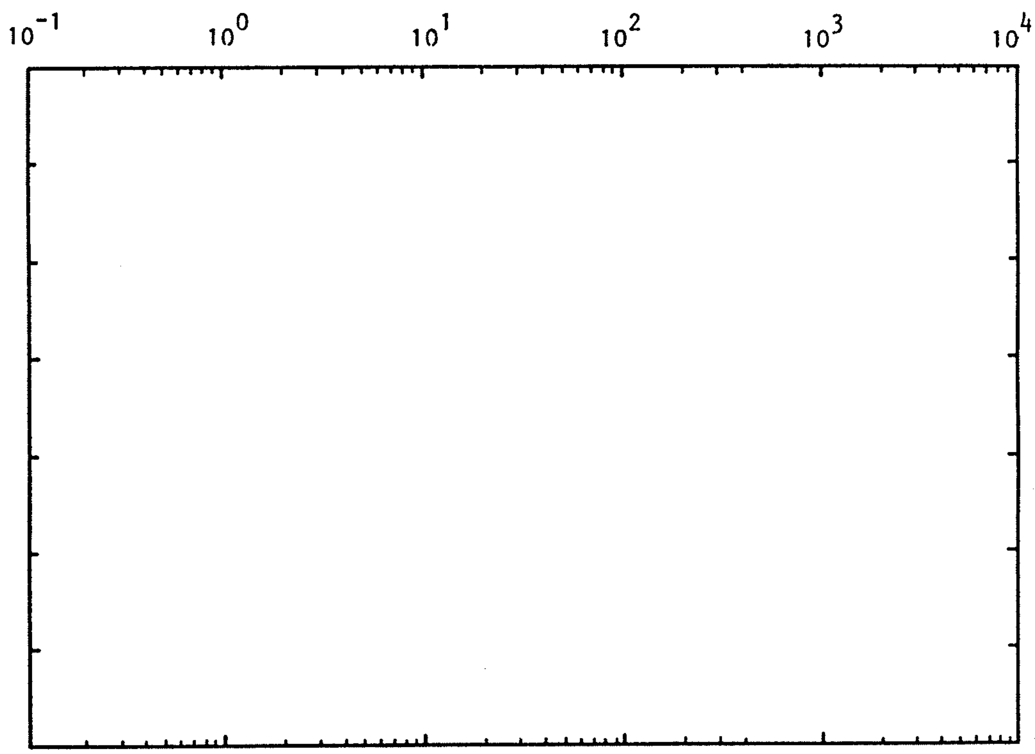
10-1
100
101
102
103
104

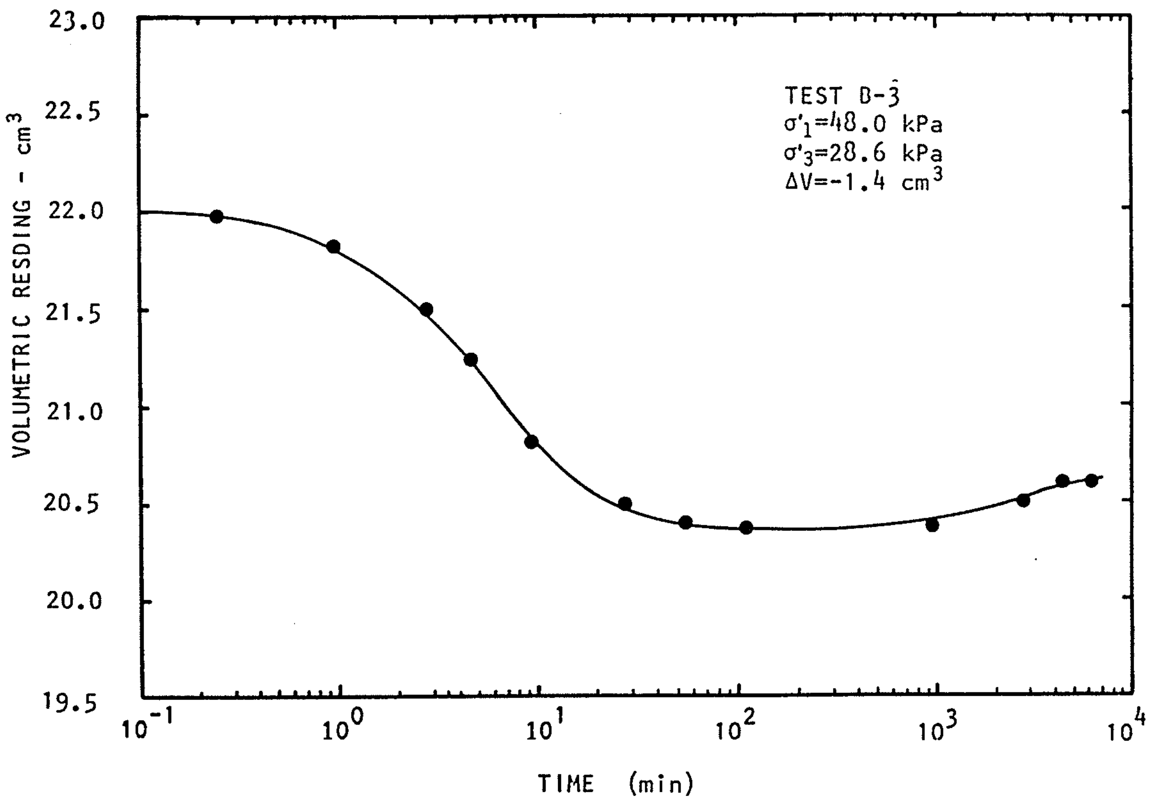
TEST B-3
σ'1=48.0 kPa
σ'3=28.6 kPa
ΔV=-1.4 cm3
VOLUMETRIC RESDING - cm3
23.0
22.5
22.0
21.5
21.0
20.5
20.0
19.5
10-1
100
101
102
103
104
TIME (min)

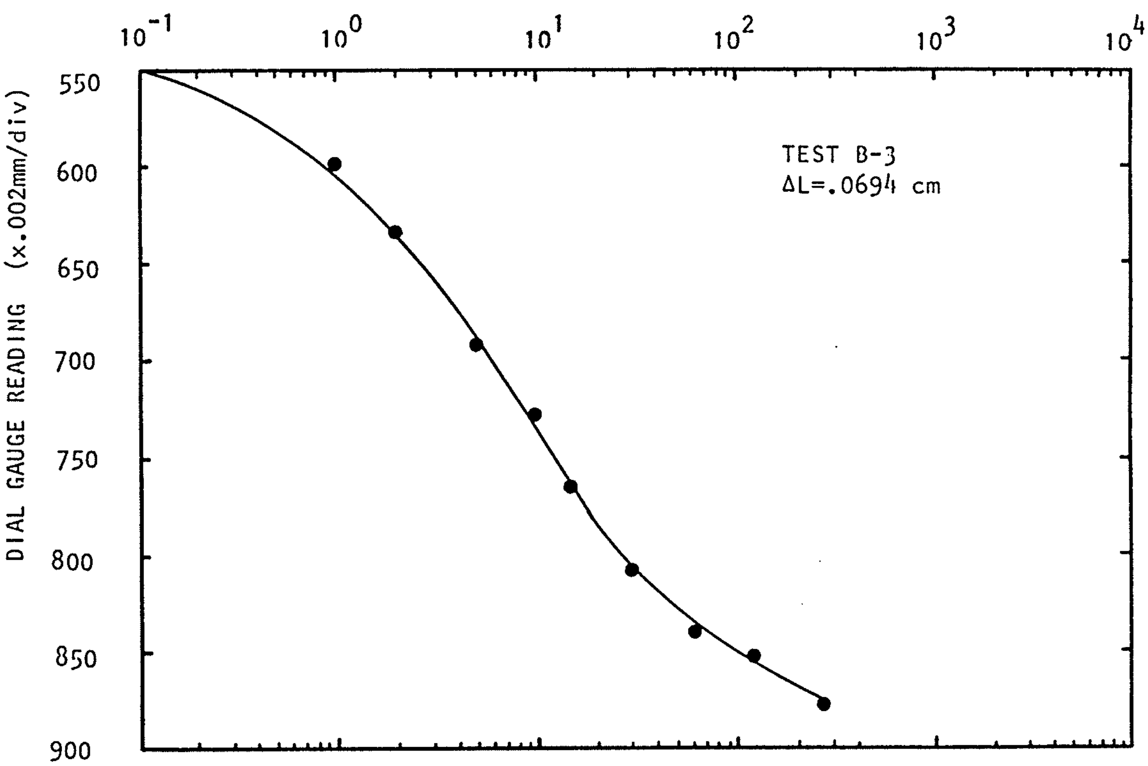
TEST B-3
ΔL=.0694 cm
DIAL GAUGE READING (x.002mm/div)
10-1
100
101
102
103
104
550
600
650
700
750
800
850
900

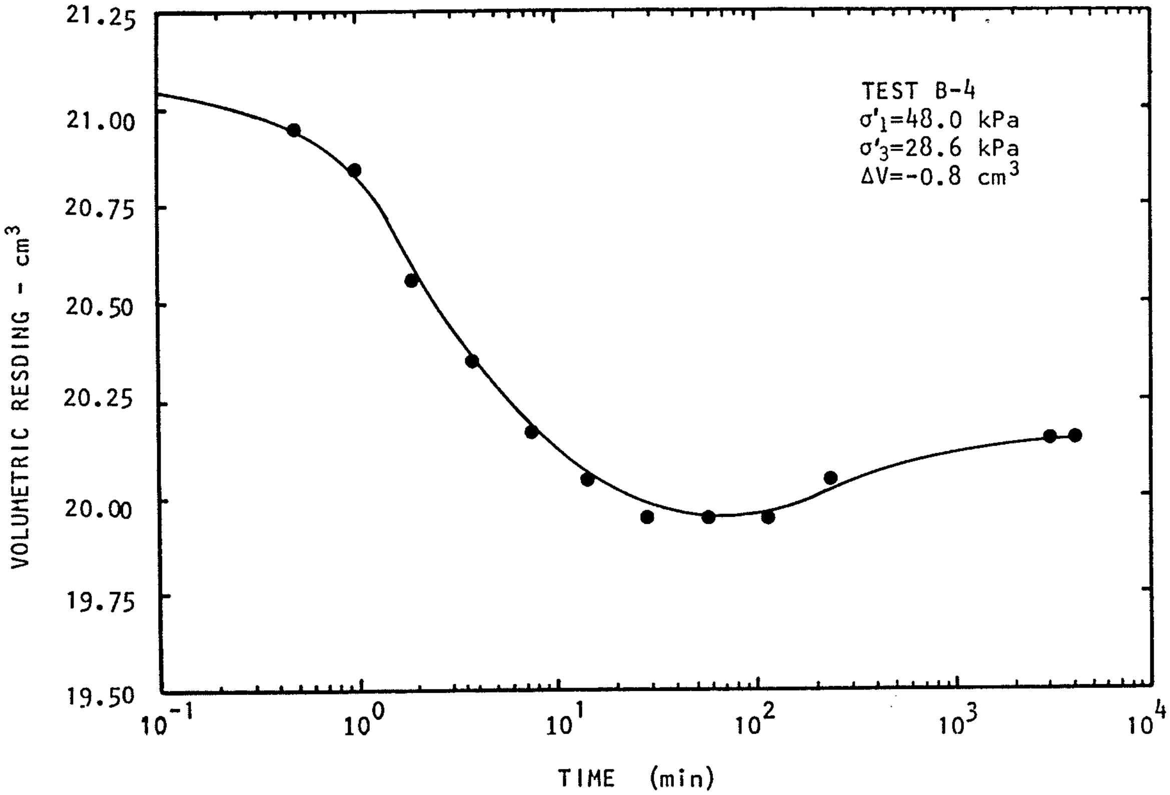

TEST B-4
σ'1=48.0 kPa
σ'3=28.6 kPa
ΔV=-0.8 cm3
VOLUMETRIC RESDING - cm3
21.25
21.00
20.75
20.50
20.25
20.00
19.75
19.50
10-1
100
101
102
103
104
TIME (min)

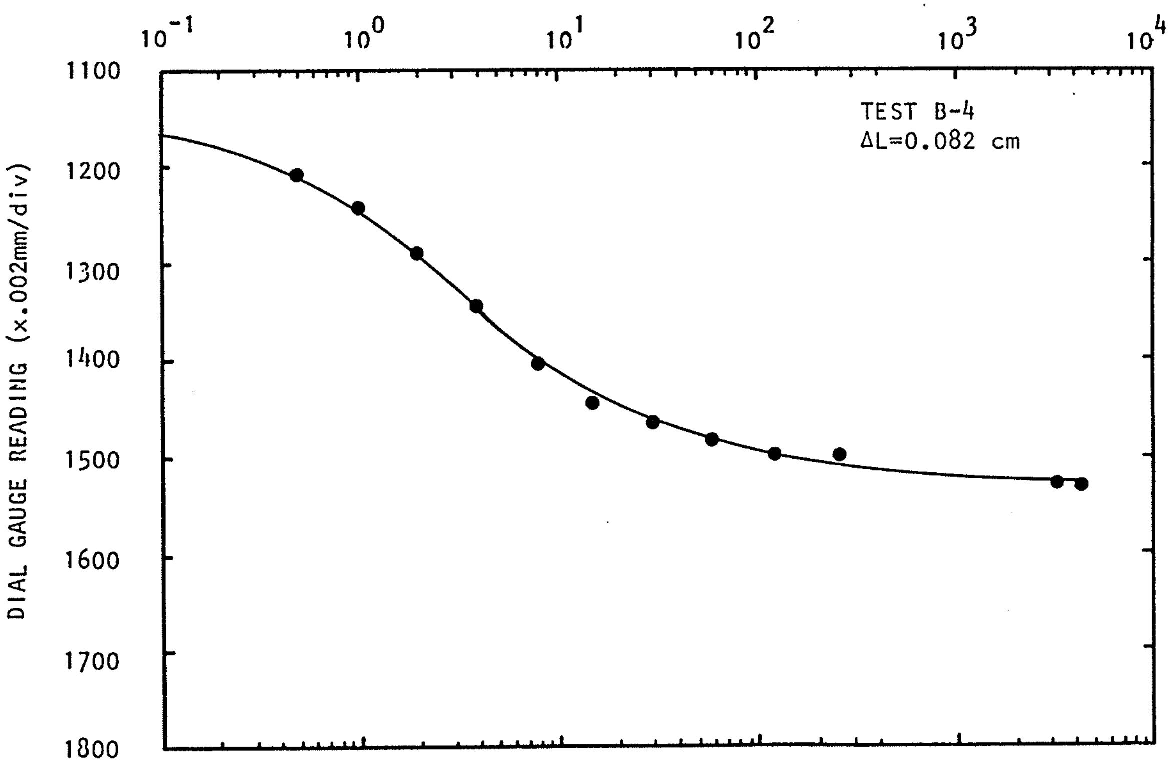

TEST B-4
ΔL=0.082 cm
DIAL GAUGE READING (x.002mm/div)
10-1
100
101
102
103
104
1100
1200
1300
1400
1500
1600
1700
1800

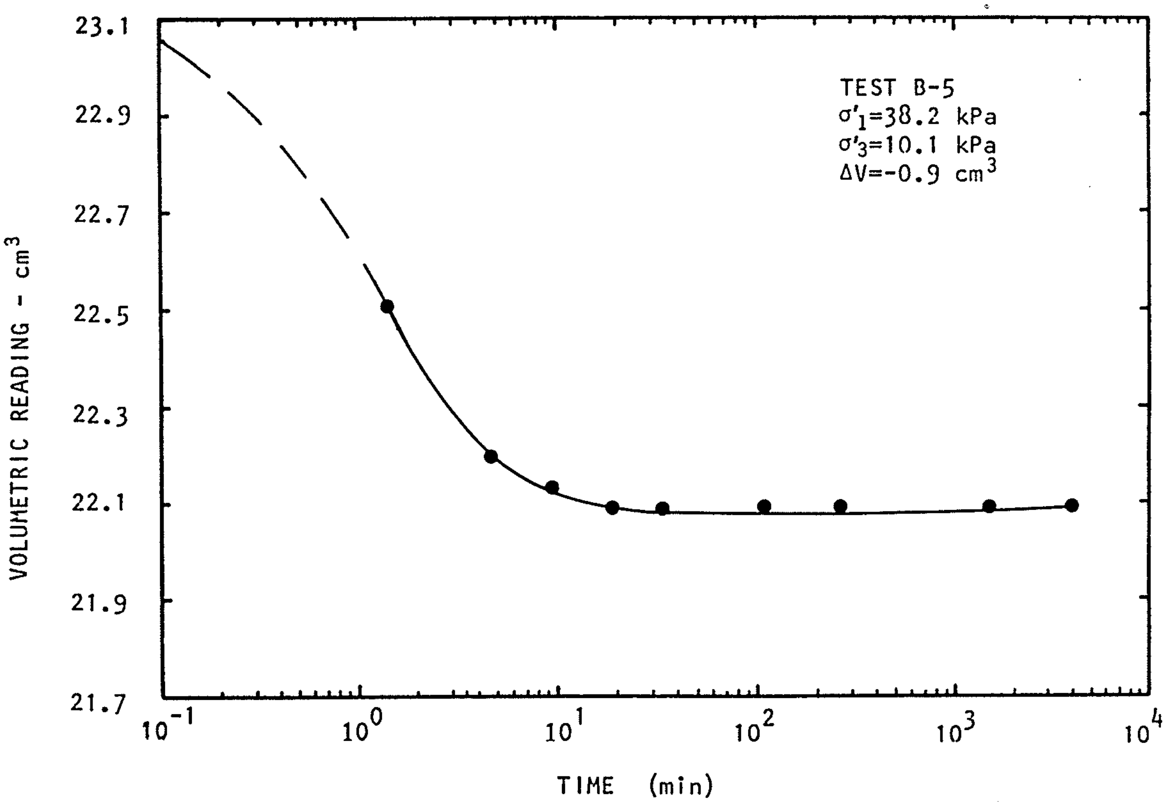

TEST B-5
σ'1=38.2 kPa
σ'3=10.1 kPa
ΔV=-0.9 cm3
VOLUMETRIC READING - cm3
23.1
22.9
22.7
22.5
22.3
22.1
21.9
21.7
10-1
100
101
102
103
104
TIME (min)

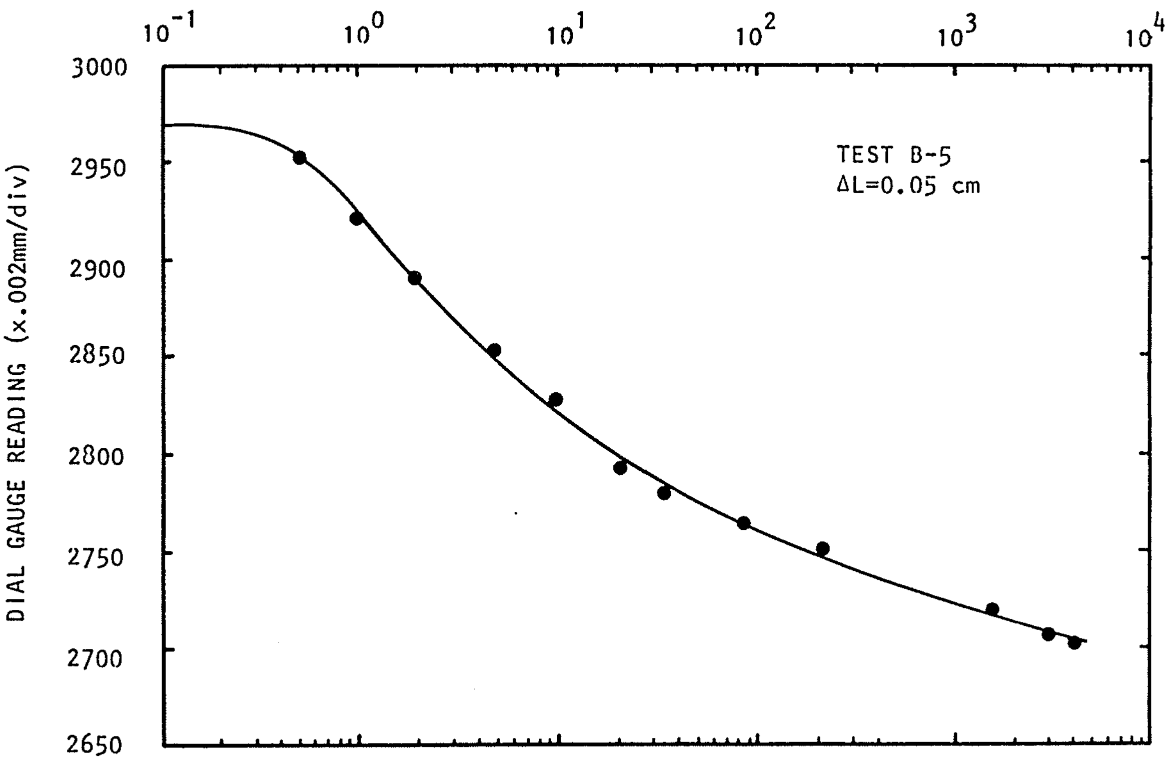

TEST B-5
ΔL=0.05 cm
DIAL GAUGE READING (x.002mm/div)
3000
2950
2900
2850
2800
2750
2700
2650
10-1
100
101
102
103
104

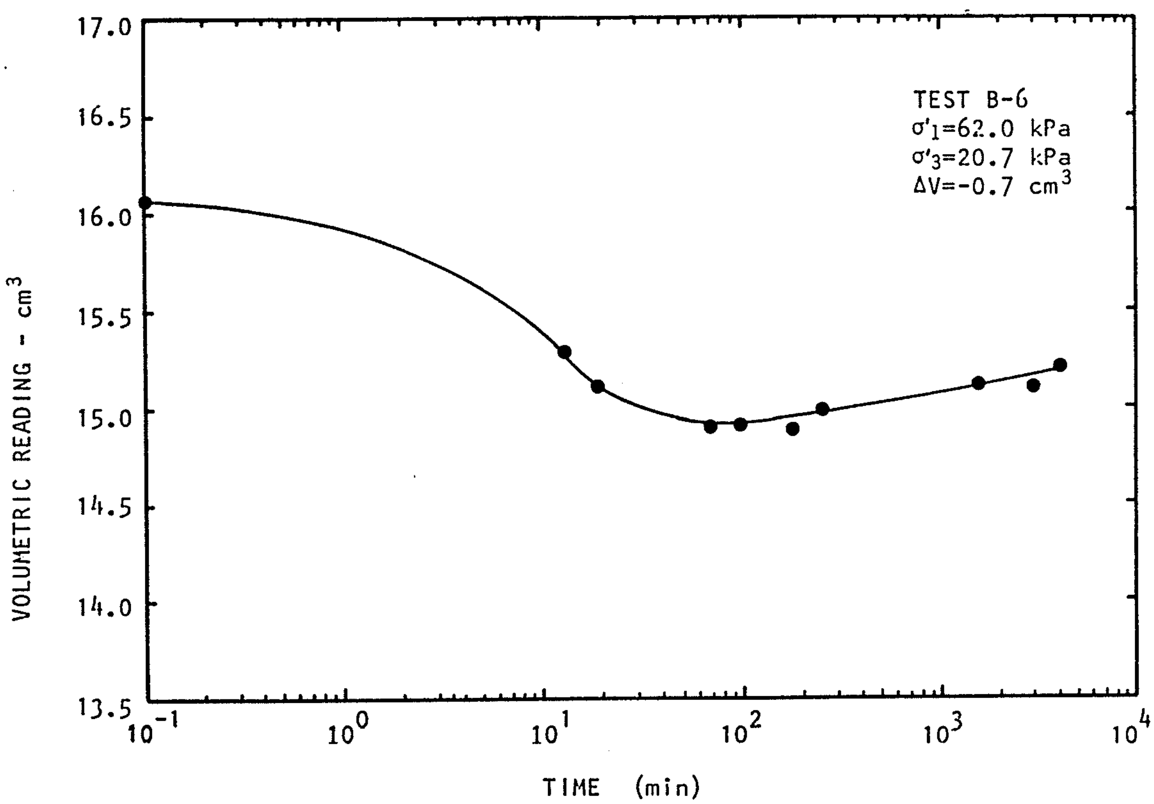
17.0
16.5
16.0
15.5
15.0
14.5
14.0
13.5
VOLUMETRIC READING - cm^3
TEST B-6
σ'$_1$=62.0 kPa
σ'$_3$=20.7 kPa
ΔV=-0.7 cm^3
10^{-1}
10^0
10^1
10^2
10^3
10^4
TIME (min)

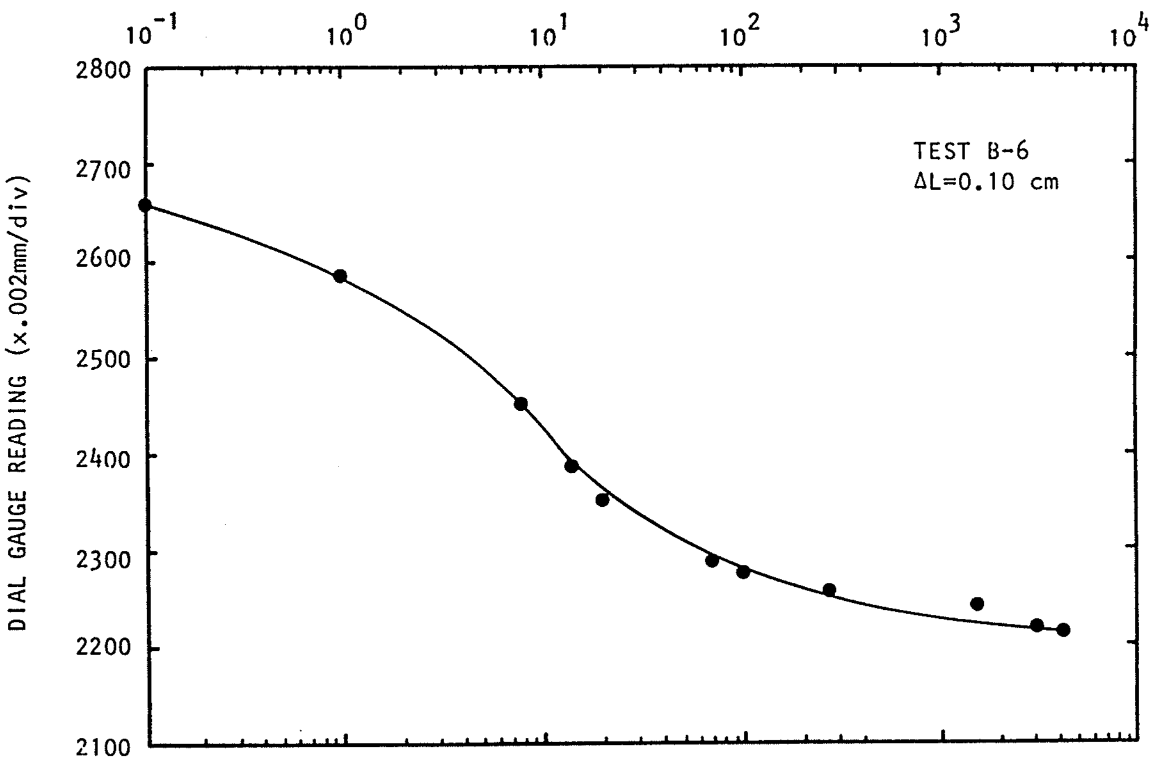
10^{-1}
10^0
10^1
10^2
10^3
10^4
2800
2700
2600
2500
2400
2300
2200
2100
DIAL GAUGE READING (x.002mm/div)
TEST B-6
ΔL=0.10 cm

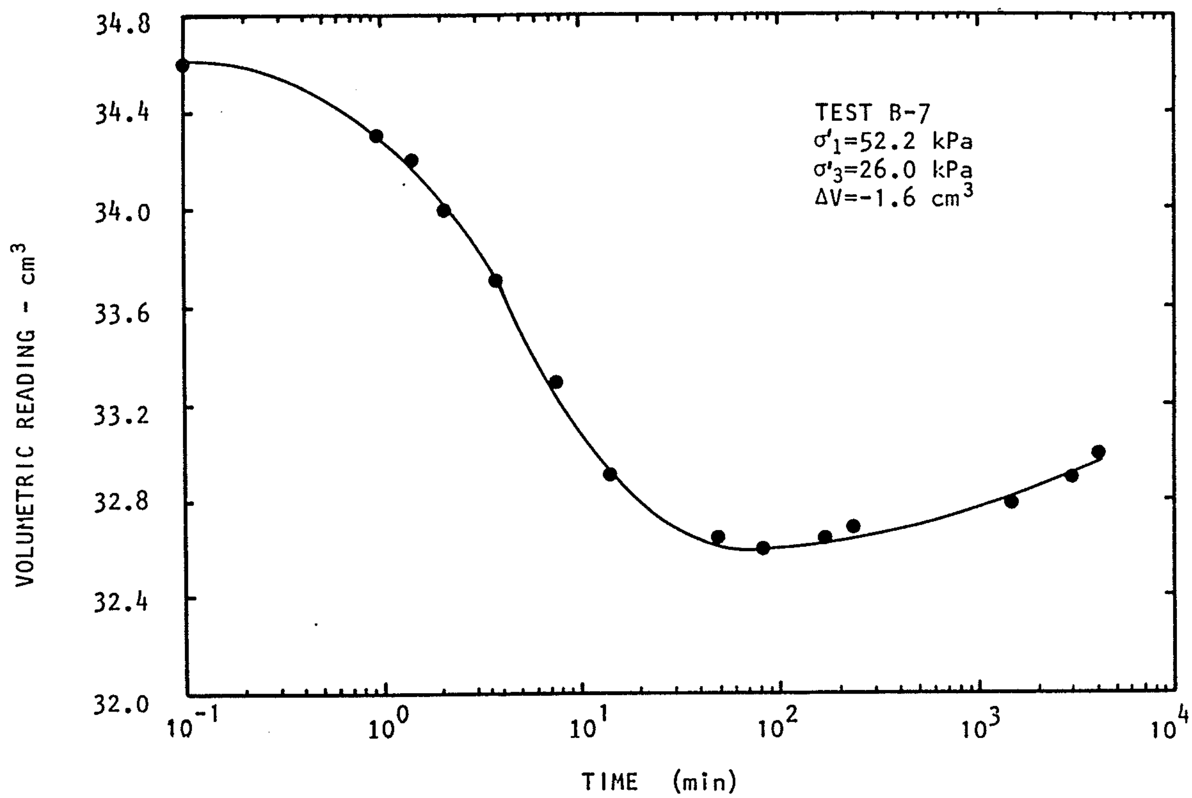
TEST B-7
σ'1=52.2 kPa
σ'3=26.0 kPa
ΔV=-1.6 cm3
VOLUMETRIC READING - cm3
34.8
34.4
34.0
33.6
33.2
32.8
32.4
32.0
10-1
100
101
102
103
104
TIME (min)

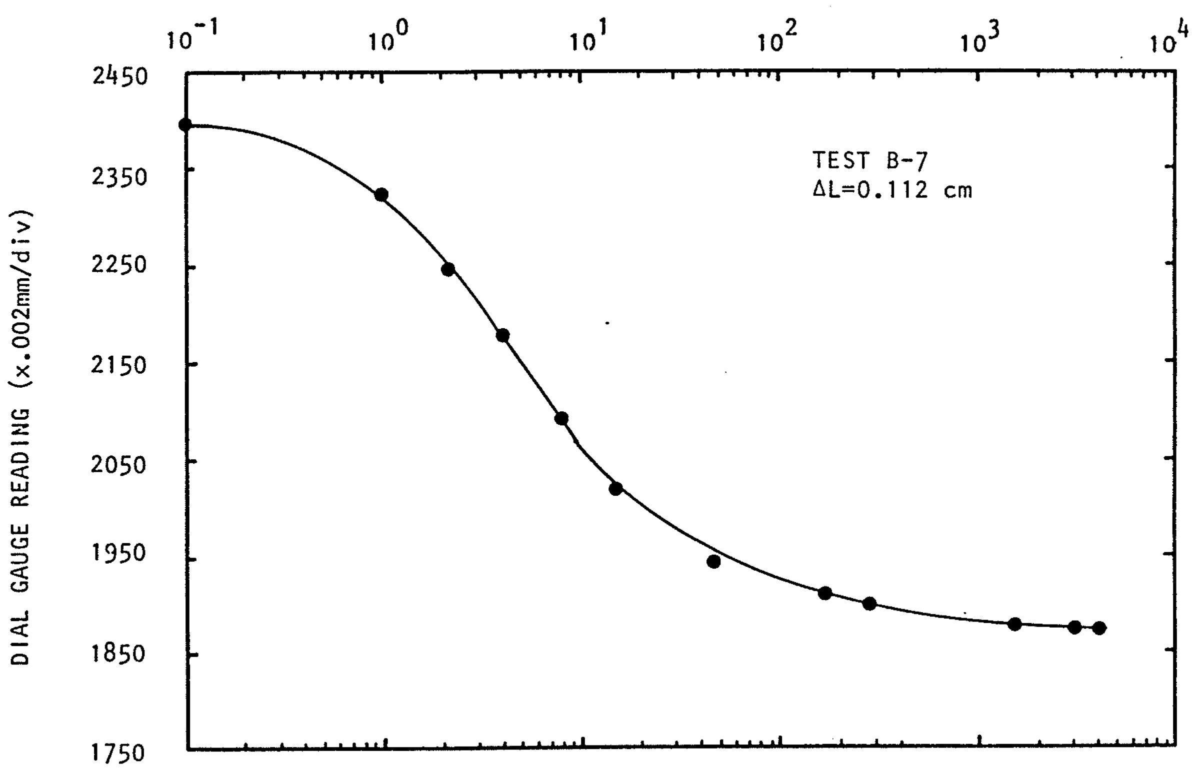
10-1
100
101
102
103
104
TEST B-7
ΔL=0.112 cm
DIAL GAUGE READING (x.002mm/div)
2450
2350
2250
2150
2050
1950
1850
1750

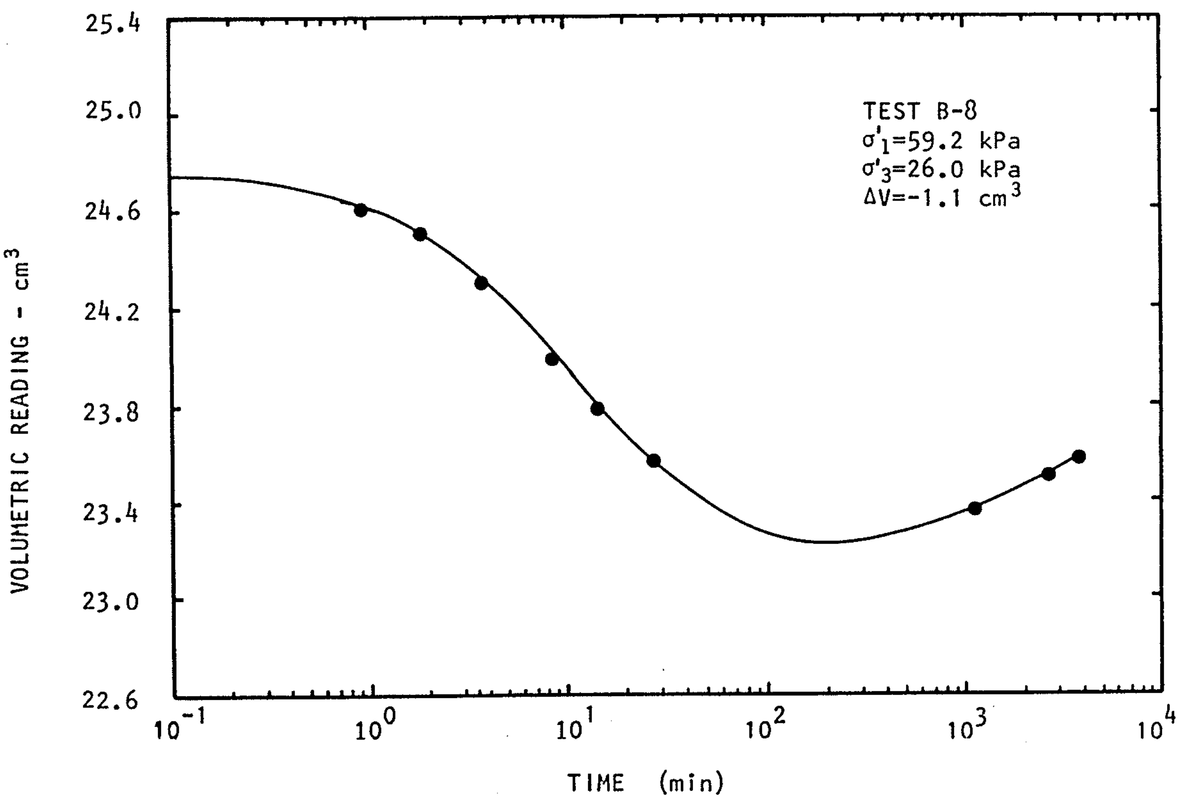

TEST B-8
σ'1=59.2 kPa
σ'3=26.0 kPa
ΔV=-1.1 cm3
VOLUMETRIC READING - cm3
25.4
25.0
24.6
24.2
23.8
23.4
23.0
22.6
10-1
100
101
102
103
104
TIME (min)

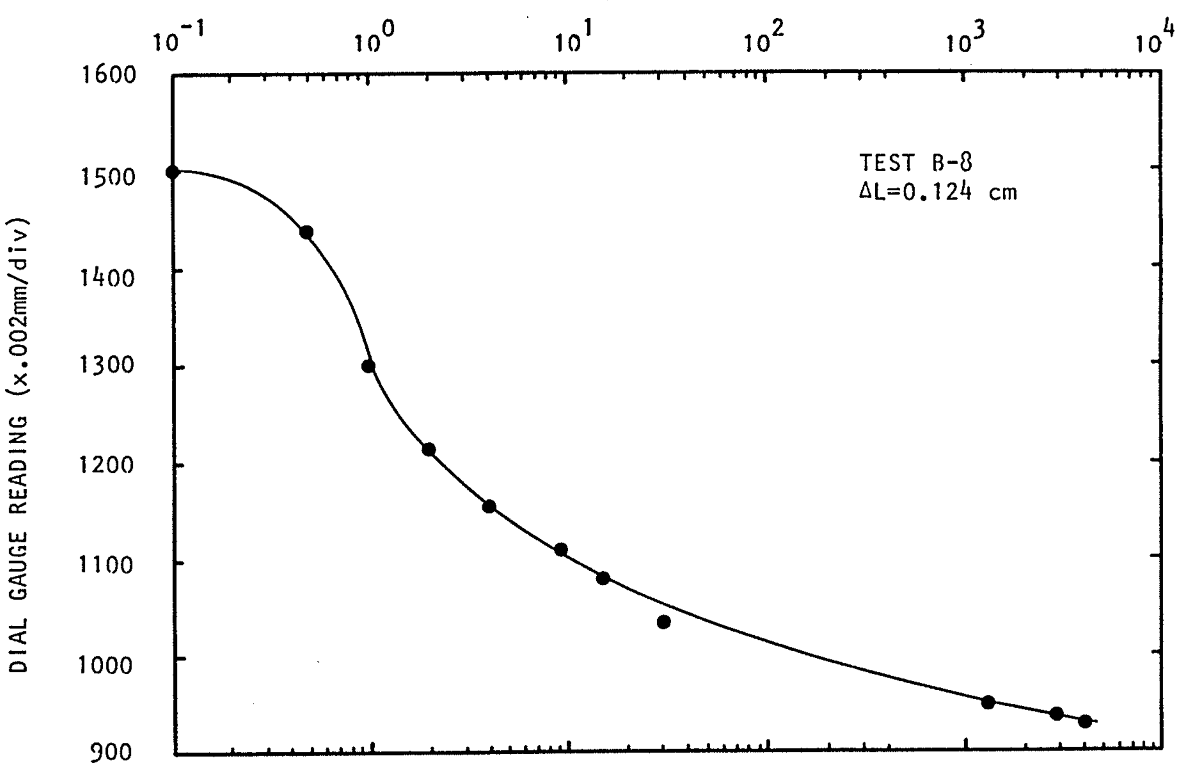

10-1
100
101
102
103
104
TEST B-8
ΔL=0.124 cm
DIAL GAUGE READING (x.002mm/div)
1600
1500
1400
1300
1200
1100
1000
900

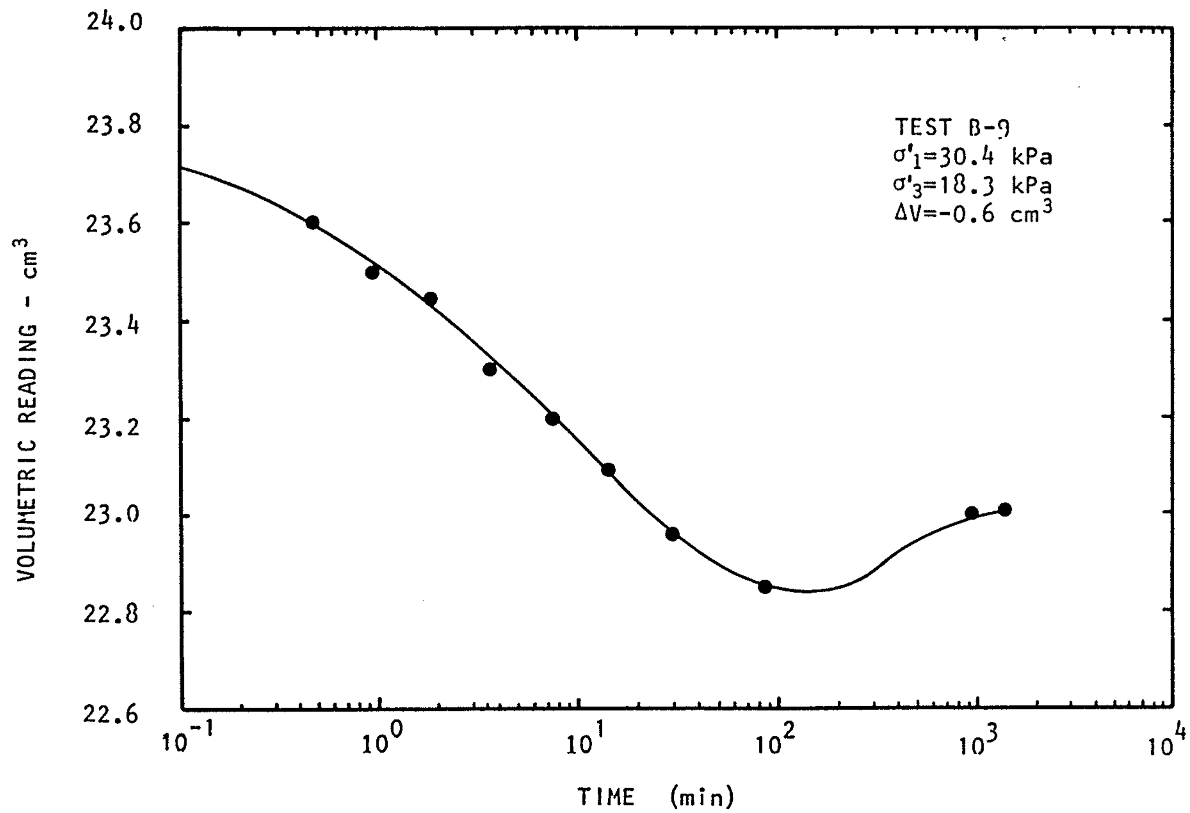

24.0
23.8
23.6
23.4
23.2
23.0
22.8
22.6
VOLUMETRIC READING - cm^3
TEST B-9
σ'_1=30.4 kPa
σ'_3=18.3 kPa
ΔV=-0.6 cm^3
10^{-1}
10^0
10^1
10^2
10^3
10^4
TIME (min)

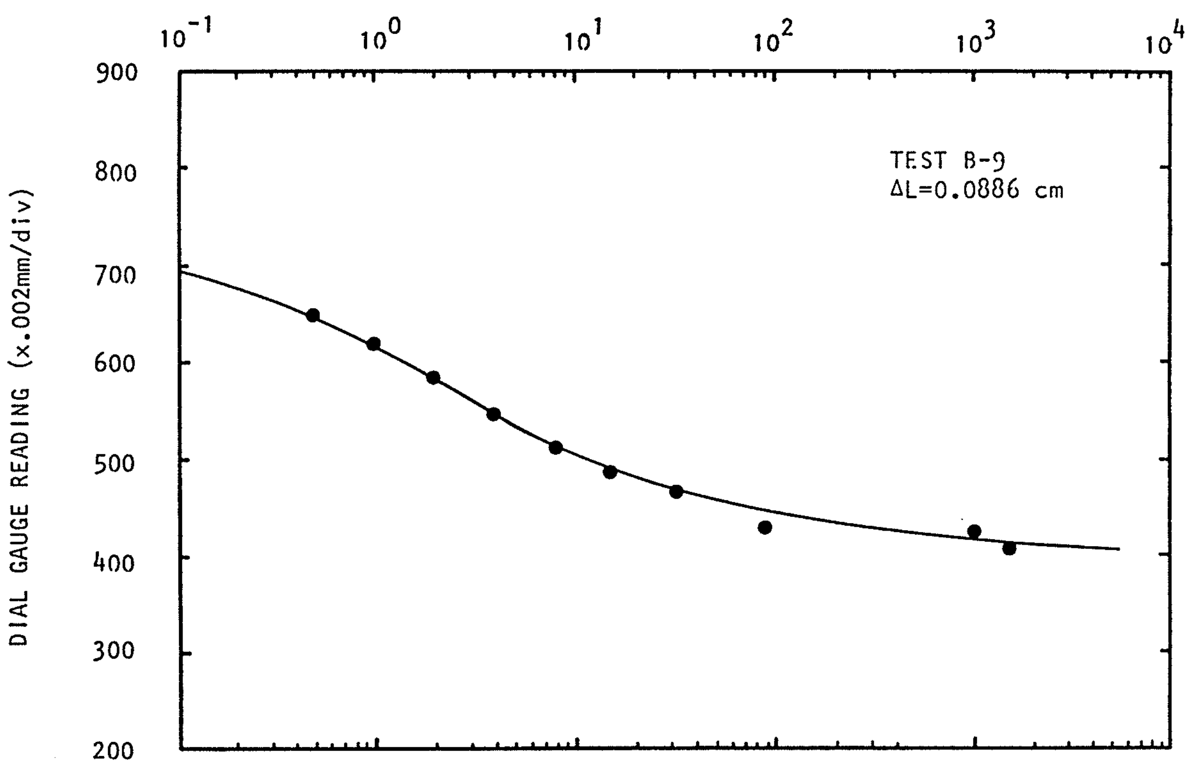

10^{-1}
10^0
10^1
10^2
10^3
10^4
900
800
700
600
500
400
300
200
DIAL GAUGE READING (x.002mm/div)
TEST B-9
ΔL=0.0886 cm

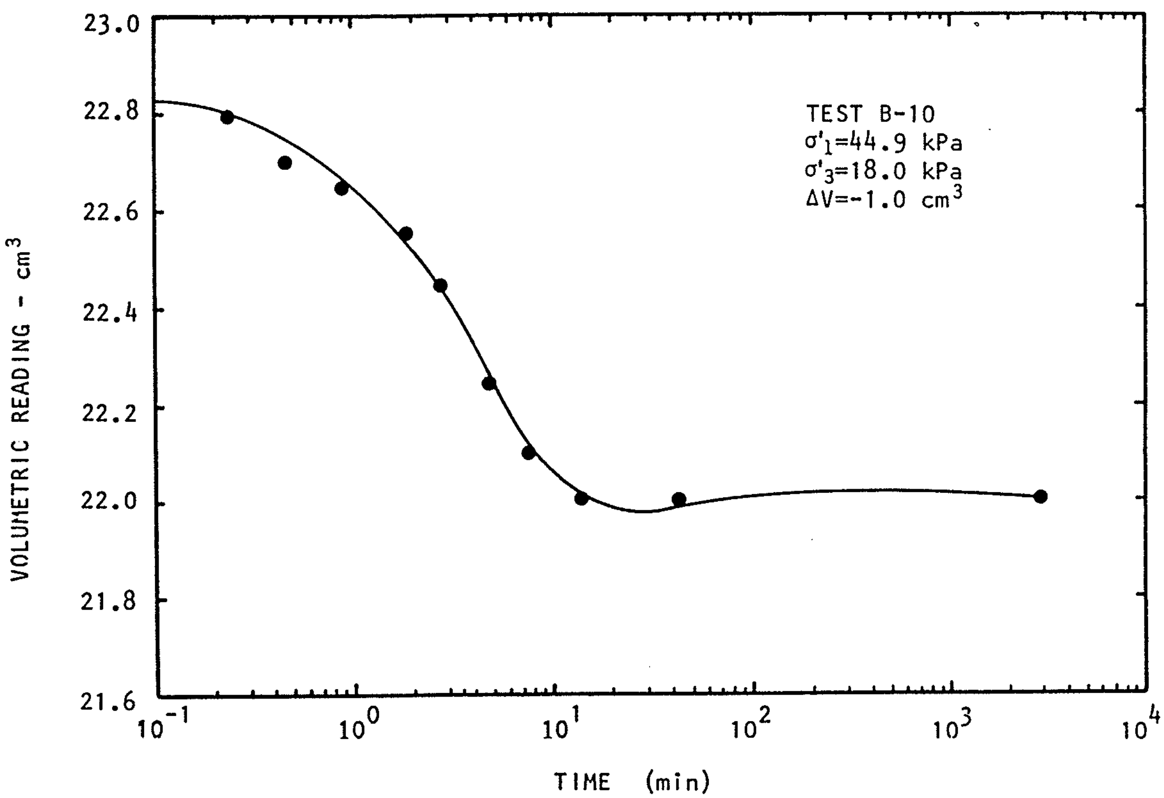
TEST B-10
σ'1=44.9 kPa
σ'3=18.0 kPa
ΔV=-1.0 cm3
VOLUMETRIC READING - cm3
23.0
22.8
22.6
22.4
22.2
22.0
21.8
21.6
10-1
100
101
102
103
104
TIME (min)

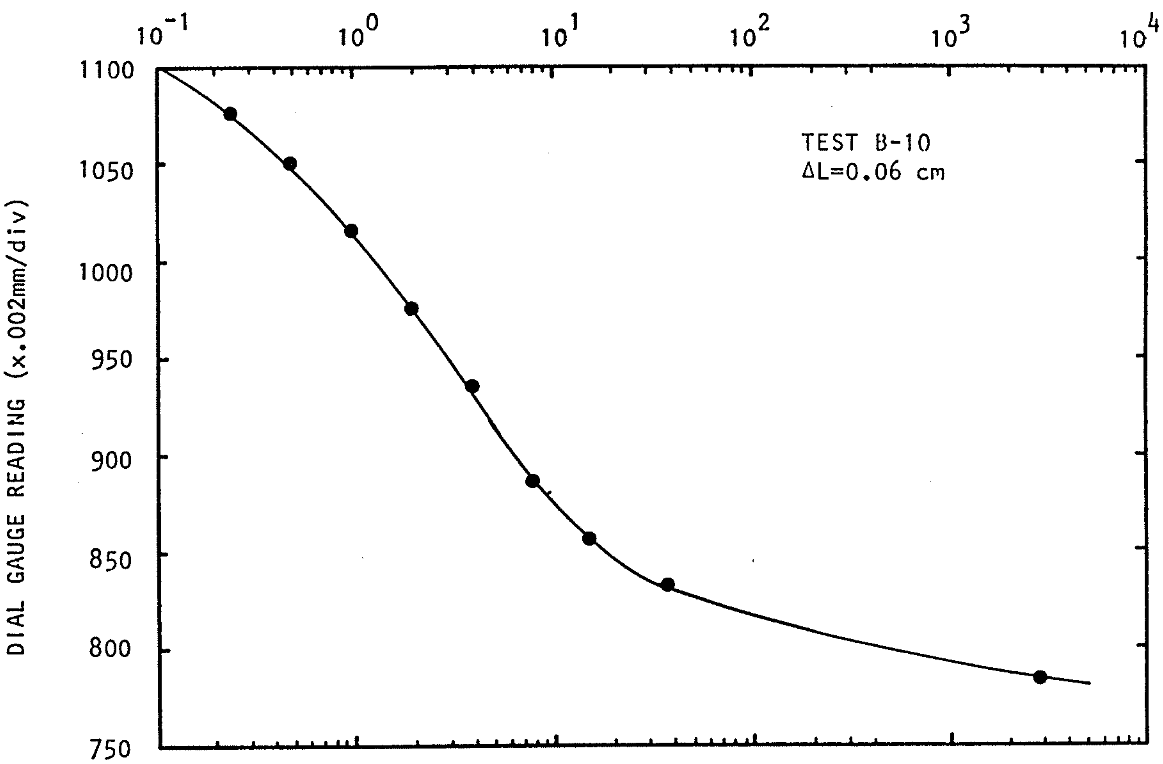
10-1
100
101
102
103
104
TEST B-10
ΔL=0.06 cm
DIAL GAUGE READING (x.002mm/div)
1100
1050
1000
950
900
850
800
750

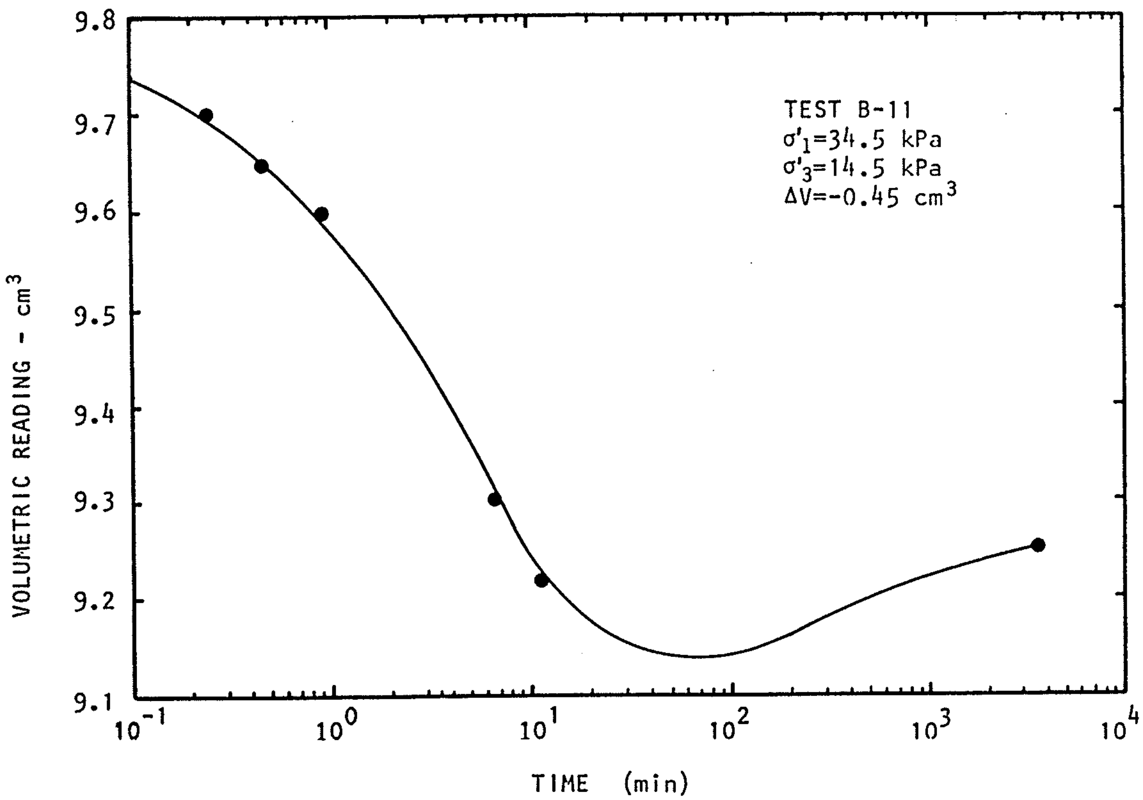

TEST B-11
σ'1=34.5 kPa
σ'3=14.5 kPa
ΔV=-0.45 cm3
VOLUMETRIC READING - cm3
9.8
9.7
9.6
9.5
9.4
9.3
9.2
9.1
10-1
100
101
102
103
104
TIME (min)

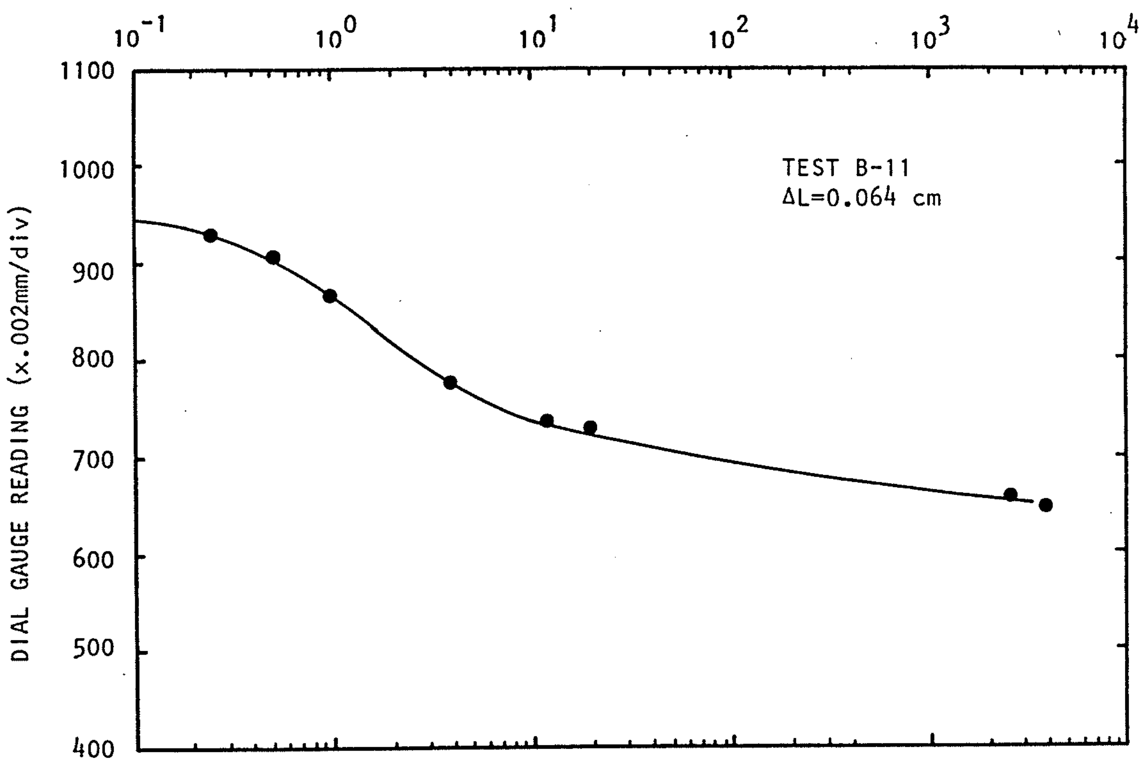

TEST B-11
ΔL=0.064 cm
DIAL GAUGE READING (x.002mm/div)
10-1
100
101
102
103
104
1100
1000
900
800
700
600
500
400

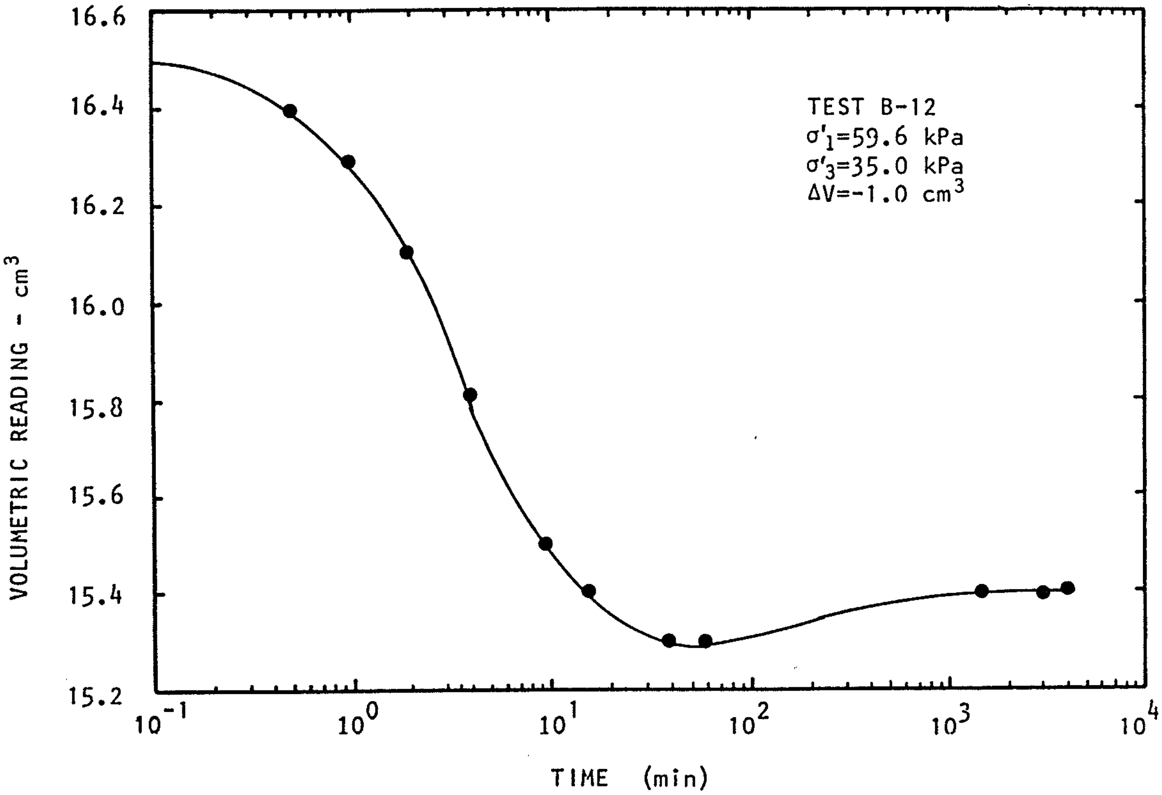
TEST B-12
σ'1=59.6 kPa
σ'3=35.0 kPa
ΔV=-1.0 cm3
VOLUMETRIC READING - cm3
TIME (min)

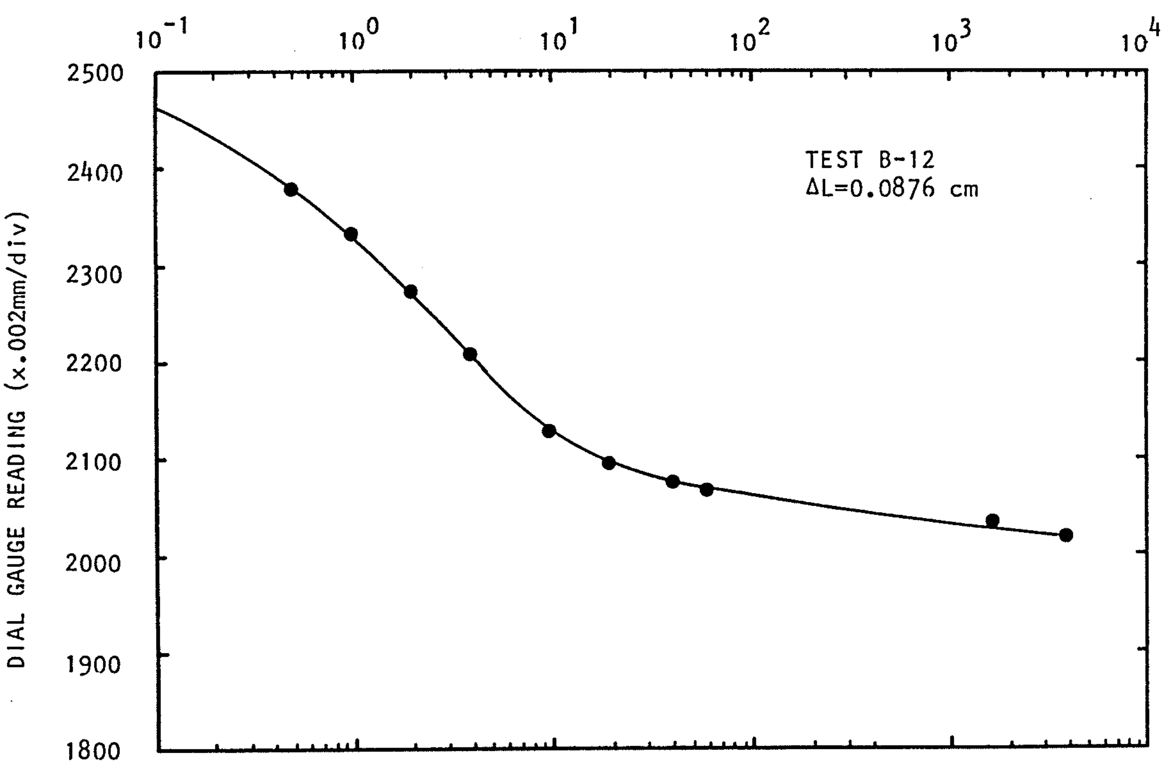
TEST B-12
ΔL=0.0876 cm
DIAL GAUGE READING (x.002mm/div)

C.2 DTTCP Test Data

TEST : B2 Date Tested : 051085

Sample Length After Consolidation : 7.787 cm $\sigma_1' = 48.0$kPa
Sample Diameter After Consolidation : 3.754 cm $\sigma_3' = 28.6$kPa
Sample Area After Consolidation : 11.069 cm^2 $\Delta u = 15.0$kPa
Sample Volume After Consolidation : 86.196 cm^3
Void Ratio After Consolidation : 0.8313
Water Content Before Consolidation :
Water Content After DTTCP Test :

END of Cycle	ΔL (cm)	E1 (cm/cm)	ΔV (cc)	Ev (cc/cc)	ΔD (cm)	E3 (cm/cm)
1	.00032	.00004	−0.06	−.00070	−.00160	−.00043
2	.00040	.00005	−0.16	−.00190	−.00370	−.00099
3	.00070	.000090	−0.26	−.00300	−.00599	−.00160
4	.00106	.00014	−0.26	−.00300	−.00610	−.00163
5	.00080	.00010	−0.36	−.00420	−.00820	−.00218
6	.00130	.00017	−0.36	−.00420	−.00830	−.00221
7	.00108	.00014	−0.42	−.00490	−.00956	−.00255
8	.00124	.00016	−0.46	−.00530	−.01050	−.00280
9	.00134	.00017	−0.46	−.00530	−.01050	−.00280
10	.00128	.00016	−0.52	−.00600	−.01180	−.00310
11	.00146	.00019	−0.54	−.00630	−.01230	−.00328
12	.00148	.00019	−0.56	−.00650	−.01270	−.00338
13	.00162	.00021	−0.62	−.00720	−.01400	−.00373
14	.00168	.00022	−0.66	−.00770	−.01480	−.00394
15	.00168	.00022	−0.71	−.00820	−.01600	−.00426
16	.00204	.00026	−0.71	−.00820	−.01610	−.00429
17	.00176	.00023	−0.82	−.00950	−.01840	−.00490
20	.00188	.00024	−1.01	−.01170	−.02260	−.00602
22	.00230	.00030	−1.06	−.01230	−.02370	−.00631
27	.00200	.00026	−1.12	−.01300	−.02500	−.00666
28	.00226	.00029	−1.11	−.01290	−.02500	−.00666
29	.00202	.00026	−1.21	−.01400	−.02700	−.00719
32	.00222	.00029	−1.21	−.01400	−.02700	−.00719
33	.00288	.00037	−1.21	−.01400	−.02700	−.00719
34	.00252	.00032	−1.24	−.01440	−.02770	−.00738
38	.00322	.00041	−1.26	−.01460	−.02830	−.00754
40	.00286	.00037	−1.31	−.01520	−.02930	−.00781
44	.00288	.00037	−1.41	−.01640	−.03140	−.00836
45	.00308	.00040	−1.41	−.01640	−.03150	−.00839
50	.00314	.00040	−1.46	−.01690	−.03260	−.00868
51	.00322	.00041	−1.48	−.01720	−.03300	−.00879
52	.00332	.00043	−1.51	−.01750	−.03370	−.00898
53	.00332	.00042	−1.51	−.01750	−.03370	−.00898
56	.00330	.00043	−1.51	−.01750	−.03370	−.00898
57	.00350	.00045	−1.51	−.01750	−.03380	−.00900
58	.00332	.00043	−1.56	−.01810	−.03480	−.00927
62	.00340	.00044	−1.61	−.01870	−.03600	−.00959
68	.00360	.00046	−1.66	−.01930	−.03700	−.00986

TEST : B2 Date Tested : 051085

Sample Length After Consolidation	: 7.787	cm	σ_1'=48.0kPa
Sample Diameter After Consolidation	: 3.754	cm	σ_3'=28.6kPa
Sample Area After Consolidation	: 11.069	cm^2	Δu=15.0kPa
Sample Volume After Consolidation	: 86.196	cm^3	
Void Ratio After Consolidation	: 0.8313		
Water Content Before Consolidation	:		
Water Content After DTTCP Test	:		

Middle of Cycle	ΔL (cm)	E1 (cm/cm)	ΔV (cc)	Ev (cc/cc)	ΔD (cm)	E3 (cm/cm)
1	-.0011	-.00021	-0.35	-.00406	-.00816	-.00218
2	-.0008	-.00010	-0.35	-.00406	-.00760	-.00202
3	-.0018	-.00023	-0.45	-.00522	-.00952	-.00254
4	-.0006	-.00008	-0.45	-.00522	-.00981	-.00261
5	-.0004	-.00005	-0.45	-.00522	-.00986	-.00263
6	-.0007	-.00009	-0.65	-.00754	-.01413	-.00376
7	-.0004	-.00005	-0.65	-.00754	-.01420	-.00378
8	-.00012	-.00002	-0.65	-.00754	-.01401	-.00373
9	0.0	0.0	-0.75	-.00870	-.01646	-.00439
10	0.0002	.00003	-0.75	-.00870	-.01651	-.00440
11	0.0004	.00005	-0.75	-.00870	-.01656	-.00441
12	0.00046	.00005	-0.85	-.00986	-.01875	-.00526
13	0.00058	.00007	-0.85	-.00986	-.01877	-.00500
14	0.00022	.00003	-0.90	-.01044	-.01977	-.00527
15	0.00018	.00002	-0.95	-.01102	-.02094	-.00555
16	0.00058	.00007	-1.00	-.01160	-.02202	-.00587
17	0.00040	.00005	-1.10	-.01276	-.02414	-.00643
21	0.00092	.00012	-1.30	-.01508	-.02859	-.00762
22	0.00078	.00010	-1.30	-.01508	-.02856	-.00761
24	0.00170	.00022	-1.30	-.01508	-.02878	-.00767
28	0.00142	.00018	-1.40	-.01624	-.03090	-.00822
33	0.00150	.00019	-1.45	-.01682	-.03200	-.00852
34	0.00180	.00023	-1.45	-.01682	-.03200	-.00854
51	0.00246	.00032	-1.70	-.01972	-.03760	-.01000
57	0.00256	.00033	-1.75	-.02030	-.03970	-.01030
58	0.00260	.00033	-1.80	-.02088	-.03980	-.01060

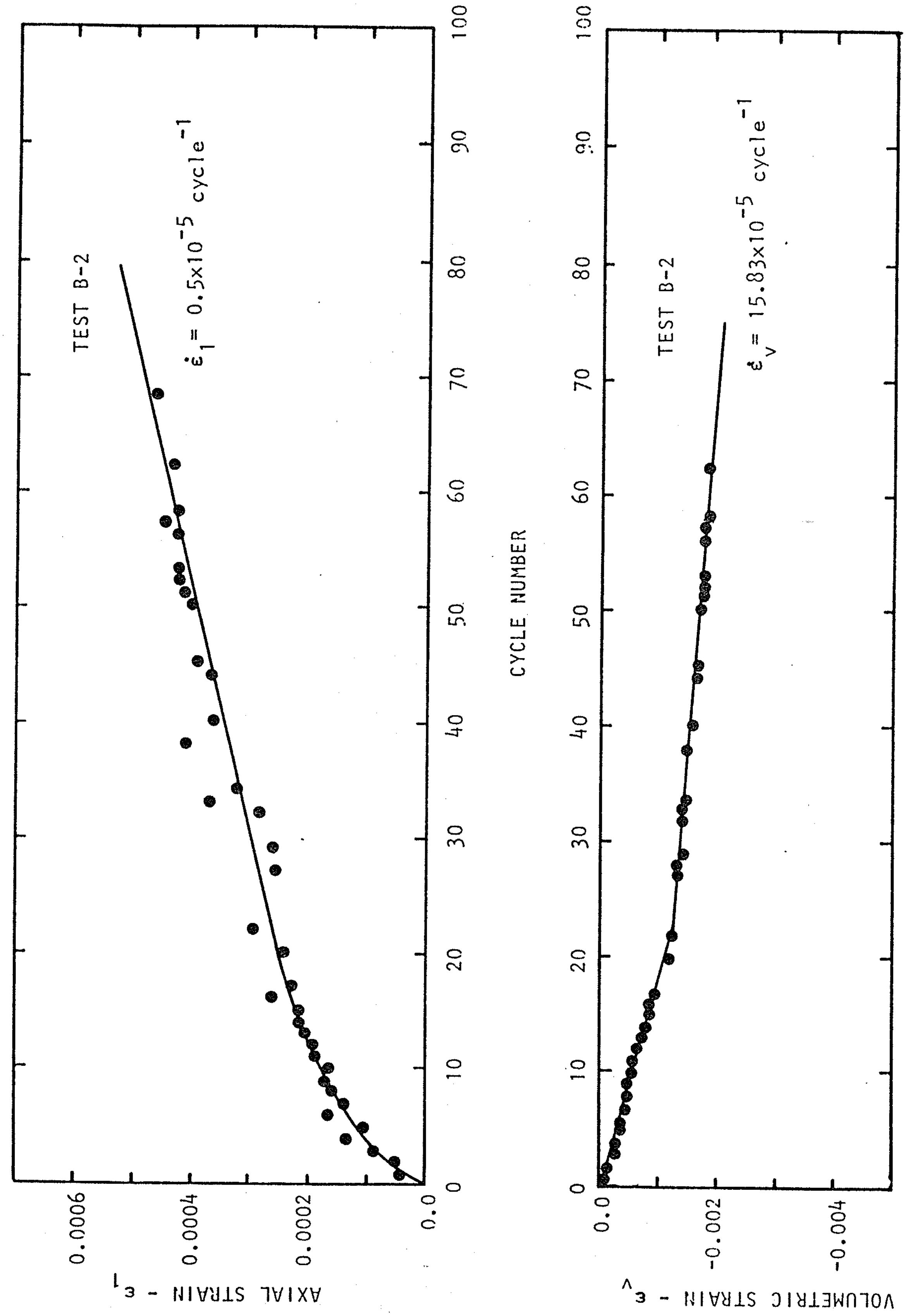
TEST B-2
$\dot{\varepsilon}_1 = 0.5\times10^{-5}$ cycle^{-1}
AXIAL STRAIN - ε_1
0.0006
0.0004
0.0002
0.0
0
10
20
30
40
50
60
70
80
90
100
CYCLE NUMBER
TEST B-2
$\dot{\varepsilon}_v = 15.83\times10^{-5}$ cycle^{-1}
VOLUMETRIC STRAIN - ε_v
0.0
-0.002
-0.004

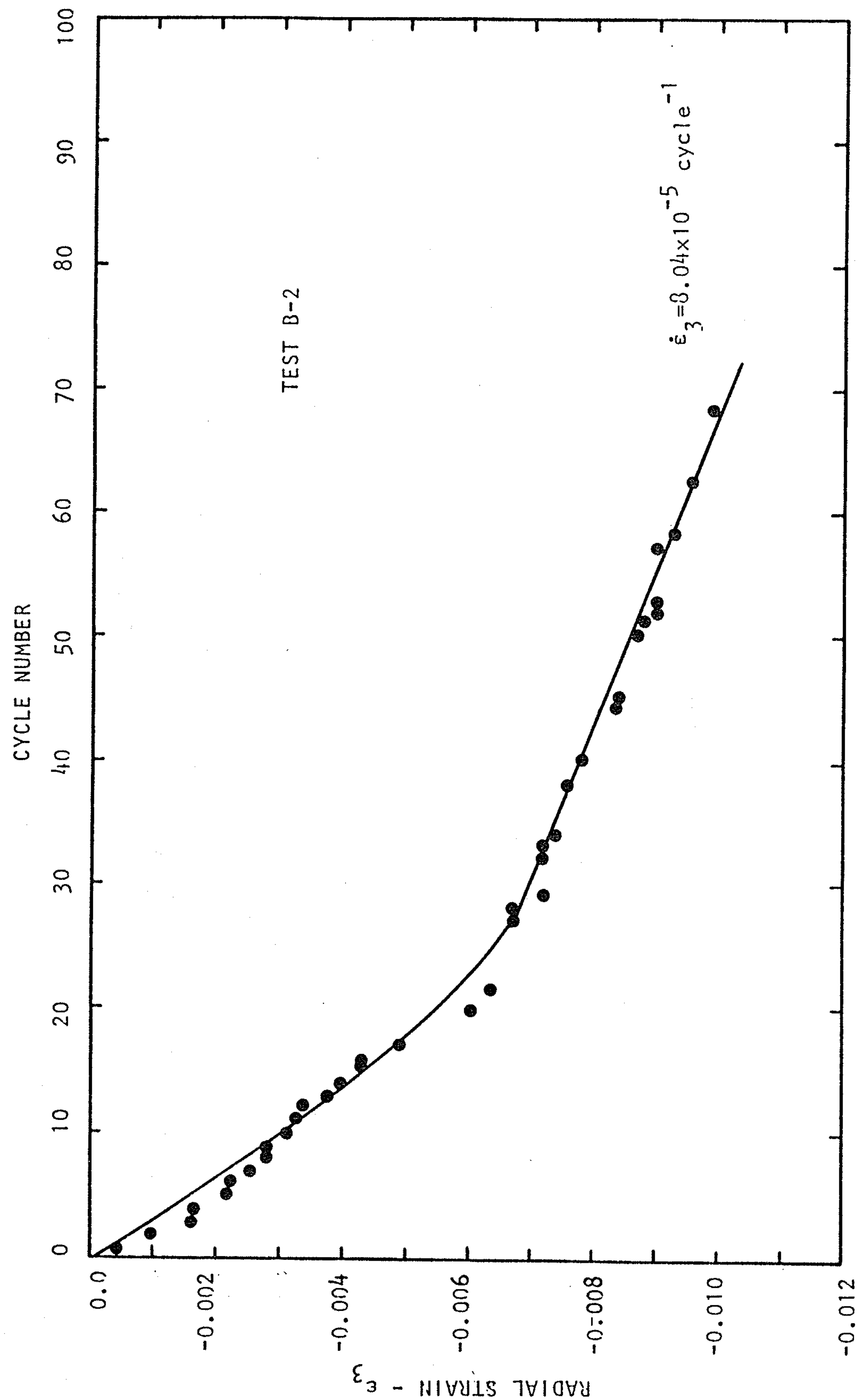
CYCLE NUMBER
0
10
20
30
40
50
60
70
80
90
100
TEST B-2
$\dot{\varepsilon}_3 = 8.04 \times 10^{-5}$ cycle^{-1}
0.0
-0.002
-0.004
-0.006
-0.008
-0.010
-0.012
RADIAL STRAIN - ε_3

TEST : B3 Date Tested : 053085

Sample Length After Consolidation : 8.585 cm σ'_1=48.0kPa
Sample Diameter After Consolidation : 3.929 cm σ'_3=28.6kPa
Sample Area After Consolidation : 12.184 cm^2 Δu=18.6KPa
Sample Volume After Consolidation : 104.058 cm^3
Void Ratio After Consolidation : 0.795
Water Content Before Consolidation : 31.5 %
Water Content After DTTCP Test : 32.6 %

End of Cycle	ΔL (cm)	E1 (cm/cm)	ΔV (cc)	Ev (cc/cc)	ΔD (cm)	E3 (cm/cm)
5	.00296	.00034	0	0	-.00067	-.00017
6	.00926	.00108	0	0	-.00212	-.00054
7	.00956	.00111	0	0	-.00219	-.00055
11	.01196	.00139	-0.05	-.00048	-.00368	-.00093
12	.01240	.00144	-0.05	-.00048	-.00378	-.00096
13	.01296	.00151	-0.10	-.00096	-.00486	-.00124
17	.01356	.00158	-0.10	-.00096	-.00499	-.00127
18	.01462	.00170	-0.10	-.00096	-.00524	-.00133
19	.01438	.00168	-0.10	-.00096	-.00518	-.00132
23	.01506	.00175	-0.20	-.00192	-.00723	-.00184
24	.01618	.00188	-0.20	-.00192	-.00748	-.00190
25	.01626	.00189	-0.20	-.00192	-.00750	-.00191
30	.01698	.00198	-0.20	-.00192	-.00766	-.00195
35	.01746	.00200	-0.30	-.00288	-.00967	-.00246
41	.01846	.00215	-0.30	-.00288	-.00990	-.00252
43	.01896	.00221	-0.30	-.00288	-.01001	-.00255
49	.01946	.00227	-0.30	-.00288	-.01013	-.00258
55	.02016	.00235	-0.35	-.00336	-.01156	-.00294
59	.02016	.00252	-0.40	-.00384	-.01217	-.00310
60	.02026	.00236	-0.40	-.00384	-.01220	-.00310
61	.02016	.00235	-0.30	-.00288	-.01029	-.00262
65	.02006	.00234	-0.40	-.00384	-.01215	-.00309
66	.02006	.00234	-0.40	-.00384	-.01215	-.00309
83	.02216	.00258	-0.50	-.00481	-.01452	-.00370
84	.02276	.00265	-0.55	-.00529	-.01560	-.00397
89	.02286	.00266	-0.60	-.00577	-.01657	-.00422
90	.02298	.00268	-0.60	-.00577	-.01660	-.00423
91	.02256	.00263	-0.65	-.00625	-.01744	-.00444
95	.02256	.00263	-0.70	-.00673	-.01838	-.00468

TEST : B3 Date Tested : 053085

Sample Length After Consolidation : 8.585 cm σ_1'=48.0 kPa
Sample Diameter After Consolidation: 3.929 cm σ_3'=28.6 kPa
Sample Area After Consolidation : 12.184 cm^2 Δu=18.6 kPa
Sample Volume After Consolidation : 104.058 cm^3
Void Ratio After Consolidation : 0.795
Water Content Before Consolidation : 31.5%
Water Content After DTTCP Test : 32.65%

Middle Of Cycle	ΔL (cm)	E1 (cm/cm)	ΔV (cc)	Ev (cc/cc)	ΔD (cm)	E3 (cm/cm)
6	-.00070	-.00008	0.50	-.0048	-.00927	-.00236
7	.00120	.00015	-0.50	-.0048	-.00972	-.00247
12	.00470	.00055	-0.55	-.0053	-.01145	-.00292
13	.00510	.00059	-0.60	-.0058	-.01248	-.00318
18	.00670	.00078	-0.60	-.0058	-.01285	-.00327
19	.00710	.00082	-0.65	-.0052	-.01387	-.00353
25	.00840	.00098	-0.70	-.0057	-.01512	-.00385
30	.00920	.00107	-0.70	-.0057	-.01530	-.00389
43	.01090	.00127	-0.80	-.0077	-.01758	-.00447
49	.01390	.00162	-0.75	-.0072	-.01733	-.00441
55	.01200	.00140	-0.85	-.0082	-.01977	-.00478
61	.01320	.00154	-0.90	-.0086	-.02000	-.00509
66	.01330	.00155	-0.90	-.0087	-.02000	-.00509
84	.01580	.00184	-1.00	-.0096	-.02246	-.00572
90	.01550	.00181	-1.10	-.0106	-.02428	-.00618

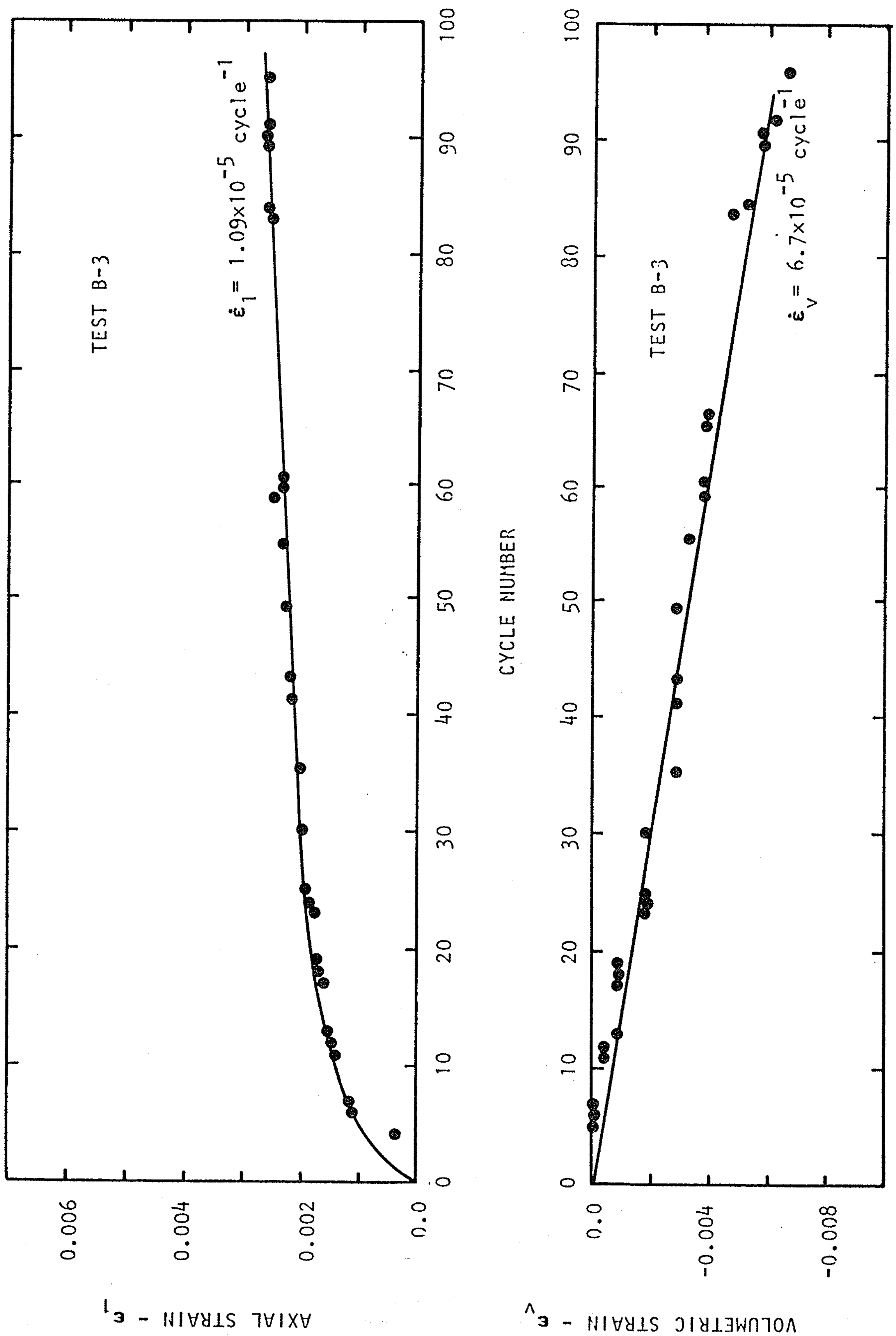
TEST B-3
$\dot{\varepsilon}_1 = 1.09\times10^{-5}$ cycle^{-1}
AXIAL STRAIN - ε_1
0.006
0.004
0.002
0.0
CYCLE NUMBER
0
10
20
30
40
50
60
70
80
90
100
TEST B-3
$\dot{\varepsilon}_v = 6.7\times10^{-5}$ cycle^{-1}
VOLUMETRIC STRAIN - ε_v
0.0
-0.004
-0.008

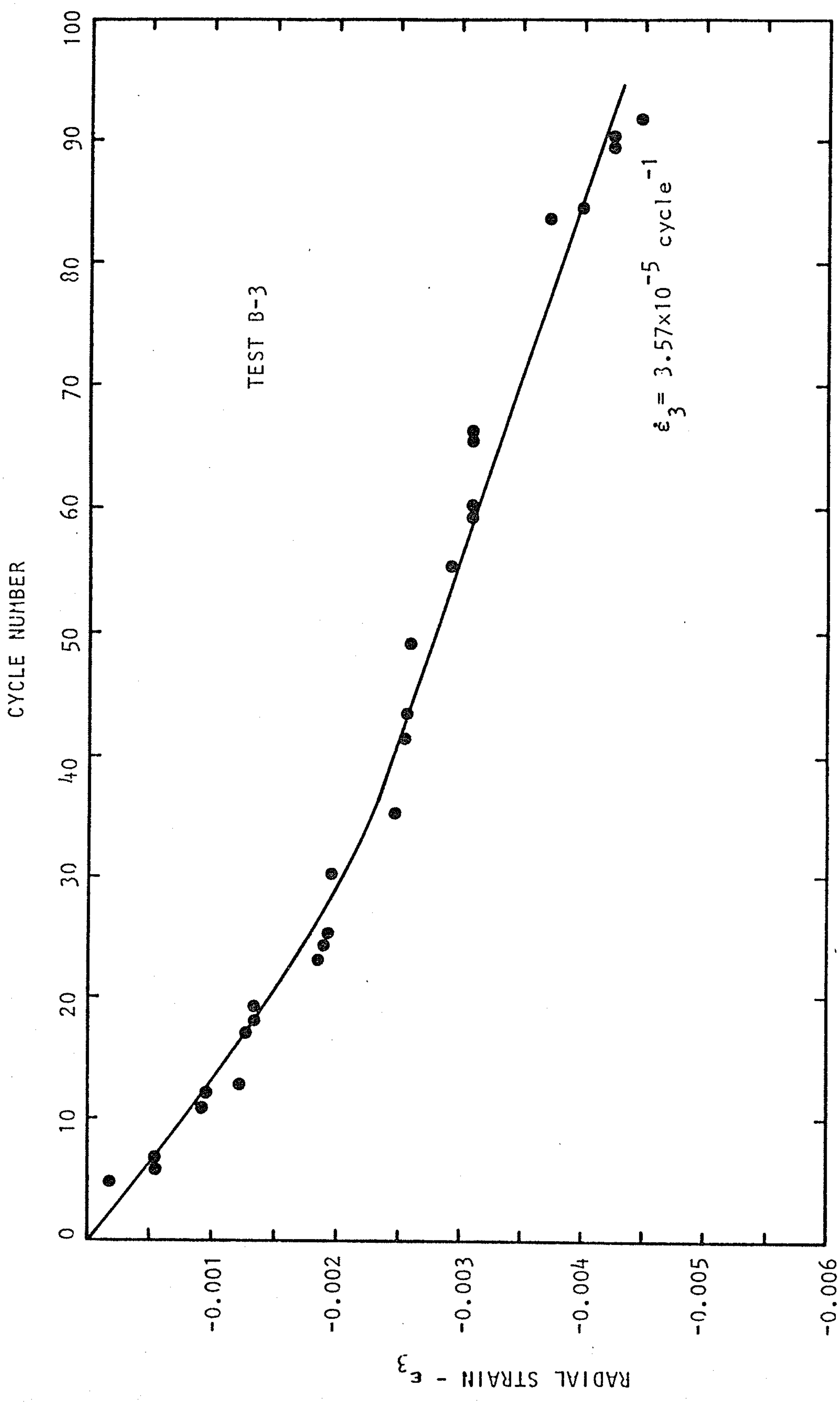

CYCLE NUMBER
RADIAL STRAIN - ε_3
TEST B-3
$\dot{\varepsilon}_3 = 3.57\times10^{-5}$ cycle^{-1}
0
10
20
30
40
50
60
70
80
90
100
-0.001
-0.002
-0.003
-0.004
-0.005
-0.006

TEST : B4 Date Tested : 062085

Sample Length After Consolidation : 8.909 cm σ'_1=48.0kPa
Sample Diameter After Consolidation : 3.918 cm σ'_3=28.6kPa
Sample Area After Consolidation : 12.034 cm^2 Δu=22.9kPa
Sample Volume After Consolidation : 107.397 cm^3
Void Ratio After Consolidation : 0.859
Water Content Before Consolidation : 31.5 %
Water Content After DTTCP Test : 30.9 %

End of Cycle	ΔL (cm)	E1 (cm/cm)	ΔV (cc)	Ev (cc/cc)	ΔD (cm)	E3 (cm/cm)
2	.00470	.00052	0	0	-.00100	-.00027
6	.00900	.00101	0	0	-.00198	-.00051
7	.00980	.00110	0	0	-.00216	-.00055
8	.01076	.00121	0	0	-.00237	-.00061
12	.01228	.00138	0	0	-.00270	-.00069
13	.01302	.00146	0	0	-.00287	-.00073
14	.01358	.00152	0	0	-.00299	-.00076
18	.01450	.00163	0	0	-.00319	-.00082
20	.01540	.00173	0	0	-.00339	-.00087
24	.01640	.00184	0	0	-.00361	-.00093
25	.01660	.00186	0	0	-.00366	-.00093
26	.01700	.00191	0	0	-.00375	-.00096
30	.01780	.00200	0	0	-.00392	-.00100
36	.01880	.00211	0	0	-.00414	-.00106
37	.01880	.00211	0	0	-.00414	-.00106

Power failure - sample reconsolidated to : V = 108.497 cm^3
L = 8.697 cm
D = 3.985 cm

End of Cycle	ΔL (cm)	E1 (cm/cm)	ΔV (cc)	Ev (cc/cc)	ΔD (cm)	E3 (cm/cm)
51	.02040	.00229	0	0	-.00471	-.00120
52	.02042	.00229	0	0	-.00471	-.00120
53	.02062	.00231	0	0	-.00476	-.00122
57	.02320	.00260	0	0	-.00535	-.00136
58	.02380	.00267	0	0	-.00549	-.00140
59	.02400	.00269	0	0	-.00554	-.00141
60	.02450	.00275	0	0	-.00565	-.00144
63	.02444	.00274	-0.10	-.00093	-.00340	-.00097
64	.02470	.00277	-0.10	-.00093	-.00386	-.00099
65	.02480	.00278	-0.10	-.00093	-.00388	-.00099
69	.02550	.00286	-0.10	-.00093	-.00404	-.00103
72	.02540	.00285	-0.10	-.00093	-.00402	-.00103
77	.02640	.00296	-0.10	-.00093	-.00425	-.00108
78	.02650	.00297	-0.10	-.00093	-.00427	-.00109
81	.02650	.00297	-0.10	-.00093	-.00427	-.00109

TEST : B4 Date Tested : 062085

Sample Length After Consolidation	: 8.909 cm	σ_1'=48.0 kPa
Sample Diameter After Consolidation	: 3.918 cm	σ_3'=28.6 kPa
Sample Area After Consolidation	: 12.034 cm^2	Δu=22.9 kPa
Sample Volume After Consolidation	: 107.397 cm^3	
Void Ratio After Consolidation	: 0.859	
Water Content Before Consolidation	: 31.5%	
Water Content After DTTCP Test	: 30.9%	

Middle Of Cycle	ΔL (cm)	E1 (cm/cm)	ΔV (cc)	Ev (cc/cc)	ΔD (cm)	E3 (cm/cm)
1	-.00920	-.00103	0.70	-.0065	-.01073	-.00274
2	-.00820	-.00092	0.80	-.0074	-.01276	-.00326
8	-.00220	-.00025	0.85	-.0079	-.01499	-.00383
13	.00040	.00004	-0.80	-.0074	-.01465	-.00374
14	.00080	.00009	-0.90	-.0084	-.01660	-.00423
20	.00260	.00029	-0.85	-.0079	-.01600	-.00410
Power failure - sample reconsolidated to : V = 108.497 cm^3, L =8.697 cm, D = 3.985 cm						
52	.01020	.00114	-0.95	-.0088	-.01979	-.00505
53	.01020	.00114	-1.00	-.0092	-.02070	-.00528
58	.01300	.00146	-0.95	-.0088	-.02043	-.00522
64	.01260	.00141	-0.90	-.0083	-.01940	-.00496
65	.01280	.00144	-0.90	-.0083	-.01947	-.00497

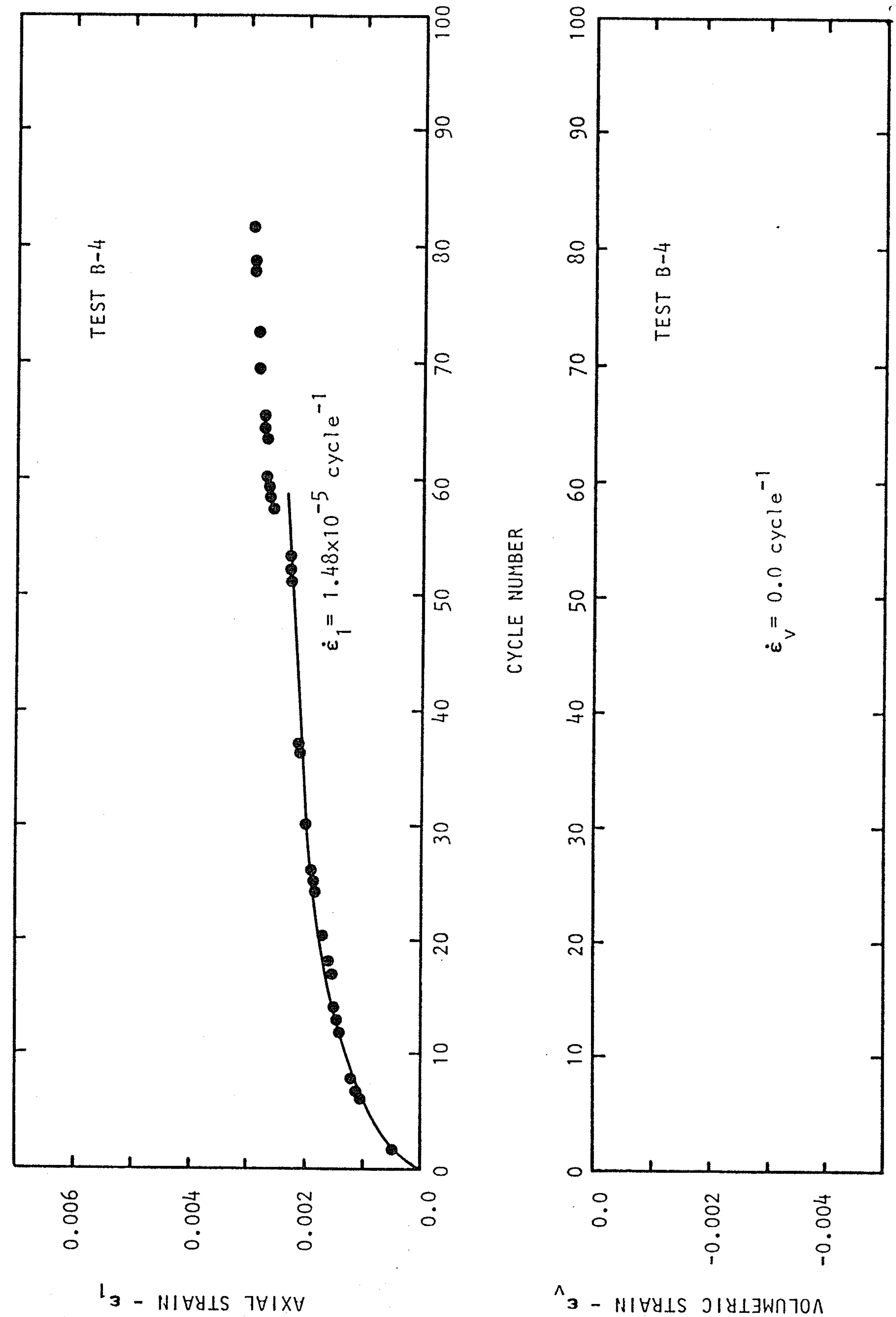

TEST B-4
$\dot{\varepsilon}_1 = 1.48 \times 10^{-5}$ cycle^{-1}
AXIAL STRAIN - ε_1
0.006
0.004
0.002
0.0
CYCLE NUMBER
0
10
20
30
40
50
60
70
80
90
100
TEST B-4
$\dot{\varepsilon}_v = 0.0$ cycle^{-1}
VOLUMETRIC STRAIN - ε_v
0.0
-0.002
-0.004

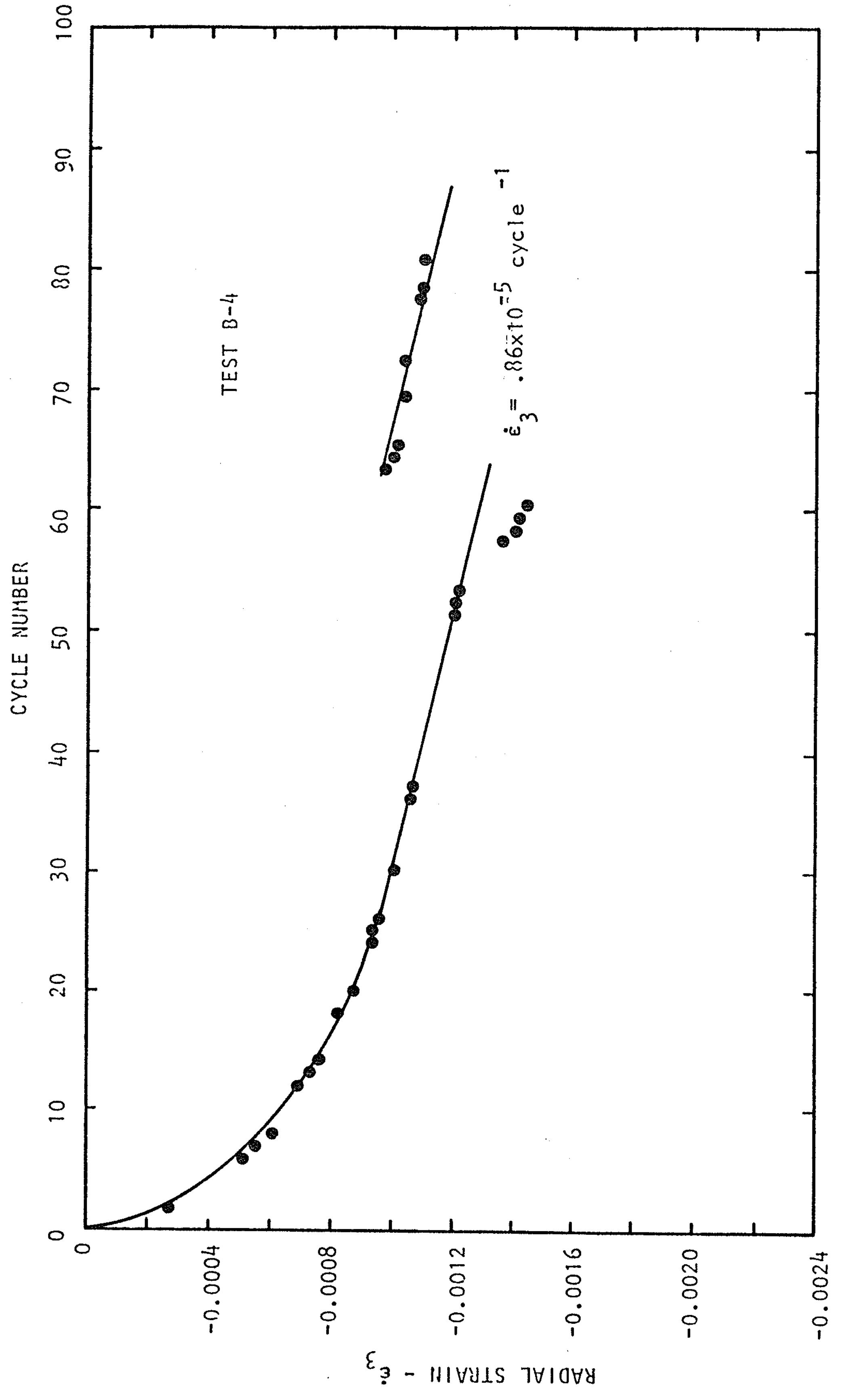

CYCLE NUMBER
0
10
20
30
40
50
60
70
80
90
100
RADIAL STRAIN - ϵ_3
0
-0.0004
-0.0008
-0.0012
-0.0016
-0.0020
-0.0024
TEST B-4
$\dot{\epsilon}_3 = .86 \times 10^{-5}$ cycle $^{-1}$

TEST : B5 Date Tested : 071985

Sample Length After Consolidation : 8.031 cm σ_1 =38.2kPa
Sample Diameter After Consolidation: 3.575 cm σ_3 =10.1kPa
Sample Area After Consolidation : 10.086 cm^2 Δu=10. kPa
Sample Volume After Consolidation : 80.602 cm^3
Void Ratio After Consolidation : 0.834
Water Content Before Consolidation : 27.0 % (air dry)
Water Content After DTTCP Test : 33.0 %

End of Cycle	ΔL (cm)	E1 (cm/cm)	ΔV (cc)	Ev (cc/cc)	ΔD (cm)	E3 (cm/cm)
1	.00770	.00096	0	0	-.00174	-.00049
5	.01530	.00191	-0.10	-.00124	-.00566	-.00158
6	.01750	.00218	-0.10	-.00124	-.00615	-.00172
7	.02010	.00250	-0.10	-.00124	-.00673	-.00188
11	.02680	.00334	-0.20	-.00248	-.01045	-.00292
12	.02900	.00361	-0.20	-.00248	-.01090	-.00306
13	.03000	.00374	-0.20	-.00248	-.01120	-.00312
17	.03210	.00400	-0.20	-.00248	-.01164	-.00326
18	.03290	.00410	-0.20	-.00248	-.01182	-.00331
19	.03340	.00416	-0.20	-.00248	-.01193	-.00334
23	.03440	.00428	-0.20	-.00248	-.01215	-.00340
24	.03500	.00436	-0.20	-.00248	-.01229	-.00344
25	.03520	.00438	-0.20	-.00248	-.01233	-.00345
29	.03570	.00445	-0.20	-.00248	-.01244	-.00348
41	.04900	.00610	-0.40	-.00496	-.01987	-.00556
42	.05040	.00628	-0.40	-.00496	-.02020	-.00565
43	.05120	.00638	-0.40	-.00496	-.02040	-.00570
44	.05120	.00638	-0.40	-.00496	-.02040	-.00570
45	.05120	.00638	-0.40	-.00496	-.02040	-.00570
46	.05160	.00643	-0.40	-.00496	-.02050	-.00572
47	.05180	.00645	-0.40	-.00496	-.02050	-.00574
48	.05260	.00655	-0.40	-.00496	-.02070	-.00579
49	.05270	.00660	-0.40	-.00496	-.02070	-.00579
50	.05270	.00660	-0.40	-.00496	-.02070	-.00579
51	.05270	.00660	-0.40	-.00496	-.02070	-.00579
52	.05280	.00660	-0.40	-.00496	-.02070	-.00579
53	.05340	.00665	-0.40	-.00496	-.02090	-.00584
54	.05330	.00664	-0.40	-.00496	-.02094	-.00583
55	.05360	.00667	-0.40	-.00496	-.02091	-.00585
56	.05360	.00667	-0.40	-.00496	-.02091	-.00585
57	.05350	.00666	-0.40	-.00496	-.02088	-.00584
58	.05360	.00667	-0.50	-.00620	-.02310	-.00647
59	.05370	.00669	-0.50	-.00620	-.02315	-.00648
60	.05450	.00679	-0.50	-.00620	-.02330	-.00653
61	.05480	.00682	-0.50	-.00620	-.02340	-.00655
62	.05480	.00682	-0.50	-.00620	-.02340	-.00655
63	.05460	.00680	-0.50	-.00620	-.02335	-.00653

TEST : B5 (cont'd)

End of Cycle	ΔL (cm)	E1 (cm/cm)	ΔV (cc)	Ev (cc/cc)	ΔD (cm)	E3 (cm/cm)
64	.05470	.00681	-0.50	-.00620	-.02340	-.00654
65	.05500	.00685	-0.50	-.00620	-.02340	-.00654
66	.05550	.00691	-0.50	-.00620	-.02360	-.00659
67	.05610	.00699	-0.55	-.00682	-.02480	-.00694
78	.05660	.00700	-0.70	-.00868	-.02824	-.00790
83	.41770	.05200	-1.90	-.02357	-.13990	-.03910
84	.42568	.05303	-2.00	-.02481	-.14400	-.04028
86	.47308	.05891	-2.10	-.02605	-.15790	-.04417
89	.68910	.08581	-2.45	-.03040	-.22042	-.06166
95	.76930	.09579	-2.30	-.02854	-.23788	-.06654

TEST : B5 Date Tested : 071985

Sample Length After Consolidation : 8.031 cm σ_1'=38.2kPa
Sample Diameter After Consolidation : 3.575 cm σ_3'=10.1kPa
Sample Area After Consolidation : 10.086 cm^2 Δu=10.1kPa
Sample Volume After Consolidation : 80.602 cm^3
Void Ratio After Consolidation : 0.834
Water Content Before Consolidation : 27.0% (air dry)
Water Content After DTTCP Test : 33.0%

Middle Of Cycle	ΔL (cm)	E1 (cm/cm)	ΔV (cc)	Ev (cc/cc)	Δ D (cm)	E3 (cm/cm)
1	.00100	.0001	-0.60	-.0074	-.01353	-.00379
6	.01530	.0019	-0.60	-.0074	-.01673	-.00468
12	.02670	.0033	-0.65	-.0081	-.02040	-.00571
13	.02770	.0034	-0.70	-.0087	-.02173	-.00608
18	.03150	.0039	-0.70	-.0087	-.02260	-.00632
19	.03180	.0040	-0.70	-.0087	-.02260	-.00634
20	.03250	.0041	-0.70	-.0087	-.02290	-.00638
21	.03350	.0042	-0.70	-.0087	-.02300	-.00644
22	.03350	.0042	-0.70	-.0087	-.02300	-.00644
23	.03290	.0041	-0.70	-.0087	-.02290	-.00640
24	.03330	.0042	-0.70	-.0087	-.02300	-.00640
25	.03400	.0042	-0.70	-.0087	-.02310	-.00650
36	.03920	.0049	-0.80	-.0099	-.02650	-.00740
42	.04860	.0061	-0.90	-.0112	-.03090	-.00860
43	.04950	.0062	-0.90	-.0112	-.03110	-.00870
44	.05040	.0063	-0.90	-.0112	-.03130	-.00870
45	.05060	.0063	-0.90	-.0112	-.03130	-.00876
46	.05080	.0063	-0.90	-.0112	-.03140	-.00877
47	.05100	.0064	-0.90	-.0112	-.03140	-.00878
48	.05090	.0063	-0.90	-.0112	-.03140	-.00878
49	.05170	.0064	-0.90	-.0112	-.03160	-.00883
50	.05170	.0064	-0.90	-.0112	-.03160	-.00883
51	.05180	.0064	-0.90	-.0112	-.03160	-.00883
52	.05200	.0065	-0.90	-.0112	-.03162	-.00885
53	.05210	.0065	-0.90	-.0112	-.03165	-.00887
54	.05260	.0066	-0.90	-.0112	-.03176	-.00889
55	.05280	.0066	-0.90	-.0112	-.03181	-.00890
56	.05280	.0066	-0.90	-.0112	-.03181	-.00840
57	.05290	.0066	-0.90	-.0112	-.03183	-.00840
58	.05310	.0066	-0.95	-.0118	-.03300	-.00923
59	.05320	.0066	-1.00	-.0124	-.03410	-.00954
60	.05350	.0067	-1.00	-.0124	-.03418	-.00856
61	.05380	.0067	-1.00	-.0124	-.03424	-.00958
62	.05430	.0068	-1.00	-.0124	-.03436	-.00961
63	.05440	.0068	-1.00	-.0124	-.03550	-.00993
64	.05460	.0068	-1.05	-.0124	-.03550	-.00994
65	.05460	.0068	-1.10	-.0136	-.03664	-.01025

TEST : B5 (cont'd)

Middle of Cycle	ΔL (cm)	E1 (cm/cm)	ΔV (cc)	Ev (cc/cc)	ΔD (cm)	E3 (cm/cm)
66	.05440	.0068	-1.10	-.0136	-.03654	-.01024
67	.05570	.0069	-1.10	-.0136	-.03675	-.01028
68	.05550	.0069	-1.10	-.0136	-.03684	-.01031
69	.05550	.0069	-1.10	-.0136	-.03684	-.01031
70	.05560	.0069	-1.10	-.0136	-.03686	-.01312
71	.05570	.0069	-1.15	-.0143	-.03799	-.01063
72	.05570	.0069	-1.15	-.0143	-.03794	-.01063
73	.05580	.0070	-1.15	-.0143	-.03901	-.01063

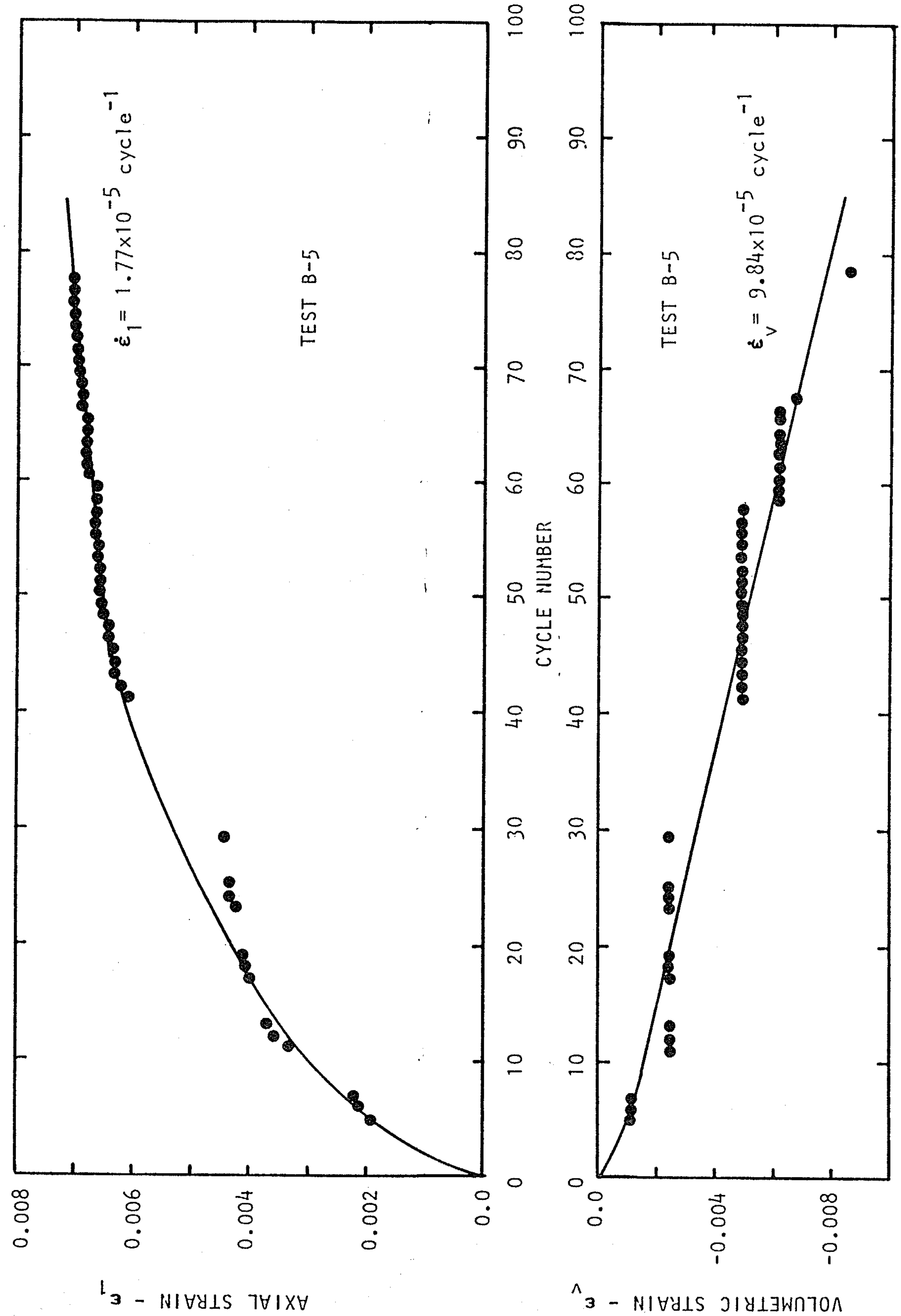

TEST B-5
$\dot{\varepsilon}_1 = 1.77 \times 10^{-5}$ cycle^{-1}
AXIAL STRAIN - ε_1
CYCLE NUMBER
TEST B-5
$\dot{\varepsilon}_v = 9.84 \times 10^{-5}$ cycle^{-1}
VOLUMETRIC STRAIN - ε_v

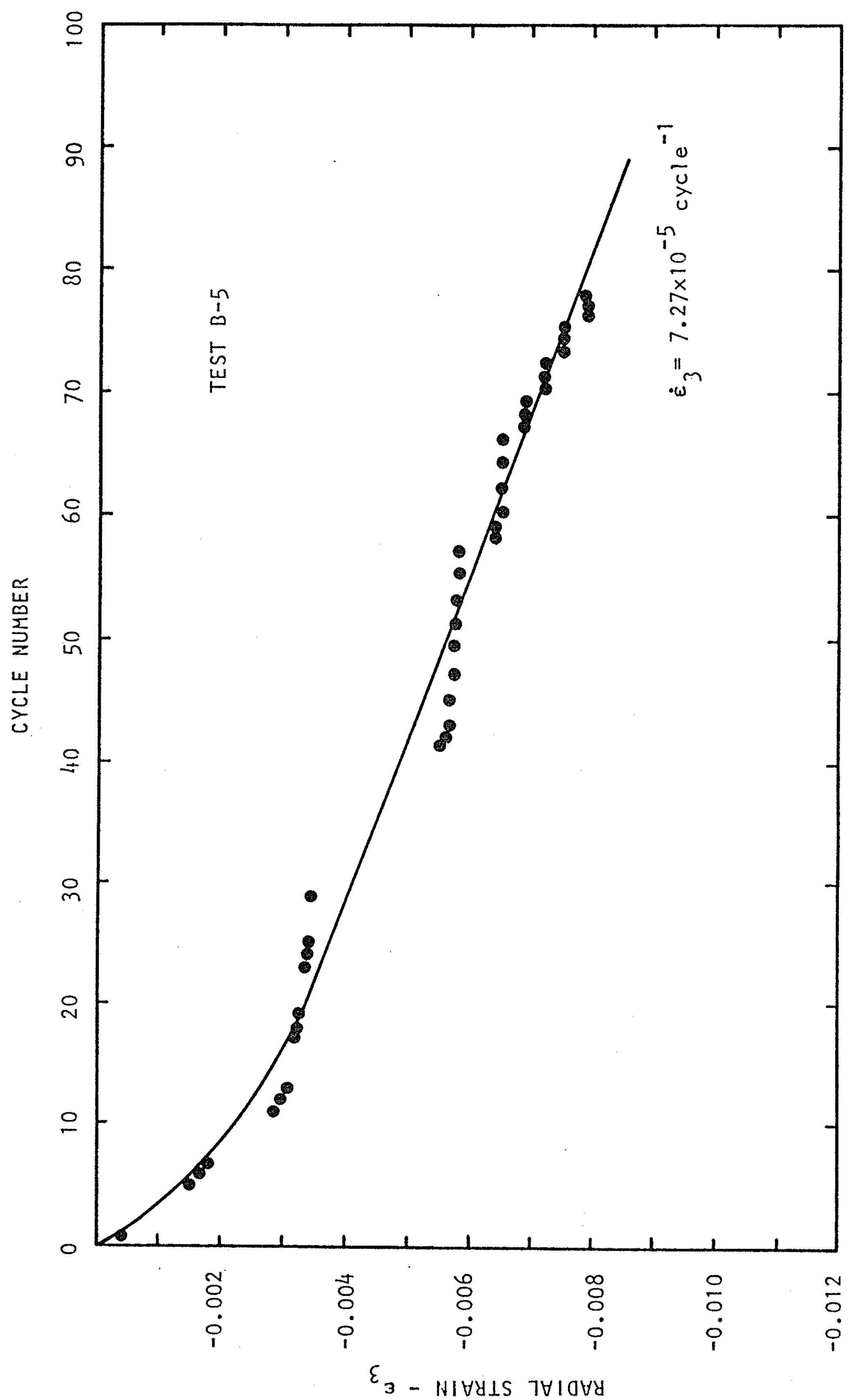
TEST B-5
$\dot{\varepsilon}_3 = 7.27\times10^{-5}$ cycle^{-1}
CYCLE NUMBER
0
10
20
30
40
50
60
70
80
90
100
RADIAL STRAIN - ε_3
-0.002
-0.004
-0.006
-0.008
-0.010
-0.012

TEST : B6 Date Tested : 072085

Sample Length After Consolidation : 7.810 cm σ_1'=62.0kPa
Sample Diameter After Consolidation : 3.615 cm σ_3'=20.7kPa
Sample Area After Consolidation : 10.262 cm^2 Δu=10.5kPa
Sample Volume After Consolidation : 80.142 cm^3
Void Ratio After Consolidation : 0.837
Water Content Before Consolidation : 26.3 % (air dry)
Water Content After DTTCP Test : 30.1 %

End of Cycle	ΔL (cm)	E1 (cm/cm)	ΔV (cc)	Ev (cc/cc)	ΔD (cm)	E3 (cm/cm)
1	.00020	.00003	-0.05	-.00062	-.00118	-.00032
5	.00050	.00006	-0.10	-.00125	-.00237	-.00066
6	.00070	.00009	-0.20	-.00250	-.00467	-.00129
7	.00090	.00011	-0.20	-.00250	-.00472	-.00131
11	.00050	.00006	-0.20	-.00250	-.00462	-.00128
12	.00210	.00027	-0.30	-.00374	-.00725	-.00200
13	.00210	.00027	-0.30	-.00374	-.00725	-.00200
17	.00160	.00021	-0.30	-.00374	-.00713	-.00197
18	.00200	.00026	-0.30	-.00374	-.00722	-.00200
19	.00230	.00029	-0.30	-.00374	-.00729	-.00202
23	.00240	.00031	-0.35	-.00437	-.00944	-.00234
24	.00290	.00037	-0.35	-.00437	-.00856	-.00267
25	.00290	.00037	-0.35	-.00437	-.00856	-.00267
26	.00270	.00035	-0.35	-.00437	-.00851	-.00235
27	.00280	.00036	-0.35	-.00437	-.00854	-.00236
28	.00280	.00036	-0.40	-.00499	-.00966	-.00267
29	.00270	.00035	-0.40	-.00499	-.00964	-.00267
41	.00320	.00041	-0.50	-.00624	-.01200	-.00332
42	.00390	.00050	-0.45	-.00562	-.01100	-.00305
43	.00390	.00050	-0.45	-.00562	-.01100	-.00305
44	.00370	.00047	-0.45	-.00562	-.01100	-.00304
45	.00370	.00047	-0.45	-.00562	-.01100	-.00304
46	.00380	.00049	-0.50	-.00624	-.01210	-.00336
47	.00360	.00046	-0.50	-.00624	-.01210	-.00335
48	.00400	.00051	-0.50	-.00624	-.01220	-.00337
49	.00410	.00052	-0.50	-.00624	-.01220	-.00338
50	.00420	.00054	-0.50	-.00624	-.01224	-.00338
51	.00390	.00050	-0.50	-.00624	-.01220	-.00337
52	.00390	.00050	-0.50	-.00624	-.01220	-.00337
53	.00390	.00050	-0.50	-.00624	-.01220	-.00337
54	.00400	.00051	-0.55	-.00686	-.01331	-.00368
55	.00410	.00052	-0.55	-.00686	-.01334	-.00369
56	.00400	.00051	-0.55	-.00686	-.01331	-.00368
57	.00390	.00050	-0.60	-.00749	-.01444	-.00399
58	.00390	.00050	-0.60	-.00749	-.01444	-.00399
59	.00380	.00049	-0.60	-.00749	-.01439	-.00398
60	.00400	.00051	-0.60	-.00749	-.01444	-.00399

End of Cycle	ΔL (cm)	E1 (cm/cm)	ΔV (cc)	Ev (cc/cc)	ΔD (cm)	E3 (cm/cm)
61	.00390	.00050	-0.60	-.00749	-.01441	-.00399
62	.00380	.00049	-0.60	-.00749	-.01439	-.00398
63	.00320	.00041	-0.60	-.00749	-.01425	-.00394
64	.00370	.00047	-0.60	-.00749	-.01437	-.00398
65	.00400	.00051	-0.60	-.00749	-.01444	-.00399
66	.00430	.00055	-0.60	-.00749	-.01451	-.00401
67	.00450	.00058	-0.60	-.00749	-.01455	-.00403
78	.00420	.00054	-0.70	-.00873	-.01673	-.00463
79	.00540	.00069	-0.70	-.00873	-.01701	-.00471
80	.00500	.00064	-0.70	-.00873	-.01692	-.00468
81	.00500	.00064	-0.70	-.00873	-.01692	-.00468
82	.00520	.00067	-0.70	-.00873	-.01696	-.00469
83	.00530	.00068	-0.70	-.00873	-.01699	-.00470
84	.00590	.00076	-0.70	-.00873	-.01713	-.00474
85	.00590	.00076	-0.70	-.00873	-.01713	-.00474
86	.00580	.00074	-0.70	-.00873	-.01710	-.00473
87	.00580	.00074	-0.70	-.00873	-.01710	-.00473
88	.00580	.00074	-0.70	-.00873	-.01710	-.00473
89	.00600	.00077	-0.70	-.00873	-.01715	-.00474
90	.00640	.00082	-0.70	-.00873	-.01724	-.00477
91	.00700	.00090	-0.70	-.00873	-.01738	-.00481
92	.00680	.00087	-0.70	-.00873	-.01733	-.00480
93	.00670	.00086	-0.70	-.00873	-.01731	-.00479
94	.00680	.00087	-0.70	-.00873	-.01733	-.00480
95	.00690	.00088	-0.70	-.00873	-.01736	-.00480

TEST : B6 Date Tested : 072085

Sample Length After Consolidation : 7.810 cm σ_1 =62.0kPa
Sample Diameter After Consolidation : 3.615 cm σ_3 =20.7kPa
Sample Area After Consolidation : 10.262 cm^2 Δu=10.5kPa
Sample Volume After Consolidation : 80.142 cm^3
Void Ratio After Consolidation : 0.837
Water Content Before Consolidation : 26.3% (air dry)
Water Content After DTTCP Test : 30.1%

Middle Of Cycle	ΔL (cm)	E1 (cm/cm)	ΔV (cc)	Ev (cc/cc)	Δ D (cm)	E3 (cm/cm)
1	-.00160	-.0002	-0.20	-.0025	-.00414	-.00114
6	-.00130	-.0002	-0.30	-.0037	-.00646	-.00179
12	-.00030	-.0000	-0.40	-.0050	-.00890	-.00247
13	.00210	.0027	-0.40	-.0050	-.00950	-.00263
18	.00060	.0001	-0.45	-.0056	-.01030	-.00284
19	.00050	.0001	-0.45	-.0056	-.01030	-.00284
20	.00050	.0001	-0.45	-.0056	-.01030	-.00284
21	.00010	.0000	-0.45	-.0056	-.01020	-.00281
22	.00050	.0001	-0.50	-.0062	-.01140	-.00315
23	.00100	.0001	-0.50	-.0062	-.01150	-.00318
24	.00110	.0001	-0.50	-.0062	-.01152	-.00319
25	.00170	.0002	-0.50	-.0062	-.01170	-.00322
36	.00150	.0002	-0.50	-.0062	-.01161	-.00321
42	.00220	.0003	-0.60	-.0075	-.01400	-.00390
43	.00250	.0003	-0.60	-.0075	-.01410	-.00390
44	.00220	.0003	-0.60	-.0075	-.01410	-.00390
45	.00200	.0003	-0.60	-.0075	-.01400	-.00387
46	.00190	.0002	-0.60	-.0075	-.01390	-.00386
47	.00210	.0003	-0.60	-.0075	-.01400	-.00387
48	.00250	.0003	-0.60	-.0075	-.01410	-.00390
49	.00280	.0004	-0.60	-.0075	-.01420	-.00392
50	.00240	.0003	-0.60	-.0075	-.01410	-.00389
51	.00250	.0003	-0.60	-.0075	-.01410	-.00390
52	.00270	.0003	-0.60	-.0075	-.01413	-.00391
53	.00270	.0003	-0.60	-.0075	-.01413	-.00391
54	.00250	.0003	-0.60	-.0075	-.01410	-.00390
55	.00310	.0004	-0.60	-.0075	-.01423	-.00394
56	.00260	.0003	-0.60	-.0075	-.01411	-.00390
57	.00250	.0003	-0.60	-.0075	-.01410	-.00390
58	.00240	.0003	-0.60	-.0075	-.01410	-.00389
59	.00180	.0002	-0.70	-.0087	-.01617	-.00447
60	.00240	.0003	-0.70	-.0087	-.01631	-.00451
61	.00270	.0003	-0.70	-.0087	-.01638	-.00453
62	.00250	.0003	-0.70	-.0087	-.01633	-.00452
63	.00270	.0003	-0.70	-.0087	-.01638	-.00453
64	.00300	.0004	-0.70	-.0087	-.01645	-.00455

TEST : B6 (cont'd)

Middle of Cycle	ΔL (cm)	E1 (cm/cm)	ΔV (cc)	Ev (cc/cc)	ΔD (cm)	E3 (cm/cm)
66	.00250	.0003	-0.75	-.0094	-.01746	-.00483
67	.00350	.0004	-0.75	-.0094	-.01764	-.00488
68	.00380	.0005	-0.75	-.0094	-.01776	-.00491
69	.00320	.0004	-0.75	-.0094	-.01762	-.00488
70	.00320	.0004	-0.75	-.0094	-.01764	-.00488
71	.00320	.0004	-0.80	-.0100	-.01874	-.00519
72	.00320	.0004	-0.80	-.0100	-.01874	-.00519
73	.00300	.0004	-0.80	-.0100	-.01870	-.00517
74	.00350	.0004	-0.80	-.0100	-.01881	-.00520
75	.00330	.0004	-0.80	-.0100	-.01877	-.00519
76	.00340	.0004	-0.80	-.0100	-.01879	-.00520
77	.00370	.0005	-0.80	-.0100	-.01886	-.00522
78	.00380	.0005	-0.80	-.0100	-.01888	-.00522
79	.00300	.0005	-0.80	-.0100	-.01888	-.00522
80	.00410	.0005	-0.80	-.0100	-.01900	-.00524
81	.00380	.0005	-0.80	-.0100	-.01888	-.00522
82	.00370	.0005	-0.85	-.0106	-.02000	-.00553
83	.00380	.0005	-0.85	-.0106	-.02000	-.00553
84	.00440	.0006	-0.85	-.0106	-.02014	-.00557
85	.00460	.0006	-0.85	-.0106	-.02019	-.00559
86	.00460	.0006	-0.85	-.0106	-.02019	-.00559
87	.00450	.0006	-0.90	-.0112	-.02130	-.00589
88	.00470	.0006	-0.90	-.0112	-.02134	-.00590
89	.00470	.0006	-0.90	-.0112	-.02134	-.00590
90	.00490	.0006	-0.90	-.0112	-.02138	-.00519

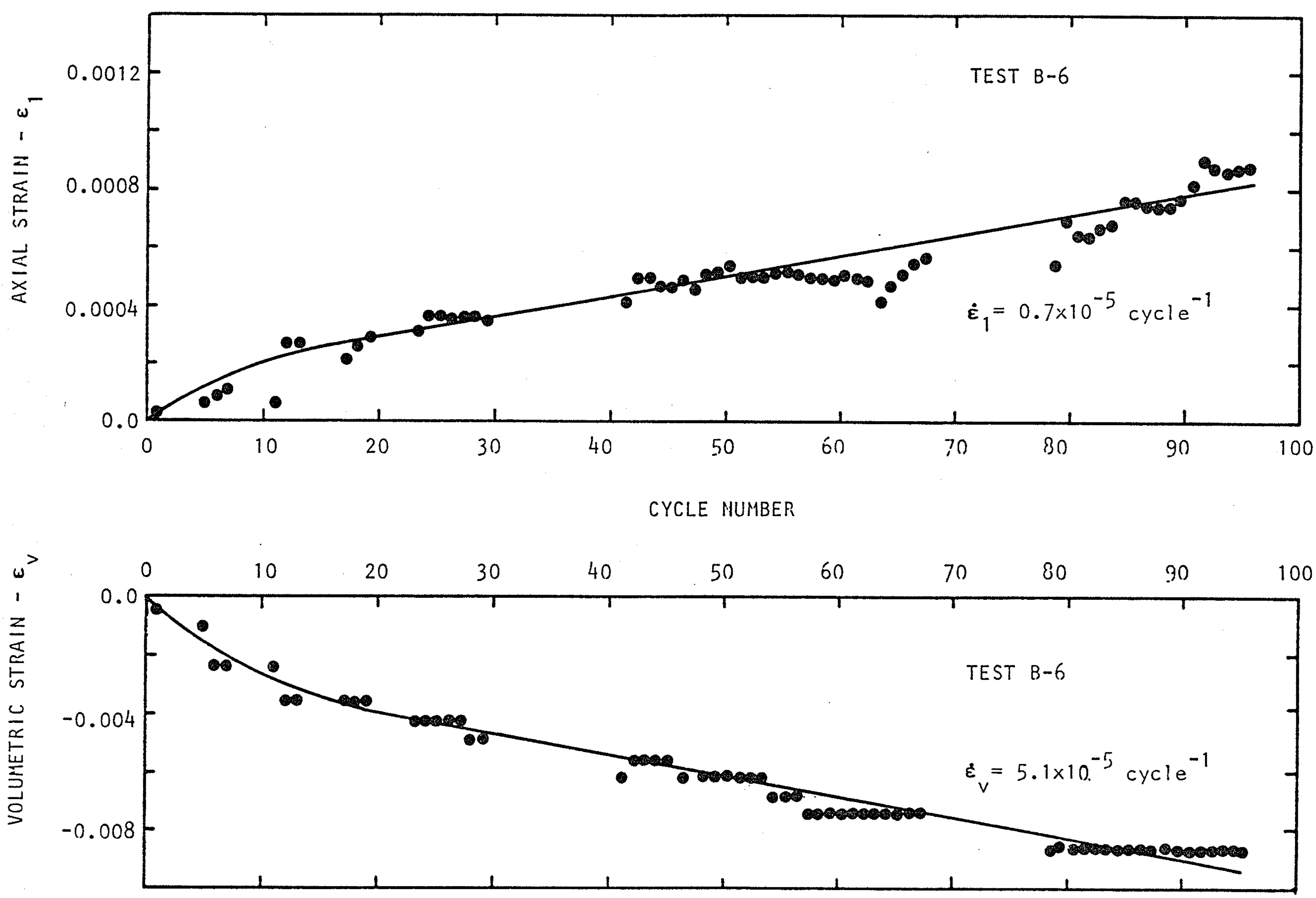

TEST B-6
$\dot{\varepsilon}_1 = 0.7 \times 10^{-5}$ cycle^{-1}
AXIAL STRAIN - ε_1
0.0012
0.0008
0.0004
0.0
0
10
20
30
40
50
60
70
80
90
100
CYCLE NUMBER
TEST B-6
$\dot{\varepsilon}_v = 5.1 \times 10^{-5}$ cycle^{-1}
VOLUMETRIC STRAIN - ε_v
0.0
-0.004
-0.008

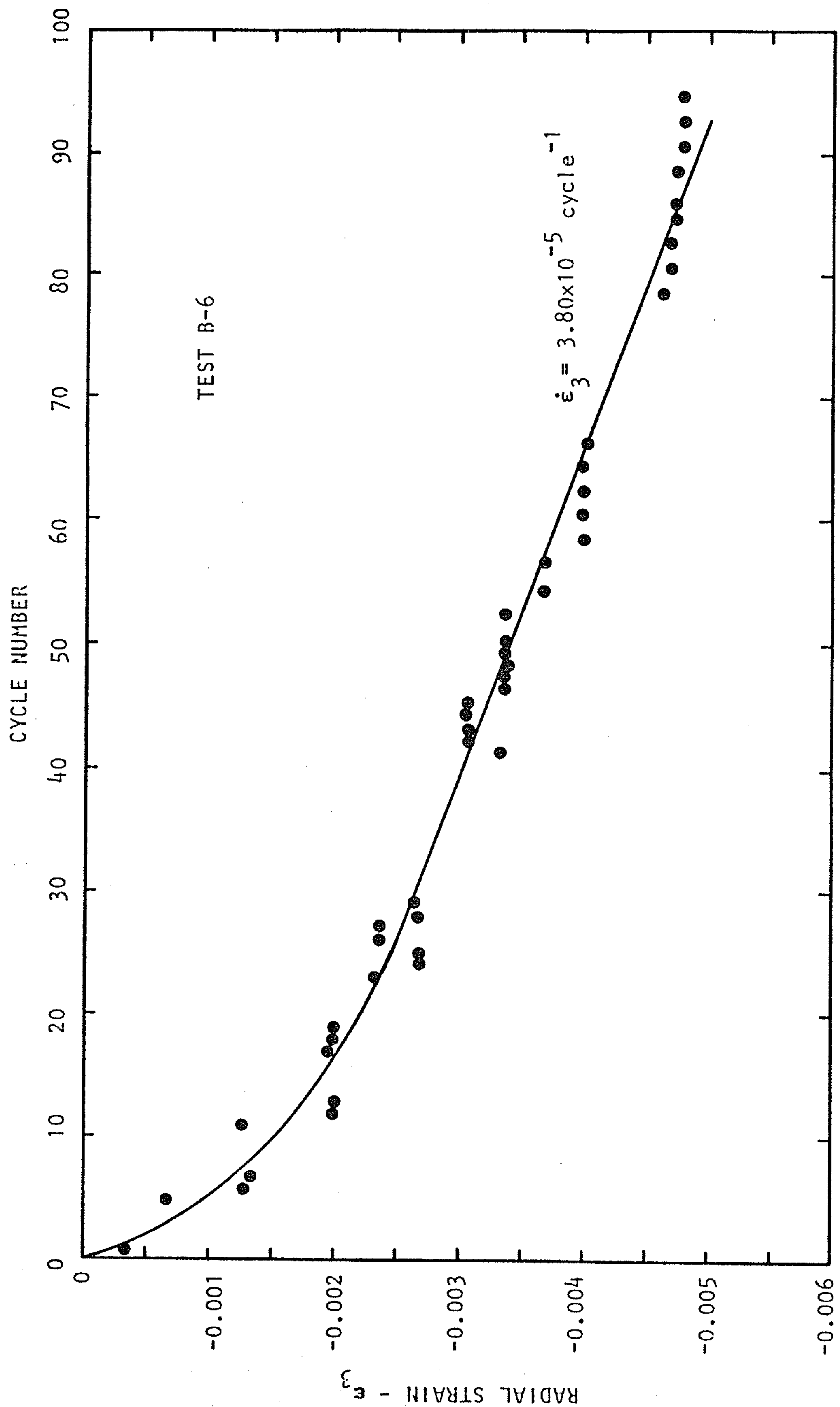

TEST B-6
$\dot{\varepsilon}_3 = 3.80\times10^{-5}$ cycle^{-1}
CYCLE NUMBER
0
10
20
30
40
50
60
70
80
90
100
RADIAL STRAIN - ε_3
0
-0.001
-0.002
-0.003
-0.004
-0.005
-0.006

TEST : B7 Date Tested : 080985

Sample Length After Consolidation : 7.598 cm σ_1' =52.2kPa
Sample Diameter After Consolidation: 3.558 cm σ_3' =26.0kPa
Sample Area After Consolidation : 9.943 cm^2 Δu=16.6kPa
Sample Volume After Consolidation : 75.547 cm^3
Void Ratio After Consolidation : 0.813
Water Content Before Consolidation : 27.7%
Water Content After DTTCP Test : 33.2%

End Of Cycle	ΔL (cm)	E1 (cm/cm)	ΔV (cc)	Ev (cc/cc)	ΔD (cm)	E3 (cm/cm)
1	.00040	.00005	0	0	-.00006	-.00002
2	.00070	.00009	0	0	-.00013	-.00004
6	.00080	.00011	-0.10	-.0013	-.00251	-.00070
7	.00020	.00003	-0.10	-.0013	-.00237	-.00067
12	.00120	.00016	-0.30	-.0040	-.00730	-.00205
13	.00110	.00014	-0.30	-.0040	-.00728	-.00205
14	.00110	.00014	-0.30	-.0040	-.00728	-.00205
18	.00140	.00018	-0.40	-.0053	-.00970	-.00273
19	.00150	.00020	-0.40	-.0053	-.00972	-.00273
20	.00210	.00028	-0.40	-.0053	-.00986	-.00277
24	.00140	.00018	-0.50	-.0066	-.01205	-.00339
25	.00180	.00237	-0.50	-.0066	-.01214	-.00341
26	.00170	.00022	-0.50	-.0066	-.01212	-.00341
27	.00140	.00018	-0.50	-.0066	-.01205	-.00339
28	.00130	.00017	-0.50	-.0066	-.01202	-.00338
29	.00140	.00018	-0.50	-.0066	-.01205	-.00339
30	.00140	.00018	-0.50	-.0066	-.01205	-.00339
31	.00140	.00018	-0.50	-.0066	-.01205	-.00339
32	.00150	.00020	-0.50	-.0066	-.01207	-.00339
33	.00140	.00018	-0.50	-.0066	-.01205	-.00339
34	.00160	.00021	-0.50	-.0066	-.01220	-.00340
35	.00180	.00024	-0.50	-.0066	-.01214	-.00341
36	.00180	.00024	-0.50	-.0066	-.01214	-.00341
37	.00180	.00024	-0.50	-.0066	-.01214	-.00341
38	.00280	.00037	-0.50	-.0066	-.01238	-.00348
39	.00270	.00036	-0.50	-.0066	-.01235	-.00347
40	.00290	.00038	-0.50	-.0066	-.01240	-.00349
41	.00300	.00040	-0.50	-.0066	-.01242	-.00349
42	.00290	.00038	-0.50	-.0066	-.01240	-.00349
43	.00400	.00053	-0.50	-.0066	-.01266	-.00356
44	.00350	.00046	-0.50	-.0066	-.01254	-.00353
45	.00360	.00047	-0.50	-.0066	-.01257	-.00353
46	.00360	.00047	-0.50	-.0066	-.01257	-.00353
47	.00390	.00051	-0.50	-.0066	-.01264	-.00355
48	.00440	.00058	-0.50	-.0066	-.01275	-.00358
49	.00460	.00061	-0.50	-.0066	-.01280	-.00360
50	.00450	.00059	-0.50	-.0066	-.01278	-.00359

TEST :B7 (cont'd)

End of Cycle	Δ L (cm)	E1 (cm/cm)	Δ V (cc)	Ev (cc/cc)	Δ D (cm)	E3 (cm/cm)
51	.00450	.00059	-0.50	-.0066	-.01278	-.00359
52	.00440	.00058	-0.50	-.0066	-.01275	-.00358
53	.00430	.00057	-0.50	-.0066	-.01273	-.00358
54	.00430	.00057	-0.50	-.0066	-.01273	-.00358
56	.00530	.00070	-0.60	-.0079	-.01531	-.00430
57	.00530	.00070	-0.60	-.0079	-.01531	-.00430
58	.00530	.00070	-0.60	-.0079	-.01531	-.00430
59	.00530	.00070	-0.60	-.0079	-.01531	-.00430
60	.00520	.00070	-0.60	-.0079	-.01529	-.00430
61	.00560	.00074	-0.60	-.0079	-.01538	-.00432
62	.00620	.00082	-0.60	-.0079	-.01552	-.00436
63	.00660	.00087	-0.60	-.0079	-.01562	-.00439
64	.00710	.00093	-0.60	-.0079	-.01574	-.00442
67	.00680	.00090	-0.60	-.0079	-.01566	-.00440
68	.00720	.00095	-0.60	-.0079	-.01576	-.00443
69	.00780	.00103	-0.60	-.0079	-.01590	-.00447
70	.00800	.00105	-0.60	-.0079	-.01595	-.00448
74	.00900	.00119	-0.60	-.0086	-.01736	-.00489
76	.00740	.00100	-0.70	-.0093	-.01915	-.00510
81	.00680	.00100	-0.75	-.0099	-.01918	-.00539
83	.00690	.00091	-0.80	-.0106	-.02038	-.00573
86	.00680	.00100	-0.80	-.0106	-.02036	-.00572
90	.00730	.00100	-0.80	-.0106	-.02047	-.00574
92	.00750	.00100	-0.85	-.0113	-.02169	-.00610
96	.00730	.00100	-0.90	-.0119	-.02282	-.00641

TEST : B7 Date Tested : 080985

Sample Length After Consolidation : 7.598 cm σ_1 =52.2kPa
Sample Diameter After Consolidation : 3.558 cm σ_3 =26.0kPa
Sample Area After Consolidation : 9.943 cm^2 Δu=16.6kPa
Sample Volume After Consolidation : 75.547 cm^3
Void Ratio After Consolidation : 0.813
Water Content Before Consolidation : 27.7%
Water Content After DTTCP Test : 33.2%

Middle of Cycle	ΔL (cm)	E1 (cm/cm)	ΔV (cc)	Ev (cc/cc)	Δ D (cm)	E3 (cm/cm)
1	-.00230	-.0003	-0.30	-.0040	-.00648	-.00182
2	-.00220	-.0003	-0.30	-.0040	-.00651	-.00183
3	-.00200	-.0003	-0.30	-.0040	-.00655	-.00184
4	-.00210	-.0003	-0.30	-.0040	-.00653	-.00184
5	-.00340	-.0004	-0.30	-.0040	-.00622	-.00175
6	-.00230	-.0003	-0.35	-.0050	-.00766	-.00215
7	-.00160	-.0002	-0.35	-.0050	-.00782	-.00220
8	-.00230	-.0003	-0.35	-.0050	-.00766	-.00215
13	-.00270	-.0004	-0.55	-.0070	-.01226	-.00344
14	-.00280	-.0004	-0.65	-.0090	-.01458	-.00410
15	-.00270	-.0004	-0.65	-.0090	-.01458	-.00410
16	-.00210	-.0003	-0.65	-.0090	-.01474	-.00414
17	-.00230	-.0003	-0.65	-.0090	-.01470	-.00413
18	-.00230	-.0003	-0.65	-.0090	-.01470	-.00413
19	-.00210	-.0003	-0.65	-.0090	-.01477	-.00415
20	-.00140	-.0002	-0.70	-.0090	-.01608	-.00452
21	-.00140	-.0002	-0.70	-.0090	-.01608	-.00452
22	-.00140	-.0002	-0.70	-.0090	-.01608	-.00452
23	-.00130	-.0002	-0.70	-.0090	-.01610	-.00453
24	-.00120	-.0002	-0.70	-.0090	-.01613	-.00453
25	-.00130	-.0002	-0.70	-.0090	-.01610	-.00453
26	-.00130	-.0002	-0.75	-.0100	-.01728	-.00486
27	-.00150	-.0002	-0.75	-.0100	-.01723	-.00484
28	-.00180	-.0002	-0.75	-.0100	-.01716	-.00482
29	-.00140	-.0002	-0.75	-.0100	-.01725	-.00485
30	-.00140	-.0002	-0.75	-.0100	-.01725	-.00485
31	-.00160	-.0002	-0.75	-.0100	-.01721	-.00484
32	-.00190	-.0002	-0.75	-.0100	-.01735	-.00482
33	-.00130	-.0002	-0.75	-.0100	-.01728	-.00486
34	-.00110	-.0001	-0.75	-.0100	-.01732	-.00487
35	-.00100	-.0001	-0.75	-.0100	-.01735	-.00488
36	-.00080	-.0001	-0.75	-.0100	-.01739	-.00489
37	-.00080	-.0001	-0.75	-.0100	-.01739	-.00488
38	-.00010	-.0000	-0.75	-.0100	-.01756	-.00494
39	.00060	.0001	-0.75	-.0100	-.01772	-.00498
40	.00070	.0001	-0.75	-.0100	-.01775	-.00499
41	.00090	.0001	-0.75	-.0100	-.01779	-.00500

Middle of Cycle	ΔL (cm)	E1 (cm/cm)	ΔV (cc)	Ev (cc/cc)	Δ D (cm)	E3 (cm/cm)
42	.00080	.0001	-0.75	-.0100	-.01777	-.00499
43	.00130	.0002	-0.75	-.0100	-.01800	-.00503
44	.00220	.0003	-0.75	-.0100	-.01810	-.00509
45	.00180	.0002	-0.75	-.0100	-.01801	-.00506
46	.00200	.0003	-0.75	-.0100	-.01805	-.00507
47	.00200	.0003	-0.75	-.0100	-.01805	-.00507
48	.00210	.0003	-0.75	-.0100	-.01808	-.00508
49	.00260	.0003	-0.75	-.0100	-.01819	-.00511
50	.00260	.0003	-0.75	-.0100	-.01819	-.00511
51	.00260	.0003	-0.75	-.0100	-.01819	-.00511
52	.00250	.0003	-0.75	-.0100	-.01817	-.00511
53	.00250	.0003	-0.75	-.0100	-.01817	-.00511
54	.00230	.0003	-0.75	-.0100	-.01812	-.00509
55	.00230	.0003	-0.75	-.0100	-.01812	-.00509
56	.00220	.0003	-0.80	-.0110	-.01927	-.00542
57	.00220	.0003	-0.80	-.0110	-.01927	-.00542
58	.00290	.0004	-0.80	-.0110	-.01944	-.00546
59	.00280	.0004	-0.80	-.0110	-.01941	-.00546
60	.00270	.0004	-0.85	-.0110	-.02056	-.00579
61	.00270	.0004	-0.85	-.0110	-.02056	-.00579
62	.00370	.0005	-0.85	-.0110	-.02080	-.00584
63	.00450	.0006	-0.85	-.0110	-.02099	-.00590
64	.00400	.0005	-0.85	-.0110	-.02090	-.00586
67	.00510	.0007	-0.85	-.0110	-.02112	-.00594
68	.00520	.0007	-0.85	-.0110	-.02115	-.00594
69	.00460	.0006	-0.85	-.0110	-.02101	-.00590
70	.00350	.0005	-0.85	-.0110	-.02075	-.00583
79	.00260	.0003	-1.05	-.0140	-.02522	-.00709
92	.00210	.0003	-1.15	-.0150	-.02751	-.00773

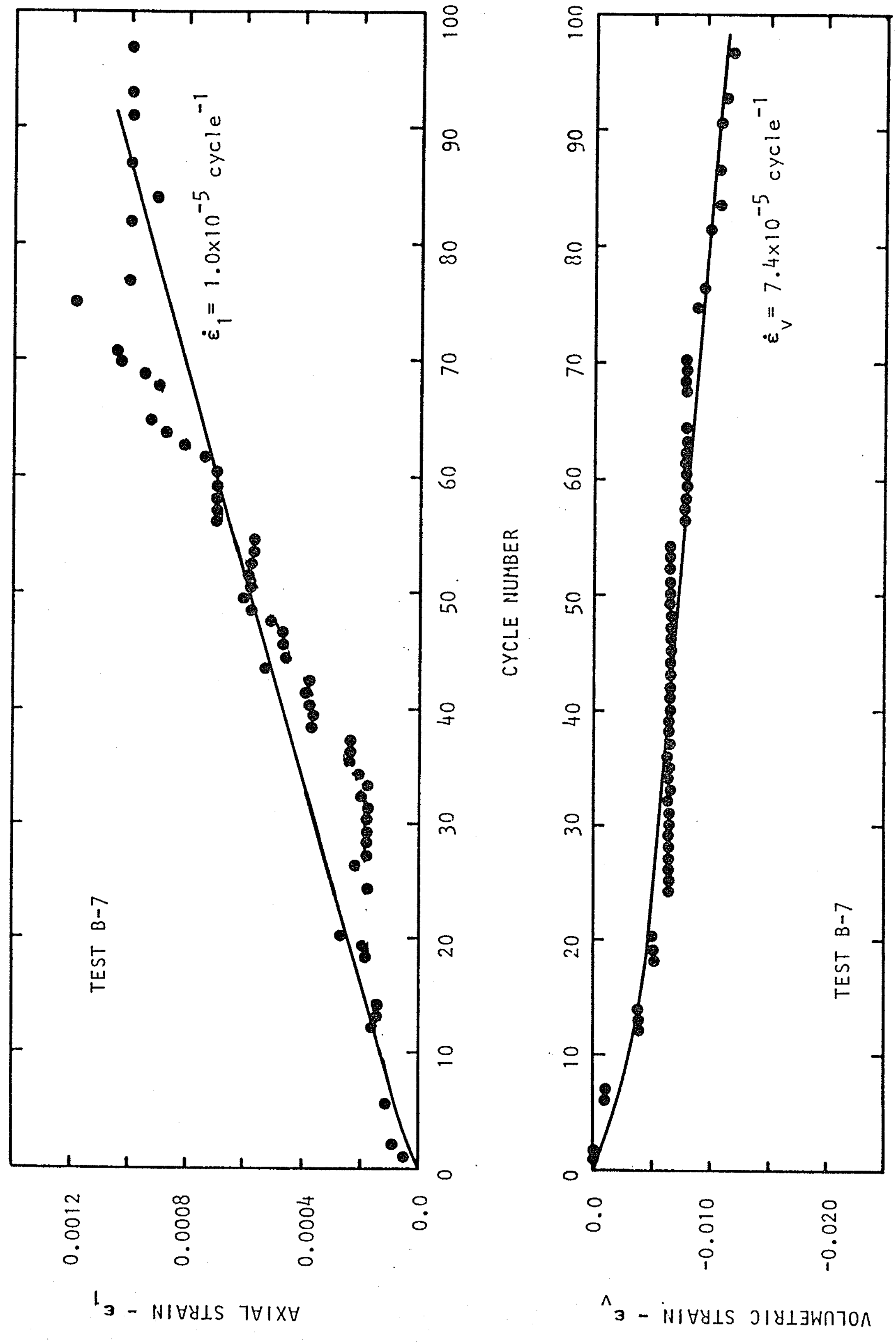

TEST B-7
$\dot{\varepsilon}_1 = 1.0 \times 10^{-5}$ cycle^{-1}
AXIAL STRAIN - ε_1
0.0012
0.0008
0.0004
0.0
CYCLE NUMBER
0
10
20
30
40
50
60
70
80
90
100
TEST B-7
$\dot{\varepsilon}_v = 7.4 \times 10^{-5}$ cycle^{-1}
VOLUMETRIC STRAIN - ε_v
0.0
-0.010
-0.020

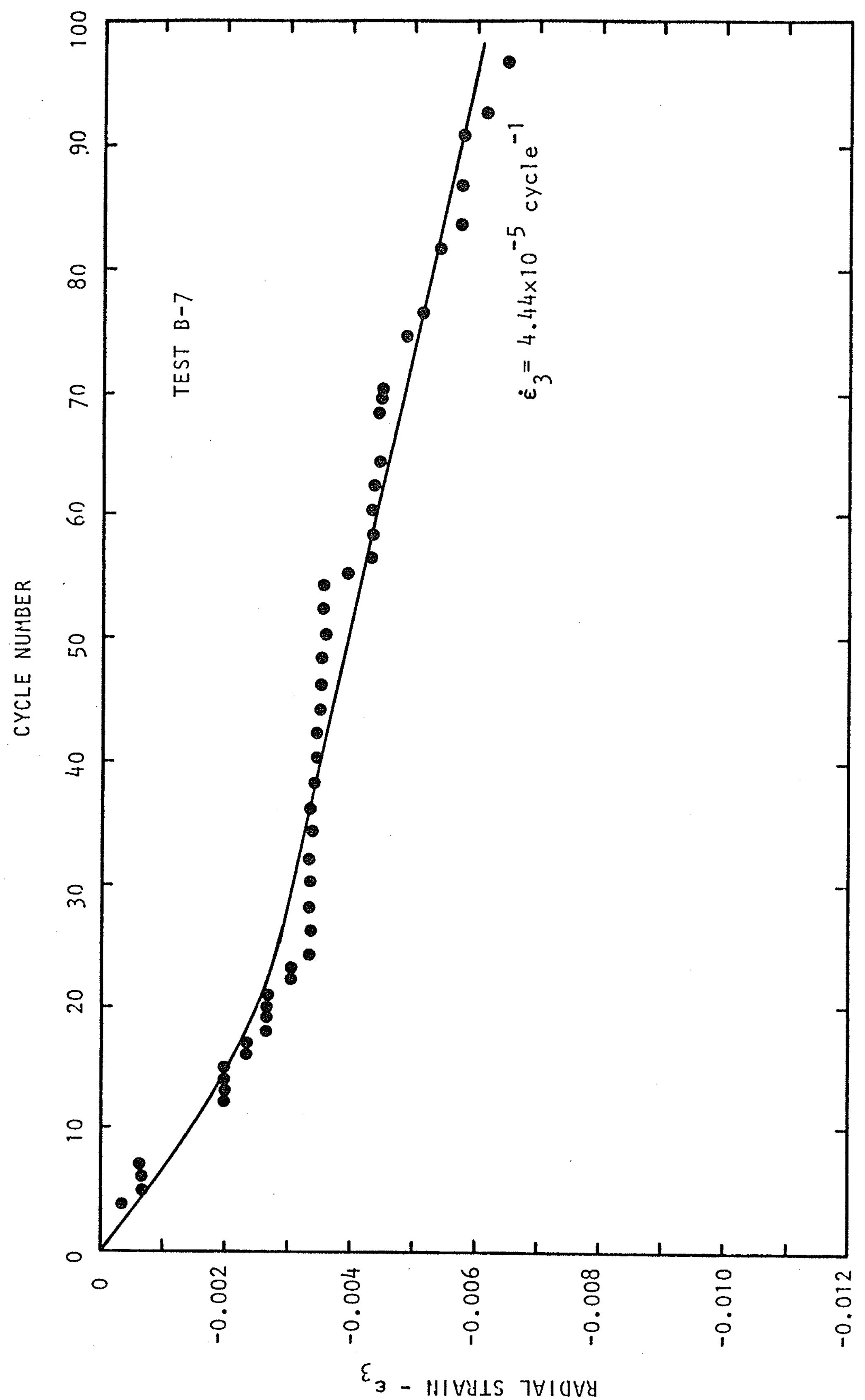
CYCLE NUMBER
RADIAL STRAIN - ε_3
TEST B-7
$\dot{\varepsilon}_3 = 4.44 \times 10^{-5}$ cycle^{-1}
0
10
20
30
40
50
60
70
80
90
100
0
-0.002
-0.004
-0.006
-0.008
-0.010
-0.012

TEST :B8 Date Tested : 080985

Sample Length After Consolidation : 7.462 cm σ_1=59.2kPa
Sample Diameter After Consolidation: 3.603 cm σ_3=16.8kPa
Sample Area After Consolidation : 10.193 cm^2 Δu=16.7kPa
Sample Volume After Consolidation : 76.059 cm^3
Void Ratio After Consolidation : 0.810
Water Content Before Consolidation : 29.5%
Water Content After DTTCP Test : 30.0%

End Of Cycle	ΔL (cm)	E1 (cm/cm)	ΔV (cc)	Ev (cc/cc)	ΔD (cm)	E3 (cm/cm)
1	.01180	.00158	0	-.0013	-.00283	-.00080
2	.02350	.00315	-0.10	-.0013	-.00904	-.00223
6	.08020	.01075	-0.30	-.0039	-.02660	-.00739
7	.10390	.01392	-0.30	-.0039	-.03248	-.00902
8	.12310	.01650	-0.40	-.0053	-.03961	-.01100
12	.46330	.06210	-1.10	-.0145	-.01441	-.04000
13	.57880	.07760	-1.40	-.0184	-.01828	-.05070

TEST : B8 Date Tested : 080985

Sample Length After Consolidation : 7.462 cm σ_1=59.2kPa
Sample Diameter After Consolidation : 3.603 cm σ_3=16.8kPa
Sample Area After Consolidation : 10.193 cm^2 Δu=16.7kPa
Sample Volume After Consolidation : 76.059 cm^3
Void Ratio After Consolidation : 0.810
Water Content Before Consolidation : 29.5%
Water Content After DTTCP Test : 30.0%

Middle Of Cycle	ΔL (cm)	E1 (cm/cm)	ΔV (cc)	Ev (cc/cc)	ΔD (cm)	E3 (cm/cm)
1	.00610	.0008	-0.50	-.0070	-.01330	-.00369
2	.01770	.0024	-0.70	-.0090	-.02080	-.00578
7	.09880	.0132	-0.85	-.0110	-.04430	-.01229
8	.11370	.0152	-1.10	-.0140	-.05390	-.01496
13	.54560	.0731	-3.50	-.0460	-.22450	-.06230

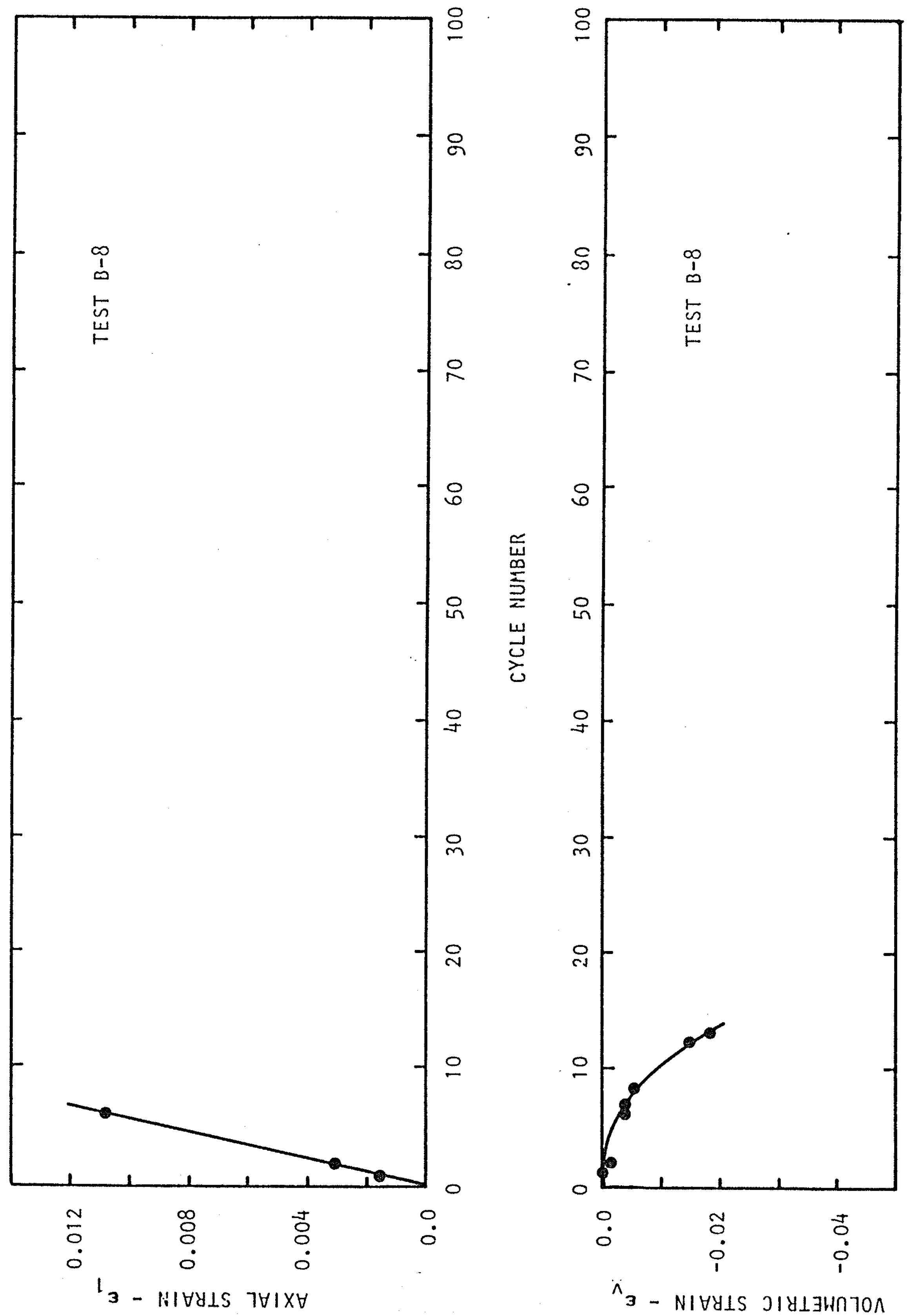

TEST B-8
AXIAL STRAIN - ε1
0.012
0.008
0.004
0.0
CYCLE NUMBER
0
10
20
30
40
50
60
70
80
90
100
TEST B-8
VOLUMETRIC STRAIN - εv
0.0
-0.02
-0.04

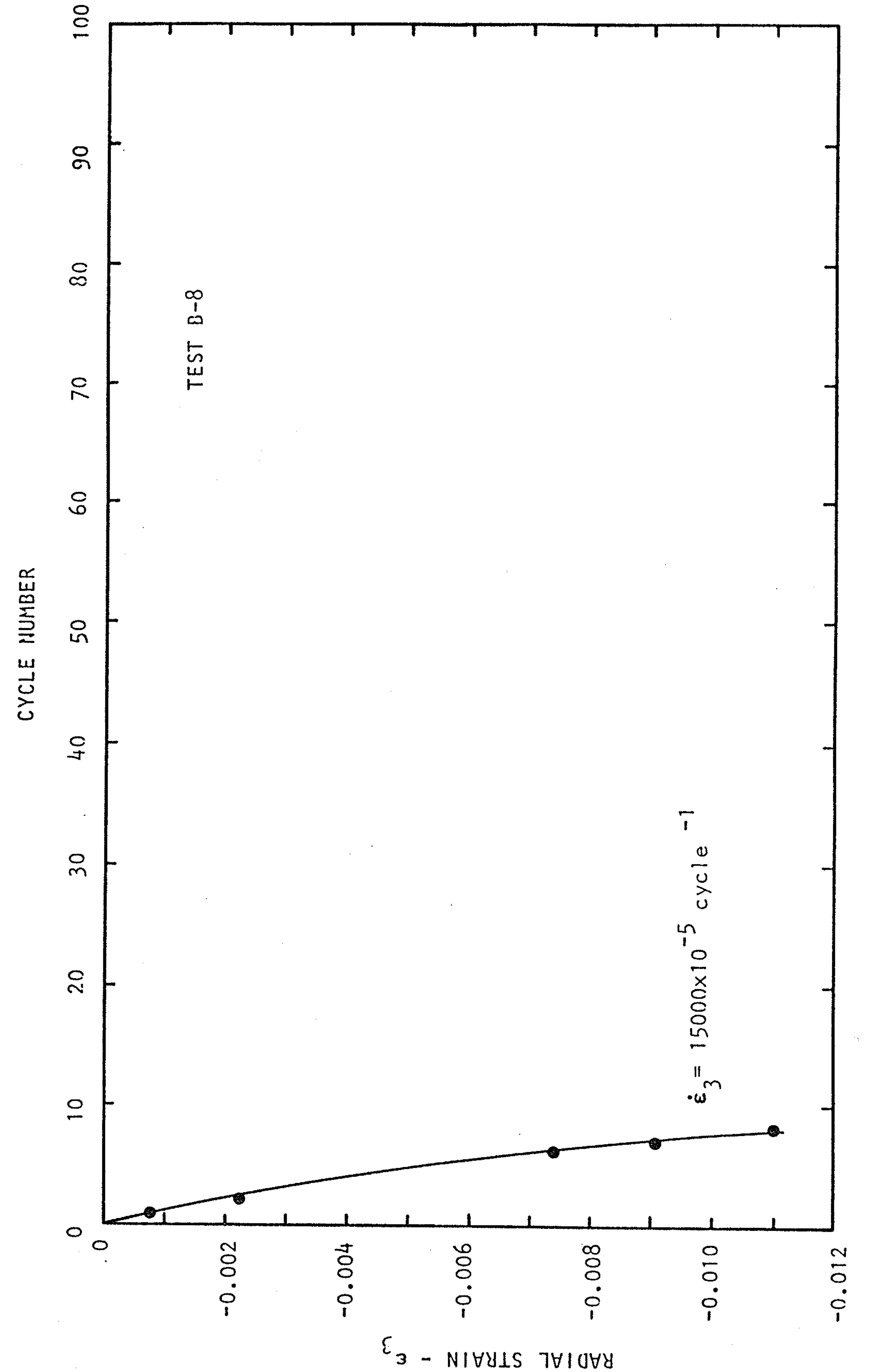
CYCLE NUMBER
RADIAL STRAIN - ε_3
TEST B-8
$\dot{\varepsilon}_3 = 15000 \times 10^{-5}$ cycle^{-1}
0
10
20
30
40
50
60
70
80
90
100
0
-0.002
-0.004
-0.006
-0.008
-0.010
-0.012

TEST :B9 Date Tested : 081485

Sample Length After Consolidation : 7.957 cm σ_1'=30.4kPa
Sample Diameter After Consolidation : 3.563 cm σ_3'=18.3kPa
Sample Area After Consolidation : 9.970 cm^2 Δu=16.7kPa
Sample Volume After Consolidation : 79.338 cm^3
Void Ratio After Consolidation : 0.806
Water Content Before Consolidation : 29.9%
Water Content After DTTCP Test : 32.3%

End Of Cycle	ΔL (cm)	E1 (cm/cm)	ΔV (cc)	Ev (cc/cc)	ΔD (cm)	E3 (cm/cm)
4	.00440	.00055	-0.05	-.0006	-.00211	-.00099
5	.00560	.00070	-0.05	-.0006	-.00238	-.00067
6	.00590	.00074	-0.10	-.0013	-.00357	-.00100
11	.00730	.00092	-0.15	-.0019	-.00501	-.00141
17	.00300	.00101	-0.20	-.0025	-.00629	-.00176
18	.00830	.00104	-0.20	-.0025	-.00635	-.00178
19	.00850	.00107	-0.20	-.0025	-.00640	-.00180
20	.00850	.00107	-0.20	-.0025	-.00640	-.00180
21	.00870	.00109	-0.20	-.0025	-.00644	-.00181
22	.00860	.00108	-0.20	-.0025	-.00642	-.00180
28	.00910	.00114	-0.25	-.0032	-.00765	-.00215
29	.00880	.00111	-0.30	-.0038	-.00871	-.00244
30	.00890	.00112	-0.30	-.0038	-.00873	-.00245
31	.00860	.00108	-0.30	-.0038	-.00866	-.00243
32	.00850	.00107	-0.30	-.0038	-.00864	-.00243
33	.00870	.00109	-0.30	-.0038	-.00869	-.00244
34	.00880	.00111	-0.30	-.0038	-.00871	-.00244
35	.00890	.00111	-0.30	-.0038	-.00873	-.00245
36	.00890	.00112	-0.30	-.0038	-.00873	-.00245
37	.00890	.00112	-0.30	-.0038	-.00875	-.00245
38	.00900	.00113	-0.30	-.0038	-.00875	-.00246
39	.00910	.00114	-0.30	-.0038	-.00878	-.00246
40	.00920	.00116	-0.30	-.0038	-.00880	-.00247
41	.00950	.00119	-0.31	-.0039	-.00909	-.00255
42	.00990	.00124	-0.31	-.0039	-.00918	-.00258
43	.00990	.00124	-0.31	-.0039	-.00918	-.00258
44	.01010	.00127	-0.31	-.0039	-.00923	-.00259
45	.01010	.00127	-0.31	-.0039	-.00923	-.00259
46	.01030	.00129	-0.31	-.0039	-.00927	-.00260
47	.01030	.00129	-0.31	-.0039	-.00927	-.00261
48	.01050	.00152	-0.31	-.0039	-.00932	-.00261
49	.01020	.00128	-0.31	-.0039	-.00925	-.00260
50	.01010	.00127	-0.31	-.0039	-.00923	-.00259
51	.01020	.00128	-0.31	-.0039	-.00925	-.00259
52	.01030	.00129	-0.31	-.0039	-.00927	-.00261
59	.01010	.00128	-0.40	-.0050	-.01124	-.00355

TEST :B9 (cont'd)

End of Cycle	ΔL (cm)	E1 (cm/cm)	ΔV (cc)	Ev (cc/cc)	Δ D (cm)	E3 (cm/cm)
61	.01000	.00126	−0.40	−.0050	−.01122	−.00315
62	.01030	.00129	−0.40	−.0050	−.01129	−.00317
64	.01030	.00129	−0.45	−.0057	−.01241	−.00348
67	.01020	.00128	−0.40	−.0050	−.01127	−.00316
68	.01020	.00127	−0.40	−.0050	−.01124	−.00316
70	.01000	.00126	−0.40	−.0050	−.01122	−.00315

TEST : B9 Date Tested : 081485

Sample Length After Consolidation : 7.957 cm σ'_1 =30.4kPa
Sample Diameter After Consolidation : 3.563 cm σ'_3 =18.3kPa
Sample Area After Consolidation : 9.970 cm^2 Δu=16.7kPa
Sample Volume After Consolidation : 79.338 cm^3
Void Ratio After Consolidation : 0.086
Water Content Before Consolidation : 29.9%
Water Content After DTTCP Test : 32.3%

Middle Of Cycle	ΔL (cm)	E1 (cm/cm)	ΔV (cc)	Ev (cc/cc)	ΔD (cm)	E3 (cm/cm)
1	-.00980	-.0012	-0.60	-.0080	-.01125	-.00316
2	-.00810	-.0010	-0.60	-.0080	-.01163	-.00327
3	-.00730	-.0009	-0.60	-.0080	-.01191	-.00332
4	-.00680	-.0008	-0.65	-.0080	-.01309	-.00367
5	-.00620	-.0008	-0.65	-.0080	-.01318	-.00370
6	-.00600	-.0008	-0.65	-.0080	-.01322	-.00371
7	-.00500	-.0006	-0.65	-.0080	-.01345	-.00377
8	-.00400	-.0006	-0.65	-.0080	-.01351	-.00379
9	-.00440	-.0006	-0.70	-.0090	-.01470	-.00412
10	-.00410	-.0005	-0.70	-.0090	-.01476	-.00414
11	-.00380	-.0005	-0.70	-.0090	-.01482	-.00416
12	-.00410	-.0005	-0.70	-.0090	-.01476	-.00414
13	-.00310	-.0004	-0.70	-.0090	-.01499	-.00421
14	-.00290	-.0004	-0.70	-.0090	-.01503	-.00422
15	-.00290	-.0004	-0.70	-.0090	-.01503	-.00422
16	-.00270	-.0003	-0.75	-.0090	-.01620	-.00455
17	-.00250	-.0003	-0.75	-.0090	-.01624	-.00456
18	-.00240	-.0003	-0.75	-.0090	-.01626	-.00457
19	-.00220	-.0003	-0.80	-.0100	-.01743	-.00489
20	-.00200	-.0002	-0.80	-.0100	-.01747	-.00490
21	-.00210	-.0002	-0.80	-.0100	-.01747	-.00490
22	-.00190	-.0002	-0.80	-.0100	-.01749	-.00491
23	-.00320	-.0004	-0.80	-.0100	-.01720	-.00483
24	-.00210	-.0003	-0.80	-.0100	-.01745	-.00490
25	-.00270	-.0003	-0.80	-.0100	-.01731	-.00486
26	-.00250	-.0003	-0.85	-.0110	-.01848	-.00519
27	-.00240	-.0003	-0.85	-.0110	-.01850	-.00519
28	-.00240	-.0003	-0.85	-.0110	-.01850	-.00519
29	-.00250	-.0003	-0.90	-.0110	-.01959	-.00550
30	-.00280	-.0004	-0.90	-.0110	-.01952	-.00548
31	-.00280	-.0004	-0.90	-.0110	-.01952	-.00548
32	-.00270	-.0003	-0.90	-.0110	-.01955	-.00549
33	-.00270	-.0003	-0.95	-.0120	-.02066	-.00580
34	-.00270	-.0003	-0.95	-.0120	-.02066	-.00580
35	-.00280	-.0004	-1.00	-.0130	-.02176	-.00611
36	-.00330	-.0004	-1.00	-.0130	-.02164	-.00608
37	-.00310	-.0004	-1.00	-.0130	-.02169	-.00609

Middle of Cycle	$\tilde{\Delta} L$ (cm)	E1 (cm/cm)	ΔV (cc)	Ev (cc/cc)	ΔD (cm)	E3 (cm/cm)
38	-.00300	-.0004	-1.00	-.0130	-.02171	-.00609
39	-.00290	-.0004	-1.00	-.0130	-.02173	-.00610
40	-.00280	-.0004	-1.00	-.0130	-.02176	-.00611
41	-.00250	-.0003	-1.00	-.0130	-.02182	-.00610
42	-.00210	-.0003	-1.00	-.0130	-.02194	-.00615
43	-.00160	-.0002	-0.95	-.0120	-.02091	-.00587
44	-.00120	-.0002	-0.95	-.0120	-.02100	-.00589
45	-.00090	-.0001	-0.90	-.0110	-.01995	-.00560
46	-.00070	-.0001	-0.90	-.0110	-.02000	-.00561
47	-.00060	-.0001	-0.90	-.0110	-.02002	-.00562
48	-.00180	-.0002	-0.90	-.0110	-.01975	-.00554
49	-.00120	-.0002	-0.90	-.0110	-.01989	-.00558
50	-.00100	-.0001	-0.90	-.0110	-.01993	-.00559
51	-.00090	-.0001	-0.90	-.0110	-.01995	-.00560
52	-.00100	-.0001	-0.90	-.0110	-.01995	-.00559
53	-.00100	-.0001	-0.95	-.0120	-.01995	-.00559
54	-.00070	-.0001	-0.95	-.0120	-.02110	-.00593
55	-.00060	-.0001	-0.95	-.0120	-.02114	-.00593
56	-.00050	-.0001	-0.95	-.0120	-.02116	-.00594
57	-.00020	-.0000	-1.00	-.0130	-.02234	-.00627
58	-.00040	-.0001	-1.00	-.0130	-.02230	-.00626
59	-.00040	-.0001	-1.00	-.0130	-.02230	-.00626
60	-.00040	-.0001	-1.00	-.0130	-.02230	-.00626
72	-.00260	-.0000	-1.20	-.0150	-.02626	-.00737

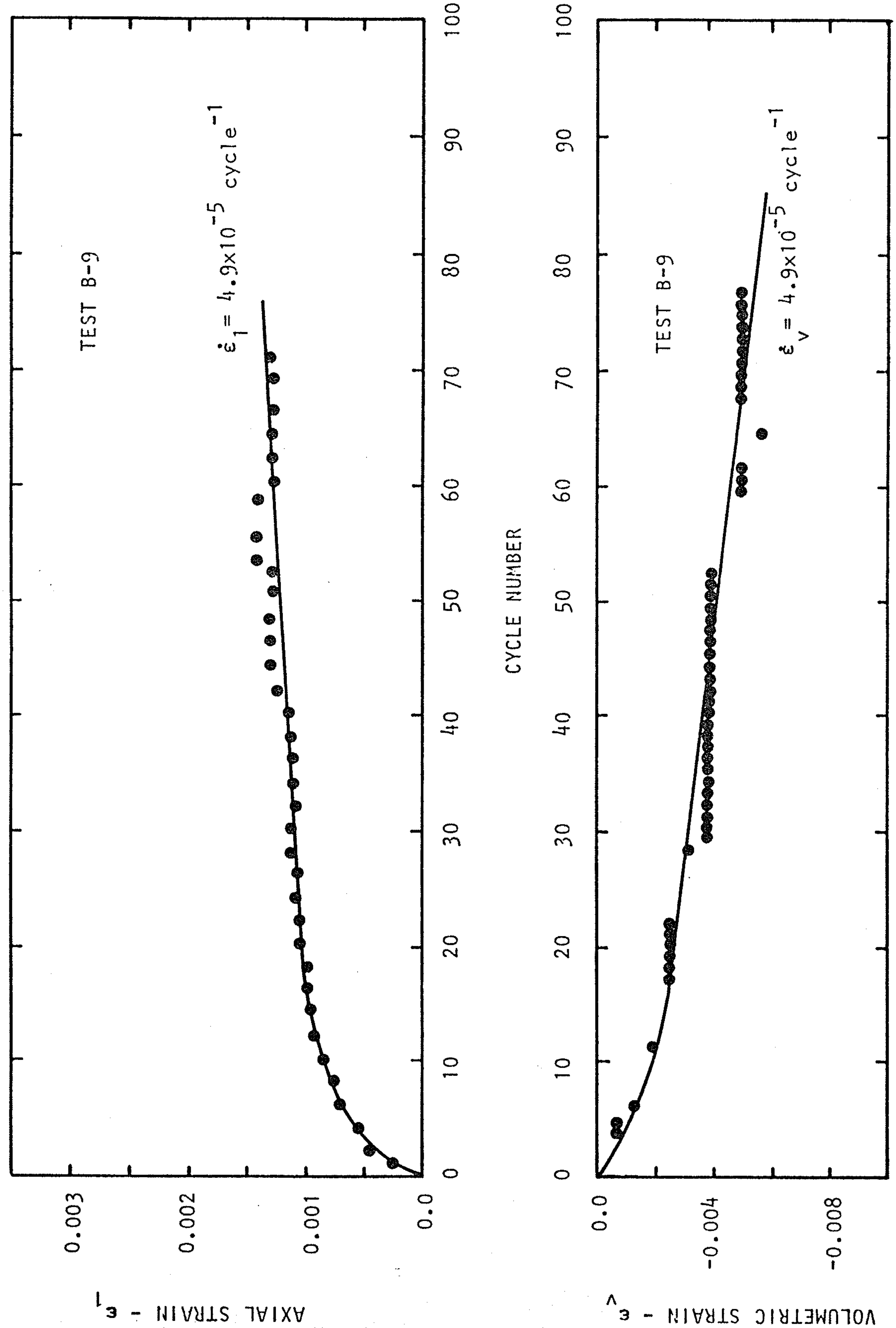
TEST B-9
$\dot{\varepsilon}_1 = 4.9\times10^{-5}$ cycle^{-1}
AXIAL STRAIN - ε_1
0.003
0.002
0.001
0.0
0
10
20
30
40
50
60
70
80
90
100
CYCLE NUMBER
TEST B-9
$\dot{\varepsilon}_v = 4.9\times10^{-5}$ cycle^{-1}
VOLUMETRIC STRAIN - ε_v
0.0
-0.004
-0.008

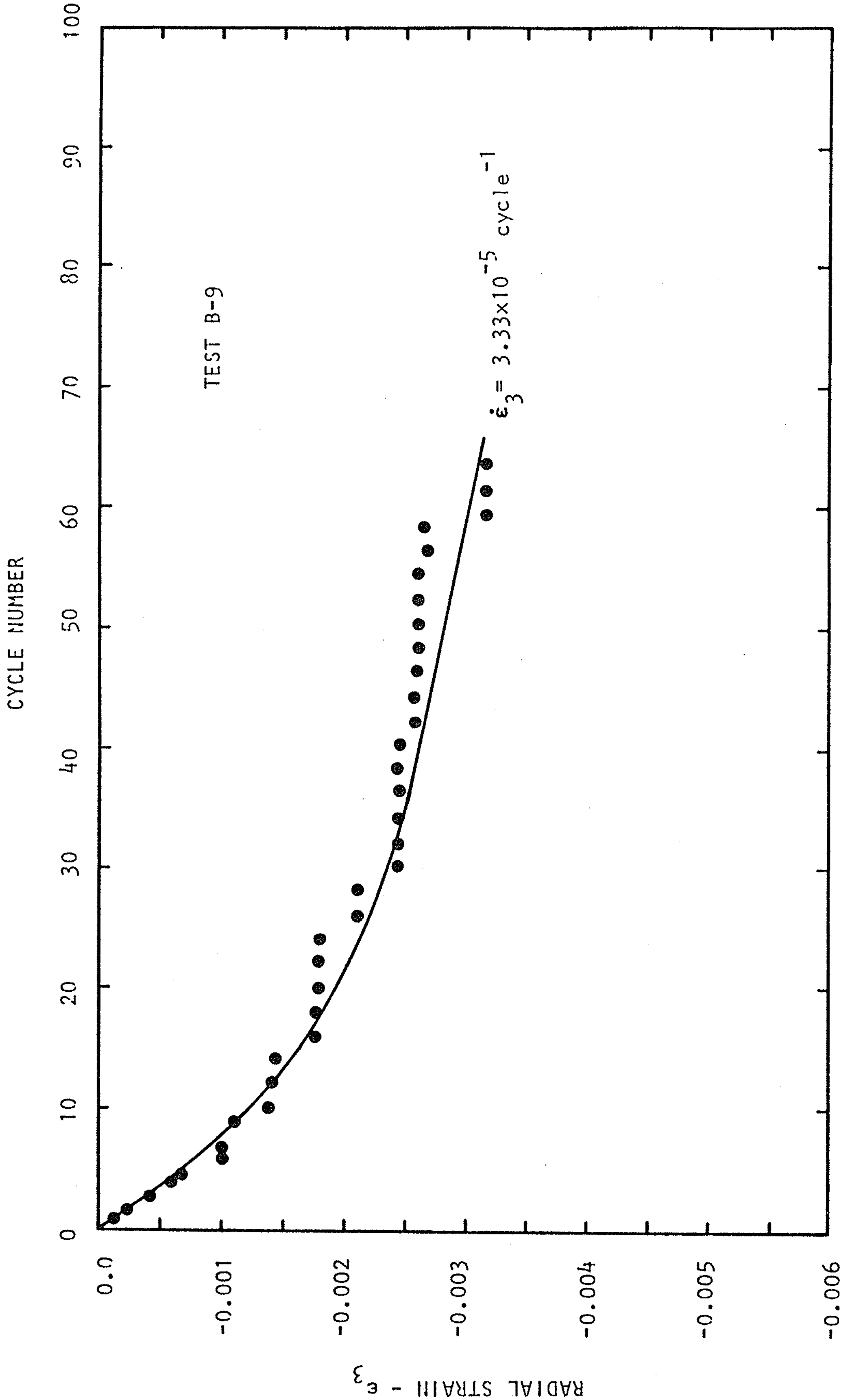
CYCLE NUMBER
0
10
20
30
40
50
60
70
80
90
100
TEST B-9
$\dot{\varepsilon}_3 = 3.33\times10^{-5}$ cycle^{-1}
0.0
-0.001
-0.002
-0.003
-0.004
-0.005
-0.006
RADIAL STRAIN - ε_3

TEST : B10 Date Tested : 090685

Sample Length After Consolidation : 7.776 cm $\sigma_1=44.9$kPa
Sample Diameter After Consolidation : 3.574 cm $\sigma_3=18.0$kPa
Sample Area After Consolidation : 10.031 cm^2 $\Delta u=5.8$kPa
Sample Volume After Consolidation : 77.996 cm^3
Void Ratio After Consolidation : 0.825
Water Content Before Consolidation : 30.2%
Water Content After DTTCP Test : 31.9%

End Of Cycle	ΔLd (cm)	E1 (cm/cm)	ΔV (cc)	Ev (cc/cc)	ΔD (cm)	E3 (mc/mc)
1	.00010	.00001	0	0	-.00002	-.00001
2	.00050	.00006	0	0	-.00007	-.00002
3	.00070	.00009	0	0	-.00012	-.00003
4	.00080	.00010	0	0	-.00014	-.00004
5	.00100	.00013	0	0	-.00012	-.00005
6	.00140	.00018	0	0	-.00028	-.00008
7	.00180	.00023	0	0	-.00037	-.00010
12	.00230	.00030	-0.05	-.0006	-.00163	-.00046
13	.00250	.00032	-0.05	-.0006	-.00168	-.00047
14	.00260	.00033	-0.05	-.0006	-.00170	-.00048
18	.00280	.00036	-0.10	-.0013	-.00289	-.00081
19	.00290	.00037	-0.10	-.0013	-.00292	-.00082
20	.00330	.00042	-0.10	-.0013	-.00301	-.00084
21	.00280	.00036	-0.10	-.0013	-.00289	-.00091
22	.00300	.00039	-0.10	-.0013	-.00294	-.00082
23	.00300	.00040	-0.10	-.0013	-.00294	-.00082
24	.00310	.00040	-0.10	-.0013	-.00296	-.00083
37	.00420	.00054	-0.10	-.0013	-.00322	-.00090
42	.00460	.00059	-0.13	-.0017	-.00399	-.00112
43	.00500	.00064	-0.15	-.0019	-.00454	-.00127
44	.00500	.00064	-0.15	-.0019	-.00454	-.00127
48	.00500	.00064	-0.15	-.0019	-.00454	-.00127
49	.00460	.00059	-0.15	-.0019	-.00445	-.00125
50	.00480	.00062	-0.15	-.0019	-.00450	-.00126
54	.00510	.00066	-0.15	-.0019	-.00457	-.00128
55	.00520	.00067	-0.15	-.0019	-.00459	-.00128
56	.00520	.00067	-0.15	-.0019	-.00459	-.00128
60	.00560	.00072	-0.15	-.0019	-.00468	-.00131
66	.00620	.00080	-0.17	-.0022	-.00528	-.00148
68	.00640	.00082	-0.15	-.0019	-.00487	-.00136
72	.00620	.00080	-0.20	-.0026	-.00597	-.00167
79	.00630	.00081	-0.25	-.0032	-.00713	-.00200
84	.00670	.00086	-0.20	-.0026	-.00608	-.00170

TEST : B10 Date Tested : 090685

Sample Length After Consolidation : 7.776 cm $\sigma_1' = 44.9$kPa
Sample Diameter After Consolidation : 3.574 cm $\sigma_3' = 18.0$kPa
Sample Area After Consolidation : 10.031 cm^2 $\Delta u = 5.8$kPa
Sample Volume After Consolidation : 77.996 cm^3
Void Ratio After Consolidation : 0.825
Water Content Before Consolidation : 30.2%
Water Content After DTTCP Test : 31.9%

Middle Of Cycle	ΔL (cm)	E1 (cm/cm)	ΔV (cc)	Ev (cc/cc)	ΔD (cm)	E3 (cm/cm)
1	-.00060	-.0001	-0.15	-.0020	-.00326	-.00091
2	-.00090	-.0001	-0.20	-.0030	-.00433	-.00121
3	.00010	.0000	-0.20	-.0030	-.00456	-.00128
4	.00030	.0000	-0.20	-.0030	-.00461	-.00129
5	.00050	.0001	-0.20	-.0030	-.00465	-.00130
6	.00070	.0001	-0.20	-.0030	-.00470	-.00132
7	.00080	.0001	-0.20	-.0030	-.00472	-.00132
8	.00100	.0001	-0.20	-.0030	-.00477	-.00133
9	.00100	.0001	-0.20	-.0030	-.00477	-.00133
10	.00090	.0001	-0.20	-.0030	-.00474	-.00133
11	.00110	.0001	-0.20	-.0030	-.00479	-.00134
12	.00140	.0002	-0.20	-.0030	-.00486	-.00136
13	.00150	.0001	-0.20	-.0030	-.00488	-.00137
14	.00170	.0002	-0.20	-.0030	-.00493	-.00138
15	.00230	.0003	-0.20	-.0030	-.00507	-.00142
16	.00210	.0003	-0.20	-.0030	-.00502	-.00141
17	.00230	.0003	-0.20	-.0030	-.00507	-.00142
18	.00220	.0003	-0.20	-.0030	-.00505	-.00141
19	.00230	.0003	-0.20	-.0030	-.00507	-.00142
20	.00240	.0003	-0.20	-.0030	-.00509	-.00142
21	.00270	.0003	-0.20	-.0030	-.00516	-.00144
22	.00250	.0003	-0.20	-.0030	-.00511	-.00143
23	.00260	.0003	-0.20	-.0030	-.00514	-.00144
24	.00260	.0003	-0.20	-.0030	-.00514	-.00144
25	.00280	.0004	-0.20	-.0030	-.00518	-.00145
33	.00340	.0004	-0.20	-.0030	-.00532	-.00149
43	.00350	.0004	-0.25	-.0030	-.00649	-.00182
49	.00420	.0005	-0.25	-.0030	-.00665	-.00186
50	.00420	.0005	-0.25	-.0030	-.00665	-.00186
55	.00490	.0006	-0.25	-.0030	-.00681	-.00191
56	.00460	.0006	-0.25	-.0030	-.00674	-.00189
61	.00490	.0006	-0.25	-.0030	-.00681	-.00191
62	.00480	.0006	-0.25	-.0030	-.00679	-.00190
67	.00520	.0007	-0.27	-.0030	-.00734	-.00205
82	.00580	.0007	-0.30	-.0040	-.00816	-.00228

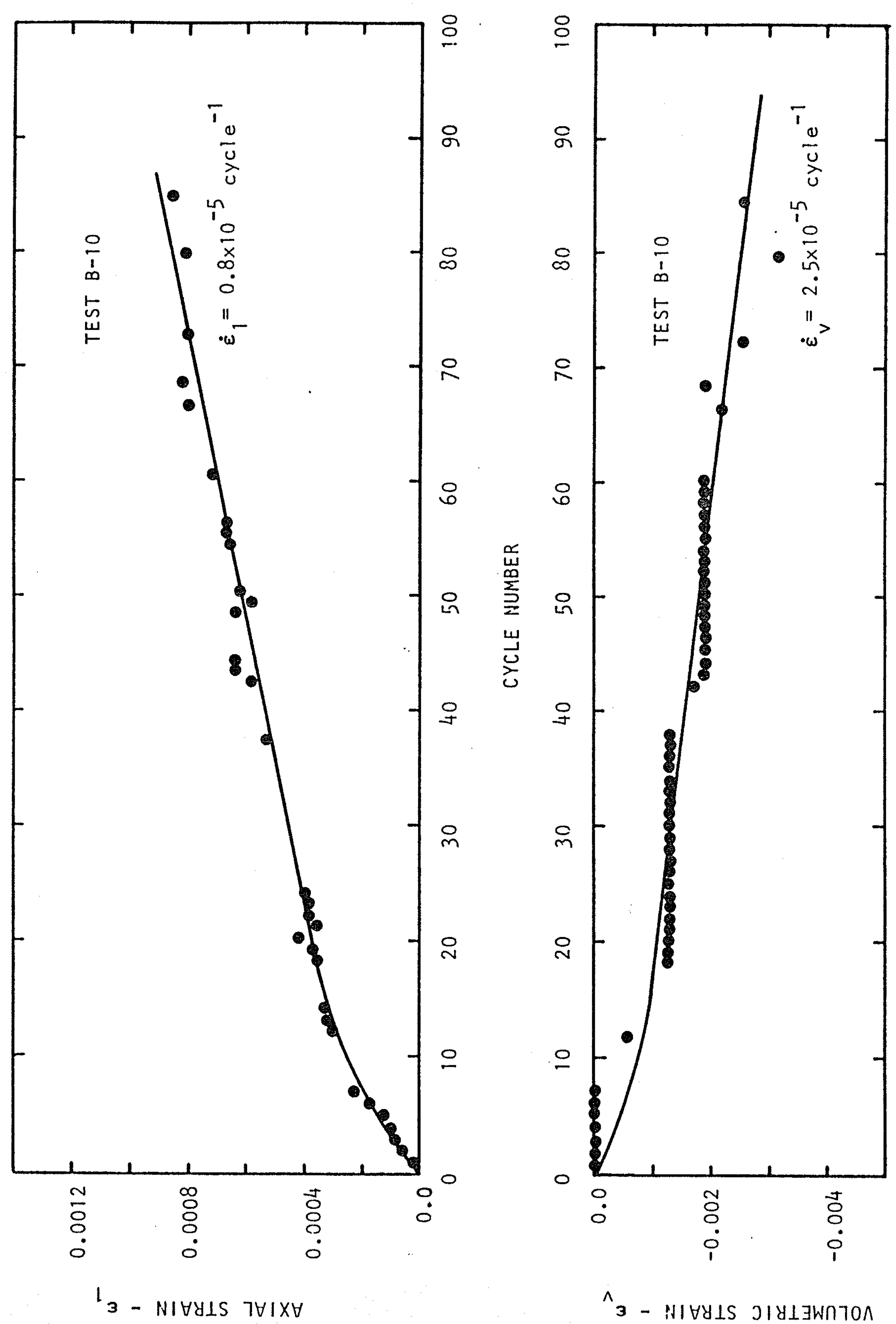
TEST B-10
$\dot{\varepsilon}_1 = 0.8\times10^{-5}$ cycle^{-1}
AXIAL STRAIN - ε_1
0.0
0.0004
0.0008
0.0012
TEST B-10
$\dot{\varepsilon}_v = 2.5\times10^{-5}$ cycle^{-1}
VOLUMETRIC STRAIN - ε_v
0.0
-0.002
-0.004
CYCLE NUMBER
0
10
20
30
40
50
60
70
80
90
100

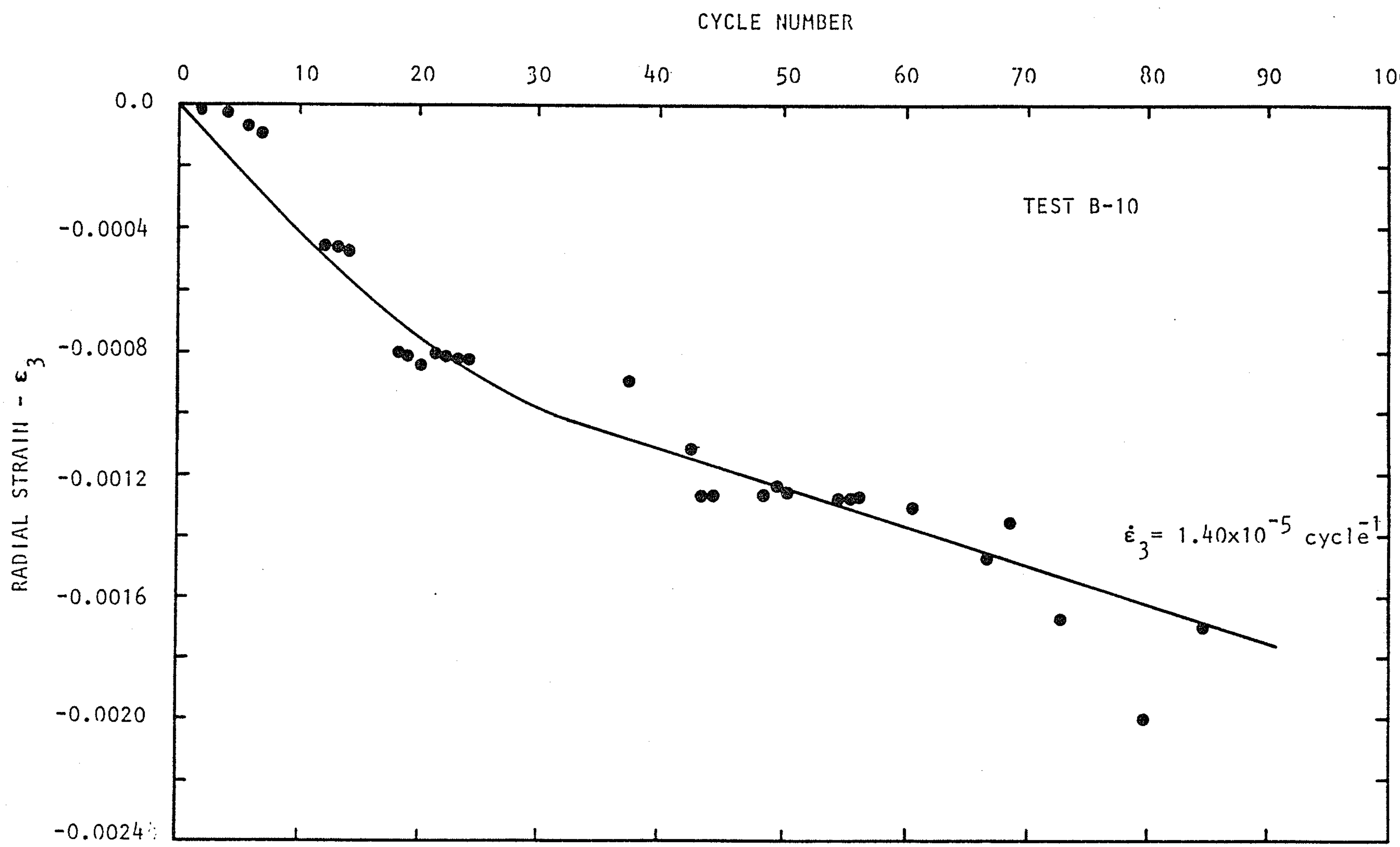
CYCLE NUMBER
0
10
20
30
40
50
60
70
80
90
100
0.0
-0.0004
-0.0008
-0.0012
-0.0016
-0.0020
-0.0024
RADIAL STRAIN - ε_3
TEST B-10
$\dot{\varepsilon}_3 = 1.40 \times 10^{-5}$ cycle^{-1}

TEST : B11 Date Tested : 090685

Sample Length After Consolidation : 7.594 cm σ_1 =34.5kPa
Sample Diameter After Consolidation : 3.584 cm σ_3 =14.5kPa
Sample Area After Consolidation : 10.088 cm^2 Δu=5.8kPa
Sample Volume After Consolidation : 74.593 cm^3
Void Ratio After Consolidation : 0.842
Water Content Before Consolidation : 30.9%
Water Content After DTTCP Test : 33.7%

End Of Cycle	ΔL (mm)	E1 (mm/mm)	ΔV (cc)	Ev (cc/cc)	ΔD (mm)	E3 (mm/mm)
1	.00010	.00001	0	0	-.00003	-.00001
2	.00010	.00014	0	0	-.00024	-.00007
3	.00160	.00022	0	0	-.00039	-.00011
4	.00170	.00023	0	0	-.00042	-.00012
5	.00160	.00022	0	0	-.00039	-.00011
6	.00220	.00030	0	0	-.00054	-.00015
7	.00270	.00037	0	0	-.00066	-.00018
12	.00310	.00042	-0.05	-.0007	-.00196	-.00055
13	.00440	.00060	-0.05	-.0007	-.00227	-.00063
14	.00430	.00058	-0.05	-.0007	-.00225	-.00063
18	.00380	.00051	-0.10	-.0013	-.00249	-.00069
19	.00420	.00057	-0.10	-.0013	-.00342	-.00096
20	.00440	.00060	-0.10	-.0013	-.00347	-.00097
24	.00400	.00054	-0.15	-.0020	-.00458	-.00128
26	.00490	.00062	-0.15	-.0020	-.00480	-.00134
37	.00520	.00070	-0.20	-.0027	-.00607	-.00169
42	.00560	.00076	-0.23	-.0031	-.00688	-.00192
43	.00580	.00078	-0.20	-.0027	-.00621	-.00173
44	.00660	.00089	-0.20	-.0027	-.00641	-.00179
48	.00620	.00084	-0.23	-.0031	-.00703	-.00196
49	.00640	.00087	-0.23	-.0031	-.00708	-.00198
50	.00690	.00093	-0.25	-.0034	-.00768	-.00214
51	.00690	.00093	-0.25	-.0034	-.00768	-.00214
54	.00700	.00095	-0.25	-.0034	-.00770	-.00215
55	.00870	.00118	-0.25	-.0034	-.00812	-.00227
56	.00890	.00120	-0.25	-.0034	-.00817	-.00228
60	.00910	.00123	-0.25	-.0034	-.00822	-.00229
66	.00900	.00122	-0.25	-.0034	-.00819	-.00229
67	.00890	.00120	-0.25	-.0034	-.00817	-.00228
72	.00850	.00115	-0.30	-.0040	-.00927	-.00259
79	.00870	.00118	-0.35	-.0047	-.01052	-.00293
84	.00920	.00124	-0.35	-.0047	-.01064	-.00297

TEST : B11 Date Tested : 090685

Sample Length After Consolidation : 7.594 cm σ_1'=34.5kPa
Sample Diameter After Consolidation : 3.584 cm σ_3'=14.5kPa
Sample Area After Consolidation : 10.088 cm^2 Δu=5.8kPa
Sample Volume After Consolidation : 74.593 cm^3
Void Ratio After Consolidation : 0.842
Water Content Before Consolidation : 30.9%
Water Content After DTTCP Test : 33.7%

Middle Of Cycle	ΔL (cm)	E1 (cm/cm)	ΔV (cc)	Ev (cc/cc)	ΔD (cm)	E3 (cm/cm)
1	-.00150	-.0002	-0.15	-.0067	-.00324	-.00090
2	-.00150	-.0002	-0.20	-.0020	-.00444	-.00124
3	-.00170	-.0002	-0.20	-.0027	-.00439	-.00122
4	-.00080	-.0001	-0.20	-.0027	-.00401	-.00129
5	-.00040	-.0001	-0.20	-.0027	-.00471	-.00131
6	-.00050	-.0001	-0.20	-.0027	-.00468	-.00131
7	.00040	.0001	-0.20	-.0027	-.00490	-.00137
8	.00070	.0001	-0.22	-.0029	-.00545	-.00152
13	.00190	.0002	-0.25	-.0034	-.00647	-.00100
14	.00230	.0003	-0.25	-.0034	-.00656	-.00183
15	.00260	.0004	-0.25	-.0034	-.00664	-.00185
16	.00210	.0003	-0.25	-.0034	-.00651	-.00817
17	.00210	.0003	-0.25	-.0034	-.00651	-.00182
18	.00200	.0003	-0.25	-.0034	-.00649	-.00181
25	.00300	.0004	-0.33	-.0044	-.00865	-.00241
26	.00410	.0006	-0.30	-.0040	-.00820	-.00229
33	.00340	.0004	-0.35	-.0047	-.00923	-.00258
43	.00480	.0006	-0.35	-.0047	-.00957	-.00267
49	.00480	.0006	-0.40	-.0054	-.01076	-.00300
50	.00520	.0007	-0.40	-.0054	-.01086	-.00303
55	.00600	.0008	-0.38	-.0051	-.01106	-.00309
56	.00750	.0010	-0.40	-.0054	-.01142	-.00319
61	.00730	.0010	-0.45	-.0060	-.01257	-.00351
62	.00720	.0010	-0.45	-.0060	-.01255	-.00350
67	.00700	.0009	-0.45	-.0060	-.01250	-.00349
81	.00740	.0010	-0.47	-.0063	-.01308	-.00365
85	.00780	.0011	-0.47	-.0063	-.01317	-.00368

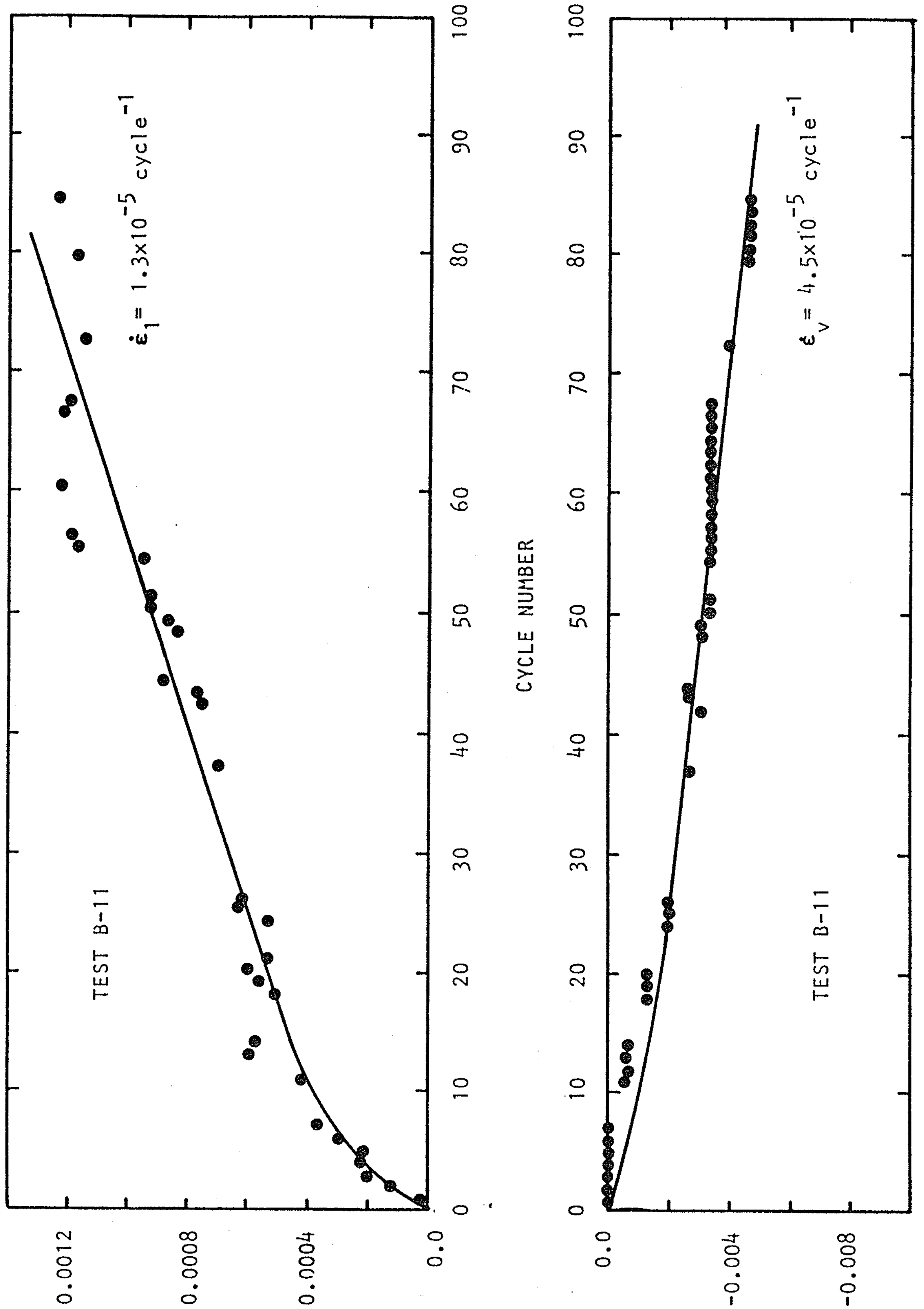
TEST B-11
ε̇1 = 1.3x10^-5 cycle^-1
TEST B-11
ε̇v = 4.5x10^-5 cycle^-1
CYCLE NUMBER
0 10 20 30 40 50 60 70 80 90 100
0.0 0.0004 0.0008 0.0012
0.0 -0.004 -0.008

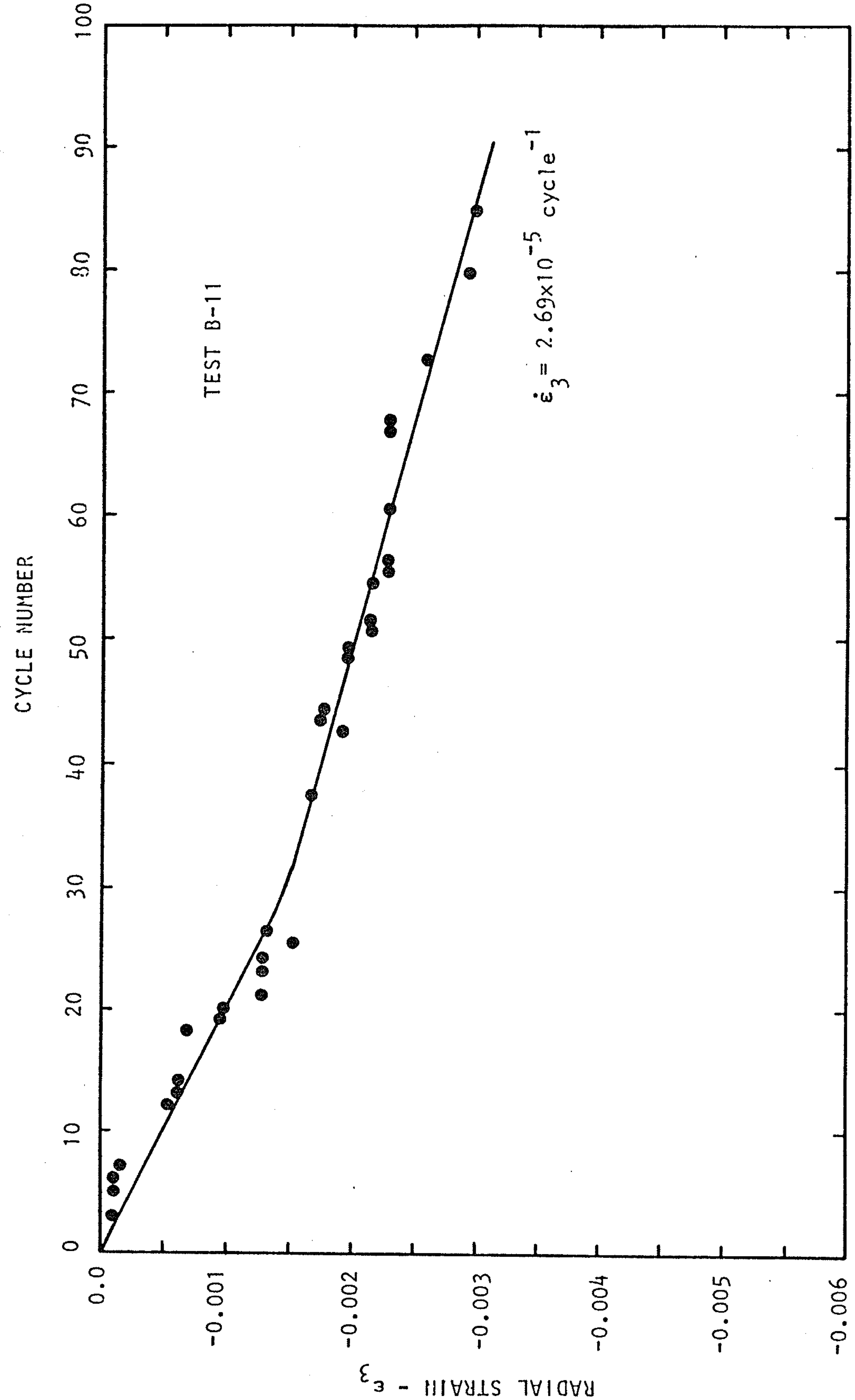

CYCLE NUMBER
RADIAL STRAIN - ε_3
TEST B-11
$\dot{\varepsilon}_3 = 2.69\times10^{-5}$ cycle^{-1}
0 10 20 30 40 50 60 70 80 90 100
0.0 -0.001 -0.002 -0.003 -0.004 -0.005 -0.006

TEST : B12 Date Tested : 093085

Sample Length After Consolidation : 7.511 cm $\sigma_1' = 59.6 kPa$
Sample Diameter After Consolidation : 3.562 cm $\sigma_3' = 35.0 kPa$
Sample Area After Consolidation : 9.965 cm^2 $\Delta u = 33.0 kPa$
Sample Volume After Consolidation : 74.852 cm^3
Void Ratio After Consolidation : 0.824
Water Content Before Consolidation : 31.9%
Water Content After DTTCP Test : 34.2%

End Of Cycle	ΔL (cm)	E1 (cm/cm)	ΔV (cc)	Ev (cc/cc)	ΔD (cm)	E3 (cm/cm)
1	.00610	.00081	0	0	−.00146	−.00041
2	.01010	.00135	0	0	−.00241	−.00068
3	.01340	.00178	0	0	−.00319	−.00090
6	.01980	.00264	0	0	−.00472	−.00132
7	.02050	.00273	0	0	−.00488	−.00137
8	.02260	.00301	0	0	−.00538	−.00151
12	.02560	.00341	0	0	−.00610	−.00171
13	.02750	.00366	0	0	−.00655	−.00184
14	.02840	.00378	0	0	−.00677	−.00190
18	.03130	.00417	0	0	−.00746	−.00209
20	.03250	.00433	−0.05	−.0007	−.00994	−.00251
24	.03480	.00463	−0.10	−.0013	−.01068	−.00300
27	.03500	.00466	−0.10	−.0013	−.01073	−.00301
30	.03640	.00485	−0.20	−.0027	−.01344	−.00377
31	.03660	.00487	−0.20	−.0027	−.01350	−.00379
36	.03750	.00499	−0.30	−.0040	−.01609	−.00452
42	.03980	.00530	−0.30	−.0040	−.01664	−.00467
43	.04020	.00535	−0.30	−.0040	−.01673	−.00470
49	.04140	.00551	−0.40	−.0053	−.01940	−.00545
50	.04200	.00559	−0.40	−.0053	−.01954	−.00549
54	.04260	.00567	−0.40	−.0053	−.01969	−.00553
55	.04340	.00578	−0.40	−.0053	−.01990	−.00558
61	.04340	.00578	−0.45	−.0066	−.02110	−.00592
62	.04350	.00579	−0.50	−.0067	−.02230	−.00626
67	.04450	.00592	−0.50	−.0067	−.02250	−.00632
68	.04450	.00592	−0.50	−.0067	−.02250	−.00632
72	.04560	.00607	−0.60	−.0080	−.02520	−.00700
78	.04830	.00643	−0.60	−.0080	−.02581	−.00725
85	.05040	.00671	−0.60	−.0080	−.02632	−.00739
91	.05180	.00690	−0.70	−.0094	−.02900	−.00815

TEST : B12 Date Tested : 093085

Sample Length After Consolidation : 7.511 cm $\sigma_1' = 59.6$kPa
Sample Diameter After Consolidation : 3.562 cm $\sigma_3' = 35.0$kPa
Sample Area After Consolidation : 9.965 cm^2 $\Delta u = 33.0$kPa
Sample Volume After Consolidation : 74.852 cm^3
Void Ratio After Consolidation : 0.824
Water Content Before Consolidation : 31.9%
Water Content After DTTCP Test : 34.2%

Middle Of Cycle	ΔL (cm)	E1 (cm/cm)	ΔV (cc)	Ev (cc/cc)	ΔD (cm)	E3 (cm/cm)
1	-.00980	-.0013	-1.00	-.0134	-.02140	-.00601
2	-.00520	-.0007	-1.05	-.0140	-.02367	-.00664
4	-.00070	-.0001	-1.05	-.0140	-.02470	-.00695
7	.00660	.0009	-1.00	-.0134	-.02530	-.00710
13	.01250	.0017	-1.05	-.0140	-.02790	-.00785
14	.01430	.0018	-1.00	-.0134	-.02710	-.00762
20	.01850	.0025	-1.00	-.0134	-.02820	-.00790
25	.02130	.0028	-1.10	-.0147	-.03119	-.00876
26	.02160	.0029	-1.10	-.0147	-.03130	-.00878
31	.02380	.0032	-1.10	-.0147	-.03180	-.00892
37	.02500	.0033	-1.30	-.0174	-.03680	-.01033
38	.02480	.0033	-1.45	-.0194	-.04030	-.01130
43	.02730	.0036	-1.40	-.0187	-.03970	-.01115
44	.02720	.0036	-1.45	-.0194	-.04088	-.01148
49	.02850	.0038	-1.45	-.0194	-.04119	-.01156
50	.02920	.0039	-1.45	-.0194	-.04140	-.01161
55	.03020	.0040	-1.50	-.0200	-.04280	-.01200
56	.03020	.0040	-1.50	-.0200	-.04250	-.01200
61	.03060	.0041	-1.50	-.0200	-.04290	-.01200
62	.03120	.0042	-1.50	-.0200	-.04300	-.01210
67	.04430	.0059	-1.50	-.0200	-.04620	-.01300
68	.03290	.0044	-1.50	-.0200	-.04340	-.01220
73	.03390	.0045	-1.80	-.0240	-.05070	-.01425
79	.03710	.0049	-1.80	-.0240	-.05150	-.01446
85	.03860	.0051	-1.85	-.0247	-.05310	-.01490
91	.04040	.0054	-1.90	-.0254	-.05470	-.01540
92	.04070	.0054	-1.90	-.0254	-.05475	-.01540

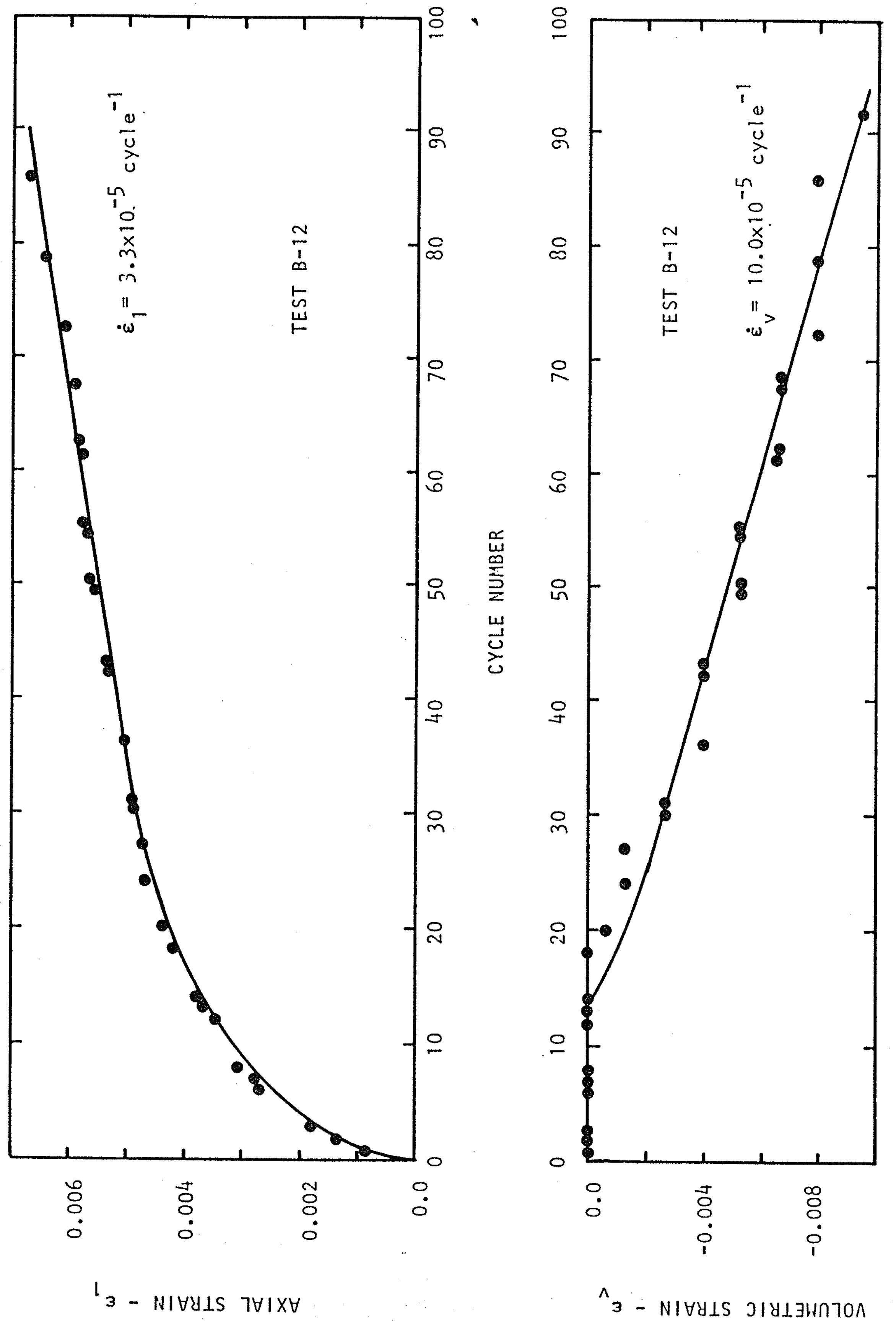

TEST B-12
$\dot{\varepsilon}_1 = 3.3\times10^{-5}$ cycle^{-1}
AXIAL STRAIN - ε_1
0.0
0.002
0.004
0.006
CYCLE NUMBER
0
10
20
30
40
50
60
70
80
90
100
TEST B-12
$\dot{\varepsilon}_v = 10.0\times10^{-5}$ cycle^{-1}
VOLUMETRIC STRAIN - ε_v
0.0
-0.004
-0.008

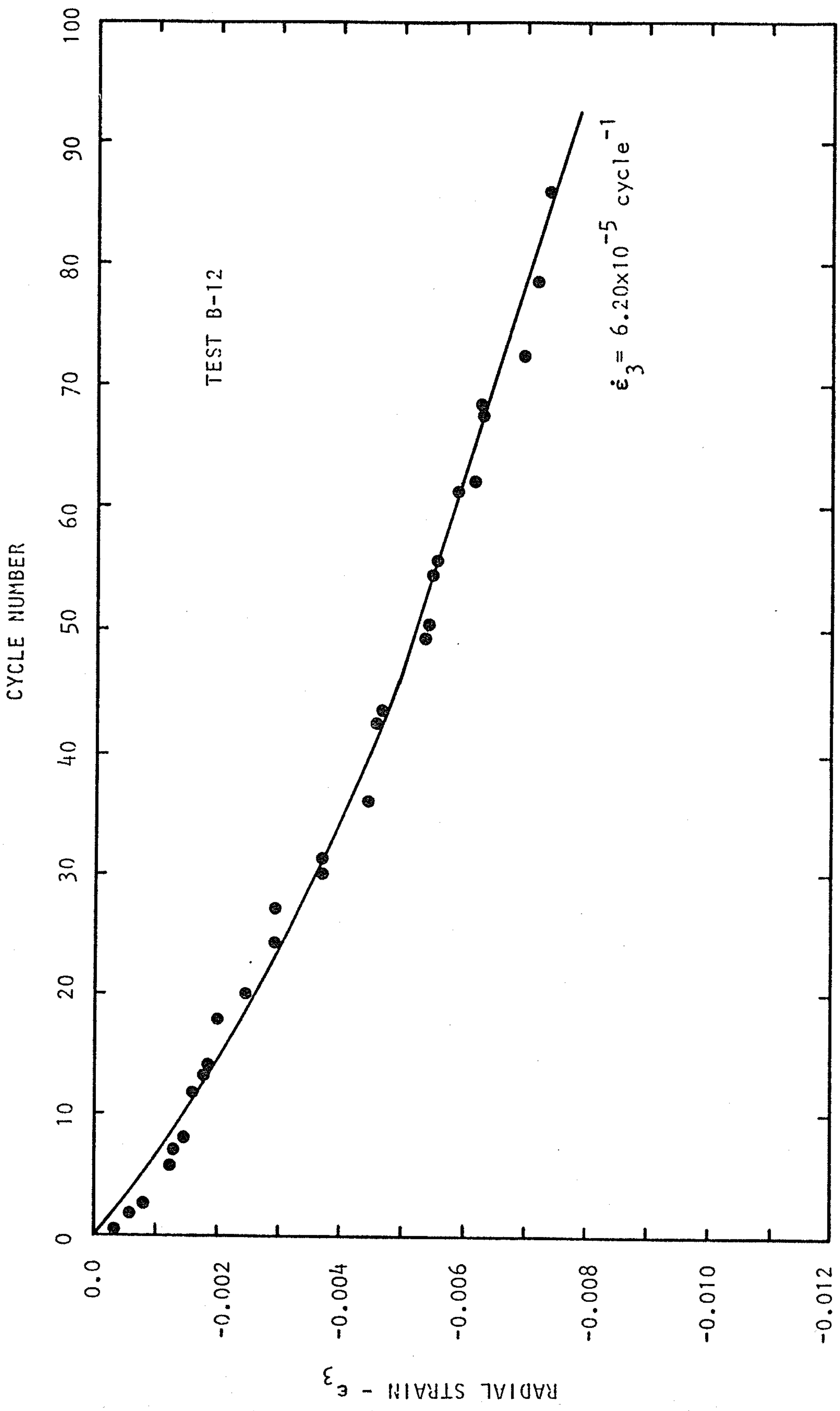
CYCLE NUMBER
0
10
20
30
40
50
60
70
80
90
100
TEST B-12
$\dot{\varepsilon}_3 = 6.20\times10^{-5}$ cycle^{-1}
0.0
-0.002
-0.004
-0.006
-0.008
-0.010
-0.012
RADIAL STRAIN - ε_3

C.3 CIU Test Results

UNIVERSITY OF MANITOBA
SOIL MECHANICS LABORATORY

SAMPLE NO. = T 1 HOLE NO. = 2 DEPTH = 1.30 METRES TO 1.60 METRES

SAMPLE HEIGHT AFTER CONSULIDATION = 7.655 CENTIMETRES
SAMPLE VOLUME AFTER CONSOLIDATION = 83.930 CUBIC CENTIMETRES
SAMPLE AREA AFTER CONSOLIDATION = 10.957 SQUARE CENTIMETRES

CONSTANT LOAD = 2.70 N .
PROVING RING FACTOR = 1.0000 N ./DIV
PISTON AREA = 1.2570 SQUARE CENTIMETRES

INITIAL DIAL READING = 0.0 DIVISIONS

SHEAR TEST RESULTS START 90285 END 100285

CONSOLIDATED UNDRAINED TRIAXIAL TEST
::

PT	TIME	DISPL DIAL RDG	PRING DIAL RDG	PORE PRESS KPA	PER CENT PCSTRN	EFFECT SIGMA1 KPA	EFFECT SIGMA3 KPA	HALF DEV STRESS KPA	DEV STRESS KPA	EFFECT OCT STRESS KPA	RATIO OF EFF SIGMA1 EFF SIFMA3	A
1	1331	0.0	35.0	209.0	0.0	24.4	16.0	4.2	8.4	18.8	1.524	0.0
2	1343	0.1	58.0	217.0	0.20	37.3	8.0	14.7	29.3	17.8	4.665	0.38
3	1402	0.4	66.0	217.0	0.50	44.5	8.0	18.2	36.5	20.2	5.562	0.28
4	1417	0.6	69.0	216.0	0.73	48.1	9.0	19.6	39.1	22.0	5.348	0.23
5	1430	0.7	71.0	215.0	0.94	50.9	10.0	20.4	40.9	23.6	5.086	0.18
6	1455	1.0	82.0	214.0	1.33	61.6	11.0	25.3	50.6	27.9	5.600	0.12
7	1518	1.3	89.0	212.0	1.70	69.7	13.0	28.3	56.7	31.9	5.351	0.06
8	1540	1.6	94.0	210.0	2.05	76.0	15.0	30.5	61.0	35.3	5.064	0.02
9	1605	1.9	103.0	208.0	2.46	85.7	17.0	34.4	68.7	39.9	5.042	-0.02
10	1625	2.1	109.0	206.0	2.77	92.8	19.0	36.9	73.8	43.6	4.885	-0.05
11	1640	2.3	112.0	204.0	3.00	97.3	21.0	38.2	76.3	46.4	4.633	-0.07
12	1658	2.5	117.0	203.0	3.29	102.5	22.0	40.2	80.5	48.8	4.659	-0.08
13	1720	2.8	122.0	201.0	3.64	108.6	24.0	42.3	84.6	52.2	4.525	-0.10
14	1738	3.0	126.0	199.0	3.93	113.8	26.0	43.9	87.8	55.3	4.379	-0.13
15	1816	3.5	132.0	196.0	4.53	121.5	29.0	46.3	92.5	59.8	4.190	-0.15
16	1842	3.8	138.0	194.0	4.95	128.3	31.0	48.7	97.3	63.4	4.139	-0.17
17	1904	4.1	144.0	192.0	5.30	136.0	34.0	51.0	102.0	68.0	4.001	-0.18
18	1936	4.4	150.0	190.0	5.72	142.8	36.0	53.4	106.8	71.6	3.965	-0.19
19	2000	4.7	157.0	187.0	6.19	151.2	39.0	56.1	112.2	76.4	3.877	-0.21
20	2015	4.9	159.0	186.0	6.44	152.7	39.0	56.9	113.7	76.9	3.916	-0.22
21	2040	5.2	165.0	184.0	6.83	159.4	41.0	59.2	118.4	80.5	3.887	-0.23
22	2105	5.5	170.0	182.0	7.24	166.0	44.0	61.0	122.0	84.7	3.772	-0.24
23	2130	5.8	175.0	180.0	7.63	171.7	46.0	62.8	125.7	87.9	3.732	-0.25
24	2200	6.2	182.0	178.0	8.11	178.9	48.0	65.4	130.9	91.6	3.727	-0.25
25	2220	6.4	185.0	176.0	8.43	182.9	50.0	66.5	132.9	94.3	3.659	-0.26
26	947	14.8	305.0	134.0	19.33	297.5	92.0	102.7	205.5	160.5	3.233	-0.38

SAMPLE NO. = T 1 HOLE NO. = 2 DEPTH = 1.30 METRES TO 1.60 METRES

CONSOLIDATION AXIAL STRESS = 225.00 KPA
PRECONSOLIDATION PRESSURE = 100.00 KPA
NORMALIZING STRESS = 225.00 KPA

NORMALIZED SHEAR TEST RESULTS START 90285 END 100285

PT	PER CENT PCSTRN	NRMLZD HALF DEV STRESS KPA	EFFECT RATIO SIGMA1 SIGMA3	NRMLZD OCT STRESS KPA	NRMLZD CHANGE IN PWP KPA
1	0.0	0.019	1.524	0.084	0.0
2	0.20	0.065	4.665	0.079	0.036
3	0.50	0.081	5.562	0.090	0.036
4	0.73	0.087	5.348	0.098	0.031
5	0.94	0.091	5.086	0.105	0.027
6	1.33	0.112	5.600	0.124	0.022
7	1.70	0.126	5.361	0.142	0.013
8	2.05	0.135	5.064	0.157	0.004
9	2.46	0.153	5.042	0.177	-0.004
10	2.77	0.164	4.885	0.194	-0.013
11	3.00	0.170	4.633	0.206	-0.022
12	3.29	0.179	4.659	0.217	-0.027
13	3.64	0.188	4.525	0.232	-0.036
14	3.93	0.195	4.379	0.246	-0.044
15	4.53	0.206	4.190	0.266	-0.058
16	4.95	0.216	4.139	0.282	-0.067
17	5.30	0.227	4.001	0.302	-0.076
18	5.72	0.237	3.965	0.318	-0.084
19	6.19	0.249	3.877	0.340	-0.098
20	6.44	0.253	3.916	0.342	-0.102
21	6.83	0.263	3.887	0.358	-0.111
22	7.24	0.271	3.772	0.376	-0.120
23	7.63	0.279	3.732	0.391	-0.129
24	8.11	0.291	3.727	0.407	-0.138
25	8.43	0.295	3.659	0.419	-0.147
26	19.33	0.457	3.233	0.713	-0.333

UNIVERSITY OF MANITOBA
SOIL MECHANICS LABORATORY

SAMPLE NO. = T 2 HOLE NO. = 2 DEPTH = 1.30 METRES TO 1.60 METRES

SAMPLE HEIGHT AFTER CONSOLIDATION = 7.546 CENTIMETRES
SAMPLE VOLUME AFTER CONSOLIDATION = 83.790 CUBIC CENTIMETRES
SAMPLE AREA AFTER CONSOLIDATION = 11.100 SQUARE CENTIMETRES

CONSTANT LOAD = 2.63 N .
PROVING RING FACTOR = 1.0000 N ./DIV
PISTON AREA = 1.2670 SQUARE CENTIMETRES

INITIAL DIAL READING = 18.40 DIVISIONS

SHEAR TEST RESULTS START 2 END 0

CONSOLIDATED UNDRAINED TRIAXIAL TEST
::::::::::::::::::::::::::::::::::::

PT	TIME	DISPL DIAL RDG	PRING DIAL RDG	PORE PRESS KPA	PER CENT PCSTRN	EFFECT SIGMA1 KPA	EFFECT SIGMA3 KPA	HALF DEV STRESS KPA	DEV STRESS KPA	EFFECT OCT STRESS KPA	RATIO OF EFF SIGMA1 EFF SIFMA3	A
1	1505	18.4	26.0	207.0	0.0	26.1	27.0	-0.5	-0.9	26.7	0.966	0.0
2	1515	18.6	66.0	219.0	0.20	50.0	15.0	17.5	35.0	26.7	3.337	0.33
3	1523	18.6	74.0	219.0	0.27	57.2	15.0	21.1	42.2	29.1	3.814	0.28
4	1550	19.0	87.0	224.0	0.80	63.6	10.0	26.8	53.6	27.9	6.361	0.31
5	1603	19.1	93.0	224.0	0.93	68.9	10.0	29.4	58.9	29.6	6.889	0.28
6	1614	19.3	95.0	223.0	1.19	71.5	11.0	30.3	60.5	31.2	6.501	0.26
7	1642	19.6	104.0	223.0	1.59	79.3	11.0	34.1	68.3	33.8	7.205	0.23
8	1700	20.0	109.0	222.0	2.12	84.3	12.0	36.1	72.3	36.1	7.024	0.20
9	1725	20.2	116.0	220.0	2.39	92.3	14.0	39.1	78.3	40.1	6.589	0.16
10	1756	20.6	125.0	218.0	2.92	101.7	16.0	42.8	85.7	44.6	6.356	0.13
11	1810	20.8	129.0	217.0	3.14	106.0	17.0	44.5	89.0	46.7	6.235	0.11
12	1842	21.2	137.0	214.0	3.71	115.4	20.0	47.7	95.4	51.8	5.770	0.07
13	1922	21.7	147.0	211.0	4.37	126.4	23.0	51.7	103.4	57.5	5.494	0.04
14	1952	22.1	156.0	208.0	4.90	136.5	26.0	55.3	110.5	62.8	5.250	0.01
15	2016	22.4	162.0	207.0	5.30	142.2	27.0	57.6	115.2	65.4	5.265	0.0
16	2050	22.8	172.0	204.0	5.84	153.0	30.0	61.5	123.0	71.0	5.099	-0.02
17	2120	23.2	179.0	202.0	6.36	160.2	32.0	64.1	128.2	74.7	5.007	-0.04
18	2142	23.5	184.0	200.0	6.76	165.9	34.0	65.9	131.9	78.0	4.878	-0.05
19	2205	23.8	188.0	198.0	7.16	170.7	36.0	67.3	134.7	80.9	4.740	-0.07
20	2235	24.2	200.0	196.0	7.69	181.9	38.0	71.9	143.9	86.0	4.786	-0.08
21	2300	24.5	202.0	194.0	8.08	184.9	40.0	72.4	144.9	88.3	4.622	-0.09
22	837	32.0	252.0	170.0	18.02	229.3	63.0	83.1	166.3	118.4	3.639	-0.22

SAMPLE NO. = T 2 HOLE NO. = 2 DEPTH = 1.30 METRES TO 1.60 METRES

ONSOLIDATION AXIAL STRESS = 234.00 KPA
.RECONSOLIDATION PRESSURE = 100.00 KPA
NORMALIZING STRESS = 234.00 KPA

NORMALIZED SHEAR TEST RESULTS START 2 END)

PT	PER CENT PCSTRN	NRMLZD HALF DEV STRESS KPA	EFFECT RATIO SIGMA1 SIGMA3	NRMLZD OCT STRESS KPA	NRMLZD CHANGE IN PWP KPA
1	0.0	-0.002	0.966	0.114	0.0
2	0.20	0.075	3.337	0.114	0.051
3	0.27	0.090	3.814	0.124	0.051
4	0.80	0.115	6.361	0.119	0.073
5	0.93	0.126	6.889	0.127	0.073
6	1.19	0.129	6.501	0.133	0.068
7	1.59	0.146	7.205	0.144	0.068
8	2.12	0.154	7.024	0.154	0.064
9	2.39	0.167	6.589	0.171	0.056
10	2.92	0.183	6.356	0.193	0.047
11	3.14	0.190	6.235	0.199	0.043
12	3.71	0.204	5.770	0.221	0.030
13	4.37	0.221	5.494	0.246	0.017
14	4.90	0.236	5.250	0.269	0.004
15	5.30	0.246	5.265	0.279	0.0
16	5.84	0.263	5.099	0.303	-0.013
17	6.36	0.274	5.007	0.319	-0.021
18	6.76	0.282	4.878	0.333	-0.030
19	7.16	0.288	4.740	0.346	-0.038
20	7.69	0.307	4.786	0.367	-0.047
1	8.08	0.310	4.622	0.377	-0.056
.2	13.02	0.355	3.639	0.506	-0.158

UNIVERSITY OF MANITOBA
SOIL MECHANICS LABORATORY

SAMPLE NO. = T 3 HOLE NO. = 2 DEPTH = 1.85 METRES TO 1.85 METRES

SAMPLE HEIGHT AFTER CONSOLIDATION = 8.415 CENTIMETRES
SAMPLE VOLUME AFTER CONSOLIDATION = 101.700 CUBIC CENTIMETRES
SAMPLE AREA AFTER CONSOLIDATION = 12.087 SQUARE CENTIMETRES

CONSTANT LOAD = 2.71 N .
PROVING RING FACTOR = 1.0000 N ./DIV
PISTON AREA = 1.2570 SQUARE CENTIMETRES

INITIAL DIAL READING = 1.00 DIVISIONS

SHEAR TEST RESULTS START 130285 END 130285

CONSOLIDATED UNDRAINED TRIAXIAL TEST
::::::::::::::::::::::::::::::::::::

PT	TIME	DISPL DIAL RDG	PRING DIAL RDG	PORE PRESS KPA	PER CENT PCSTRN	EFFECT SIGMA1 KPA	EFFECT SIGMA3 KPA	HALF DEV STRESS KPA	DEV STRESS KPA	EFFECT OCT STRESS KPA	RATIO OF EFF SIGMA1 EFF SIGMA3	A
1	952	1.0	24.0	200.0	0.0	36.9	40.0	-1.5	-3.1	39.0	0.924	0.0
2	959	1.1	78.0	217.0	0.12	64.6	23.0	20.8	41.6	36.9	2.807	0.38
3	1035	1.4	92.0	219.0	0.48	73.9	21.0	26.5	52.9	38.6	3.521	0.34
4	1120	2.0	111.0	217.0	1.19	91.1	23.0	34.0	68.1	45.7	3.951	0.24
5	1201	2.6	127.0	214.0	1.90	106.6	26.0	40.3	80.6	52.9	4.100	0.17
6	1230	3.0	139.0	212.0	2.38	117.9	28.0	44.9	89.9	58.0	4.211	0.13
7	1306	3.5	153.0	209.0	2.97	130.7	30.0	50.3	100.7	63.6	4.356	0.09
8	1334	3.9	163.0	206.0	3.39	141.2	33.0	54.1	108.3	69.1	4.280	0.05
9	1410	4.3	176.0	203.0	3.92	154.0	36.0	59.0	118.0	75.3	4.277	0.02
10	1430	4.6	184.0	201.0	4.22	162.0	38.0	62.0	124.0	79.3	4.262	0.01
11	1455	4.8	192.0	198.0	4.49	170.9	41.0	65.0	129.9	84.3	4.159	-0.02

SAMPLE NO. = T 3 HOLE NO. = 2 DEPTH = 1.85 METRES TO 1.85 METRES

CONSOLIDATION AXIAL STRESS = 240.00 KPA
PRECONSOLIDATION PRESSURE = 100.00 KPA
NORMALIZING STRESS = 240.00 KPA

NORMALIZED SHEAR TEST RESULTS START 130285 END 130285

PT	PER CENT PCSTRN	NRMLZD HALF DEV STRESS KPA	EFFECT RATIO SIGMA1 SIGMA3	NRMLZD OCT STRESS KPA	NRMLZD CHANGE IN PWP KPA
1	0.0	-0.006	0.924	0.152	0.0
2	0.12	0.087	2.807	0.154	0.071
3	0.48	0.110	3.521	0.161	0.079
4	1.19	0.142	3.961	0.190	0.071
5	1.90	0.168	4.100	0.220	0.058
6	2.38	0.187	4.211	0.242	0.050
7	2.97	0.210	4.356	0.265	0.037
8	3.39	0.226	4.280	0.288	0.025
9	3.92	0.246	4.277	0.314	0.012
10	4.22	0.258	4.262	0.330	0.004
11	4.49	0.271	4.169	0.351	-0.008

SAMPLE NO. = T 4 HOLE NO. = 2 DEPTH = 1.85 METRES TO 1.85 METRES

CONSOLIDATION AXIAL STRESS = 500.00 KPA
PRECONSOLIDATION PRESSURE = 100.00 KPA
NORMALIZING STRESS = 500.00 KPA

NORMALIZED SHEAR TEST RESULTS START 150285 END 160285

PT	PER CENT PCSTRN	NRMLZD HALF DEV STRESS KPA	EFFECT RATIO SIGMA1 SIGMA3	NRMLZD OCT STRESS KPA	NRMLZD CHANGE IN PWP KPA
1	0.0	0.001	1.004	0.583	0.0
2	0.50	0.182	1.927	0.513	0.190
3	0.69	0.222	2.238	0.505	0.224
4	1.04	0.253	2.512	0.502	0.248
5	1.32	0.269	2.663	0.504	0.258
6	2.30	0.345	3.198	0.544	0.268
7	2.78	0.365	3.279	0.563	0.262
8	3.09	0.376	3.320	0.575	0.258
9	3.29	0.394	3.387	0.593	0.252
10	3.66	0.411	3.309	0.630	0.226
11	3.91	0.425	3.312	0.652	0.214
12	5.05	0.479	3.418	0.715	0.186
13	5.36	0.491	3.430	0.731	0.178
14	5.99	0.502	3.367	0.759	0.158
15	7.34	0.533	3.338	0.811	0.124
16	23.15	0.507	2.673	0.944	-0.026

UNIVERSITY OF MANITOBA
SOIL MECHANICS LABORATORY

SAMPLE NO. = T 4 HOLE NO. = 2 DEPTH = 1.85 METRES TO 1.85 METRES

SAMPLE HEIGHT AFTER CONSOLIDATION = 7.926 CENTIMETRES
SAMPLE VOLUME AFTER CONSOLIDATION = 93.900 CUBIC CENTIMETRES
SAMPLE AREA AFTER CONSOLIDATION = 11.846 SQUARE CENTIMETRES

CONSTANT LOAD = 2.71 N .
PROVING RING FACTOR = 1.0000 N ./DIV
PISTON AREA = 1.2670 SQUARE CENTIMETRES

INITIAL DIAL READING = 1.00 DIVISIONS

SHEAR TEST RESULTS START 150285 END 160285

CONSOLIDATED UNDRAINED TRIAXIAL TEST
::

PT	TIME	DISPL DIAL RDG	PRING DIAL RDG	PORE PRESS KPA	PER CENT PCSTRN	EFFECT SIGMA1 KPA	EFFECT SIGMA3 KPA	HALF DEV STRESS KPA	DEV STRESS KPA	EFFECT OCT STRESS KPA	RATIO OF EFF SIGMA1 EFF SIFMA3	A
1	955	1.0	62.0	209.0	0.0	292.1	291.0	0.6	1.1	291.4	1.004	0.0
2	1030	1.4	277.0	304.0	0.50	377.7	196.0	90.9	181.7	256.6	1.927	0.53
3	1045	1.6	325.0	321.0	0.69	400.6	179.0	110.8	221.6	252.9	2.238	0.51
4	1104	1.8	363.0	333.0	1.04	419.6	167.0	126.3	252.6	251.2	2.512	0.49
5	1117	2.1	384.0	338.0	1.32	431.4	162.0	134.7	269.4	251.8	2.653	0.48
6	1230	2.8	479.0	343.0	2.30	502.0	157.0	172.5	345.0	272.0	3.198	0.39
7	1304	3.2	505.0	340.0	2.78	524.7	160.0	182.4	364.7	281.6	3.279	0.36
8	1318	3.4	520.0	338.0	3.09	537.8	162.0	187.9	375.8	287.3	3.320	0.34
9	1338	3.6	543.0	335.0	3.29	558.8	165.0	196.9	393.8	296.3	3.387	0.32
10	1406	3.9	566.0	322.0	3.66	589.0	178.0	205.5	411.0	315.0	3.309	0.28
11	1430	4.1	585.0	316.0	3.91	609.3	184.0	212.7	425.3	325.8	3.312	0.25
12	1544	5.0	658.0	302.0	5.05	676.8	198.0	239.4	478.8	357.6	3.418	0.19
13	1607	5.3	675.0	298.0	5.36	692.8	202.0	245.4	490.8	365.6	3.430	0.18
14	1652	5.8	693.0	288.0	5.99	713.8	212.0	250.9	501.8	379.3	3.357	0.16
15	1818	6.8	742.0	271.0	7.34	761.0	228.0	266.5	533.0	405.7	3.338	0.12
16	1100	19.4	842.0	196.0	23.15	810.0	303.0	253.5	507.0	472.0	2.673	-0.03

C.4 X-Ray Diffraction Results

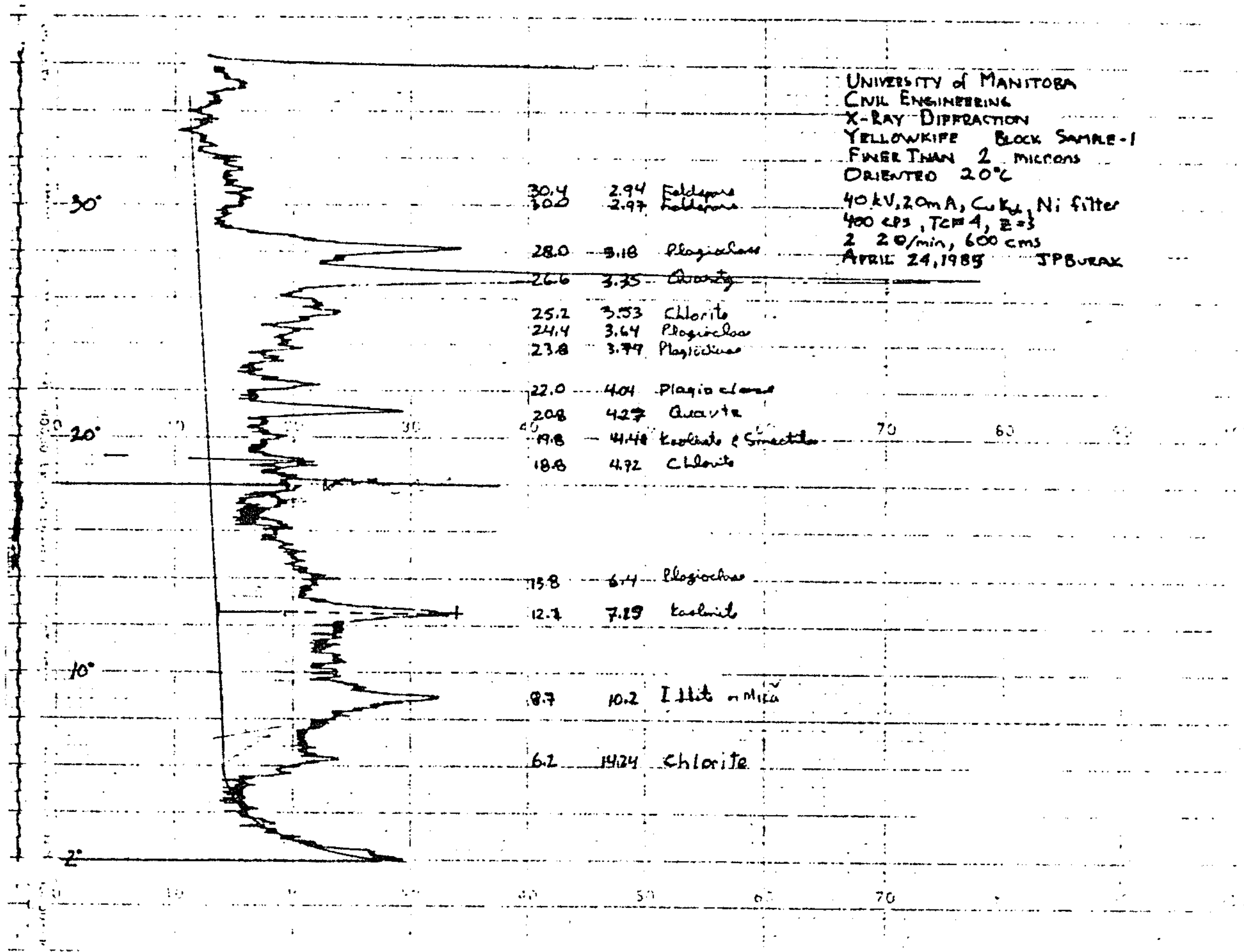

University of Manitoba
Civil Engineering
X-Ray Diffraction
Yellowknife Block Sample-1
Finer Than 2 microns
Oriented 20°C
40 kV, 20 mA, Cu Kα, Ni filter
400 cps, TC=4, Σ=3
2 2θ/min, 600 cms
April 24, 1985 JPBurak
30°
20°
10°
2°
30.4 2.94 Feldspars
30.0 2.97 Feldspars
28.0 3.18 Plagioclase
26.6 3.35 Quartz
25.2 3.53 Chlorite
24.4 3.64 Plagioclase
23.8 3.74 Plagioclase
22.0 4.04 Plagioclase
20.8 4.27 Quartz
19.8 4.48 Kaolinite & Smectite
18.8 4.72 Chlorite
13.8 6.4 Plagioclase
12.4 7.15 Kaolinite
8.7 10.2 Illite mica
6.2 14.24 Chlorite

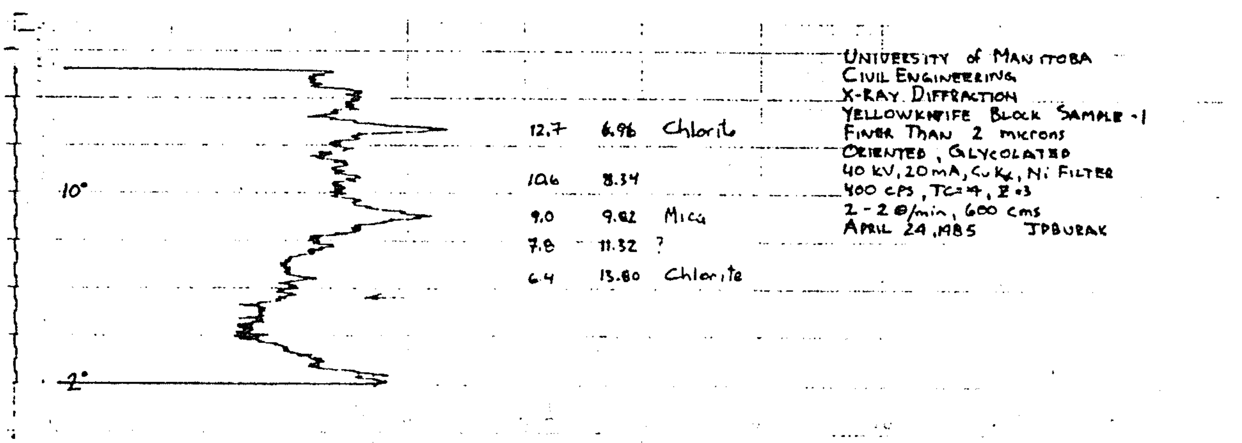

University of Manitoba
Civil Engineering
X-Ray Diffraction
Yellowknife Block Sample-1
Finer Than 2 microns
Oriented, Glycolated
40 kV, 20 mA, Cu Kα, Ni Filter
400 cps, TC=4, Σ=3
2-2θ/min, 600 cms
April 24, 1985 JPBurak
10°
2°
12.7 6.96 Chlorite
10.6 8.34
9.0 9.82 Mica
7.8 11.32 ?
6.4 13.80 Chlorite

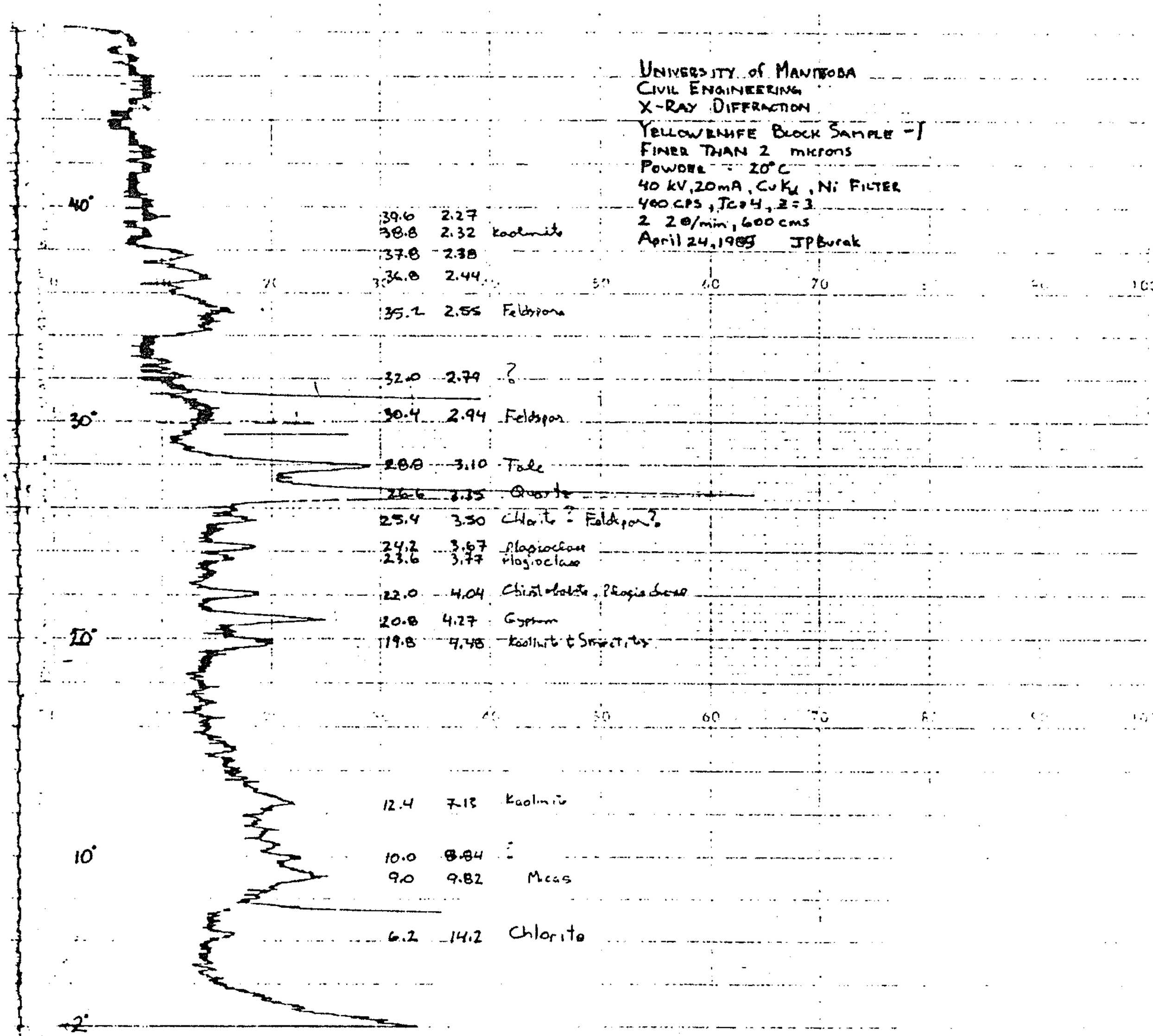

UNIVERSITY of MANITOBA
CIVIL ENGINEERING
X-RAY DIFFRACTION
YELLOWKNIFE BLOCK SAMPLE - I
FINER THAN 2 microns
POWDER - 20°C
40 kV, 20mA, Cu Kα, Ni FILTER
400 CPS, Tc = 4, z = 3
2 2θ/min, 600 cms
April 24, 1985 JPBurak
40°
30°
20°
10°
2°
39.6 2.27
38.8 2.32 Kaolinite
37.8 2.38
36.8 2.44
35.2 2.55 Feldspar
32.0 2.79 ?
30.4 2.94 Feldspar
28.8 3.10 Talc
26.6 3.35 Quartz
25.4 3.50 Chlorite ? Feldspar ?
24.2 3.67 Plagioclase
23.6 3.77 Plagioclase
22.0 4.04 Christobalite, Plagioclase
20.8 4.27 Gypsum
19.8 4.48 Kaolinite + Smectites
12.4 7.13 Kaolinite
10.0 8.84 ?
9.0 9.82 Micas
6.2 14.2 Chlorite

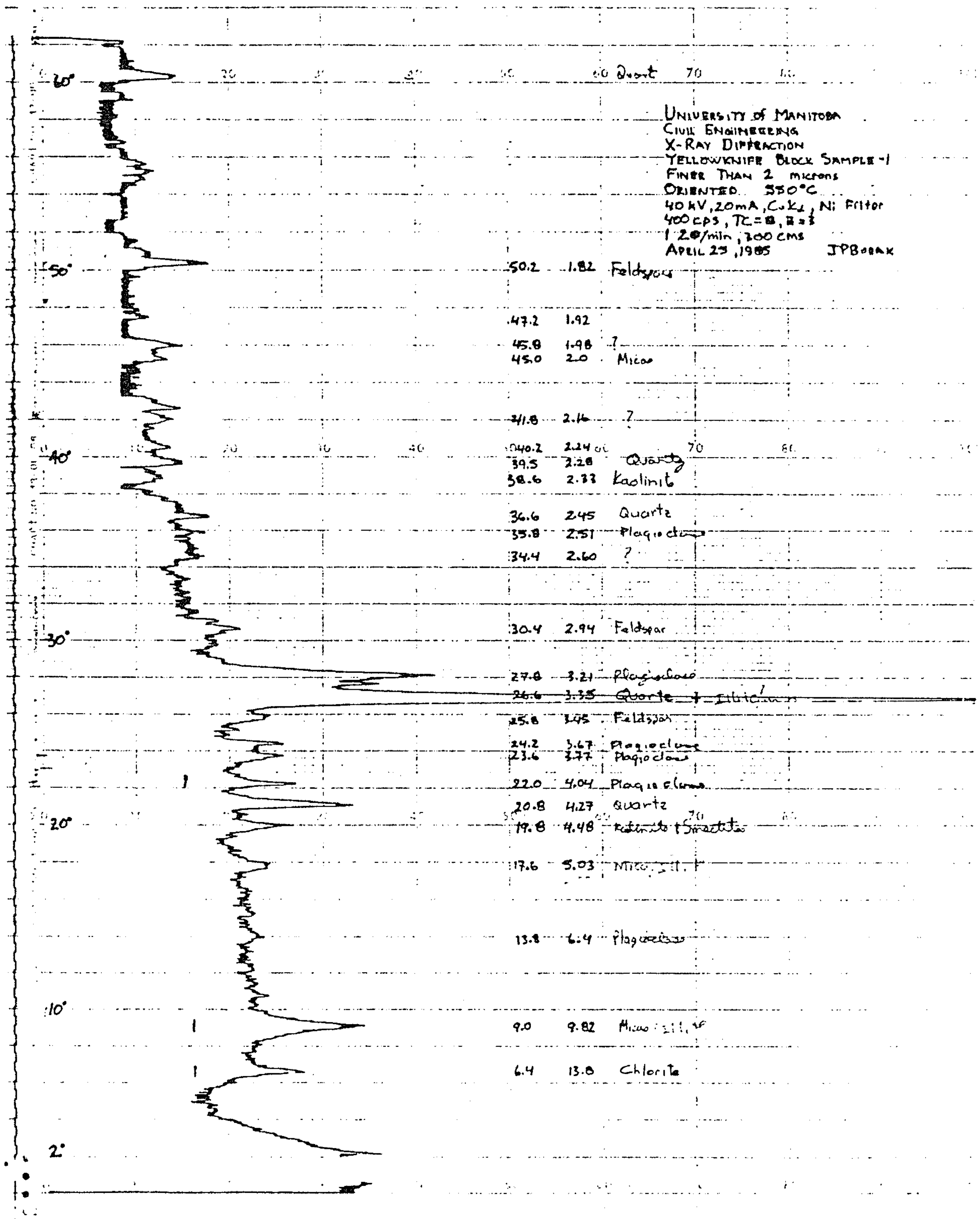
University of Manitoba
Civil Engineering
X-Ray Diffraction
Yellowknife Block Sample -1
Finer Than 2 microns
Oriented 550°C
40 kV, 20 mA, CuKα, Ni Filter
400 cps, TC=8, 2:1
1 2θ/min, 300 cms
April 25, 1985 JPBorak
60° Quartz
50° 50.2 1.82 Feldspar
47.2 1.92
45.8 1.98 ?
45.0 2.0 Mica
41.8 2.16 ?
40° 40.2 2.24
39.5 2.28 Quartz
38.6 2.33 Kaolinite
36.6 2.45 Quartz
35.8 2.51 Plagioclase
34.4 2.60 ?
30° 30.4 2.94 Feldspar
27.8 3.21 Plagioclase
26.6 3.35 Quartz + Illite
25.8 3.45 Feldspar
24.2 3.67 Plagioclase
23.6 3.77 Plagioclase
22.0 4.04 Plagioclase
20.8 4.27 Quartz
20° 19.8 4.48 Kaolinite + Smectite
17.6 5.03 Mica; Illite
13.8 6.4 Plagioclase
10° 9.0 9.82 Mica; Illite
6.4 13.8 Chlorite
2°

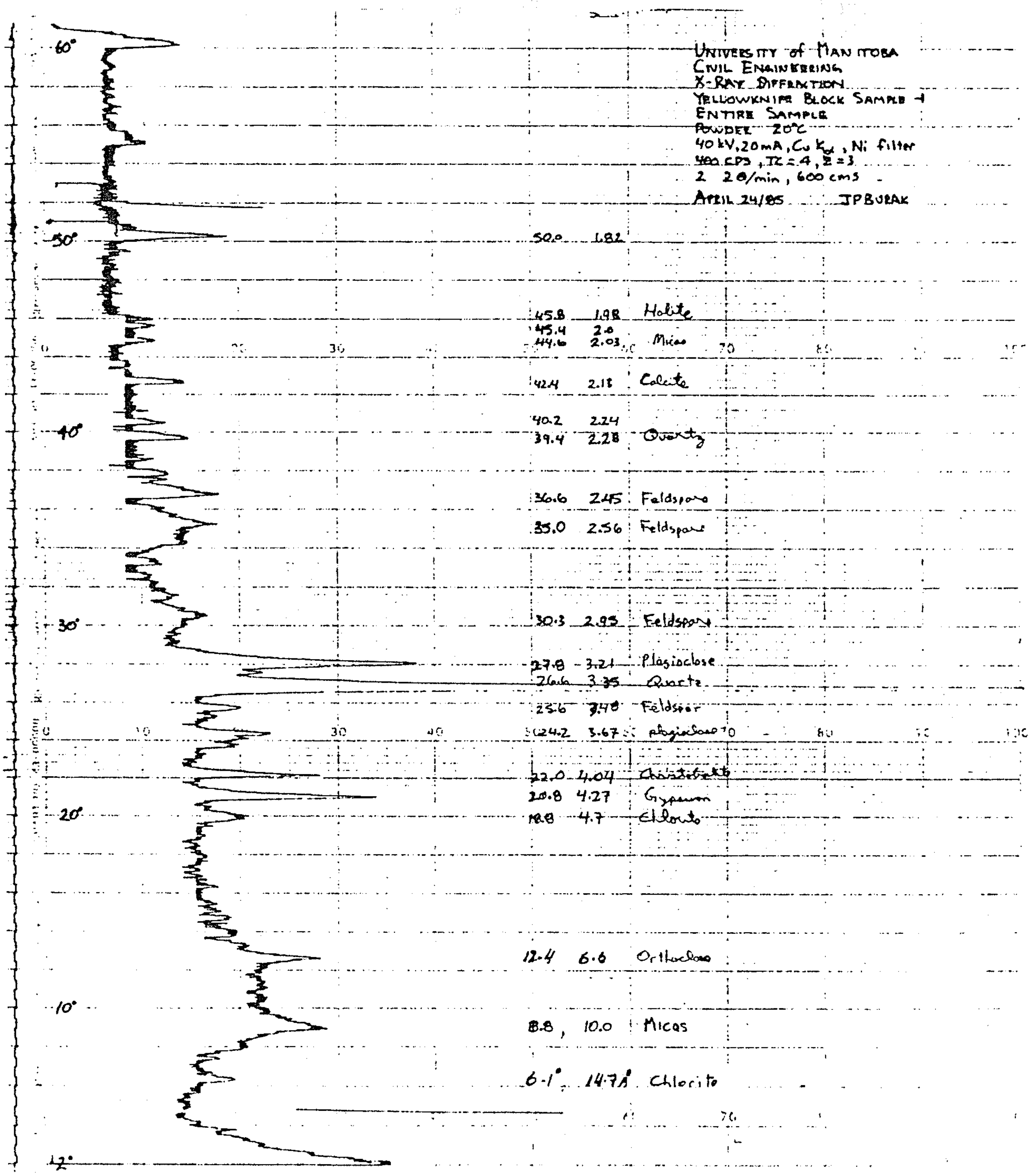

University of Manitoba
Civil Engineering
X-Ray Diffraction
Yellowknife Block Sample 4
Entire Sample
Powder 20°C
40 kV, 20 mA, Cu K_{α}, Ni filter
400 CPS, TC = 4, Σ = 3
2 2θ/min, 600 cms
April 24/85
JPBurak
60°
50°
40°
30°
20°
10°
50.0 1.82
45.8 1.98 Halite
45.4 2.0
44.6 2.03 Micas
42.4 2.13 Calcite
40.2 2.24
39.4 2.28 Quartz
36.6 2.45 Feldspars
35.0 2.56 Feldspars
30.3 2.95 Feldspars
27.8 3.21 Plagioclase
26.6 3.35 Quartz
25.6 3.48 Feldspar
24.2 3.67 plagioclase
22.0 4.04 Christobalite
20.8 4.27 Gypsum
18.8 4.7 Chlorite
12.4 6.6 Orthoclase
8.8, 10.0 Micas
6.1° 14.7Å Chlorite